TABLE OF CONTENTS

LIST OF TABLES

LIST OF FIGURES

LIST OF ABREVIATIONS

AHS	American Helicopter Society
AIAA	American Institute of Aeronautics and Astronautics
ASC	American Society for Composites
ASCE	American Society of Civil Engineers
ASME	American Society of Mechanical Engineers
ASTM	American Society for Testing and Materials
ATM	Accelerated testing methodology
ATM-2	Advanced accelerated testing methodology
BAC	bisaminomethylcyclohexane
BSI	Boltzmann superposition integral
BSP	Boltzmann superposition principle
CA, CAF	Constant amplitude (fatigue)
CAH	Constant amplitude fatigue at high frequency
CAM	Constant amplitude fatigue at intermediate frequency
CANWEA	Canadian Wind Energy Association
CDF	Cumulative density function of a statistical distribution
CDS	Characteristic damage state
CEM	Critical element model
CFRP	Carbon fibre reinforced polymer

CHF	Cumulative hazard function of a statistical distribution
CLD	Constant life diagram
CLT	Classical laminate theory
COE	Cost of energy
DFT	Discrete Fourier transform
DGEBA	Diglycidyl ether of bisphenol A
DMA	Dynamic mechanical analysis (or analyser)
DMTA	Dynamic mechanical-thermal analysis (or analyser)
DSC	Differential scanning calorimetry
ERF	Error function
ETS	École de technologie supérieure
ETT	Effective time theory
EU-FP6	European Union 6th Framework Programme
FLD	Fatigue life diagram
GFRP	Glass fibre reinforced polymer
HCF	High cycle fatigue ($10^3 \leq N \leq 10^8$ cycles)
HF	Hazard function of a statistical distribution
IEA	International Energy Agency
ISO	International Organization for Standardization
KAHR	Kovacs-Aklonis-Hutchinson-Ramos

KWW	Kohlrausch-Williams-Watts
LCF	Low cycle fatigue ($N < 10^3$ cycles)
LSQ	Least square regression
ML, MLE	Maximum likelihood (estimation)
NREL	National Renewable Energy Laboratory
NSERC	National Sciences and Engineering Research Council of Canada
PDF	Probability density function of a statistical distribution
PEEK	Polyether-ether ketone
PES	Polyether sulfone
PP	Polypropylene
P-S-N	Probabilistic stress-life (fatigue curve)
RoM	Rules of mixture
SEI	Strength evolution integral
SF	Survival function of a statistical distribution
SLERA	Strength-life equal rank assumption
S-N	Stress-life (fatigue curve)
TASP	Time-age superposition principle
TNM	Tool-Narayanaswamy-Moynihan
TPU	Thermoplastic poly eurethane
TSTSP	Time-stress-temperature superposition principle

TTSP	Time-temperature superposition principle
UD	Unidirectional reinforced fibre composite
VAF	Variable amplitude fatigue
VFT	Vogel-Fulcher-Tammann
VHCF	Very high cycle fatigue ($N > 10^8$ cycles)
WESNet	Wind Energy Strategic Network
WLF	Williams-Landel-Ferry
WMC	Knowledge Centre Wind turbine Materials and Constructions

LISTE OF SYMBOLS AND UNITS OF MEASUREMENTS

A	Arrhenius pre-exponential factor, or general empirical model parameter, or specimen cross section, mm^2
a	General empirical model parameter
a_e	Ageing shift factor
$a_i(T)$	Slope correction factor
$a_i^{S'}$	Modified static strength shift factor
a_T	Horizontal temperature shift factor
a_ϵ	Strain shift factor
a_σ	Stress shift factor
B	Fatigue sensitivity parameter
b	General empirical model parameter
b_i	Fatigue slope parameter
b_T	Vertical temperature shift factor
C	Relaxation modulus, Pa, or fatigue stress intercept, Pa, or empirical model parameter
C_{LM}	Larson-Miller empirical material constant, dimensionless
C_{SD}	Sherby-Dorn empirical material constant, dimensionless
CTE	Coefficient of thermal expansion, $^\circ\mathrm{C}^{-1}$
CV	Coefficient of variation, %
c	Specific heat, $\mathrm{J\,K^{-1}\,kg^{-1}}$, or general empirical model parameter
D	Damage parameter, dimensionless
d	Displacement, mm, or fatigue slope parameter, $\mathrm{cycle\,Pa^{-1}}$
E	Elastic (Young's) modulus, Pa
$E^\star$	Complex or dynamic axial modulus, Pa
E'	Storage axial modulus, Pa
E''	Loss axial modulus, Pa
E_a	Arrhenius activation energy, $\mathrm{J\,mol^{-1}}$ or J/molecule
e	Random error
F	(log-)Normal distribution cumulative density function
$\mathbf{F}$	Fisher matrix
F_a	Failure function, dimensionless
F_m	Hygrothermal matrix property reduction factor, dimensionless
F_r	Failure mode dependent remaining strength, Pa
f	Frequency, Hz, or (log-)Normal distribution probability density function
f_0	Pre-exponential frequency factor, Hz
$G^\star$	Complex or dynamic shear modulus, Pa

G'	Storage shear modulus, Pa
G''	Loss shear modulus, Pa
g_i	Stress dependent material parameters (with $i = 0, 1, 2$)
H	(log-)Normal distribution cumulative hazard function
$H(t)$	Heaviside step function
H_i	Magnitude of the ith structural transition, Pa
h	Specimen thickness, mm, or (log-)Normal distribution hazard function, or function of a statistical model
h_i	Strain dependent material parameters (with $i = 0, 1, 2$)
Im	Imaginary scale
i	Imaginary operator ($\sqrt{-1}$), or iterative index
K	Empirical constant, or heat transfer coefficient, $\mathrm{W\,m^{-2}\,{}^{\circ}C^{-1}}$
K_γ	$100(1+\gamma)/2$th standard normal percentile
k	Arrhenius rate constant, or, spring constant, $\mathrm{N\,mm^{-1}}$, or strength degradation rate exponent, or general empirical parameter
k_i	Weibull shape parameter of the ith structural transition
k_B	Boltzmann constant (1.3806×10^{-23} $\mathrm{J\,K^{-1}}$)
k_D	Fatigue accumulation index, dimensionless
$k_0,\ k_1$	Rate exponent empirical parameters
L	Likelihood
LMP	Larson-Miller parameter, K
M	Absorbed moisture fraction, dimensionless
$\overline{M}_n$	Number average molecular weight, $\mathrm{g\,mol^{-1}}$
$M^\star$	Complex or dynamic modulus (tensile, shear, bulk, viscosity ,etc.)
M'	Storage modulus (tensile, shear, bulk, viscosity ,etc.)
M''	Loss modulus (tensile, shear, bulk, viscosity ,etc.)
MHP	Manson-Haferd parameter, K
m	Fatigue life or strength degradation exponent, dimensionless, or general empirical parameter
m'	Empirical temperature dependent material constant, $\mathrm{s^{-}}^{n}$
N	Fatigue life, cycle
$N_f,\ N_{f_1}$	Fatigue life at frequency f and f_1, cycle
n	General empirical parameter, or actual cycle count, cycle, or summation limit
n_f	Material parameter, dimensionless
n_f^*	Material parameter, dimensionless
n_r	Failure mode dependent material parameter, dimensionless

P	Load, N, or arbitrary material property
P_f	Probability of failure, dimensionless
$P(T)$	Any temperature dependent property
q	Generated heat rate, W
R	Fatigue stress ratio $\sigma_{min}/\sigma_{max}$, dimensionless or, ideal gas constant (8.314 $\mathrm{J\,mol^{-1}K^{-1}}$)
Re	Real scale
r^2	Coefficient of determination, dimensionless
S	Strength, Pa, or creep compliance, $\mathrm{Pa^{-1}}$
S^*	Viscoelastic parameter, $\mathrm{Pa^{-1}}$
S_c	Matrix compliance, $\mathrm{Pa^{-1}}$
S_{eq}	Equivalent initial static strength, Pa
$\mathbf{S}_{ij}$	Reduced compliance matrix, $\mathrm{Pa^{-1}}$
$\bar{\mathbf{S}}_{ij}$	Reduced transformed compliance matrix, $\mathrm{Pa^{-1}}$
$\mathbf{S}_{ij}(\tau)$	Time-dependent strength field, Pa
S_m	Empirical temperature dependent material constant, Pa
S_r	Residual strength, Pa
S_u	Ultimate static strength, Pa
S_u^*	Lower static strength asymptote, Pa
S_{ut}	Ultimate tensile static strength, Pa
$S_{xx},\ S_{yy},\ S_{xy}$	Sum of squares
S_ϵ	Empirical temperature dependent material constant, Pa
s	Stress, Pa, or Laplace variable, or standard deviation of lognormal distribution
s'	Pooled estimate of the log-standard deviation based on the lack of fit
SDP	Sherby-Dorn Parameter, dimensionless
T	Temperature, ℃ or K
T_a	Manson-Haferd temperature intercept, K
T_{cure}	Cure temperature, ℃ or K
T_e	Exposure temperature, ℃ or K
T_f	Fictive temperature, ℃ or K
T_g	Glass transition temperature, ℃ or K
$T_{g,end}$	Glass transition temperature based on the storage modulus rubbery plateau, ℃ or K
$T_{g,loss}$	Glass transition temperature based on the loss modulus peaks, ℃ or K
$T_{g,onset}$	Glass transition temperature based on the onset of the storage modulus drop, ℃ or K
$T_{g,peak}$	Glass transition temperature based on the peak of loss factor, ℃ or K
$T_{g,s}$	Static glass transition temperature, ℃ or K
T_{gw}	Wet glass transition temperature, ℃ or K

$T_{g,\infty}$	Maximum glass transition temperature, ℃ or K
T_m	Melting or fusion temperature, ℃ or K
T_n	Normalized temperature, dimensionless
T_r	Room (ambient) temperature, ℃ or K, or temperature fitting parameter, ℃ or K
T_{ref}	Reference transition temperature, ℃ or K
T_s	Midplane transient temperature, ℃ or K
T_{se}	Midplane equilibrium temperature, ℃ or K
$T_{s=0}$	Stress free temperature
$T_{\alpha,\beta,\gamma \text{ or } \delta}$	Structural transition temperatures ($T_\alpha = T_g$, temperature is lower with ascending Greek alphabetical order), ℃ or K
t	Time, s
t'	Reduced time to failure
t_a	Manson-Haferd time intercept, h
t_c	Time at censoring, s or h
t_{cl}	Time at left censoring, s or h
t_{cr}	Time at right censoring, s or h
t_e	Exposure time, s
t_f	Failure time, s or h
$\tan\delta$	Loss factor, dimensionless
V	Volume, m^3
$\mathbf{V}$	Asymptotic covariance matrix
v_f	Fibre volume fraction, dimensionless or %
W	Specimen width, mm
$\overline{X}$	Average value of X (any statistical variable), units of X, or upper bound on the value of X (any statistical variable), units of X, or Laplace transform of X
$\underline{X}$	Lower bound on the value of X (any statistical variable), units of X
$\hat{X}$	Estimator of X (any statistical variable), units of X
$\dot{X}$	Rate of change of X (any variable), units of $X\,\text{s}^{-1}$
z_p	Standard normal percentile
α	Weibull shape parameter, or general empirical parameter, or aerodynamic angle of attack, ° linear coefficient of thermal expansion, $℃^{-1}$, or distribution percentile
α'	Student t-distribution percentile
β	Stretched exponential exponent, or Weibull characteristic value, or surface to volume ratio, or general empirical parameter, or coefficient of hygral expansion, $\%M^{-1}$

γ	Shear strain, dimensionless, or Zhurkov constant, m^3, or power law fatigue parameters, or Gompertz distribution scale parameter, dimensionless
ΔH	Enthalpy, J
ΔH_f	Enthalpy of fusion, J
ΔT_f, ΔT_{f_1}	Temperature differential at frequency f and f_1, ℃ or K
$\Delta\sigma$	Mechanical stress increment, Pa, or stress range, Pa
δ	Phase lag (also known as loss angle), radian
δ_X	Deviation from reference X (any variable), units of x
ϵ	Strain, dimensionless
ϵ_c	Composite (or fibre) static failure strain, dimensionless
ϵ_m	Matrix static failure strain, dimensionless
ϵ_{max}	Maximum strain at first cycle, dimensionless
ϵ_u	Ultimate failure strain, dimensionless
ϵ'_0	Empirical temperature dependent material constant, dimensionless
ζ	Characteristic time, or damping function
η	Model parameter, dimensionless, or Gompertz distribution shape parameter
η_p	Normal percentile rank, dimensionless
Θ	Arbitrary transition temperature, ℃ or K
θ	Blade pitch angle, °, or fibre angle, °, or general statistical distribution parameter
λ	Effective time, s
μ	Coefficient of viscosity, Pa s, or Normal distribution mean
$\mu^\star$	Complex or dynamic coefficient of viscosity, Pa s
μ'	Storage coefficient of viscosity, Pa s
μ''	Loss coefficient of viscosity, Pa s
μ_e	Ageing shift factor rate
ν	Poisson's ratio, dimensionless, or statistical degree of freedom
ρ	Mass density, dimensionless
σ	Mechanical stress, Pa, or (log-)standard deviation of (log)Normal distribution
σ_a	Cyclic stress amplitude, Pa
σ_f	Failure stress, Pa
$\boldsymbol{\sigma}_{ij}(\tau)$	Time-dependent stress field, Pa
σ_m	Mean cyclic stress, Pa
σ_X	Standard deviation of X (any variable)

$\sigma_0(t'_0, T_0)$	Weibull scale parameter of S_u at the reference t' and T, Pa
τ	Shear stress, Pa, or relative time
$\hat{\tau}$	Characteristic action time
Φ	Flow angle, °or standard Normal distribution cumulative density function
ϕ	Relaxation function of any property, or fibre angle, °, or standard Normal distribution probability density function
χ	Critical stress ratio, dimensionless
Ψ	Shifted stress/strain dependent time scales
ψ	Stress ratio function, dimensionless
ω	Angular frequency $2\pi f$, s^{-1}
£	Log-likelihood

Superscripts

$T{+}H$	Temperature and humidity
$+$	Tensile
$-$	Compressive

Subscripts

f	Fibre property
i	Ordinal position i (with i any integer), or orthogonal principal directions i =1, 2, 3, or general orthogonal directions for i =x, y, z
L	Longitudinal/fiberwise direction
m	Matrix property
max	Maximum value (absolute or cyclic)
min	Minimum value (absolute or cyclic)
model	From model
ref	Reference value
reg	From regression
T	Transverse direction
0	Nominal (reference) condition

SI units

Base units

A	ampere, electric current
g	gram, mass
K	kelvin, thermodynamic temperature
m	meter, length
mol	mole, quantity of matter
s	second, time

Derived units

J	joule, energy, $\mathrm{N\,m}$
Hz	hertz, frequency, s^{-1}
h	hour, time, 60 min
min	minute, time, 60 s
N	newton, force, $\mathrm{kg\,m\,s}^{-2}$
Pa	pascal, pressure, $\mathrm{N\,m}^{-2}$
TEX	linear mass density of textile thread, $\mathrm{g\,km}^{-1}$
V	volt, electric potential, $\mathrm{kg\,m}^2\,\mathrm{A}^{-1},\mathrm{s}^{-3}$
W	watt, power, $\mathrm{J\,s}^{-1}$
Ω	ohm, electrical resistance, $\mathrm{kg\,m}^2\,\mathrm{A}^{-2},\mathrm{s}^{-3}$

Other units

°	degree
℃	celsius degree, temperature

Unit prefixes

μ	micro, $\times 10^{-6}$
m	mili, $\times 10^{-3}$
k	kilo, $\times 10^{3}$
M	mega, $\times 10^{6}$
G	giga, $\times 10^{9}$

INTRODUCTION

An increasingly dominant preoccupation of western societies in the late 20th and early 21st centuries is the sustainability of the modern way of life and its effect on Earth's ecosystems. In particular, the upcoming scarcity and associated price rise of fossil fuels (see e.g. (1)) and the raising concerns over the potential impacts of climate changes from anthropic causes (2; 3) has led to an increased interest in renewable energies. As a result, the wind energy sector is enjoying a rapid and sustained growth in the Americas, Asia and Europe (4; 5; 6; 7).

Many factors are important for the success of wind energy projects. Among them, one of the most determinant parameters is the cost of energy (COE). This parameter sets the price for producing a given amount of electric energy from a specific method and its main drivers are:

- The initial cost of the energy plant and of its financing.
- The operation and maintenance costs of the plant.
- The total energy output over the period for which costs are accounted for.

As wind energy production requires no fuel, turbine costs is one of the main factors influencing COE. The cost of a turbine — and that of its installation and maintenance — must therefore be minimized. However, as the energy output of a wind turbine is part of the calculation of COE and as it depends on the prevailing wind conditions at the site, wind turbine siting is also a major factor.

According to the United States Department of Energy (8), the rotor's cost accounts for 20% to 30% of total turbine costs, with the rotor including both the blades and hub. The blades — which are accountable for a large part of the rotor cost — are made at

95% from composite materials, with the remaining 5% being metallic materials at the hub interface. Moreover, as the rotor is matched to the nacelle, which sits atop the tower, its weight has a cascading effect on the structural requirements of the tower and foundations of a turbine. It is therefore evident that minimizing blade weight and cost are key objectives in turbine design.

However, structural requirements are also extensive. First, most turbines are of the horizontal axis type, with an upwind rotor. Because of aerodynamic performance requirements, the turbine blades are based on relatively thin aerofoil cross-sections that provide only minimal section moment of inertia in the main load direction. It follows that in order to minimize the deflection of the blades and avoid the risk of them striking the tower or of excessively altering their aerodynamic performances, relatively stiff materials are required. As discussed before, the weight and cost of the rotor are determinant factors of wind energy economics and thus the material stiffness to weight ratio needs to be maximized.

Wind turbines are also exposed to extremely variable loads that will need to be endured over a lifetime of 20 to 30 years (9). They are part of the man-made structures that need to withstand the most extreme fatigue loading conditions (8; 10). For example, compared to airframe structures which are expected to last 60 000 hours (11) while receiving careful maintenance, a wind turbine blade running only 50% of the time over its 25 years design life would run close to twice as many hours, while receiving only minimal maintenance. This would induce a number of fatigue cycles in the range of 10^8 to 10^9 (12). Accounting for the fact that these operating hours are undergone under loads and environmental conditions that are highly variable and that creep can also become a problem for the larger turbines (9), challenges for designers become evident.

Furthermore, the shape of a wind turbine blade, a wing-like structure with a tapering chord, significant amount of twist and continually changing cross-section is also relatively complex. Considering that a single blade can reach several tens of metres in length (with prototypes exceeding 100 m) and weight in tens to hundreds of metric tons, manufacturability can also become one of the important aspects of the turbine blades costs.

Of course, the ideal solution would involve a low-cost material, with easy manufacturability and high performance-to-weight ratio. It is clear, however, that these are competing requirements and that trade-off will need to be balanced. Up to now, the most common answer to these challenges is that of using thermoset matrix composites, mainly glass fibre reinforced polymers.

0.1 Wind energy in Canada

According to the Canadian Wind Energy Association (CANWEA), the total installed wind energy capacity increased from 137 MW in year 2000 to 11 205 MW as of December 2015, making Canada the seventh-largest wind energy producer in the world. Moreover, between 2011 and 2015, the sustained growth of the wind energy capacity has been 23 %. Thus, with over 1 500 MW installed in 2015, Canada was also the sixth country for added capacity for that same year (5; 6).

Looking at the distribution of wind energy potential over Canada from the wind energy atlas by Environment Canada (13) — which shows the wind energy potential in $\mathrm{W\,m^{-2}}$ of rotor swept surface (Figure 0.1) — or the 'Wind Energy in Canada' map of Canadian Geographics (15), it is clear that a significant part of the best resources are set in the northernmost and remotest part of the country.

However, there are little operational data for wind turbines and wind plants in cold climates such as that of Northern Canada. Combined with the fact that Canada is a

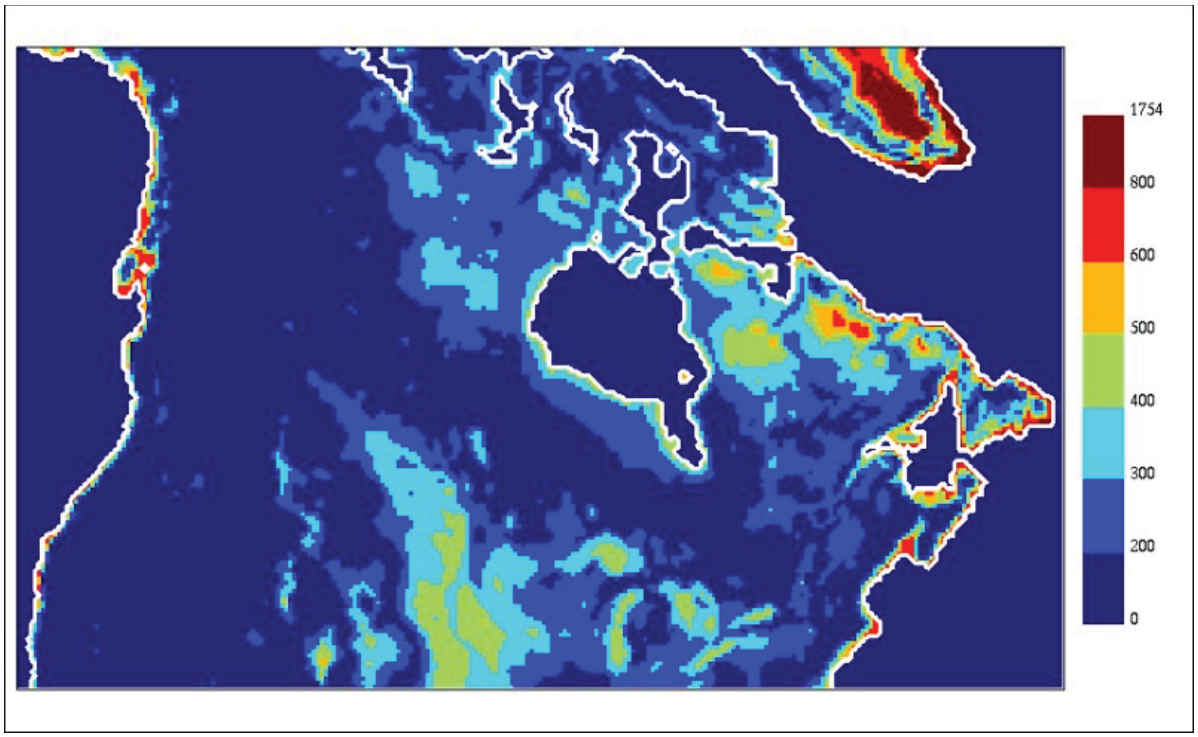

Figure 0.1 Environment Canada Canadian Atlas Level 0 of five years mean wind energy potential per rotor area ($W\,m^{-2}$) at 50 metres above ground. The colour code matches the Battelle-NREL classes, where Class 3 (300–400 $W\,m^{-2}$, turquoise colour) and above is deemed suitable for wind energy generation. Map from reference (13) and Batelle-NREL wind classes description in reference (14)

large country with a low population density, the remoteness of many interesting sites would mean that in case of low turbine availability due to reliability issues, the COE could easily become excessive.

The Wind Energy Strategic Network (WESNet) was founded in order to tackle the technical challenges associated with wind energy production in the distinctive climate and geography of Canada. WESNet was a five years endeavour regrouping 16 Canadian universities collaborating with 15 partners from industry, wind institutes and governments. The research programme was organized in the four following wind energy themes.

Theme 1 Wind resource assessment and forecasting in the Canadian climate and geography.

Theme 2 Wind energy extraction in a Nordic setting, including wind turbine performance assessment and wind turbine design.

Theme 3 Technologies for integration of wind power into the electrical grids.

Theme 4 Simulation and optimization technologies to maximize the economic benefits of wind energy for Canada.

In particular, the project described in this thesis is part of Theme 2.

0.2 The research problem and objective

The climate and geography of Canada are atypical for the wind energy sector. One of the consequences of this situation is an unacceptable level of uncertainties regarding the lifetime estimates of wind turbine components. Despite the very strong wind energy potential of northern Canada, these uncertainties cast doubts on the economic viability of developing wind energy plants in some of the most windy regions of the country. In order to fully realize the wind energy potential of Canada, wind turbine manufacturers and wind energy plant installers need to be provided with information and tools to alleviate those uncertainties.

Thus, in a broad perspective, the objective of the WESNet programme is to reduce the incertitude related to the operation of wind energy plants in Canada's northern climate. The general objective of this thesis is to characterize and model the temperature effects on the mechanical behaviour of representative wind turbine blade materials. Because of the Canadian context, a particular attention is given to the effects of low temperature. Specific objectives of the project detailed in this thesis are:

a. Experimentally assess, on laboratory samples of unidirectional and $[\pm 45]_2 s$ glass–epoxy composite materials representative of wind turbine blades components, the effects of:

   - Temperature on the materials tensile and compressive static strengths and stiffnessess.
   - Temperature and frequency on the materials tensile and fully reversed stress-life fatigue curves.

b. Model the effects of temperature on:

   - The material's strength and stiffness under static loading.
   - The stress–life fatigue curve of unidirectional materials under tensile fatigue loading.
   - The probability of fatigue failures.

c. Model the effects of temperature and frequency on the materials dynamic behaviour and glass transition temperature.

These points have been specifically addressed because:

- Glass fibre-epoxy composite is the most common material for wind turbine blades.
- Effects of low temperatures on the mechanical response of composites are scarcely documented, but important in the Canadian climate.
- Fatigue is the main loading mode of wind turbine blades.
- Synergies may exist between static, dynamic and fatigue loadings.

Note that many other technical, economical or social concerns exist related to wind energy production in the Canadian context. For example, plant accessibility, freeze-thaw cycles effects, plant-grid interconnection, icing conditions prediction and effects, labour availability, lubrication are all sources of uncertainties. However, they are not considered in the present thesis.

0.3 Organization of the thesis

At the end of this chapter, the author's contributions to solving the research problem, as well as the significance of these contributions are discussed. In Chapter 1, a critical review of the literature on the topic of temperature and time dependence of the mechanical response of polymers and composites is provided. As will be seen from the literature review, fundamental knowledge surrounding the effects of temperature and frequency on the fatigue behaviour of composite materials is still quite weak, yet it is known that interactions exist between static, dynamic and fatigue failure modes. Therefore, the project presented in this thesis is quite exploratory in nature. The main problem of characterizing and modelling the effect of temperature on the mechanical response of wind turbine blade materials was thus broken down into more manageable sub-problems. Each of these sub-problem is then resolved by building on the knowledge acquired in previous steps and the thesis will mimic this breakdown. Consequently, the following topics are discussed as individual chapters within the core of the thesis:

Chapter 2 Experimental study of temperature and fatigue load frequency effects on unidirectional glass–epoxy composites under static and fatigue loading.

Chapter 3 Experimental study of low temperature effects on $[\pm 45]_{2s}$ glass–epoxy composites under static and fatigue loads.

Chapter 4 Probabilistic modelling of the stress-life fatigue curve of glass fibre reinforced polymer composites loaded in tension along the fibre direction, including temperature and frequency effects.

Chapter 5 Modelling the transition temperature and time-temperature superposition characteristics of the storage modulus of epoxies and their composites.

Chapter 6 Modelling the loss modulus of polymers and composites.

Chapter 7 Modelling the effect of temperature on the instantaneous static strength of polymer composites.

Chapters 2 and 3 are associated with objective a. from the previous section. Chapters 4, 5 and 7 are the outcome of research objective b., while chapters 5 and 6 relate to objective c.

It may appear that this structure does not evolve from the simplest to the most complex topic or from the most specific to the most most general one. Indeed, these criteria were not the main ones for the thesis organization. However, it will be seen that each section builds on the experimental and modelling outcome of the previous ones and that a natural flow across the various section is maintained with this structure, while minimizing repeated information.

Finally, a discussion regarding the multiple research outcomes, their significance in the broad context of composite materials and energy production is provided.

0.4 Contribution to solving the research problem

Several novel contributions were generated while attempting to solve the research problem. These have been or are planned to result in conference and journal publications as follows. A first publication (conference article, Chapter 2) provides a discussion on the ef-

fects of temperature and frequency on the fatigue durability of unidirectional glass-epoxy composites. The novelty of this work stands from:

a. The production of an original fatigue dataset for a material representative of a wind turbine blade's structural components and covering both low and high temperatures as well as frequency effects.

b. The recognition that fatigue properties appear to be less sensitive to low temperature than static properties.

The second paper (Chapter 3) summarizes, within a journal article, both qualitative and quantitative results for fatigue tests at stress ratios $R = 0.1$ and $R = -1$ and at 23℃ and -40℃ on $[\pm 45^\circ]_{2s}$ glass-epoxy laminates. The main novel results are:

a. A demonstration that, for glass–epoxy composites typical of current wind turbine blade materials, the loss of strength at lower temperature reported for various composites in the previous literature (up to the early 2000's) is not representative anymore.

b. An analysis of the fatigue failure showing that in the high cycle fatigue regime under $R = 0.1$ loading, the performance is generally improved at low temperature.

c. A description of changes in failure mechanisms between -40℃ and 23℃ for both $R = 0.1$ and $R = -1$ fatigue loads.

d. The recognition that a rise in the loss modulus of polymers at low temperatures may increase creep-fatigue interactions. Thus, combining low temperature and low cyclic stresses (i.e. very high cycle counts) may reduce fatigue life of composites compared to that at room temperature.

The third publication (Chapter 4) proposes and validates a methodology for predicting the effects of temperature on tensile fatigue life of glass-epoxy composites loaded in the fibre direction. The main novel contributions are:

a. An empirical model describing the evolution of static strength as a function of temperature based on tests at a minimum of four temperatures.

b. A model for predicting the probabilistic S–N curve of glass fibre reinforced polymers in tension over a wide range of temperature based on static strength prediction as a function of temperature (low experimental burden).

The last journal article (Chapter 5) covers a novel approach, based on dynamic mechanical analysis, to obtain time-temperature (or frequency-temperature) superposition characteristics of epoxies and for evaluating their glass transition temperature. The novelty of this work emanates from:

a. The proposition of a new model to evaluate the glass transition temperature and describe the evolution of the storage modulus as a function of temperature and frequency based on a statistical distribution of secondary bonds breakage in polymers and fibre reinforced polymer matrix composites.

b. The demonstration that, across the glass transition region, the logarithm of the time-temperature shift factor as a function of the logarithm of the frequency is continuous if the effects of strain rates on the glass transition temperature are accounted for (as opposed to the usual Williams-Landel-Ferry equation which predicts discontinuities).

Finally, preliminary results for novel approaches in the modelling the effects of temperature on the loss modulus and strength of polymers and composites are also presented (Chapters 6 and 7).

0.5 Significance of the work

Findings from this research project are significant for the wind energy industry, not only because they provide reliable methods to evaluate temperature effects on the fatigue performance of composites, but also because they do so while minimizing the experimental burden to obtain the required model parameters. The approach proposed here therefore provides a cost-effective way to assess the material behaviour through relatively short and easily performed tests. In doing so, uncertainties relating to the structural durability of wind turbine blade in the Canadian climate are reduced.

Moreover, the approach used in this research broke down the complex and synergistic effects of temperature and time dependence in a way that allowed for the observation of some simple facts that challenge common beliefs with regards to temperature and load rate effects on composites. The main common beliefs that are challenged are:

Low temperature effects on strength and modulus of composites are small: challenged by static results under tension and compression loading for unidirectional and for $\pm 45^\circ$ laminates.

Viscous effects mainly relate to high temperatures: challenged by fatigue results obtained at -40℃ for $\pm 45^\circ$ laminates.

Discontinuous time-temperature superposition at glass transition: challenged by the applicability of the proposed model across a much broader temperature range than is typically possible.

It thus appears that the findings presented here have a reach that exceeds the application to the initial context of wind energy and should be of interest to a much broader commu-

nity of users and researchers involved in the general fields of the mechanics of polymers and polymer matrix composites.

CHAPTER 1

LITERATURE REVIEW

Part of the complexity in analysing the mechanical behaviour of composites comes from the heterogeneity of the media. The response of composites to thermomechanical loads is no exception to that rule.

In this specific domain, the material's heterogeneity plays a role in two main parts. First, due to discrepancies between constituents thermal expansion coefficients, internal stresses develop under temperature differentials. Second, the behaviour of constituent fibres and matrix, as well as at the interphase between these two entities, differs from medium to medium.

The current review of the state of the art will therefore try to conform to this reality by mimicking the multi-scale nature of the composite in the description of the material behaviour. The thermomechanical behaviour of composites will thus be discussed first from the level of the constituent materials, before moving to the description of the global behaviour of composites. The effect of temperature and strain rate on the static and fatigue failure of composites will be discussed. Despite the existence of synergistic effects between temperature and other parameters like solvent absorption, oxidation or radiation effects on the material properties and the failure of fibre reinforced polymers, these will not be covered in the current review.

1.1 The nature of polymeric matrices and their composites

Polymer composites are made using a wide variety of matrices including both thermoset polymers and thermoplastics. Because of the possibilities for increased production rates and refusing of the polymer matrices for assembly, non-structural applications often make use of thermoplastic resins reinforced with short fibres. However, most structural

applications use thermosetting resins — often simply called thermosets — for their greater stiffness and stability once cured.

During manufacturing of composite parts, thermoset polymers go from a fluid state where the resin is forced through the network of reinforcing fibres using pressure (mechanical, atmospheric, autoclave,...) and capillarity. The resin is then cured through heating (self-heating due to exothermic chemical reactions or external heat source) and the initially fluid material irreversibly polymerized to an amorphous state. Cured thermoset resins are highly reticulated (cross-linked). This characteristic cross-linking of polymer branches hinders chain reorganizations and prevents the formation of a crystalline structure, but provides good strength and stiffness performances as well as good thermal and chemical stability.

As opposed to thermoset, thermoplastic resins undergo a reversible hardening process and solidify mostly due to weak interaction forces and entanglement rather than through reticulation. Because of the greater freedom of movement allowed by the absence of cross-links in thermoplastic polymers, some thermoplastics exhibit a tendency to partially crystallize upon solidification. Manufacturing of composites using thermoplastics can either be done through in-situ polymerization (see e.g. Joncas (16)), or by diffusion of melted resin through the reinforcements. Because of the relatively high viscosity of thermoplastic melts, they are used essentially in conjunction with short fibres.

Considering that most structural composites use amorphous matrices and that this class of materials behaves differently to most conventional (crystalline) engineering materials, it is useful to consider their peculiarities.

1.2 The formation, structure and properties of amorphous solids

From a practical standpoint, solids are usually considered to be stable entities. This implies the assumption that their properties remain unchanged over extended periods of times, with the term 'extended' being put in relation to the timescale that is significant for

humans. For crystalline solids such as metals, the stability assumption is quite satisfying from an engineering point of view since unless a significant amount of energy is provided, the structure of crystalline solids is indeed stable. This is due to the fact that the solid phase of crystalline materials is in thermodynamic equilibrium.

Amorphous solids, of which polymers are an important subset, behave differently. But first, what is an amorphous material to start with? It is a material that has hardened from its liquid phase without undergoing a true phase change to the solid state. Upon polymerization in the case of thermosetting resins (or on cooling down through the fusion temperature T_m for semicristalline thermoplastics) the liquid phase experiences a rapid reduction of molecular mobility. On the timescale of the cooling, or polymerization in the case of thermosets, molecular rearrangement is eventually very restrained. The liquid phase becomes trapped in its configuration and starts hardening. This phenomenon is called the glass transition — even though it is not an actual phase transition in the thermodynamic sense.

The result is a structure that is more or less disordered and that lacks the structural periodicity encountered in crystalline solids. Amorphous solids, although they appear stable on a first approximation, show complex time-dependent behaviour. Furthermore, their mechanical response shows a sensitivity to the history and rate of solicitation, of temperature, of pressure and of external work to which they are submitted (e.g. Struik (17) or Chow (18)). However, given a relatively short time scale, these structures may still be seen as stable, or rather 'metastable'.

The fundamental reasons for this so-called metastability are yet to be fully understood (19). Still, the landmark review paper by Kauzmann (20) still provides many good insight on the physical process underlying the glass transition.

It is strongly believed that the root causes for the reduced stability of glasses lies in the fact that their passage from the liquid phase to the solid state is not an actual phase change. As stated earlier, amorphous materials — also often called glasses —

rather undergo a process of supercooling (cooling below the normal freezing point) and vitrification where the material passes from a liquid state at melt, to a supercooled liquid form and finally settle in a glassy, solid like state.

For thermoplastics above the melt temperature T_m or in uncured thermosets, the constituent molecules have high mobility (or self-diffusivity) and the material has a purely viscous behaviour. The higher the temperature is, the weaker the intermolecular interaction forces are and the lower the viscosity is. As this state is of little relevance for structural applications of polymers, the physics behind the behaviour of liquids won't be the subject of further discussion here.

In a conventional solidification phase change, free energy (the energy available to perform work in the material system) is expended in the formation and growth of crystals, resulting in a discontinuity in the energy content of the solid phase and the liquid phase at a given temperature (enthalpy of fusion). For crystallization to occur, two energy barriers need to be overcome. First, the energy barrier related to nucleation of crystals and second, that of crystal growth.

In the case of amorphous solids, Kauzmann suggests that either or both of these energy barriers must be too high for the material. It thus has no choice but to settle in a low energy state that exhibit some short-range order at the atomic level, but lacks the long-range order and periodicity of crystals.

In other words, on passing under T_m, crystalline materials undergo an instantaneous phase change. As this phase change occurs, the material's enthalpy (and volume) shows a discontinuity on passing from a state of high enthalpy liquid to an equilibrium crystalline state with lower enthalpy (and volume). On the other hand, amorphous materials will cross over their melting temperature without the formation of crystals. They rather go into a supercooled liquid form where viscosity and rigidity increase — i.e. they turn into a viscoelastic material with a dominant viscous behaviour. Upon further cooling, the supercooled liquid moves into a glassy, solid like state where the elastic behaviour is

most significant. This is the process commonly called the glass transition or vitrification. It is interesting to note that as vitrification, as opposed to crystallization, is not an equilibrium process and there is no cohabitation of phases with different energy states (solid-liquid or the triple-point) and the process is not accompanied by energy release (e.g. fusion latent heat) (20). In this glassy state, the material will share, on different time scales, properties of solids — that is elasticity and relatively high stiffness — and of fluids — a tendency to flow and permanently dissipate mechanical energy.

1.2.1 Vitrification and the glass transition

On the one hand, the solidification and the melting processes of crystalline materials are well defined thermodynamic processes that are mutually opposite. On the other hand, the process of vitrification, that is of forming a solid like structure from a fluid upon cooling, and the fluidification process occurring upon heating are not thermodynamically reversible (see e.g. Kauzmann (20), Chow (18) or Stillinger (19)). Correspondingly, there is no discontinuity in the enthalpy curve of glasses as a function of temperature. Yet, it is observed that there are abrupt changes in other properties such as the coefficient of thermal expansion (CTE), the specific heat (c) and the elastic moduli (E).

Kauzmann suggests that in the glassy state, matter conserves the structure, energy and volume of the liquid, but changes in energy and volume become more akin to those of crystals. He suggests that this is the result of the restriction imposed on some molecular degrees of freedom of the liquid, impeding on their contribution to some material properties.

Two mechanisms are considered for the restriction of molecular movements in glasses leading to changes in measured properties. A first possibility is that the changes in measured properties are due to thermodynamic equilibrium considerations, resulting in permanent restrictions on the degrees of freedom. The second possibility is that restriction occurs because of relaxation mechanisms and that kinetic theories of molecular

motions represent the behaviour rather than thermodynamics. Under the latter hypothesis, it is believed that given enough time for changes in molecular configurations to occur, properties might not be found to differ. Experimental evidence suggests that the relaxation effect is dominant (20).

It is also interesting to note that Kauzmann identified an apparent paradox in the thermodynamics of the glass transition. This paradox lies in the fact that extrapolating the rapid decrease in entropy in glasses at the glass transition, the entropy becomes negative at temperatures well above the absolute zero. Since the entropy of a liquid cannot be lower than that of a glass of the same enthalpy, this paradox suggested that an 'ideal' thermodynamic glass-transition might actually exist. However, neither the absence nor the existence of such a second-order thermodynamic transition — transition where the first derivative of the thermodynamic free energy or one of its proxies with regards to another thermodynamic quantity (e.g. density vs pressure) is continuous but the second derivative is discontinuous — have been definitively demonstrated (21; 22; 19).

Yet, in their landmark paper, Gibbs and DiMarzio (23) have presented a quasi-lattice model (statistical mechanics framework) based on chain stiffness that predict a second-order transition. It is proposed that the temperature at which this transition occurs can be assimilated to the lower bound of T_g. Their formulation has been used successfully to predict qualitatively the influence of molecular weight on T_g, the volume-temperature and volume-molecular weight relationships as well as several other behaviours. Most significantly, it resolves Kauzmann's paradox by showing that there is a discontinuity in the configurational entropy–temperature relationship.

Other empirical or phenomenological relationships have been proposed to describe the evolution of material properties with time and temperature. In the framework of kinetic theories, the Arrhenius relationship (equation 1.1) is one of the most (perhaps even THE most) used formulation. It was thus natural that attempts to represent the glass transition with this equation were made. However, although it appears that it offers a

reasonable approximation of the evolution of properties such as stiffness, compliance or viscosity with temperature below the glass transition ($T_g/T < 0.75$) and terminal flow region ($T_g/T > 1.3$), the relationship appears to break down at higher temperatures (24).

$$k = A \exp \frac{-E_a}{RT} \tag{1.1}$$

In equation 1.1 k is the rate constant, A is the (empirical) pre-exponential factor, E_a is the activation energy, R is the ideal gas constant (8.314 J/mol K) and T is the absolute temperature. Note that the Boltzmann constant $k_B = 1.380648 \times 10^{-23}$ J/K is sometimes used instead of R, yielding E_a in the units of J/molecule instead of J/mol.

Originally formulated by Fulcher (25) for describing the effect of temperature on the viscosity μ of silicate glasses, the Vogel-Fulcher-Tammann (VFT) equation (1.2) is now used to describe the effect of temperature on other physical properties of amorphous materials such as the characteristic times for viscoelastic models.

$$P = P_0 \exp\left(\frac{A}{T - T_0}\right) \tag{1.2}$$

In equation 1.2, P is an arbitrary material property, A is an empirical model parameter, T is the temperature and the $_0$ subscript denotes the reference condition.

An alternative framework for explaining the glass transition is that of the free volume. It is easily imagined that molecular chains in a polymer, even though they are mingled, are not in direct contact with each because of the electronic forces at play. Therefore, the polymer chains have some room around them that can accommodate some amount of movement. Since the volume of a solid or liquid increases and its density decreases as the temperature rises, it can be assumed that there is more 'free room' inside the material at high temperature than there is at low temperature. Therefore, according to this theory, movement of molecular chains are gradually hindered as the temperature decreases. The glass transition thus occurs when the space around polymer chains becomes too

constrained to allow for movement of parts of the polymer chain — a movement called segmental motions.

The free volume theory has been the basis of multiple interpretation of the behaviour of polymers. However, despite its apparent simplicity, it is not always used coherently. For example, White and Lipson (26) interestingly reminds us that atoms and molecules are not static, they constantly vibrate. Thus, free volume should not be seen as a static setting. This further implies that some of the free volume might actually be occupied by those vibrating motions and only a fraction of the actual free volume might be left for segmental motions. A valuable review of the different interpretations of the free-volume theory in the most influential early literature on the glass formation is also discussed in (26).

It can be anticipated that the free volume in a polymer would be a function of many internal factors such as molecular weight, cross-link density, chain configuration, pressure, etc. Indeed, it appears that such factors influence the glass transition temperature. The molecular weight dependence of T_g was demonstrated by Fox and Flory (27), given by:

$$T_g = T_{g,\infty} - \frac{K}{\overline{M}_n}, \tag{1.3}$$

where $T_{g,\infty}$ is the maximum glass transition, K is an empirical factor representative of free-volume and $\overline{M}_n$ is the number average molecular weight. The explanation advanced for this behaviour is that chain ends have more free volume around them as they are tied to other chains by weak interactions. Thus, the lower the molecular weight, the more free ends which in turns provide more 'free volume', thus lowering T_g.

The cooling rate dependency of T_g is briefly discussed by Debenedetti and Stillinger (21). Basically, looking from the solidifying liquid viewpoint, the slower the rate of cooling, the more time the molecules have to reorganize in a way that the systems remains a liquid. However, upon fast cooling, the molecular structures becomes trapped in a configuration that cannot be changed to adapt to the temperature change and solidification occurs.

The result is that the higher the cooling rate is, the higher T_g remains. That is to say that the temperature and rate of temperature change history of an amorphous material will influence its physical properties as the molecular organization will change. However, in the case of T_g, the change remains of the order of a few degrees. The cooling rate effects on the solidification of polymers has implications in the manufacturing of composites as it will influence not only the mechanical properties of the final part, but also its geometric stability and residual stresses. Such considerations are discussed in White and Hahn (28).

The effects of cross-link density on the mechanical properties of polymers is discussed by Nielsen in (29) and his book on the mechanical properties of polymers (30). Relationships (empirical or based on the kinetic theory) for T_g, the shear modulus G or volumetric properties as a function of the polymer chain structures are proposed. However, most of these only relate to lightly cross-linked materials in the rubbery state. Although relatively old, these references still provide a good insight on the general behaviour of polymers.

Considering the effects of molecular weight, cross-link density and cooling-rate on the glass transition, one is forced to realize that the curing conditions of a polymer will influence its final properties. The relationships between cure conditions and polymer properties of thermoset polymers are discussed by Enns and Gillham (31). They proposed a time-temperature-transition cure diagram which allows to anticipate the polymer state based on its cure schedule.

As the glass transition is the result of the timescale of molecular motions becoming longer, it is intuitive to think that the rate of loading (or the frequency f of an oscillating load) will influence T_g. Results from Barral et al. (32), Li, Lee-Sullivan and Thring (33) and Goertzen and Kessler (34) have shown that in the case of epoxies and carbon–epoxy composites, an Arrhenius relationship provides a very good description of the frequency dependence of T_g measured by dynamic mechanical analysis (DMA) over the practical

range of $0.1 \leq f \leq 100$ Hz. This relationship is given by:

$$f_{\mathrm{M},\, T_g} = f_0 \exp\left(\frac{-E_a}{RT_g}\right), \tag{1.4}$$

where the glass transition activation energy E_a and the pre-exponential frequency f_0 for the rate constant $f_{\mathrm{M},\, T_g}$ are obtained from a linear regression of $\ln f$ over $1/T_g$. It is interesting to note that this Arrhenius relationship fits much better on the T_g obtained from the peak of the loss modulus (E'') than with that obtained at the onset of the storage modulus (E') drop.

Based on the observation that in equation 1.4 f_0 often reaches very high values that do not make sense physically, Bai and Jin (35) suggested that a VTF type relationship might provide a better fit of T_g over broad frequency ranges. The VTF formulation of $T_g(f)$ is given by:

$$f = f_0 \exp\left(\frac{-E_a}{R(T_g - T_{g,s})}\right), \tag{1.5}$$

where $T_{g,s}$ is called the static glass transition temperature, which is the temperature where the thermally activated processes become impossible. This formulation thus implies that there would be a temperature above $T = 0$ K where the molecular mobility would be completely restrained. This brings the advantage that the VTF approach provides a pre-exponential frequency f_0 that is more physically plausible than that obtained from the Arrhenius relationship of equation 1.4. It also appears that the difference between the Arrhenius and VTF estimates becomes more pronounced at higher heating rates in DMA experiments.

All this can be summarized by Figure 1.1, which illustrates the different possible states of the matter in a volume (or enthalpy) versus temperature plot (see e.g. Hertzberg (36) or White and Lipson (26)). In Figure 1.1, starting with a melt at high temperature (right of point I), if the temperature goes down, there is a corresponding decrease in volume and enthalpy. This change of volume is a result of the lowering enthalpy, which translates to reduced amplitude of the vibrations of atoms. If the material is prone to crystallization,

there is a sudden change of state (I-II) where the molecules reorganize into a structured crystal and this change is accompanied by heat release, the fusion enthalpy ΔH_f. This is a first order thermodynamic transition, meaning that there is a discontinuity in volume and enthalpy between the former and latter states of the matter. Cooling the material further, the volume and enthalpy keep reducing, although at a somewhat slower rate.

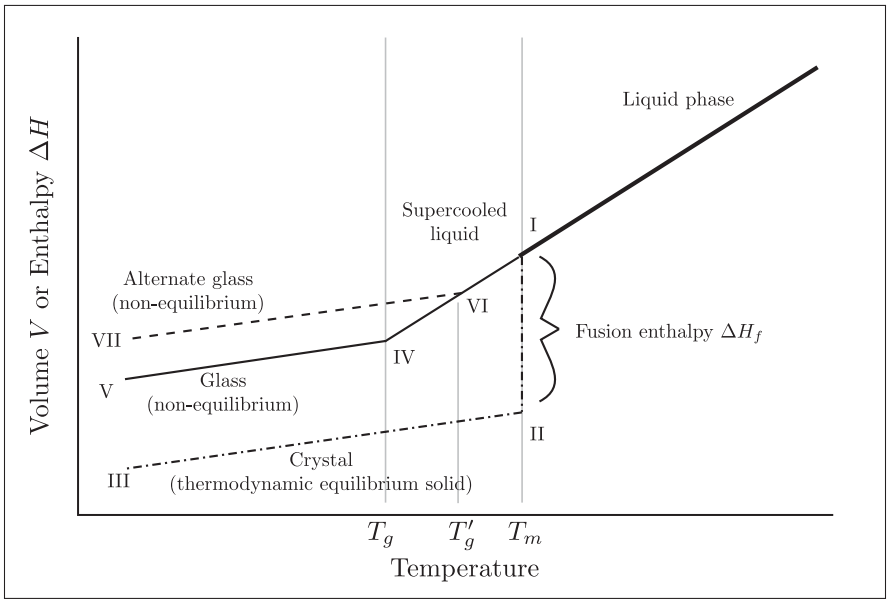

Figure 1.1 Volume–temperature plot of the state of matter

However, for amorphous (and for the amorphous portion of semi-crystalline materials), this phase change is not possible. The material thus goes through point I and keeps gradually losing volume and enthalpy while cooling and goes to the state of supercooled liquid (I to IV). However, at point IV the molecular mobility is reduced to a point where the reorganization of molecules to maintain thermodynamic equilibrium is no more possible. At this point, the glass transition temperature is reached. From this point (IV), as the temperature keeps decreasing, the material will still lose volume and enthalpy, but at a rate lower than before (similar to that of the crystalline solid). It is interesting to note that the volume of a glass is higher than that of the crystalline solid of similar constitution because the crystal is the densest possible state of solids. This difference

between crystalline and amorphous volume is an indication of the material relative free volume.

As noted before, the glass transition is a likely kinetic phenomenon and is a factor of the cooling rate. The effect of a higher cooling rate would be to limit the time for molecular rearrangement to occur, thus resulting in a higher T_g (depicted by point VI). In section VI-VII of Figure 1.1, the material cooled at a higher rate has formed a glass, but one of higher volume and enthalpy than that formed at a slower cooling rate (i.e. section IV – V).

Note that in the previous discussion, T_g is given as the intersection of the glass line with the liquid equilibrium line, as measured in a cooling experiment. Recalling that the glass transition is not a thermodynamically reversible process, there exist another reference temperature, called the fictive temperature T_f, which is obtained from a heating experiment starting in the glassy state into the rubbery state (37). In practice, T_g and T_f are not very different, thus the distinction between T_g and T_f is mainly a concern for physicists rather than for engineers.

1.2.2 Low temperature transitions

Despite the fact that the glass transition has been the subject of a great deal of interest and research efforts over the years, the physics behind the phenomenon remains somewhat controversial. However, it appears that the glass transition is not the only transition that is observable in polymers and that a few more occur at even lower temperatures.

Because of the practical importance of the glass transition from an engineering standpoint and since lower temperature transitions are generally less pronounced than the former, low temperature transitions have been the subject of much less research. Early work by Takayanagi (38) suggests molecular mechanisms that cause the various transitions. Note that there is no standardized nomenclature for the material transitions in the literature. The method used herein will identify the transitions by the α, β, γ and δ prefixes, with

the glass transition being α and each lower temperature transition named in increasing Greek alphabetical order. According to Takayanagi, and as is generally accepted, the passage from melt to rubber corresponds to the formation of crystals in semi-crystalline materials and entanglements in amorphous materials.

Upon cooling though the α-transition (glass transition), large scale molecular motions of the amorphous portion of the material that resulted in a reorganization of the local structure of the material without long-range effects become frozen. These motions are sometimes referred to as micro-Brownian motions and can occur (above T_g) in the main chains of the polymer as well as in long side chains.

If the temperature continues to decrease, segments of the main chains and long side chains that were able to rotate (crankshaft motion), stretch or rock, between different equilibrium positions also become fixed at the β-transition temperature T_β. In some materials such as polycarbonate, this transition may also be associated with changes in the three-dimensional configuration of a molecule (stereoisomerism).

At still lower temperatures, conformational changes of small segments of side chains or side groups (rotation, stretching, rocking) are also limited, resulting in the γ and δ-transitions. These would each correspond to different side groups or chain ends.

At each transition temperature (T_α, T_β, T_γ and T_δ), the reduction in molecular mobility as temperature drops translates to an increase in storage modulus and a peak in structural damping and loss modulus. Takayanagi also demonstrated that the simpler the molecular chain was (e.g. non-branched linear polymers with small side groups), the sharper and the stronger the damping peaks are. The existence of large side groups and side chains hinders many modes of self-diffusion of the molecule and results in a broadened range of interactions with the neighbouring molecules. The damping peak is thus broadened as the chain gets a more complex structure. An idealized representation of a DMA trace over a wide temperature range is illustrated in Figure 1.2. Note that transitions are not always as well defined and sometimes overlap significantly.

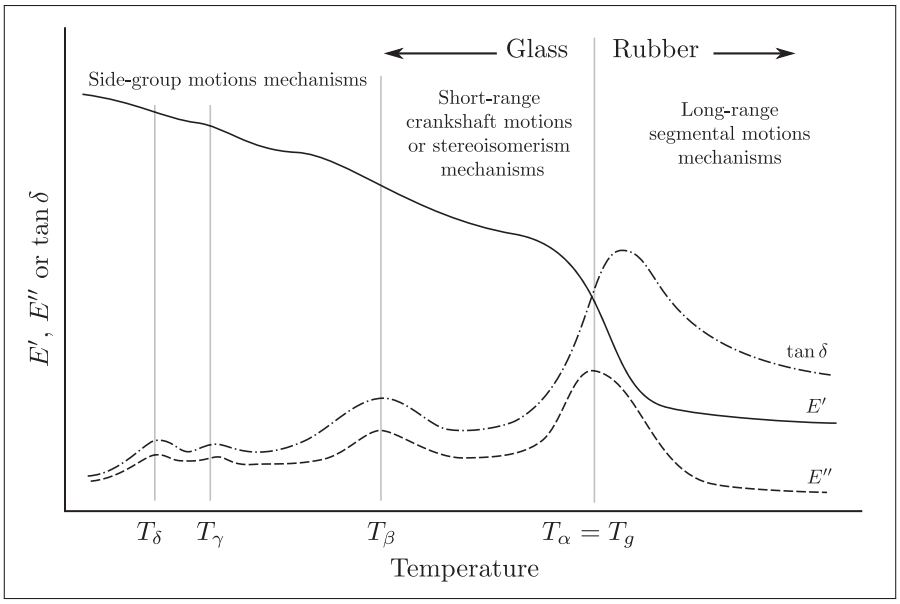

Figure 1.2 Typical DMA trace for a polymer

Cross-linking is expected to modify the behaviour of thermosets compared to that of thermoplastics. The effect of low temperatures and water absorption in virgin PEEK (a semi-crystalline thermoplastic) and three epoxies as well as in glass or carbon reinforced composites made with the same resins have been studied by Adams and Singh (39). Their results showed that epoxies and their composites have a $T_\beta \approx -40$℃ at the specimen resonant frequency ($20\ Hz < f < 30\ Hz$). This β-transition of epoxy based composites may thus be relevant to the context of the current study since it implies increased viscous effects at low temperatures, a phenomenon that may in turn impact the fatigue behaviour of the material. Another fact demonstrated by Adams and Singh is that low-temperature transitions may be useful for understanding the glass transition by allowing to make effects that would be transient at higher temperatures (e.g. moisture uptake) more stable.

1.2.3 Time dependent mechanical response of amorphous solids

As discussed before, temperature influences the molecular mobility within amorphous materials and thus, their response to external loads. This molecular mobility implies

that if a load is applied (i.e. there is an energy input) for a period of time, some of the molecules may become mobile enough to move in search of a lower energy state. Effectively, this translates into a viscoelastic behaviour. As a general rule, if loads are applied rapidly or over short periods of time, the molecules are not able to reorganize and the stiffness remains high (compliance is low). Conversely, for slow loading or long periods under load, molecules may have time to reorganize and stiffness may be reduced (compliance is high). An interesting introductory text to viscoelasticity is provided in the first chapter of Vincent's book (40) while a more detailed treatment is available in Gutierrez-Lemini (41).

In an ideal elastic (Hookean) solid, the energy required to deform the material under load is entirely stored as elastic energy. On the other end of the spectrum, a viscous fluid (Newtonian) can only dissipate the energy input of a non-hydrostatic stress state through shear flow. In a viscoelastic material, both processes are possible. A practical consequence of viscoelasticity is that after removal of an external stress, a viscoelastic body maintains some strains over a period of time after the load is removed, while an elastic body would "instantaneously" recover its stress-free state. Put otherwise, the mechanical response of viscoelastic material is delayed and dependent on the load history.

According to Gibson (42), there are four main manifestations of visocelasticity that are commonly encountered in engineering. Those are:

Creep: an increase in strain with time under a constant load (and the reverse operation of recovery where strain is retained after load removal).

Relaxation: a reduction in stress with time under a constant strain.

Strain-rate ($\dot{\epsilon}$) dependence of the stress-strain (σ–ϵ) curve: where the stiffness of a material increases (compliance decrease) with the loading rate.

Hysterisis: the irreversibility of the σ–ϵ path in a cyclic stress.

The classical approach for modelling linear viscoelasticity is the Boltzmann Superposition Integral (BSI). This method is based on the Boltzmann Superposition Principle (BSP), which states that for all linear systems, the response of the system at a given time (and place) and under the effect of a group of stimuli is the same as the sum of the effect of each stimulus considered by itself. Mathematically, this would translate to:

$$\sigma(a\epsilon_1 + b\epsilon_2) = a\sigma(\epsilon_1) + b\sigma(\epsilon_2), \tag{1.6}$$

where a and b would just be scaling constants accounting for the stress–strain relationship (stiffness).

If we consider that at a constant temperature, the net response at a time t of a material — which is non-ageing (i.e. time alone does not change the material properties) — that is subjected to a load at instant t_{ref} which precedes t is a function of the intensity of the load and of the elapsed time $t - t_{\text{ref}}$ only, we may pose:

$$\epsilon(t) = \Delta\sigma S(t - t_{\text{ref}}), \tag{1.7}$$

where $\epsilon(t)$ is the strain at time t and $S(t)$ is the material's time-dependent creep compliance. Gibson suggests that $S(t)$ can often be approximated by a power law such as:

$$S(t) = S_0 + S_1 t^x, \tag{1.8}$$

with S_0 the initial elastic compliance while S_1 and x are empirical constants.

The BSP stipulates that the strain response to a series of stress increments $\Delta\sigma$ at different times would be proportional to the sum of the individual strain amplitudes. Thus, given n stress increments, we get:

$$\epsilon(t) \approx \sum_{i=1}^{n} \Delta\epsilon_i(t) = \sum_{i=1}^{n} \Delta\sigma_i S(t - t_{\text{ref},\,i}),\ t > t_{\text{ref},\,i}, \tag{1.9}$$

which can, by passing to the limit as $n \to \infty$, be generalized to the BSI for arbitrarily complex time histories.

$$\epsilon(t) = \int_{-\infty}^{t} S(t-\zeta)\frac{\mathrm{d}\sigma(\zeta)}{\mathrm{d}\zeta}\mathrm{d}\zeta. \tag{1.10}$$

In equation 1.10, ζ is the characteristic time, which is the continuous spectrum of times $t_{\mathrm{ref},i}$ and $\sigma(\zeta)$ is the stress function . An analogous form of equation 1.10 can also be found to evaluate stresses as a function of strains. It thus becomes:

$$\sigma(t) = \int_{-\infty}^{t} C(t-\zeta)\frac{\mathrm{d}\epsilon(\zeta)}{\mathrm{d}\zeta}\mathrm{d}\zeta. \tag{1.11}$$

where $C(t)$ is the time-dependent relaxation modulus. Note that in equations 1.10 and 1.11, $S(t<0) = 0$ and $C(t<0) = 0$. Recalling the power law of equation 1.8, taking the constant term out of the integral, equation 1.10 and 1.11 can be rewritten as:

$$\epsilon(t) = S_0\sigma_0(t) + \int_{0^+}^{t} S(t-\zeta)\frac{\mathrm{d}\sigma(\zeta)}{\mathrm{d}\zeta}\mathrm{d}\zeta, \tag{1.12}$$

$$\sigma(t) = C_0\epsilon_0(t) + \int_{0^+}^{t} C(t-\zeta)\frac{\mathrm{d}\epsilon(\zeta)}{\mathrm{d}\zeta}\mathrm{d}\zeta, \tag{1.13}$$

where time 0^+ is the time just after the first loading step and the first term (outside the integral) represents the elastic part of the response.

The BSI formulation, although quite useful, does not lend intuitively interpretable results. However, if one looks at the problem of viscoelasticity from a mechanistic perspective, it is possible to assimilate the viscous behaviour of a material to a Newtonian fluid damper such that:

$$\frac{\mathrm{d}\epsilon}{\mathrm{d}t} = \frac{\sigma}{\mu} \tag{1.14}$$

where μ is the viscosity and the elastic behaviour to a spring of stiffness k obeying Hooke's law:

$$\epsilon = \frac{\sigma}{k}. \tag{1.15}$$

It turns out that through a Laplace transform, the BSI can be rearranged into an ordinary differential equation of the form:

$$\sum_{i=0}^{n} a_i \frac{\mathrm{d}^i \epsilon}{\mathrm{d}t^i} = \sum_{i=0}^{n} b_i \frac{\mathrm{d}^i \sigma}{\mathrm{d}t^i} \tag{1.16}$$

which corresponds to the requirements of the spring and dashpot mechanistic model. An infinite number of springs and dampers configurations are, however, imaginable for equation 1.16. The most common models are:

- The Maxwell model consisting of a spring and damper in series and which is known to provide an adequate description of relaxation, but not of creep.
- The Kelvin-Voigt model made of a set of spring and damper in parallel, which is adequate for creep description (apart from the initial elastic response), but is not for relaxation.
- The Zener standard linear solid consists of a Maxwell element in parallel to a second spring element, which is the simplest arrangement that models all the aspects of the creep and relaxation.

The mathematical derivation of these models is provided in most textbooks dealing with viscoelasticity (see e.g. Hertzberg (36), Gibson (42), Vincent (40) or Gutierrez-Lemini (41)).

It is interesting to note that the Laplace transform (here denoted by the overline symbol) of the creep compliance is:

$$\overline{S}(s) = \frac{1}{s^2 \overline{C}(s)} \tag{1.17}$$

and thus $S(t)$ is not strictly equal to $1/C(t)$. However, if $t \to 0$ or $t \to \infty$, it can be proven that $S(t) = 1/C(t)$ and thus the approximation may be acceptable in many cases where t is either very short or very long. This is important in that simply substituting an elastic solution to a viscoelastic problem defined in equations 1.10 or 1.11 may not yield accurate

answers at moderate times or non-constant stress. In such cases, it is either necessary to solve in the Laplace space in order to maintain the stiffness-compliance relationship or to impose a model of relaxation which implies the relaxation (or retardation) times.

However, if transformed in the Laplace space, the BSI may be expressed in a way that is analogous to Hooke's law. Elastic solutions can then be solved by an inverse Laplace transform to obtain the linear viscoelastic solution. In the case of sinusoidal stresses, a Fourrier transform also yields a form similar Hooke's law. This particularity is referred to as the correspondence principle. Discussions on this topic are found, for example, in (43; 42; 44).

Note that for the special case of a constant stress (mathematically equivalent to Heaviside's step function), it can be shown that the solution of the BSI is directly analogous to the elastic solution. This is called the quasi-elastic analysis.

1.2.3.1 Viscoelasticity under sinusoidal loads

For a constant or monotonous external loads, equations 1.10 and 1.16 usually reduce to simple algebraic equations. However, in the case of oscillating loads, it may not be so. A special case of oscillating load that is of interest for the engineer is the sinusoidal loading of angular frequency $\omega = 2\pi f$ (with f the actual frequency), such as would be encountered in a rotating machine or in a DMA experiment.

A stress that varies sinusoidally with time t at an angular frequency ω in an homogeneous and isotropic sample would be represented by the real part of the complex stress function:

$$\sigma^*(t) = \sigma_0(\cos\omega t + i\sin\omega t) = \sigma_0 \exp(i\omega t), \tag{1.18}$$

where $i = \sqrt{-1}$ is the imaginary operator and σ_0 is the complex amplitude of the stress.

Substituting this definition of the complex stress in equation 1.10, we get:

$$\begin{aligned}\epsilon^*(t) &= \int_{-\infty}^{t} S(t-\zeta)\frac{\mathrm{d}\sigma_0 \exp(i\omega\zeta)}{\mathrm{d}\zeta}\mathrm{d}\zeta; \\ &= \int_{-\infty}^{t} S(t-\zeta)\sigma_0 i\omega \exp(i\omega\zeta)\mathrm{d}\zeta; \\ &= \sigma_0 i\omega \int_{-\infty}^{t} S(t-\zeta)\exp(i\omega\zeta)\mathrm{d}\zeta.\end{aligned} \tag{1.19}$$

Posing that $X = t - \zeta$, recalling that $S(t) = 0$ for $t < 0$ and taking the constants out of the integral, equation 1.19 can be rearranged in:

$$\epsilon^*(t) = \sigma_0 i\omega \exp(i\omega t)\int_{-\infty}^{\infty} S(X)\exp(-i\omega X)\mathrm{d}X. \tag{1.20}$$

It occurs that the integral from equation 1.20 is the Fourier transform (denoted by the caret symbol $\hat{}$) of the creep compliance $S(t-\zeta)$, which is by definition $S(\omega)$ (see e.g. Gibson, Hwang and Sheppard (45)).

$$\hat{S}(t-\zeta) = S(\omega) = \int_{-\infty}^{\infty} S(X)\exp(-i\omega X)\mathrm{d}X. \tag{1.21}$$

The expression may thus be rewritten to:

$$\epsilon^*(t) = \sigma_0 i\omega \exp(i\omega t)S(\omega). \tag{1.22}$$

Recalling equation 1.18 and posing that the complex compliance is given as $S^*(\omega) = i\omega S(\omega)$, equation 1.22 further reduces to:

$$\epsilon^*(t) = \sigma^*(t)S^*(\omega). \tag{1.23}$$

Alternatively, by substituting sinusoidally varying strain $\epsilon^*(t) = \epsilon_0 \exp(i\omega t)$ in equation 1.11 and applying a similar reasoning, the expression of viscoelastic stress may

be given as:

$$\sigma^*(t) = \epsilon^*(t)C^*(\omega), \tag{1.24}$$

where $C^*(\omega) = i\omega C(\omega)$ and $C(\omega)$ is the Fourier transform of the relaxation moduli $C(t-\zeta)$.

The analogy between Hooke's law in 1D for elastic materials and the viscoelastic stress-strain relationship from equation 1.24 is evident. However, it must be emphasized that the strain is now related to stress by a compliance or modulus which is complex.

From there, it is informative to rewrite the complex modulus in terms of real and imaginary parts as it provides an interesting insight on the physics of viscoelasticity.

Specifically, considering a unidirectional loading, the complex relaxation modulus may be simplified to any complex modulus M^* (where M^* may stand for any complex modulus such as tensile, shear bulk or viscosity). A visual representation of the dynamic modulus in the complex plane is shown in Figure 1.3. From this image, it is easily seen that the modulus (in the mathematical sense) of $M^\star$ is given by:

$$|M^\star| = \sqrt{M'^2 + M''^2} = \frac{|\sigma(t)|}{|\epsilon(t)|} \tag{1.25}$$

where M' is the storage modulus and M'' is the loss modulus. These two parameters, M' and M'', are the real and imaginary part of M^*. They are respectively associated with the elastic energy storage and viscous energy dissipation or internal damping of the material. These parameters are also be given by:

$$M' = |M^\star|\cos\delta = \frac{\sigma_0}{\epsilon_0}\cos\delta \tag{1.26}$$

$$M'' = |M^\star|\sin\delta = \frac{\sigma_0}{\epsilon_0}\sin\delta \tag{1.27}$$

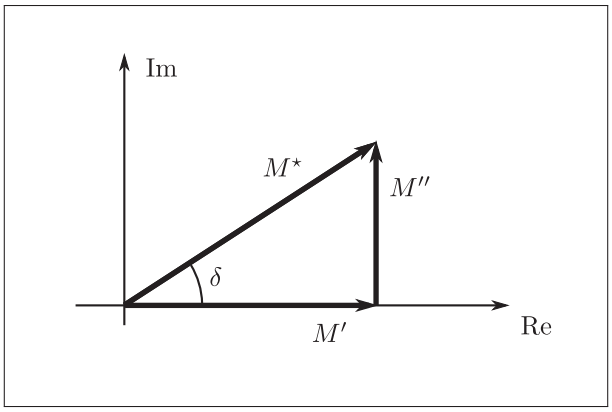

Figure 1.3 Schematic representation of the dynamic modulus

The complex modulus is then given by:

$$M^*(\omega) = M'(\omega) + iM''(\omega). \tag{1.28}$$

The loss factor, defined as $\tan\delta(\omega) = M''(\omega)/M'(\omega)$, is often used as a measure of the relative damping of a viscoelastic material. Introducing this definition in equation 1.28, it becomes:

$$M^*(\omega) = M'(\omega)(1 + i\tan\delta(\omega)); \tag{1.29}$$

$$= |M^\star(\omega)| \exp(i\delta(\omega)); \tag{1.30}$$

$$= \frac{\sigma'}{\epsilon} + i\frac{\sigma''}{\epsilon}. \tag{1.31}$$

In equation 1.31, $\delta(\omega)$ is the phase lag of the strain $\epsilon(t)$ over the stress $\sigma(t)$. Correspondingly, $M'(\omega)$ is the ratio of the in-phase (real) component of the stress σ' over the actual strain ϵ, while $M''(\omega)$ is that of the out-of-phase (imaginary) component of the stress (σ'') over ϵ.

It is worth noting that, as is shown by the previous development, in an actual experiment the strain will lag the stress independently of the control mode (stress or strain control).

For a dynamic shear test, it is also possible to relate the viscosity μ to the dynamic shear modulus $G^\star$ by the following relationships

$$\mu^\star = \frac{G^\star}{\omega} \tag{1.32}$$

$$\mu' = \frac{G''}{\omega} \tag{1.33}$$

$$\mu'' = \frac{G'}{\omega}. \tag{1.34}$$

Finally, it was demonstrated that creep, relaxation and dynamic viscoelasticity all emanate from the same physical mechanisms, so it is possible to relate the results of the former two types of experiment to the latter. However, in practice, experimental data are discrete and only obtained over finite time or frequency ranges so the solution of the improper integral in the Fourier transform is problematic.

Nevertheless, Gibson et al. (45) showed that through a discrete Fourrier transform (DFT) and numerical integration, the frequency domain complex modulus $M^\star$ could be used to evaluate the creep compliance $S(t)$ or relaxation modulus $C(t)$. However, it was unclear if the time frame of experiments were required to be similar for accurate predictions. Parot and Duperray (46) used another kind of DFT to assess the time-domain relaxation from frequency-domain experiments. The use of numerical integration was in part due to the Fourrier integral being infinite, while experimental data can only be finite in nature. Guedes et al. (47) have thus proposed integration-free method to achieve an estimate of the time-domain master curve from frequency domain experiments. Their approach is based on the property that if the time-temperature superposition principle (TTSP, see next section) applies to the material, it should apply to its viscoelastic spectrum. This spectrum is not directly measurable experimentally, but can be approximated efficiently by numerical methods. Application of their algorithm to simulated data showed that

the approach could provide a useful approximation of the creep master curve from the dynamic data.

1.2.3.2 The time-temperature superposition principle

Experience has shown that a relationship exists between the effects of time and temperature on amorphous materials mechanical response. The time-temperature superposition principle (TTSP) stipulates that the mechanical response at a given load and temperature and at a certain time scale (or frequency) is equivalent to the response to the same load at other combinations of temperatures and time scales. This means that if one is to look at a curve of an instantaneous material property (e.g. the storage modulus, loss modulus or creep compliance) of a material over time for a given temperature, the shape of the curve would remain constant, while it would undergo a shift in both the initial property and the time scale. The parameters representing these shifts are commonly called the vertical shift parameter (b_T) — associated with the change of property along the dependent variable axis — and the horizontal shift (a_T) along the time axis — the independent variable.

This simple shift behaviour means that a single master curve of the behaviour at one temperature could be expected to represent the behaviour for any time scale if the amplitude of the shift is known. Alternatively, it should be possible to reconstruct a master curve over a larger time scale based on the behaviour of the material over smaller time scales, but at multiple temperatures. That is actually the most common use of the TTSP since it allows accelerated testing of the long-term behaviour of materials by using higher temperatures than those found in service.

Both a_T and b_T are functions of temperature and time scale. It is interesting to note, however, that b_T is expected to be close to unity. Thus, it is sometimes neglected in the evaluation of the shift factors. A way to determine b_T is to plot the loss angle δ or the

damping coefficient $\tan\delta$ against frequency as these values are supposed to be frequency independent (48). The horizontal shift factor a_T, on the other hand, is not negligible.

As shifting curves by a_T and b_T is the result of empirical observation, no theory can predict the values of the shift parameters, they need to be found experimentally by fitting results to a model. Moreover, there are discontinuities in the shift factors where the physical mechanisms that affect the material properties change (49). Therefore, shift factors would not follow the same trend above and below T_g and multiple fits would be required.

Currently, the two most common approaches for evaluating a_T are the empirical formulation of an Arrhenius type relationship (48) and the Williams-Landel-Ferry (WLF) equation from (50). The Arrhenius equation for TTSP is usually given as:

$$\ln a_T = \frac{E_a}{R}\left(\frac{1}{T} - \frac{1}{T_{\text{ref}}}\right) \tag{1.35}$$

where E_a denotes the Energy of activation of the process, R is the ideal gas constant (8.314 J/mole℃) and T_{ref} is a reference temperature. This equation is usually expected to work best at $T \ll T_g$ or $T \gg T_g$ (i.e. fully glassy state or when an amorphous solid approaches the liquid state).

Closer to T_g, the WLF model is usually preferred. It is given by the following equation:

$$\ln a_T = \frac{-C_1(T - T_{\text{ref}})}{C_2 + (T - T_{\text{ref}})} \tag{1.36}$$

in which C_1 and C_2 are empirical constants. Despite WLF's equation being better suited to model the behaviour for $T \geq T_g$, a second fit is sometimes used below T_g instead of the Arrhenius equation. A demonstration of this, as well as an interesting discussion on the use of horizontal shift factors, can be found in Sullivan (51).

A special case of the WLF equation exists for $T_{\text{ref}} = T_g$. In such a case, it has been shown that for many polymers $C_1 = 17.44$℃ and $C_2 = 51.6$℃. It is interesting to note that the

VFT and WLF equations are known to be equivalent forms, as discussed for example by Liu and Jin (24), or White and Lipson (26).

The so-called 'universal' constants C_1 and C_2 proposed by Williams, Landel and Ferry were soon challenged however. For example, Adams and Gibbs [(52), p.140] note that:

> So the "universality" of Eq.(5) [equation 1.36 from this document with $T_{\text{ref}} = T_g$, $C_1 = 17.44$℃ and $C_2 = 51.6$℃] seems quite poor insofar as quantitative description is attempted.

A limit of the TTSP is that it is only valid for linear viscoelastic materials that are thermorhologically simple (e.g. where variations of a_T are log-log linear). Thermorheological simplicity can be seen as an equivalent of all relaxation times having the same temperature dependence. However, thermorheological simplicity is not always easy to ascertain and it is sometimes useful and even preferable to check results in the linear space to verify that the fit is indeed good (53).

Also, the TTSP assumes that the shift factors do not vary over time. However, polymers age and the shift factors do vary over time. To model long-term behaviour from short time data, ageing thus needs to be accounted for.

1.2.3.3 Ageing

Ageing of amorphous materials happens below the glass transition and occurs as a result of all the molecular movements discussed earlier. In some instance, such a molecular movement brings the structural configuration to a lower energy, more stable one where the material remains temporarily. This new configuration reduces the enthalpy and also potentially the free volume of the material (some configurational changes may be made without affecting the latter), whilst increasing its stiffness and lowering its T_g. Thus, the very nature of ageing — a reduction in enthalpy and/or free volume — means that as time goes by, the process occurs at an ever-decreasing pace.

It is evident that ageing thus depends on the initial state of the amorphous material and, remembering the discussion around Figure 1.1, on the cooling rate below T_g. This is called the quenching condition of the material. It is worth noting that bringing a material somewhat above its T_g for some time brings the material back to the rubbery condition, erasing previous ageing and making a new quench possible. This process is called annealing (or sometimes rejuvenation). According to Cowie (reported by Odegard and Bandyopadhyay [(54) p.1699]), bringing the material to a temperature 40℃ above T_g for a period of 10-15 minutes is adequate for annealing. Ageing of polymers is well documented and the seminal work of Struik (17) provides much information on dealing with ageing from an experimental and engineering point of view.

It should now be clear though that ageing will affect the time-temperature superposition shift factors of a material and that if the experiments are comparable in length to the ageing time of the material, the superposition will not work. As a result, Barbero (49) suggests that experiments for TTSP should be performed on a timescale at least ten times shorter than the ageing time of the sample. Yet, this approach has the drawback of providing a master curve under a given set of time-temperature and age conditions. These are called momentary master curves.

Sullivan (51), Brinson (55) and Barbero (49) describe a time-age superposition principle (TASP) — in the context of creep — which is conceptually similar to the TTSP, but which relates the effects of ageing time on the mechanical behaviour instead of that of temperature. From this approach, ageing shift factors a_e and the ageing shift factor rate μ_e, the latter being assumed to remain constant when well below T_g, are obtained.

These two parameters can then be used in Struiks (17) effective time theory (ETT). According to the ETT, the effective time λ is given by

$$\lambda = \int_0^t a_e(\zeta)\mathrm{d}\zeta. \tag{1.37}$$

It is this effective time that would be used in the TTSP of an application where ageing occurs.

Of particular interest for the current research question is the specific ageing of epoxy resins as they are a very popular choice for wind turbine blades composites. Odegard and Bandyopadhyay (54) reviewed the ageing behaviour of epoxy polymers. Some of the most relevant points they relate are:

- The ageing process of epoxies is slow.
- The elastic modulus of epoxies shows negligible to small increases with ageing.
- The hardness and tenacity of epoxies decreases with age.
- The ageing process may change the mode I crack propagation from an initially unstable crack propagation to an 'unstable stick-slip' mode.
- The quasi-static tensile yield stress of epoxies decreases with age, possibly due to microcracking and reduction in tenacity.
- The quasi-static yield stress in compression and shear increases significantly with ageing.

As examples of the magnitude of the ageing effects, they report changes in the yield strength of epoxy of 15% over about three decades of ageing time, a reduction of critical energy release rate of about a decade over two decades of ageing time, a doubling of the relaxation modulus over two decades of ageing or a fourfold increase in a_e over two decades of ageing time.

It is worth mentioning that Struik (17) reported that at medium to high stresses, but below yield, a kind of mechanical rejuvenation is possible. The mechanisms for this rejuvenation — and even its existence — is the subject of some controversy (54). Struik's

original explanation was that mechanical strains resulted in large-scale motions of molecular segments and increased free volume, resulting in the erasure of thermal history. Odegard and Bandyopadhyay (54), however, report several studies showing that the time for ageing equilibrium appears to be independent of the load and that the relaxed volume of periodically highly loaded samples was the same as that of samples that were only lightly loaded. This suggests that the structure of the polymer might not be strongly affected, contradicting Struik's hypothesis. The alternative explanation is that the apparent rejuvenation would result from non-linear viscoelastic behaviour. Nevertheless, whatever the mechanism being active, it is easy to see implication of stress induced rejuvenation in the context of fatigue of composites. One could indeed wonder if the level of the load in structural composites would be enough to prevent ageing and thus, promote creep-fatigue interactions by favouring a state of maximum compliance.

1.2.3.4 Relaxation functions

Relaxation functions are relatively simple empirical models used to describe the relaxation of physical properties (stiffness, volume, enthalpy) of glasses with time — either due to viscoelasticity or ageing. The Maxwell and Zener standard linear solid solution for example provides an exponential solution of the type:

$$\phi(t) = \exp(-t/\zeta), \tag{1.38}$$

where $\phi(t)$ would be the normalized relaxing physical property, t the time and ζ the characteristic time for the process (ageing or viscoelastic). Although equation 1.38 shows the right overall trend for most materials, it may not fit data very well over long periods of times. Propositions such as the improved Zener model with multiple characteristic times (see e.g. Gibson (42)) or its stretched exponential counterpart (the relationship between multiple exponential functions and the stretched exponential function is discussed by Stillinger and Debenedetti in (19)) may fit much better over long times. This stretched

exponential function takes the form

$$\phi(t) = \exp\left[(-t/\zeta)\right]^{\beta}. \tag{1.39}$$

Equation 1.39 is often referred to as the Kohlrausch-Williams-Watts (KWW) formulation, named after Rudolf Kohlrausch (56) who first used it in physics to model the discharge of capacitors after remarking that the simple exponential did not fit well and his son Friedrich Wilhelm Georg Kohlraush (57) used it for mechanical relaxation (58; 59). Williams and Watts further applied the principle to dielectric spectroscopy (60). In the KWW equation, $\beta = 1$ falls back to the basic exponential function and for $0 < \beta < 1$ stretches the function towards longer times as $\beta \to 0$.

Another approach to improving the exponential model of equation 1.38 is to consider ζ as a distribution of relaxation times. The Kovacs-Aklonis-Hutchinson-Ramos (KAHR) and Tool-Narayanaswamy-Moynihan (TNM) frameworks are often cited examples of such an approach (54).

1.2.3.5 Non-linear viscoelasticity

As discussed before, the linear viscoelastic behaviour of polymeric materials is often limited to quite low stresses and strains. For a more general treatment of viscoelasticity, non-linear effects need to be accounted for. This non-linearity may be the result of the material's behaviour itself (material non-linearity), of large strains (geometric non-linearity) or of stress interactions in complex stress states (interaction non-linearity). However, since this topic is quite complex and potentially only tangentially related to the problem attacked in this dissertation (i.e. although the stress state in composites is almost always complex, the strains in the polymer matrix are usually relatively small), only a superficial discussion will be provided. An introductory text to non-linear viscoelasticity is provided in Brinson and Brinson (44).

An obvious way of introducing non-linearity in the traditional modelling approaches is to use non-linear elements in the springs and dashpots models discussed earlier (Maxwell, Kelvin-Voigt or Zener). This makes the model much more flexible, at the expense of multiplying the number of material parameters to be identified (44).

In the case of non-linear viscoelasticity, the BSI is not valid anymore since it relied on the linearity of the phenomenon. Thus, in the case of step or continuously variable loadings, much more complex approach needs to be used. For example, the single integral for the BSI may be substituted by a series of integrals, which are interdependent and require creep tests with multiple loadings steps to identify the model parameters (44).

Alternatively, the constitutive equation of the BSI may be made time dependent. Such a formulation was used by one of the most influential authors on the topic of non-linear viscoelasticity, Richard Allan Schapery. He is the author of numerous papers including, but not limited to, (61; 62; 63; 64). His work has concentrated on the use of state variable in a thermodynamic description of the constitutive equations to be used in a single integral formulation. The resulting expression for strain is:

$$\epsilon(t) = g_0 S_0 \sigma(t) H(t) + g_1 \int_{0^-}^{t} S_1(\Psi - \Psi') \frac{\mathrm{d}\left[g_2 \sigma(\zeta) H(\zeta)\right]}{\mathrm{d}\zeta} \mathrm{d}\zeta, \tag{1.40}$$

where the stress (or strain) dependent timescale is:

$$\Psi(t, \sigma) = \int_0^t \frac{1}{a_\sigma(t)} \mathrm{d}t, \tag{1.41}$$

$$\Psi(\zeta, \sigma)' = \int_0^\zeta \frac{1}{a_\sigma(\zeta)} \mathrm{d}\zeta. \tag{1.42}$$

In equations 1.40 to 1.41, parameters g_0, g_1, g_2 and a_σ are stress dependent material parameters. In particular, a_σ is a stress-time shift factor akin to a_T in the TTSP. Stress under a variable strain would be given by:

$$\sigma(t) = h_0 C_0 \epsilon(t) H(t) + h_1 \int_{0^-}^{t} C_1(\Psi - \Psi') \frac{\mathrm{d}\left[h_2 \epsilon(\zeta) H(\zeta)\right]}{\mathrm{d}\zeta} \mathrm{d}\zeta, \tag{1.43}$$

where:

$$\Psi(t,\epsilon) = \int_0^t \frac{1}{a_\epsilon(t)} \mathrm{d}t, \tag{1.44}$$

$$\Psi(\zeta,\epsilon)' = \int_0^\zeta \frac{1}{a_\epsilon(\zeta)} \mathrm{d}\zeta. \tag{1.45}$$

Note that because of the irreversibility of the non-linear creep-recovery process (i.e. the stress dependency of g_1, g_2), even for the simplest case of loading and unloading, the parameter set g_1, g_2 is different in each stage. Thus, a minimum of seven material parameters (including the exponent from equation 1.8 and accounting for those of the linear part that are equal to one) are required for the complete characterization of a material non-linear creep behaviour. It is important to note that this approach is mainly useful for short to medium term effects and that long-term predictions may yield large errors. Also, in the case of polymers, it is mostly applicable to cross-linked materials as linear polymers tend to accumulate permanent strains under load and these are not accounted for in the previous treatment (44).

Finally, the time-stress superposition principle (TSSP) — an empirical approach similar to the TTSP — is also available for dealing with non-linear viscoelasticity (65; 66; 44). This approach relies on empirically determined horizontal and vertical stress shift factors to obtain a master curve of stress effects. It can then be combined with other with a TTSP master curve to obtain a time-stress-temperature superposition principle (TSTSP) master curve (66; 44).

1.2.3.6 Creep failure models

While the TTSP applies to physical properties such as stiffness or viscosity, its use is rarely seen when strength is discussed. Empirical relationships have been introduced for metals in the mid-20th century and are sometimes successfully used for polymers if the failure mode remains constant (see e.g. Shcherbak and Gol'dman (67) or Brinson and

Brinson (44)). Among those formulation, the most popular probably is a concept similar to the TTSP that has been proposed by Larson and Miller (68) for predicting failure times of a material based on temperature and creep stress. It relies on the empirical observation that at a given stress, the product of the absolute temperature and of the sum of the logarithm of time to failure and a material constant does not change. It is based on the initial assumption that creep rate can be modelled by an Arrhenius type relationship and is inversely proportional to time. Thus, the Larson-Miller parameter (LMP) is expressed as:

$$LMP = T(C_{\mathrm{LM}} + \log t_f) = f(\sigma). \tag{1.46}$$

In this equation, LMP remains constant for a given load level (but varies with stress) and the time to failure t_f is obtained from a regression on creep results to obtain C_{LM}, an empirical material constant. This relationship has been successfully used for some polymers, mostly thermoplastics. A similar model from Orr, Sherby and Dorn where the temperature effect is directly integrated in the Arrhenius relationship also exists, and takes the following form.

$$SDP = \log t_f - \frac{C_{\mathrm{SD}}}{T} = f(\sigma). \tag{1.47}$$

In equation 1.47, SDP is the Sherby-Dorn parameter (constant for a given stress level), C_{SD} is a material constant and T is the absolute temperature.

Still in the context of metals, Manson and Haferd (69) have shown that the Larson-Miller relationship — which implies a linear behaviour in the $1/T$ vs $\log t_f$ space with curves at different stresses converging at $1/T = 0$ — provided a poor fit to measured data at long-term (in the ten thousand hours range) based on tests at short times ($t \leq 100$ hours). This was attributed to non-linearity, mostly at higher stresses. To correct this problem, they proposed a relationship based on the observation that for failure times above 10 hours ($\log t > 1$), the increase in the logarithm of failure time was linear with decreasing T. Assuming that all lines converge to $(T_a, \log t_a)$, the Manson-Haferd parameter is given

as:

$$MHP = \frac{T - T_a}{\log t_f - \log t_a}. \tag{1.48}$$

Note that MHP is the slope of the T vs $\log t$ curve, which is stress dependent.

Rarely discussed in the Western scientific literature is the work of Zhurkov (70). In this paper, Zhurkov summarized work on creep performed at the USSR academy of Science and proposed a creep strength model based on the kinetic theory and tested it on more than fifty materials, including polymers. This model takes the form:

$$t_f = t_0 \exp \frac{E_a - \gamma\sigma}{k_B T}. \tag{1.49}$$

In equation 1.49, t_0 and γ are constants, E_a is the creep failure activation energy (also constant for a given temperature), σ is the applied stress, k_B is Boltzmann's constant and T is the absolute temperature. One of Zhurkov main observation is that for all tested materials, the parameter t_0 — which he associated with the material structure's natural oscillation period — would be a constant. Also, for many materials, E_a was found to be equal to the product $\gamma\sigma$ at t_0, meaning that a stress exists so that $t_f = t_0$ and is independent of temperature. Note that although there are evidences of the physical basis behind Zhurkov model, the relationship is considered to be more empirical than theoretical in the Western science community. Also worth noting is that these creep strength models do not provide very different strength estimates and rely on somewhat similar modelling approaches (71).

1.3 Thermal stability of inorganic reinforcements

Although many materials used as reinforcement in polymer-based composites are themselves amorphous or contain amorphous phases (e.g. glass, basalt, graphite), the temperature at which their glass transition occurs is usually much higher than for organic matrices (or fibres such as nylon). Therefore, in most instances they can be considered as thermally stable and their time-dependent nature can be neglected.

For example, E-glass fibres have a lower limit of softening temperature of 820℃ (72) while a basic epoxy would have a $T_g \approx 50°C$ and a typical high-performance room temperature cured epoxy would have a $T_g \approx 160°C$ (73). Based on such numbers, it is evident that a polymer would be degraded beyond usability well before fibres would be significantly affected by temperature.

1.4 Thermomechanics of polymer matrix composites

The thermomechanics of polymer matrix and inorganic reinforcements have been discussed in the previous section. The discussion now turns towards the effects of time and temperature on the composites themselves. The topic of internal stresses in composites under thermal loading will first be briefly discussed. The viscoelastic effects will then be addressed in terms of material properties. The topic of temperature effects on quasi static and fatigue failure will finally be treated.

1.4.1 Internal stresses in fibrous composites

Internal 'residual' stresses in composites mainly result from two similar processes. First, during the polymer cure, the chemical contraction of the resin results in residual stresses. Second, temperature differentials encountered both during manufacture and service also influence the state of internal stresses.

Examples of work dealing with chemical and thermal shrinkage upon resin curing are those of Koufopoulos and Theocaris (74) or White and Hahn (28). Koufopoulos and Theocaris demonstrated, through photoelastic experiments on cast epoxy, that the stress distribution in the matrix depends on the fibre packing arrangement (square vs triangular), the ratio of fibre diameter over the inter-fibre distance and relative stiffness of the inclusion with relation to that of the matrix medium. It was also demonstrated that the curing stress can exceed the matrix strength and result in fracture. One of the main advantages of this study is that by allowing the resin to cure around the inclusions—

as opposed to press-fitting inclusion into holes in the matrix —, it very closely mimics the actual kinetics of the stress development in composites and allows for some stress redistribution upon cure.

The work of White and Hahn (28) also deals with the development of internal stresses during cure. However, their study focused on the effect of the cure cycle on internal stresses. Their results suggest that residual stresses mainly depend on the cure temperature, with cure temperature being a good indicator of the stress-free temperature. Therefore, a cure temperature closer to ambient reduces the stress level at the expense of additional cure time.

Internal stresses also exist in composites due to the discrepancy in CTE between fibre and matrix materials. With fibres CTE often being one or two orders of magnitudes lower compared to that of the matrix, significant stresses may result upon temperature change (75). This is of particular interest for the strength of composite structures exposed to cold climates as the temperature differential between the operational and stress-free (cure) temperatures becomes more important. Lord and Dutta studied the stress formation and distribution in composites exposed to low temperature (76). Dutta (75; 77) also provides an analytical approach for estimating matrix and fibre stresses in composites subject to cold temperature environment. From this work, it is clear that a high fibre content, which is often desirable in structural applications, tends to increase the internal thermomechanical stresses developed on cooldown. It is also suggested that such stresses due to cooldown may be sufficient to result in crack formation. The possibility of freeze-thaw cycles acting as a crack driving force is also discussed.

The effect of viscoelastic relaxation of stress around a reinforcing fibre is briefly discussed in (43). It is illustrated that below (but close to) T_g, very long times are required to relax the shrinkage stresses. Therefore, once cured and cooled to ambient temperature, the stress state in a fibre reinforced composite is not excessively time dependent.

Finally, one should be aware that matrix swelling caused by moisture diffusion can also generate (or relieve) other residual stresses due to cure or thermal stresses (76).

1.4.2 Time dependent mechanical response of polymer matrix composites

In the case of anisotropic materials, equation 1.10 and 1.11 have to be adapted to account for the tensor form of the creep compliance and relaxation modulus. This transformation was first detailed for linear viscoelasticity, including thermodynamic arguments for some symmetry in the compliance and stiffness matrices, in (43). This formulation includes the effect of transient temperatures. For the classical material assumptions of a plane-stress state and of a specially orthotropic lamina, the time-dependent creep compliance would be given as:

$$\mathbf{S}_{ij}(t) = \begin{bmatrix} S_{11}(t) & S_{12}(t) & 0 \\ S_{21}(t) & S_{22}(t) & 0 \\ 0 & 0 & S_{66}(t) \end{bmatrix} = \begin{bmatrix} S_{11} & S_{12} & 0 \\ S_{21} & S_{22}(t) & 0 \\ 0 & 0 & S_{66}(t) \end{bmatrix}. \tag{1.50}$$

The treatment of this problem is described by Sullivan (51) in the ply natural coordinates and by Brinson and Gates (55) for an orthotropic laminate in arbitrary directions and for laminates (under a constant load). It is also discussed in Gibson (42). It is interesting to note that Sullivan (51) has shown experimentally that in the ply natural axis, $S_{12}(t) = S_{21}(t)$, but that the time dependence of this compliance, as well as that of S_{11} were negligible. It was however shown that S_{22} and S_{66} were strongly time dependent. As discussed by Brinson and Gates, this means that off-angle plies have all nine positions of their stiffness or compliance tensors which can be strongly time-dependent, such that:

$$\bar{\mathbf{S}}_{ij}(t) = \begin{bmatrix} \bar{S}_{11}(t) & \bar{S}_{12}(t) & \bar{S}_{16}(t) \\ \bar{S}_{21}(t) & \bar{S}_{22}(t) & \bar{S}_{26}(t) \\ \bar{S}_{61}(t) & \bar{S}_{62}(t) & S_{66}(t) \end{bmatrix}, \tag{1.51}$$

with the overline denoting the transformed creep compliance in the analysis direction rather than in the ply natural axis. This coordinate transformation is performed in a way that is analogous to the regular transformation for elastic strains (78) thanks to the elastic-viscoelastic correspondence principle. It is also worth noting that the symmetry of the elastic stiffness or compliance matrices also holds true for the viscoelastic creep-compliance and relaxation-modulus matrices.

Note that the assumption of linear viscoelasticity (thermorheological simplicity) is likely acceptable in many instances, but that if both the matrix and reinforcements are linear viscoelastic medium, then the global behaviour is non-linear viscoelastic unless the a_T shift factors of both materials are identical (43).

Griffith (66; 71) has proposed ways to deal with temperature and stress as accelerating factors (non-linear viscoelasticity) for a single unidirectional ply through the time-stress-temperature superposition principle (TSTSP). He also proposed that through the use of an orthotropic transformation equation, the compliance of a laminate oriented at an arbitrary angle could be obtained from tests on the lamina in other directions. Griffith also discusses the importance of laminate postcure in viscoelastic analysis. He notes the importance of postcure both in the experimental analysis of viscolelastic parameters (ensuring that the sample state is comparable to the final part state) and to stabilize the ageing of the material. It is interesting to note that Beckwith (79) reported that non-linear viscoelasticity might result from microdamages induced in the composites even at moderate stress levels. This has obvious implications for operational considerations. However, Beckwith also mentioned that this makes the identification of viscoelastic material parameters quite hard as they change significantly with each loading cycle, stabilizing only after many (around ten) stress cycles. This is also discussed in Brinson and Brinson (44), who discuss the importance of sample conditioning (i.e. repeated stress cycling) before the experimental measurement of creep compliance.

Dillard (80) has modelled the creep strength of graphite–epoxy composites including non-linear viscoelasticity based on ply level viscoelastic properties. He used a power law relaxation function for the creep compliance and a modified Tsai-Hill failure criterion to account for the time-dependent strength. The non-linear stress effects were introduced using a hyperbolic sine function in a viscoelastic model by Findley. The form of the viscoelastic model including stress effects is:

$$\epsilon(t) = \epsilon_0' \sinh\left(\frac{\sigma}{S_\epsilon}\right) + m' \sinh\left(\frac{\sigma}{S_m}\right) t^n, \tag{1.52}$$

where ϵ_0', S_ϵ, m' and S_m are temperature dependent material constants. An important element discussed in (80) is that a singularity exists where the power law exponent is zero where the other model parameter diverge. Since in viscoelastic materials, the exponent is usually well below unity, it is likely that a small error in the exponent results in large discrepancies of the other power law parameter. Note that in non-linear viscoelasticity, the stress transformation is no longer a direct analogue to the elastic case. Dillard suggested linearization of the relationship around the current stress state and interactions of multiaxial stresses was considered. Complex stress histories are dealt with through a numerical approach that sums the effect of small stress steps, an approach that Dillard accepts as oversimplified, but simple to implement for a first approximation. Predictions for the laminate creep strength were mainly lower than experimental measurements and decreased more rapidly with accelerating factors.

Sullivan (51) has shown that matrix dominated compliance (shear and transverse) of unidirectional composites — 30% v_f glass–Derakan 470-36 epoxy vinyl ester (Novolac based) — exhibit ageing characteristics similar to that of the bulk resin. However, as a fibre dominated property, the longitudinal compliance was not subject to ageing. Sullivan's experiments confirmed that Struik's (17) statement that polymers only reach ageing equilibrium in a practical time frame for $T \geq T_g - 15$℃ remains valid for composites. The suggestion that for matrix dominated properties of composites, ageing effects may be comparable to temperature effects was also supported by the experiments. It is worth

noting that Sullivan also demonstrated that the linear viscoelasticity regime of composites may be limited to quite low stress level. Indeed, non-linear behaviour was observed with shear stress as low as 8 MPa. Beckwith (79) also report non-linear behaviour at low stress, but at temperatures close to T_g. The applicability of the TTSP and TASP for momentary creep as well as that of the ETT for long-term creep to composite materials was demonstrated by Sullivan (51). All of these conclusions appear to be supported in the review by Odegard and Bandyopadhyay (54).

For the viscoelastic response to a sinusoidal loading, the development proposed for amorphous solids (equations 1.23 and 1.24) still holds, but the stresses and strains need to be taken in their tensor form to account for possible material level stress and strain couplings. Such an approach is detailed in Gibson's (42), which has a thorough chapter on viscoelastic analysis in the context of composite materials structures.

The effects of physical ageing on the long-term behaviour of composites at both the lamina and laminate level has also been investigated by Brinson and Gates (55). The applicability of TTSP, TASP and ETT were verified for composites and a formulation of ETT in the framework of the classical laminate theory (CLT) was proposed. It was also reported that because the ageing shift constants $\nu_{22} \neq \nu_{66}$ as well as characteristic times $\zeta_{22} \neq \zeta_{66}$, the creep-ageing compliance behaviour of off-axis composites may become quite unintuitive.

According to Guedes (81), the shift factor a_T found for the compliance of a material is often valid for its strength properties. Interestingly, Bosze et al. (82) have also found the shape of curves for storage modulus as a function of temperature to provide a good description of the shape of strength as a function of temperature for a hybrid glass-carbon-epoxy composites. Beckwith (79) has also suggested that the creep compliance exponent of equation 1.8 is the same for the matrix dominated properties of composites as for the neat matrix.

The Larson-Miller and Sherby-Dorn relationships have proven to work for polymer matrix composites (44), but have a major limitation. The LMP and SDP are empirical parameters that are only valid for a given laminate configuration. Alternate models based on lamina properties are discussed in Brinson and Brinson (44). Guedes (81) provides a review of several time-to-failure criteria for composites that are based on continuum mechanics and thermodynamics of rupture, kinetic failure theory and viscoelastic fracture mechanics. He concludes that all the tested relationships provide comparable results for the two materials tested.

1.4.3 Effects of temperature on the static strength and modulus of composites

A brief discussion on the literature regarding the effects of temperature on the static strength of composite materials is provided. It is based on the belief that part of the knowledge accumulated about those effects may be transferable to the problem of fatigue. Most of the literature deals with the effects of high temperatures, but some discussions on low temperatures are also presented.

Previous work performed Cormier and Joncas (83; 84) as part of the WESNet programme was devoted to the study of cold temperature on the static strength of unidirectional epoxy. These propose a recension of earlier work showing that there is a lack of consensus regarding the effects of low temperatures on the strength of composites. These also propose some new experimental results, suggesting that the textbook approach of using micromechanics models and Chamis's (85; 86) equations did not provide a good prediction of the effects of low temperatures on unidirectional glass–epoxy under tension, compression or short-beam shear loadings. For tensile and compressive stresses, this was confirmed in a report from the Upwind programme (87). In both cases, the strength of unidirectional glass-epoxy composites in the fibre direction was much improved at -40°C compared to that at room temperature. This conclusion is traditionally not expected for fibre dominated properties. However, according to Christensen's (88) prediction of me-

chanical properties with common micro-mechanics equations such as the rules of mixtures (RoM) can show significant discrepancies with experimental results.

Polynomials were also used to model temperature effects on properties of polymers and composites. For example, a third-degree polynomial was proposed by Liu et al. (89) as an empirical model to describe the evolution of the modulus of a laminate exposed to heat. However, such an approach lacks any physical meaning and polynomials are likely to provide meaningless minima or maxima as well as spurious behaviour outside of measurement points.

Gibson et al. (90) propounded two empirical degradation models for mechanical properties of composites under high temperature. These were meant to be incorporated in a more general model for predicting reduction of properties after the onset of matrix degradation due to heat. The two deterministic models are based respectively on the error function (ERF) and on a modified hyperbolic tangent function. It was suggested that both formulations had equivalent predictive performance but that the hyperbolic tangent was marginally simpler, so the latter was retained. The justification for the use of an anti-symmetric function such as the hyperbolic tangent was the relatively symmetric nature of the loss factor ($\tan\delta$) curve from DMA tests around T_g. An important element of the discussion found in the work of Gibson and his colleagues is that when the temperature is high enough to decompose the matrix, the level of decomposition should also be taken into account in determining the remaining laminate properties.

Cao et al. (91) also suggested that a modified hyperbolic tangent gave a good approximation of the degradation of ultimate strength at elevated temperature. However such a formulation suggests that the strength at low temperature would remain the same as that at room temperature, an expectation which, as discussed earlier, has not been borne out by experimental results for unidirectional glass polymer composites (84; 92; 93; 94; 95).

As part of their model for temperature and stress ratio effects on the fatigue properties of carbon fibres, Kawai and his colleagues (96) also retained a modified hyperbolic tangent,

but this time to curve fit the static strength as a function of temperature. However, their modifications to the hyperbolic tangent function meant that it would only be representative of one side of the glass transition, limiting its use to relatively narrow temperature ranges.

As they provide stronger theoretical support than purely empirical models such as those discussed before, the kinetic theory and the Arrhenius type relationships were also extensively used in the past to describe the evolution of properties of polymers and their composites with temperature. For example, in recent work by Bai and Keller (97), an Arrhenius relationship was used to model the stiffness-temperature relationship. In former work, Bai and his colleagues (98) also emphasized the time dependent behaviour of polymers and their composites at elevated temperature, as well as the role of the decomposition level of the matrix in predicting the residual mechanical properties.

Still, in search of improved theoretical support, Mahieux and Reifsnider (99) suggested a Weibull based formulation to predict the elastic modulus of polymers as a function of temperature. The model has the ability to describe the evolution of matrix modulus across multiple relaxation phases encountered at different temperatures and the approach relies on a physical concept — the stochastic nature of the secondary atomic bond strength — instead of being purely empirical. The Weibull distribution survival function (SF) was chosen to represent the statistical nature of the breakage of secondary atomic bonds within the polymer as the temperature increases. In later work, Mahieux et al. (100) used the polymer modulus prediction from this model as an input for estimating tensile strength of a composite based on an earlier micro-mechanics model by Case and Reifsnider. The strength prediction was acceptable, but required a further assumption on the efficiency of load transfer at the fibre-matrix interface.

Correia et al. (101) proposed an adaptation of the Gompertz distribution cumulative density function (CDF) to describe the evolution of mechanical properties undergoing a single relaxation phase at elevated temperatures. Incidentally, Correia et al. also

demonstrated the applicability of Mahieux et al.'s formulation — formally limited to the description of matrix modulus temperature dependence — to provide an adequate representation of many of the composite's mechanical properties under temperature changes. Both of these considerations, although not commented by Correia and his colleagues, bear some significance as the hypothesis of breakage of secondary atomic bonds posed by Mahieux and Reifsnider might be transferred to the whole composite by realizing that the changes in the composite's properties are likely governed by alterations of matrix and interphase properties.

To the author's knowledge, few formulations explicitly account for estimation of tensile strength at low temperatures apart from AbdelMohsen's (102) statistical simulation and Dutta's (103) micromechanics model. AbdelMohsen has used Monte-Carlo simulations to predict low temperature strength of composites based on the strength distribution of fibres (Weibull) and using the shear lag theory to account for the temperature effects on strength redistribution around fibre breaks. The model shows evidence of bias when showing the results in Weibull plots and to the author's own admission, the fit is sometimes poor, particularly at low temperature. Possibilities for explaining this poor fit are:

- The matrix is only considered as a medium to transfer loads to the fibres, and its failure is not included in the model.
- The evolution of the matrix modulus is not accounted for.
- The coefficient of thermal expansion varies significantly over the temperature range of the analysis.

Dutta also admits poor agreement of his model with experiments and predictions being off by an order of magnitude. Moreover, Dutta's formulation cannot account for high temperature or the glass transition since it relies on the hypothesis that strength is

degraded at low temperature due to compressive stresses in the fibres that promote misalignment and fibre micro-buckling.

1.5 Fatigue of composite materials

Although the study of fatigue in composites has been an active research area from the onset, from an engineering point of view composites have long been considered as fatigue insensitive. The 'misconception' arose from the combination of two simple facts. First, high performance composites are indeed quite resistant to fatigue compared to metals. Second, they were mostly used in life-critical systems (aircraft and spacecraft) were impact damage and high static load cases (e.g. crash cases) had to be accounted for. This led to low stress or strain allowable and to relative fatigue safe products (104).

The recognition that fatigue could be a problem for composite structures lead to the study of the fatigue process of damage accumulation. As opposed to metals where a fatigue loading leads a single crack to gradually extend until it reaches a critical length where it becomes unstable, fatigue damage is characterized by several mechanisms concurrently occurring, but spatially distributed over the material volume.

The failure process of unidirectional composites was described by Reifsnider (105). Synthetically, manufacturing defects induce cracks that create stress concentrations, leading to further fibre breaks (possibly at some distance from the initial flaw), eventually leading to failure. However, additional important aspects of unidirectional ply failures are also discussed. First, it is to be understood that within a unidirectional ply or laminate, failure also occurs in a distributed and progressive manner, not just because the properties of the constituent are statistically distributed, but because composite manufacturing generates irregularities in the microstructure of the ply that in turn affect the stress and strain fields. Second, in a unidirectional ply, because of the inhomogeneity of the material, strength and stiffness gradients exist between the different phases (fibre, matrix and interphase). This means that even if a transverse crack was to appear in

the weak phase (matrix), it would either be stopped at the fibre surface, or deviated to continue growing in the weak phase. This has for consequence that either a severe stress concentration may appear at the fibre surface or fibre debonding may result from fatigue loading. Third, effects of cracks or notches have an influence that may reach out to several fibre diameters. Therefore, the increased stress at a notch or crack tip may produce breakage of a weaker fibre at a distance, thus creating a new crack site.

A consequence of the damage distribution over the material volume is that although strength might not be much affected by fatigue cycling (with most fibre breaks occurring just before failure), the stiffness may be much degraded long before failure occurs.

Failure of laminates can be seen somewhat as a generalization of unidirectional ply failures where inhomogeneity not only results from the difference in the properties of constituent phases, but also from the differences in ply orientations, creating property gradients through the thickness. Five major mechanisms can be identified for multiaxial laminates (e.g. quasi-isotropic laminates) (106). Those are:

a. matrix cracking,

b. fibre breakage,

c. crack coupling,

d. delamination initiation,

e. delamination growth.

These damage mechanisms would each be associated with a different stage of the fatigue damage evolution and are illustrated in Figure 1.4.

In the first stage, flaws that are dispersed in the material volume induce stress or strain concentrations and lead to the birth of matrix cracks, particularly in the off-axis plies.

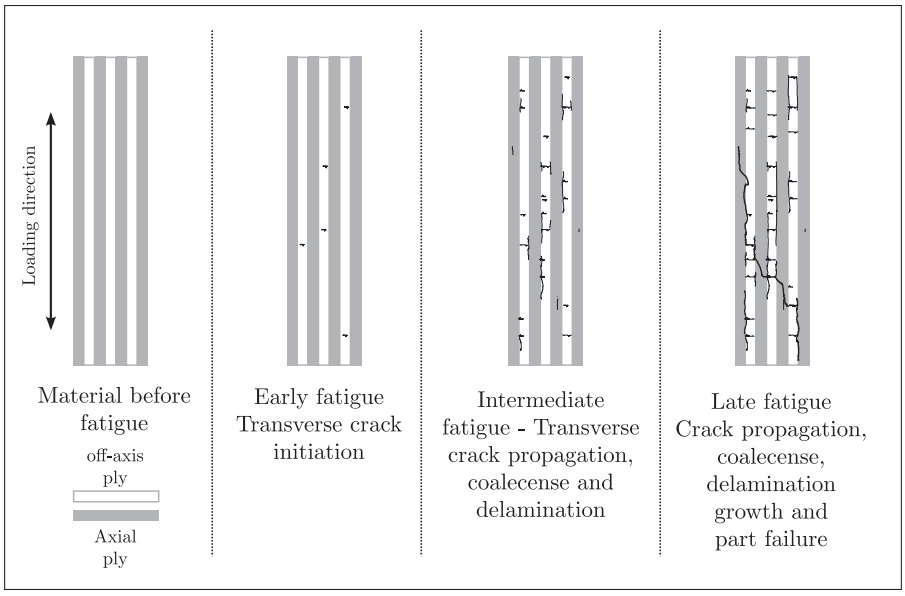

Figure 1.4 Illustration of fatigue damage formation in composites)

These initial matrix cracks appear early in the fatigue life and do not result in a significant strength degradation although stiffness can be affected. The first phase accounts for about 10% of the fatigue life. Hashin and Rotem (107) have shown empirically and theoretically that there is a critical angle at which the failure passes from a fibre dominated mode to a matrix dominated mode. Moreover, they have shown that this angle is quite shallow, of the order of two degrees for a glass fibre reinforced polymer composites.

Once cracks in the matrix of off-axis plies reach the surface of longitudinal plies, these cracks create stress concentrations and fibre breaks or deviate along the stiffer longitudinal ply and initiate longitudinal cracks. By growing from several different sites emanating from transverse crack tips, these longitudinal cracks can coalesce, leading to a phenomenon called crack coupling. Eventually, the damages result in delamination initiation between adjacent plies. These processes are characteristic of the second stage of fatigue life. In this second stage, damage progression is much slower than in the first. Consequently, it covers the best part of the fatigue process (70%-80%).

In the third and last stage, the longitudinal cracks have become so important that fibres cannot share load as effectively through the matrix. Delamination also becomes so extended that plies cannot effectively share load either. Eventually, failure results from the loss of strength occasioned by the damage state.

An interesting note is that because of the separation of plies and fibres, these are not able to resist buckling as effectively. Thus, the laminate may become much weaker in compression. Also note that in the presence of a free edge on the laminates, severe through-the-thickness stresses may occur and induce early delamination.

Reifsnider and Talug (105) and Masters and Reifsnider (108) also report the existence of a characteristic damage state (CDS) in composite laminates. The CDS follows from the observation that after cyclic loading, the number of cracks in an off-axis ply stabilizes and that the crack density at saturation is governed by elastic properties of the plies and their stacking sequence. According to the CDS, the distance between two cracks would be that required for the adjacent (unbroken) ply to transfer a load equal to the breaking strength of the cracked ply. The static and fatigue failure process are also discussed in (109). It is generally accepted that fatigue damage can reduce both the residual strength of a laminate and it stiffness. Discussions on these strength and modulus degradation are discussed in Nijssen (10).

In the present section, the most common approaches for modelling the fatigue of composites will be introduced. The non-deterministic nature of fatigue in composites and its implication in fatigue life prediction will also be addressed, followed by a discussion on the temperature and strain rate effects on the fatigue behaviour of composites.

1.5.1 Modelling approaches in fatigue of composites

Modelling the fatigue of continuous fibre reinforced polymer composites is excessively challenging due to the heterogeneous, anisotropic and discontinuous nature of the material. Moreover, as discussed earlier the constituents often exhibit important ageing,

time-dependent, strain rate and environmental sensitivity. In addition to these already stringent requirements, experience has shown that mechanical properties of composites exhibit high scatter, in part because of the complex structure of the materials and in part as a result of the uncertainties related to unavoidable manufacturing defects (see e.g. Mesogitis et al. (110)).

Fatigue strength in particular has proven to be sensitive to the inherent presence of manufacturing defects such as voids, broken fibres, fibre misalignment and waviness and delaminations or of geometric features such as the fibre volume fraction, the stacking sequence, the laminate type and thickness, and the existence of ply-drops or edges (111; 112; 113; 114).

Modelling of constant amplitude fatigue (CAF) has been an active research topic for decades. In a book chapter published in the early 1990s Sendeckyj (115) reviewed fatigue modelling approaches in composite materials and proposed three categories into which models would essentially fall. These categories would be: empirical methods, phenomenological approaches (strength and stiffness degradation theories) and finally damage modelling theories. It is noteworthy that the project presented in this dissertation will make use of empirical and strength degradation approaches for fatigue modelling.

In the early 2000s Degrieck and Paepegem (116) proposed another review of modelling methodologies, albeit with an emphasis on damage modelling. In their review, Degrieck and Paepegem still used a classification somewhat similar to that of Sendeckyj, indicating that the older theories had not been particularly challenged by newer modelling approaches. However, Degrieck and Paepegem made an important distinction for damage mechanics models by attributing them to two subcategories. The first subcategory uses the actual damage as the metric whilst the second uses damage progression as an input in a strength or stiffness reduction scheme.

Another general discussion on composite fatigue modelling is found in the review by Wicaksono and Chai (117). The evolution of damage, the influence of various parameters

and failure criterion are mainly discussed. The thesis by Rogier Nijssen (10) also includes an important review of the composite fatigue literature. Although these reviews are still very significant, it is believed that at least one modelling approach needs to be introduced: stochastic modelling. This approach relies on reliability functions to describe the fatigue process and is exemplified by the work of Castillo et al. (118) or Kassapoglou (119).

In practice, parts made of composite materials are seldom subjected to CAF loadings. Most of the time, the fatigue load profile will exhibit at least some variability and CAF fatigue modelling approaches are not all equal in dealing with this variability of the load spectrum. Since the present study only makes use of empirical models and strength degradation models, only these approaches will be discussed in detail.

1.5.1.1 Empirical models

The empirical approach to the fatigue problem is dominated by the Wöhler (S-N) stress-life diagram. In such an approach, the life (in logarithm of cycle counts) of test specimens loaded in fatigue at a given load ratio $R = \sigma_{\min}/\sigma_{\max}$ and is plotted as a function of stress (Figure 1.5). In such plots, although life is the dependent variable, it is plotted as the abscissa. Note that in the S-N diagram representation, stress may have many definitions, the most important being:

a. minimum stress $\sigma_{\min}$,

b. maximum stress $\sigma_{\max}$,

c. stress amplitude $\sigma_a = \sigma_{\max} - \sigma_{\min}/2$,

d. mean stress $\sigma_m = (\sigma_{\max} + \sigma_{\min})/2$,

e. normalized stress, any of the above stresses divided by a reference such as ultimate strength S_u.

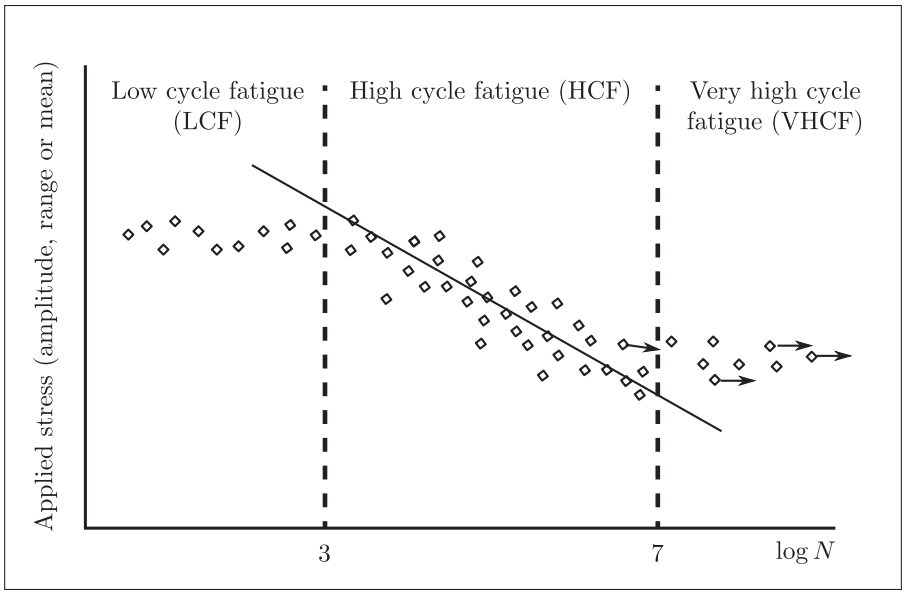

Figure 1.5 Schematic stress-life ($S-N$) curve. Applied stress may be either linear or logarithmic. Diamonds represent data points and arrows are runouts (censored results)

It is important to note that as a design tool for composite parts, the S-N curve is of limited use since it is only valid for a specific laminate under a specific loading and environmental condition. However, for research purpose, it easily shows changes in the overall material behaviour when curves obtained under different loading and environmental conditions are compared. As such it is often used in research.

The S-N curve is based on a multitude of measured life versus stress data points, over which a model is fitted. In most cases a linear model (either in the log-log or lin-log space) is used. If tensile loading is assumed, the most basic form is the power law model (120):

$$\sigma = CN^{-1/m} \rightarrow \log\sigma = \log C - \frac{1}{m}\log N, \tag{1.53}$$

where N is the number of cycles to failure under a stress σ and m is the fatigue exponent. Note that because in the overwhelming majority of cases, fatigue life is a decreasing function of stress, the fatigue exponent is explicitly negative. The parameter C is the

stress that would lead to a single cycle life, and is sometimes set equal to the static strength, although the model seldom naturally converges to the static strength. If the log-linear alternative is preferred, the fatigue relationship becomes:

$$\sigma = C - \frac{1}{m} \log N. \tag{1.54}$$

Again, parameter C may or may not be set to equal the static strength. As a single curve is usually insufficient to describe the fatigue life in low-cycle, high cycle and very high-cycle fatigue, it is generally advisable not to use the static strength in equation 1.53 or 1.54. However, for the purpose of comparing material performances, results are often plotted in terms of normalized stresses, even if the S-N curve does not converge to one.

There are two important advantages to these formulations. Firts, the model parameters for the median curve (50% survival) are easily obtained through linear regression analysis. Second, by assuming a log-normal distribution of life, a S-N curve for any desired probability of survival is easily obtained (121). It is also relatively simple to include fatigue runouts as censored data point in the assessment of fatigue curves through the use of the maximum likelihood estimation (MLE) method. Appendix I provides a summary of the least-square and MLE approaches for the evaluation of S-N curves at arbitrary probability of survival.

The most significant weakness of the S-N curve concept certainly is that it is only valid for one specific laminate under a given set of loading and environmental parameters. It is thus hard to generalize results and extensive testing is required to obtain sufficient information on the material. Other forms of empirical S-N relationships that relate to static strength or account for mean stress or stress amplitude effects are described in (115).

The empirical representation of fatigue data has been used to study the effect of material and load parameters on the fatigue of composites. The general effect of increasing mean stress for a given maximum stress level is to reduce the rate of fatigue damage. However,

the higher the mean stress, the more important time at load effects become, meaning that the fatigue lifetime approach the static fatigue (i.e. creep) behaviour (122). It is generally accepted that the most severe fatigue loading includes both tension and compression ($-\infty \leq R \leq 0$), followed by pure compression ($R > 1$) and pure tension ($0 < R < 1$) – (see e.g. (122; 123; 124)). Demers (125) also confirms that in tension-tension fatigue of glass-polyester coupons, the closer to unity R is, the longer the life.

A common representation of a material fatigue life, including the effect of R is the constant life diagram (CLD). CLDs are typically shown with σ_m as the abscissa and σ_a as the ordinate and where isolife lines (lines of constant life) are plotted. Often the only isolife represented is that of the endurance limit, i.e. for infinite life. Note that the existence of a fatigue limit in composites is debated.

An interesting historical review of the CLD concept is provided by Sendeckyj (126). The most common form of CLD probably is the (ill-named (126)) Goodman diagram, where a line tying the static strength on the abscissa to the endurance limit (or a fraction of the endurance limit) on the ordinate is the only isoline. A version of the Goodman diagram that can be shifted towards positive mean stress to account for the increased sensitivity of composites to reversed loading is typically used in the design of wind turbine blades (127; 128). Several other forms of CLD are available. Vassilopoulos, Manshadi and Keller discuss the performance of some formulation, underlining the fact that the simpler model, which linearly interpolates between S-N data at various R ratios, appears to be the most reliable, although it requires the most fatigue tests (129). They also note that the Goodman type formulation is usually conservative in its fatigue life assessment. This, combined with the limited testing it requires, is probably the main reason for its broad adoption.

Effects of multiaxial stresses are generally dealt with by using the S-N curves with a fatigue failure criterion adapted from static failure criteria, as exemplified by Hashin and Rotem (107). El Kadi and Ellyin (123) used a multiaxial strain energy criterion to assess

the effects of stress ratio and fibre angles. Their results showed that the slope of the fatigue curve is not strongly affected by the fibre angle, but that a significant downward shift of the whole curve occurs for small fibre angles. Assuming that damage was mainly due to the tensile load, they proposed a normalization scheme to deal with the effect of R.

Flore and Wegener (130) have proposed a phenomenological CLD based on four damage parameters accounting for mean stress and stress amplitude in tension and compression. Their model also used two weighting parameters for the damage due to tension and compression, which are shown to be relatively constant for different fibre dominated materials. Furthermore, by using the experimental observation that on a normalized stress basis, the S-N curves at $R = 0.1$ and $R = -1$ superimpose, they proposed that only $R = 0.1$ and static tension and compression data is required. They calibrated their model on four laminates and obtained good prediction for two other materials based on the calibrated model. One notable result is that the tension weighting parameter largely exceeds the compression one, confirming El Khadi and Ellyin's hypothesis that tensile stress dominate the damage process.

The S-N curve and CLD concepts are both limited to CAF. In practice, however, it is common that a fatigue load is not of constant amplitude. Despite the fact that it is known to be quite imprecise for composites, the miner's sum (or derivatives) is still mainly used to account for variable amplitude fatigue (VAF). The Miner's sum is given as:

$$\sum_{i=1}^{k} \frac{n_i}{N_i} = 1. \tag{1.55}$$

In equation 1.55, n_i is the actual number of cycles at the ith of k load levels, while N_i is the number of cycles at failure for the same load level. Failure of the laminate occurs when the summation equals unity (124).

In the context of wind energy materials, extensive material databases exist that cover static and fatigue properties of various materials under a multitude of loading conditions

and sample geometry. Two of the best known are the SNL/MSU/DOE Composite Material Database (131) and OptiDAT (132), which also includes the former FAST database. Multiple reports about these databases are also available.

An interesting article by Demers (125) reviewed fatigue results for several glass-polymer composites under tension-tension CAF. It is suggested that, if all fatigue data is pooled in terms of normalized fatigue stress $\sigma_{\max}/S_u$, a universal lower bound fatigue can be obtained, independent of material and test parameters. It is suggested that the 95% and 99% survival curves would respectively be given by:

$$\frac{\sigma_{\max}}{S_u} = -0.078 \log N + 0.790, \tag{1.56}$$

$$\frac{\sigma_{\max}}{S_u} = -0.078 \log N + 0.737. \tag{1.57}$$

The slope of 0.078 is relatively shallow considering the general rule of thumb that for unidirectional glass polymer composites in tension, the slope is about 0.1 for tension-tension fatigue. Sutherland (120) reports upper (good) and lower (poor) limits of slope parameters material as [0.1, 0.14] for tension-tension loading, [0.12, 0.18] for reversed loading and [0.07, 0.08] for compression fatigue. It is interesting to note that Nijssen (10) reports large errors in predicted fatigue life for very small discrepancies in the slope parameter. For variable amplitude fatigue, he reports that a 1% error in the S-N slope parameter may produce a 20% error in life, while a 5% change in slope may produce a 100% change in predicted life.

Finally, one last concept spurring from the empirical approach of the fatigue problem is Talreja's fatigue life diagram (FLD) concept (133; 134). Developed over several years, it is a representation similar to the S-N curve, but with the load expressed in the form of the maximum strain at the first cycle ϵ_{max}. However, the fatigue life diagram differs from the S-N curve by the fact that it is broken into three zones, each reflecting a different failure mode (Figure 1.6). At high strains (zone I), the failure is dominated by fibre breakage and statistical distribution of the fibre strength. Since fibre breakage will

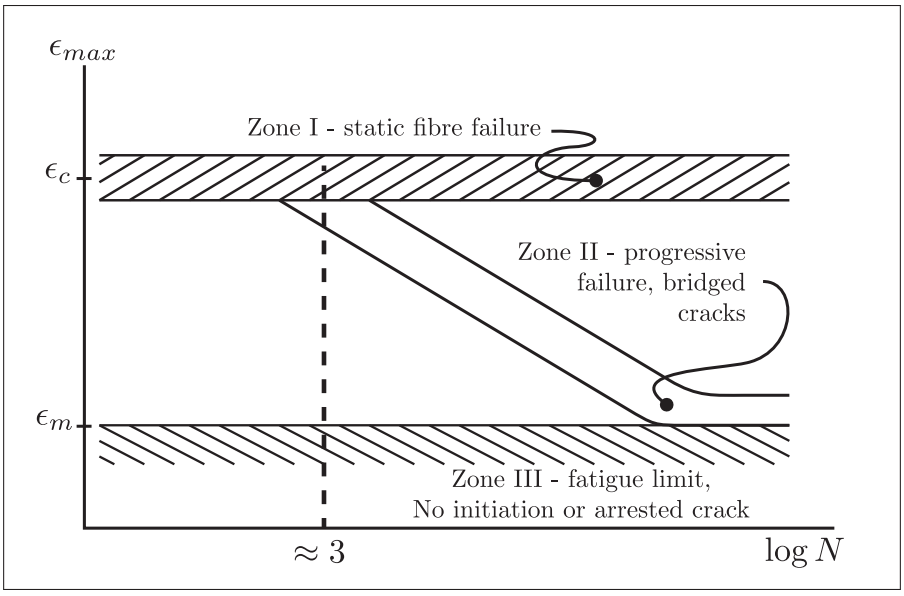

Figure 1.6 Fatigue life diagram for a hypothetical unidirectional composite

induce a significant stress concentration at the break and can quickly result in a cascade effect of further fibre breakage to failure, the life is short in this region — typically $N < 1000$ cycles for stiff fibres. This region is bounded by the fibre or composite static failure strain ϵ_c. The lower region (zone III) of the fatigue life diagram is bounded by the fatigue limit of the epoxy ϵ_m. In this lower region, either no damage occur, or cracks are arrested at fibres. In between is the region of fibre-bridged matrix cracking (zone II), where progressive matrix and fibre failure occurs. This intermediate region is the one typically represented by the S-N diagram. The interesting peculiarity of the FLD approach is that it allows one to anticipate the fatigue behaviour and failure mode of a laminate based on applied cyclic strains.

1.5.1.2 Strength degradation models

The strength degradation approach to fatigue modelling is possibly one of the most established approaches and is very present in the literature. In this approach, the hypothesis that a deterministic relationship exists between the number of load cycles that

a material has undergone, and the remaining strength of the material. This relationship would account for all the damage that accumulated due to fatigue loading. It is then assumed that the material fails when the remaining strength reduces to the applied stress or that a relationship exists between remaining strength and fatigue failure. It is also assumed that the ranking of a part on the static strength, residual strength distribution and fatigue life scale is the same. Put otherwise, it is assumed that the specimen which is initially the weakest of a sample in terms of static strength remains the weakest at any given number of fatigue cycle and that it would fail at the lowest cycle count. This latter assumption is often called the strength-life equal rank assumption (SLERA). By integrating the relationship between $N = 1$ (static failure) and $N = \infty$ (at zero load), the residual strength S_r as a function of N is obtained. By rearranging the equation and accounting for failure at $S_r = \sigma_{max}$ then provides the S-N relationship.

Advantages of the strength degradation approach include the ability to account for a cycle by cycle effect of the fatigue damage without the need for detailed analysis of the damage. The damage state is simply phenomenologically linked to the residual strength. Moreover, by explicitly stating a static strength distribution, the probabilistic assessment of failure is also allowed. Furthermore, using the static life distribution to assess the probability of fatigue failure reduces the number of fatigue tests required for assessing the fatigue life distribution. The main weakness of the method is that each of the tests that allow for the verification of one of the three hypotheses is destructive. It is thus impossible to verify all hypotheses for all specimens. Only either the static strength (initial strength and specimen ranking), the residual strength or the fatigue life can be measured for any given specimen. A select review of the literature about strength degradation models is provided here. Both early models and more recent formulations are discussed.

Sendeckyj (115) attributes the concept to Halpin, Johnson and Waddoups (135), who showed that Weibull statistics and a power law growth equation for a crack in a homogeneous material where the pre-exponential factor is proportional to the far field work

input could, under the hypothesis that the failure load is proportional to the root of the crack length, predict the failure time under a random load spectrum.

However, Broutman and Sahu (136) also proposed a linear strength degradation model at about the same time. Their strength degradation rule (for CAF) took the form:

$$S_r = S_0 - (S_0 - \sigma_{max})\frac{n}{N}, \tag{1.58}$$

with S_0 being the initial static strength, while n and N respectively stand for the actual and failure cycle count. Based on this formulation, they proposed a cumulative damage rule in the form of:

$$\sum_{i=1}^{k}\left(\frac{S_0 - \sigma_{max,i}}{S_0 - \sigma_{max,n}}\right) = 1. \tag{1.59}$$

Hahn and Kim (137) used the concept for the case of static-fatigue (creep) in composites, but rather than considering a single crack extension, they modelled a rate phenomenon. They used a strength degradation rule in the form of:

$$\frac{\mathrm{d}S(t)}{\mathrm{d}t} = -AS(t)^{-m}, \tag{1.60}$$

where S is the strength, A is a stress-dependent parameter and m is a material constant independent of stress or time t. They showed that if the static strength distribution is known and the relationship between residual strength and life is known, then the distribution of life is also known (both two-parameter Weibull).

Yang and Liu (138) demonstrated similar principles for the fatigue of composites using a two-parameter Weibull distribution of shape parameter α and characteristic strength β for strength and a power law equation for strength degradation in the form:

$$\frac{\mathrm{d}S_r(n)}{\mathrm{d}n} = -\frac{f(\sigma_{max})}{cS_r(n)^{c-1}}, \tag{1.61}$$

where n is the cycle count and c is a constant. It was shown that for long life at low stress, the life distribution would also be a two-parameter Weibull and from there obtained that $f(\sigma_{max}) = \beta^c K \sigma_{max}^b$, with K and b respectively standing for the intercept and slope parameter of the resulting power law S-N curve. On the other hand, when σ_{max} is high, the life distribution is a three-parameter Weibull that needs to be truncated at one cycles to account for first cycle failure. Note that K and b are not obtained from fatigue data alone, but rather from specific statistical procedures. A reasonable fit was obtained between the measured and predicted S_r. The model was later modified through the addition of other parameters to account for stress ratio and fatigue life fraction dependence of strength degradation, but according to Philippidis and Passipoularidis (139), these modifications do not really improve the model fit, but render the experimental evaluation of model parameters extremely burdensome.

Withney (140) used a power law fatigue curve with a two-parameter Weibull fatigue life distribution to obtain probabilistic fatigue curves. By assuming that the Weibull shape parameter is independent of the stress amplitude σ_a, he proposed a data pooling technique in order to maximize the confidence for a given fatigue data set. He also demonstrated that his approached could be obtained from a strength degradation model. By proposing the use of the maximum likelihood method for parameter estimates, Whitney also allows for the inclusion of runouts in the parameter assessment.

Sendeckyj (141) proposed a method based on the following degradation equation:

$$S_r = \sigma_{max} \left[\left(\frac{S_{eq.}}{\sigma_{max}} \right)^{1/d} - c(n-1) \right]^d . \tag{1.62}$$

In equation 1.62, $S_{eq.}$ is the equivalent static strength of a fatigue specimen, which is its initial static strength as obtained from fatigue results, c is a parameter which would represent the length of the low cycle fatigue plateau and d is a slope parameter. $S_{eq.}$ would be obtained by solving equation 1.62 for $S_{eq.}$ based on $S_r = \sigma_{max}$ at $n = N$, the number of cycles at failure. Combining this degradation rule with the hypothesis that $S_{eq.}$ follows

a Weibull distribution, it is possible to assess the probabilistic S-N curve. A landmark review of the best practices for modelling using the strength degradation approach is also proposed by Sendeckyj (115), which proposes modifications to the original model to account for the effect of R and fatigue life fraction dependence of strength degradation.

Reifsnider and Stinchcomb (142) used a strength degradation equation similar to equation 1.58, but where an exponent is added to the last term to allow for a non-linear effect of the life fraction. The equation is used in their 'critical-element model' which assumes that one 'critical element' of a laminate (e.g. type of ply) will be responsible for fatigue failure through strength degradation, but other plies — as 'subcritical elements' will contribute to the strength degradation.

More recently, D'Amore and multiple collaborators (143; 144; 145) provided a simple two parameter strength degradation rule of the form:

$$\frac{\mathrm{d}S_r(n)}{\mathrm{d}t} = -An^{-m}. \tag{1.63}$$

An interesting aspect of the work is that it included an explicit for the effect of stress ratio R in the form of a linear relationship:

$$A = A_0\sigma_{max}(1-R). \tag{1.64}$$

These equations were proven to provide relatively good S-N curve prediction. This model was modified by Epaarachchi and Clausen (146) so that it could account for the effects of frequency, of R and of the main fibre angle.

Nijssen (147) reviewed and explored the assumptions and formulation of strength degradation models in the VAF context. A notable particularity of his work is that it explored the effect of compressive fatigue loads on S_r. He concluded that strength degradation due to compression only occurred abruptly towards the end of the fatigue life. Also,

he concluded that as far as fatigue modelling is concerned, the use of a linear strength degradation might be adequate.

In most of the previously discussed instances, the actual strength degradation rule was not verified, but was deemed adequate based on the fatigue curve prediction. Philippidis and Passipoularidis (139) reviewed and tested many S_r predictions against experimental results for four materials (carbon-epoxy and glass-polyester) and found that they were, in most cases, inadequate. They also found that the more complex models seldom paid back by with improved predictions. In this work, they also modified Broutman and Sahu's (136) linear model (equation 1.59) so that it could provide a stochastic evaluation of the strength. Furthermore, they provided a way to make the model non-linear by adding a life-fraction dependent exponent k to the last term of equation 1.58 with:

$$k = k_0 \exp(k_1 n/N), \tag{1.65}$$

where k_0 and k_1 are empirical parameters. Based on their results, it was determined that while their own model provided the best probabilistic residual strength prediction, it required significant experimental efforts to evaluate its parameters. On the other hand, Broutman and Sahu's linear model fared relatively well at higher stresses and was consistently conservative at lower stress. It was therefore recommended over models based on degradation rules by Yang (equation 1.61) or Sendeckyj (equation 1.62). Passipoularidis and Philippidis (148) obtained similar results for unidirectional glass-epoxy.

D'Amore et al. (149; 150), reported that their earlier model prediction of S_r was consistently low when compared to experimental data. In fact, the predicted strength decay was too gradual. The approach modelled a wear-out of S_r while experiments showed that the behaviour was more that of a sudden drop. Relying on the SLERA hypothesis, they took a new look at their original model and proposed to use the life distribution reliability function to model the residual strength distribution. They showed that the confidence bounds of the predicted residual strength distribution were very representative

of the available residual strength data. According to the authors, based on the calculated confidence bounds, the wear-out model they used turns out to be a special case of a sudden drop model that is a good predictor of the residual strength. The model was used by Ma et al. (151) in exploring the fatigue behaviour of $\pm 45^\circ$ carbon-epoxy and carbon-PA6. It was found that even up to 10^7 cycles, carbon-epoxy laminates showed no significant strength degradation at $R = 0.1$ below $\sigma_{max} = 0.63 S_u$, while carbon-PA6 strength did not degrade at 4×10^6 cycles at $R = 0.1$ below $\sigma_{max} = 0.48 S_u$, suggesting the existence of a fatigue limit.

1.5.2 Statistical considerations

Fatigue is a stochastic process which exhibits great variability and is often heteroscedastic (i.e. the variance is not homogeneous). As for most fatigue problems a given reliability is targeted, the basic S-N curve representing a 50% probability of survival is unsuitable. Various methods are available for estimating the S-N relationship at other given probability of survival.

The traditional approach, reflected in standards such as ASTM E739 (152) or ASTM STP313, (121) is to assume a normal distribution of the logarithm of life N to obtain an estimate of the life at a given probability of survival and stress level. An approximate S-N curve at 95% probability of survival is often obtained by simply shifting the S-N curve by two standard deviations to towards shorter lives.

A problem of the traditional approach is that of extrapolation of confidence intervals outside the data range. It usually deemed unsafe to use the classical approach beyond the data range. However, many industries — wind energy being one of them — require structural durability up to a life which cannot be practically simulated in laboratory experiments. Sutherland and Veers (153) propose a method to account for the reduced reliability of the prediction outside of the data range. This approach is based on previous work by Ronold and Echtermmeyer (154).

Although this simple approach may be sufficient in many applications, it does not reach the level of accuracy that is required by safety or cost-critical industries such as civilian aviation or alternative energy production. This is one of the drivers that led to the many probabilistic strength degradation and stochastic models discussed previously. For the aerospace industry, more stringent approaches are discussed in a FAA report (155).

It is interesting to note that because of the possible extrapolation of the fatigue curves outside of the data range and because of the heteroscedasticity of fatigue life, traditional balanced experimental plans such as those in standards such as ASTM E739 (152) may not be the most efficient in producing accurate estimate of fatigue life at a given probability of failure. Also, the usual approach of performing a linear regression on the logarithm of life as a function of stress or strain cannot deal with runouts — test interrupted before failure or due to technical problems or because a predefined maximum test time was reached. This inability to deal with runouts results in the loss of information contained in those samples and in inefficient test methodologies.

Alternative analysis methods such as the MLE can deal with runouts effectively and provide improved estimates of S-N curves at different probabilities of survival. A good reference on the subject is Nelson (156). Some information on the application of MLE to the fatigue problem and a comparison with the traditional approach are given in Appendix I.

Unbalanced test plans where the load levels and number of specimens per load levels are not uniformly distributed may increase test efficiency by improving estimates of the variability while testing fewer specimens. Such approaches are discussed in Nelson (156) and in the recent paper by King et al. (157).

1.5.3 Effects of load rate and temperature on the fatigue performance of composite materials

As the mechanical behaviour of polymer matrix composites is strain-rate sensitive, researchers often try to account for the effect of frequency when modelling fatigue. Moreover, from a practical standpoint, the frequency at which fatigue tests are conducted is one of the main determinants of a test duration, and thus of resource requirements for a given test programme. It is therefore desirable to use the highest possible frequency that does not influence the test outcome. Finding the 'safe' frequency is, however, easier said than done and is most likely to rely on preliminary experiments. As a reference, ASTM D 3479 (158) warns that a temperature increase of 10℃ due to hysteretic heating at higher frequency results in a significant change in fatigue strength.

A discussion on the trends in fatigue frequencies used for research on composite materials durability is proposed by Kotik and Ipiña (159). From their report, it appears that there may be a trend towards lower test frequencies in recent years.

Bailey et al. (160; 161) propose methods to track the specimen temperature and to adjust the frequency during the test so that a target temperature is maintained throughout the test while maximizing the test frequency and minimizing test duration (note that ASTM D 3479 prescribes a constant frequency for a given test and for all load levels meant to build a S-N curve). By the use of an adaptive frequency up to 15 Hz, Bailey (161) obtained a S-N curve for woven carbon–epoxy laminate that was very close to that obtained at a constant frequency test at 4 Hz.

In the context of very high cycle fatigue (VHCF), Adam and Horst (162) have suggested that a way to limit specimen hysteretic heating would be to limit the loaded volume to a fraction of the specimen. Their report states that four-point bending appears to be the optimal loading mode for this purpose. The problems related to VHCF should be of particular interest for the wind energy sector, where turbine life would reach 30 years of almost continuous operation.

In the work of Apinis (163) results obtained for LM-L1 unidirectional glass–polyester composite at $f = 17$ Hz and $f = 400$ Hz suggest that, if specimen temperature is controlled in order to avoid hysteretic heating of the specimen, comparable fatigue life can be obtained. However, this may not be the case with angle-ply composites or more complex laminates where the viscoelastic response may be more affected by strain rates.

Kahirdeh, Naderi and Khonsari (164) used thermography and acoustic emissions to monitor the damage in reversed bending specimens of woven glass-epoxy composites at 10 Hz. Their results suggest that cooling may have a significant effect on the rate of acoustic emissions and fatigue life of the composite.

The expected effect of frequency on the fatigue strength of composites has been summarized by Hahn and Turkgenc ((165), p.17) as:

> [...] at low frequency ranges where there is negligible heat dissipation, as the load frequency increases, cycles to failure increase also. As higher frequency ranges are considered this increase is at a slower rate. When there is excessive heat dissipation, however, a reverse trend can be observed.

This quote would be in agreement with results from Mandell and Meier (122) who tested glass–epoxy composites at 0.01 Hz, 0.1 Hz and 1 Hz under square-wave loading. Mandell and Meier suggest that this may be due in part to time under load considerations. On a cyclic basis and from a strength degradation modelling perspective, Mandell and Meier argue that the effect of frequency would be dependent on the rate of strength degradation, load range and cyclic load waveform (influencing the time-at-load). For a given maximum stress, lowering the stress amplitude increased the failure time towards that for creep failure. Nevertheless, failure times were consistently lower for fatigue than for creep. Note, however, that this work is performed at high stress and for relatively short fatigue lives.

Eftekhari and Fatemi (166) studied the effect of frequency on the fatigue of short fibre thermoplastic composites and observed that the negative effect of hysteretic heating could

in some cases occur even at frequency below 1 Hz. In their analysis, they state that the reduced hysteresis loop at higher frequency may explain, at least partially, the fatigue life improvement related to a frequency increase (in the absence of excessive heat). Another possible explanation would be a result of heating at crack tips that could result in crack blunting.

Masters and Reifsnider (108) have reported that load frequency may have an effect on the number of cycles required to attain the CDS. For example, the CDS was reached in about 1000 cycles at 1 Hz and 1×10^6 cycles at 15 Hz for quasi-isotropic graphite-epoxy laminates in $R = 0.1$ fatigue.

Sun and Chan (167) proposed a relationship based on crack propagation theory in viscoelastic media for predicting frequency effects and also including temperature effects. The model is fitted to fatigue results from $[\pm 45]_{2S}$ carbon–epoxy laminates with a centre-hole. Test frequencies were 1 Hz, 3 Hz, 10 Hz and 30 Hz. Interactions between frequency and load levels were noted, with higher load level showing peak life at lower frequencies. Sun and Chan's model is as follows:

$$N_f = N_{f_1} \frac{f}{f_1} \exp\left[\eta \left(\frac{\Delta T_{f_1} - \Delta T_f}{T_0}\right)\right]. \tag{1.66}$$

In equation 1.66, N is the fatigue life f is the frequency, ΔT is the temperature rise near the hole (average), T_0 is room temperature and η is a material parameter (in the range of nine for the reported results). Subscripts f and f_1 respectively stand for the desired and reference frequencies. Prediction and experiments were in relatively good agreement.

Sun and Chim (168) studied time at load effect on the same material and geometry as Sun and Chan (167). The effect was studied by periodically interrupting the fatigue cycling and statically loading the material at the maximum cyclic stress. It was surprisingly found that such creep-fatigue tests resulted in higher lives that ordinary fatigue. It was hypothesized that the effect was due to plastic strains accumulating at matrix crack tip that results in compressive stresses at the crack tip when cyclic loading was resumed,

thus improving fatigue life. To verify the hypothesis, two-block tests were performed, where frequency was varied from 1 Hz in the first block to 10 Hz in the second block or vice-versa. According to the postulated hypothesis, the low-high frequency cycles should show higher lives due to increased time-at-load at low cycles. Even though the number of specimens was limited, the hypothesis was clearly verified with a threefold increase in life for the tests started at low frequency.

Saff (169) also provides results for frequency effects on carbon-epoxy laminates. $[\pm 45]_{2S}$ (as Sun and Chan), and laminates [48/48/4] and [4/80/16] (in percent of $0°/\pm 45°/90°$), but the specimens were cooled by air between -7℃ and -1℃ during fatigue cycling. However, contrary to expectations, cooling the specimens did not appear to reduce the frequency effects. The results for the different laminates suggest that the frequency effect may be related to the level of shear stress in the matrix. Saff also proposed the following relationship to predict the temperature rise at the hole for a given frequency (ΔT_f), which is meant to be used with equation 1.66.

$$\Delta T_f = \frac{f}{\alpha}\left[\left(\frac{\Delta\sigma}{S_u}\right)^2 - \beta\right] \tag{1.67}$$

In equation 1.67, α and β are empirical parameters, $\Delta\sigma$ is the stress range and S_u is the static strength.

An estimate of specimen temperature rise based on viscoelasticity and heat transfer was proposed by Hahn and Kim (170). This midplane transient temperature T_s estimate at time t is given by:

$$\left(\frac{T_s - T_r}{T_{se} - T_r}\right) = 1 - \exp\left(\frac{-\beta K t}{\rho c}\right), \tag{1.68}$$

where K is the heat transfer coefficient, ρ is the mass density, c is the specific heat, T_r is the ambient temperature and where β is the surface to volume ratio:

$$\beta = \frac{2(W+h)}{Wh} \tag{1.69}$$

with W and h respectively standing for the specimen width and thickness. Finally, T_{se} is the equilibrium temperature given by:

$$T_{se} - T_r = \frac{q}{\beta K}. \tag{1.70}$$

In equation 1.70, q is the heat generated by unit of time. Although scatter was important, agreement was relatively good with experimental measurements.

By combining linear viscoelasticity relationships with heat transfer equations, Katunin et al. (171) were able to obtain equations for the temperature field within a composite sample. This estimate of the temperature field relies on DMA tests at various temperatures and frequencies and the resulting TTSP master-curve and $T_g(f)$ Arrhenius relationships to provide information on the hysteretic heating behaviour of the material. However, the model was not validated experimentally and its reliability remains to be challenged.

Strain-rate effect on the static and fatigue strength of $[\pm 45]_{5S}$ glass–epoxy composites was also investigated by Kujawski and Ellyin (172). Test frequencies were 0.417 Hz and 3.6 Hz. They have shown that an important accumulation of viscous cyclic strain occurred during fatigue loading and that the rate of accumulation varied with both the frequency and the expanded life fraction. The rate of cyclic strain accumulation was initially high, but decreased sharply in the first part of the test, before reaching an approximately stable value. Just before failure, the cyclic strain accumulation rate would increase dramatically. Also, as expected, higher strain rates resulted smaller hysteresis loops. This is of particular interest to the current project as DMTA analyses under shear loading by Adams and Singh (39) have shown that for epoxy resins, low-temperature transitions could occur at temperatures likely to occur in northern regions (around $T = -40$℃). As this low temperature transition is associated to a marked increase of loss factor, it is possible that low temperatures have deleterious effects on fatigue performance of matrix dominated composites.

Lin et al. (173) also studied the effect of frequency on the fatigue of ±45 laminates, but made from carbon-PEEK (semi-crystalline thermoplastic) composites with a $v_f = 0.6$ and $T_g = 143°C$. They performed $R = 0.1$ fatigue tests at 1 Hz, 5 Hz and 10 Hz and measured very high temperature increases. At 1 Hz, the temperature rose to a peak of about 80℃, but exceeded 170℃ at 5 Hz and 10 Hz. However, after those peak temperatures were reached at about 100, 1000 and 10000 cycles respectively for 1 Hz, 5 Hz and 10 Hz, the temperature decreases substantially because the softened resin allowed for a fibre realignment to 33°, thus reducing the viscoelastic and hysteretic effects. The resulting S-N curves were, of course, strongly non-linear.

Kharrazi and Sarkani (174) performed similar tests to those of Sun and Chan or Saff, but on centre-hole specimens of glass–vinylester composites with $[0/90]_{nS}$ and $[\pm 45]_{nS}$ specimens loaded at 0.3 Hz, 1 Hz and 3 Hz. On the one hand, fatigue lives at the two lower frequencies did not differ significantly. On the other hand, the fatigue life at 3 Hz was significantly lower than at the lower frequencies. For the cross-ply laminate, the difference was most important at higher loads and the log-log linear curves converged at lower stresses. For the angle ply laminate, however, a much steeper slope in the low cycle region was reported at 3 Hz, accompanied by a feature that was absent from other conditions, that is an apparent fatigue limit. Kharrazi and Sarkhani have also shown that the damage growth rate, as measured by stiffness degradation, is fatigue sensitive and that there are synergistic effects with the cycle count and load level. Other results were in agreement with the literature previously cited.

Shah and Chamis (11) have performed a sensitivity analysis on fatigue life for random parameters such as constituent properties, ply thickness, constituent ratios and frequency. Their simulations computed the cumulative probability density distribution of fatigue life for a $[0/\pm 45/90]_S$ graphite–epoxy laminate subject to sinusoidal tensile loading. First-ply failure is considered as the failure criterion. Their simulations are in qualitative agreement with the literature previously discussed, that is a reduction of fatigue life at high loads when the frequency is increased. Other interesting results include the conclusion that ply

thickness is the most significant driver of fatigue life at low frequency and low load, while the matrix strength, constituent stiffnesses and proportions were most determinant at higher frequencies and load amplitudes. This finding is of particular interest in the wind energy sector where the combination of thick laminates (and Plies) are used in relatively lightly loaded structures (as expected lifetimes are high).

Even though some would argue that time and temperature effects need to be considered together, the effect of temperature alone on the fatigue behaviour has also been the subject of several studies. As will be seen, a large fraction of the work on the topic is qualitative. Moreover, it mostly relates to aerospace materials such as carbon prepregs exposed to either very high or cryogenic temperatures. The materials and environmental conditions are therefore quite different to those encountered in the wind energy industry.

Rotem and Nelson (175) proposed a model for the effect of temperature on the fatigue of graphite-epoxy composites by applying a vertical shift factor to the static strength and changing the slope of the S-N curve. Their model predicts failure when the fatigue function F reaches unity, with F being given by:

$$F_i = a_i(T)\left(\frac{1}{a_i(T)} - b_i \log N\right) - a_i^{S'}. \tag{1.71}$$

In equation 1.71, b_i is the fatigue slope and $a_i(T)$ is the slope correction factor and $a_i^{S'}$ is the modified static strength shift factor, given by:

$$1 - a_i^{S'} = \sqrt{\frac{T_0}{T}}. \tag{1.72}$$

In equations 1.71 and 1.72, T and T_0 respectively represent the analysis and reference temperatures. Note that according to the experiments by Rotem and Nelson, if the modified static strength — that is shifted by $a_i^{S'}$ — is used in the fatigue function, $a_i(T) = 1$. This model was adapted by Xiao (176) for taking frequency effects into

account. He used Hahn and Kim (170) temperature increase prediction to iteratively shift the S-N curve.

Chamis and Sinclair (177) performed a sensitivity analysis of 15 parameters on the fatigue resistance of Boron-epoxy, graphite epoxy and carbon-epoxy unidirectional laminates through a multi-step regression analysis. The parameters included initial static strength $S_{u,0}$, test temperature T, the glass transition temperature of the matrix in the dry and moisture saturated (wet) condition T_g, T_{gw}, previous exposure time t_e, temperature T_e and number of fatigue cycles N. Quadratic interactions between the parameters were also studied and interactions were indeed significant in the case of T, M and N. The resulting generalized prediction equation is as follows:

$$\frac{\sigma_{\max}}{S_{u,0}} = \sqrt{\frac{T_{gw} - T}{T_g - T_0}} - 0.10 S_{u,0} \log N. \tag{1.73}$$

The slope predictions for carbon-epoxy composites appear to be in adequate agreement with experimental results, but the global prediction is quite conservative.

The work of Sims and Gladman(92) deals with the $R = 0.1$ fatigue of woven glass–epoxy composite loaded in the fibre direction at temperatures ranging from -150℃ to 150℃. Their results show that the S-N curves at different temperatures are superimposed when plotted relative to σ_{max}/S_u (with S_u being that at the specified temperature).

Hartwig and Knaak (178) report fatigue strength (stress for a life of 10×10^7 cycles) for different fibre reinforced epoxy composites. For example, they report that the fatigue strength of unidirectional glass-epoxy at 77 K is only $0.25S_u$, while it is about $0.65S_u$ for unidirectional Kevlar and $0.85S_u$ for carbon. The fatigue strength of quasi-isotropic carbon composites is reported at $0.65S_u$. Although there is no room temperature benchmark in the article, this would represent a small improvement when compared to contemporary data from Weeton et al. (179).

Further experimental work by Toth et al. (93) showed that cryogenic temperatures (20 K, -253℃) led to an increase in static tensile strength and $R = -1$ fatigue lives in triaxial $[-45/0_3/45/0_3/\pm 45/0_3/45/0_3/-45]$ laminates. However, they were unable to quantify the increase in static strength as their test frame was not strong enough to break the cold specimens. Furthermore, all their tests resulted in lives shorter than 100 000 cycles at loads less than 20 % of the laminate ultimate tensile stress and at a temperature of 300 K. Such short lives appear to be improbable for modern laminates.

Sys (180) also provides some $R = 0.1$ and $R = -1$ fatigue test data on $\pm 10^\circ$ glass–unsaturated polyester composite of $v_f = 0.5$. Tests are performed at -20℃, 20℃ and 50℃. Although very little analysis is provided, results suggest that on a strain basis, the low temperature had little effects on fatigue performance.

Tang et al. (181; 182) propose a cumulative damage model with a damage parameter D given by $D = 1 - E/E_0$, where E_0 is the initial modulus and E, the residual modulus after N cycles. The degradation model, which incorporates the maximum stress $\sigma_{\max}$, fatigue stress ratio R and frequency f is given by:

$$\frac{\mathrm{d}D}{\mathrm{d}N} = \left(C_1 + \frac{C_2}{f}\right) \frac{(\sigma_{\max}(1-R))^m N}{(1-D)^n}, \tag{1.74}$$

with C_1, C_2, m and n being empirical material parameters. The rationale for the frequency effect is based on two considerations. First is the empirical observation that the m and n parameters were not affected by frequency in their experiments on glass-vinylester composites of $v_f \approx 36\%$ tested under $R = 0.1$ fatigue loading at 2 Hz and 10 Hz. Second is the previously discussed assumption that the fatigue strength is proportional to the test frequency. After expansion in Taylor's series and noting that for their material $C_1 = 0$, equation 1.74 can be rewritten as:

$$2m \log \sigma_{\max} + \log N_f = \log C_2, \tag{1.75}$$

where N_f is the number of cycles at failure. Assuming that the slope followed an Arrhenius relationship with temperature, it follows that:

$$m = m_0 \exp \frac{E_a}{RT}, \tag{1.76}$$

with m_0 being the pre-exponential slope factor, E_a the activation energy, R the gas constant and T, the temperature. The model provided an adequate fit to the experiments. It is interesting to note that Tang et al. (181) report that the S-N curve plotted on a normalized stress basis appear to rotate around a fulcrum at 1000 cycles (clockwise rotation of the S-N curve with increasing temperature). This would be consistent with Talreja's fatigue life diagram which locates the passage from a stochastic (static) fibre break failure mode below 1000 cycles to a progressive fibre bridged matrix cracking mode above that threshold (see e.g. (134)). However, their temperature tests were run at 10 Hz, which might have been high enough to result in hysteretic heating. Moreover, their lowest test temperature was limited to 4℃.

Reifsnider's and his co-workers have also devised an elaborate method, called the critical clement model (CEM) and strength evolution integral (SEI), to predict long-term behaviour of composite materials. The model is the result of many years of research and has been synthesized by Reifsnider, Case and Duthoit (183). The major hypothesis of the CEM is that failure of a laminate is driven by the failure of one of its constituent laminae or regions, namely the critical element. Modelling the failure of the critical element thus allows for prediction of the laminate failure. In practice, the critical element is often the plies oriented in the main load direction, possibly nearby to a defect or geometric feature such as a hole. All other parts of the laminate are considered subcritical elements and the effect of them being damaged or failed will translate in a stress redistribution to the critical element. The model is meant to predict material behaviour under various environments and can incorporate many combined damage mechanisms such as creep, fatigue and thermo-oxidation. The approach relies on kinetic theory and point-wise definition of stress and strength over the material and appears to have the capacity to accurately

model the evolution of strength in the critical element through the SEI:

$$F_r = 1 - \int_0^{\tau_1} 1 - F_a \left(\frac{\boldsymbol{\sigma}_{ij}(\tau)}{\mathbf{S}_{ij}(\tau)} \right) k\tau^{k-1} \mathrm{d}\tau. \tag{1.77}$$

In equation 1.77, F_r is the remaining strength for the designated failure mode, k is a material parameter, $\tau = t/\hat{\tau}$ is the time relative to the characteristic (or average) action time $\hat{\tau}$, $\boldsymbol{\sigma}_{ij}(\tau)$ and $\mathbf{S}_{ij}(\tau)$ are the time-dependent stress field and strengths in the i, j materials principal directions. Finally, F_a is a scalar failure function such as the maximum stress criterion:

$$F_a = \left[\frac{\sigma_{11}}{S_{11}}, \frac{\sigma_{22}}{S_{22}}, \frac{\sigma_{12}}{S_{12}} \right] \leq 1. \tag{1.78}$$

In the particular case of fatigue, posing a power law fatigue strength equation with failure at N cycle and recalling that the number of cycles n at frequency f is given by $n = ft$, the SEI can be rewritten as:

$$F_r = 1 - \int_0^{t_1} 1 - F_a \left(\frac{\boldsymbol{\sigma}_{ij}(t)}{\mathbf{S}_{ij}(t)} \right) k \left(\frac{ft}{N(t)} \right)^{k-1} \mathrm{d} \left(\frac{ft}{N(t)} \right). \tag{1.79}$$

The main strength of this model, its flexibility, is also its main weakness. Indeed, the approach relies on an extremely detailed knowledge of a material's behaviour and of its evolution, as well as the evolution of the stress field over time. Unfortunately, such detailed knowledge can only be obtained through considerable experimental efforts. Note that since the method was incorporated in a commercial computer code (MRLife) extensive documentation seems difficult to find in the public domain.

Epaarachchi and Clausen (146) have developed a model based on equation 1.63, with provisions for dealing with temperature effects. However, they did not model such effects explicitly. Their work included a discussion and some data on the effect of temperature on fatigue and the model fit on fatigue data was generally quite good.

Bureau and Denault (184) studied the effect of temperature in the range between -40 ℃ and 50 ℃ on the $R = 0.1$ flexural fatigue of two composites, namely 2-2 glass twill–

polyester and biaxial glass fabric–polypropylene composites. Both laminates had $v_f = 0.6$. According to their results, if normalized by the static strength at their respective temperatures, S-N curves for the glass–polyester were superimposed, while those of the glass–polypropylene matrix composite showed a small improvement in fatigue life. This was attributed to a possible transition region in the thermoplastic that was absent in the thermoset. The superimposed curves found by Bureau and Denault are in agreement with the earlier results by Sims and Gladman. However, even for thermosetting matrix composites, this simple behaviour is not always borne out by experiment. Brassard (185) found a statistically significant downward shift of the normalized fatigue curve at low temperature under $R = 0.1$ fatigue for UD glass–epoxy at -40℃ and 20℃.

Kumagai et al. (186) and Shindo et al. (187) report static and $R = 0.1$ fatigue results for plain weave E glass-epoxy composites at room, liquid nitrogen (77 K) and liquid helium (4 K) temperatures. Their results show a change in static behaviour from a non-linear response with brittle failure at room temperature to an almost bilinear response with some evidence of progressive failure at cryogenic temperature. The tensile modulus of the composite increased by about 20% and 25% at 77 K and 4 K, while the S_u increased by 89 % and 92 % at the same temperatures. Failure strains also almost doubled at low temperatures, from about 1.5 % to around 3 % at cryogenic temperatures. At around 1 % strain, the inflection point of the stress-strain curve at low temperature is lower than the initial (room temperature) failure strain. The stress at the inflection point is also about 10 % lower than the room temperature failure stress. These changes in static behaviour translated into comparable changes in the low-cycle fatigue behaviour of the composite. However, in the high cycle fatigue regime, the slope of the S-N curve seems to gradually increase, resulting in lower fatigue life at 4 K compared to 77 K, but still higher (for a given maximum stress) than at room temperature at least up to 10^6 cycles. If the stress is normalized by S_u, it appears that the fatigue limit is somewhat reduced at 4 K, from around $0.3S_u$ at room temperature and 77 K, to $0.2S_u$.

Kumagai (186) also report strength and stiffness degradation result for the same plain-weave E glass-epoxy material and temperatures. It is seen that at room temperature, a small initial increase in the strength and stiffness (up to 10^3 cycle) was noted, followed by an abrupt degradation to approximately $0.9E_0$ and $0.65S_{u,0}$ at 10^5 cycles (with the 0 subscript standing for the initial value). On the other hand, at cryogenic temperatures, the stiffness degradation with increasing log-cycles was almost linear from the start and down to $0.68E_0$ at 10^5 cycles for fatigue at 77 K and down to $0.65E_0$ for 10^4 cycles at 4 K. The stiffness degradation rates are thus markedly increased at cryogenic temperatures. Strength degradation at cryogenic temperatures showed a slow decay up to $0.95S_{u,0}$ for 10^3 cycles at 77 K or 10^2 cycles at 4 K, followed by an increasing degradation rate leading to strength reductions to $0.7S_{u,,0}$ for 10^5 cycles at 77 K and $0.45S_{u,0}$ for 10^4 cycles at 4 K. Strength degradation rates at room temperature and 77 K are thus comparable, but increase significantly between 77 K and 4 K.

Jen et al. (188) provide static and fatigue results, including strength and stiffness degradation measurements, for cross-ply and quasi-isotropic AS4-PEEK laminates at temperatures ranging from 25℃ to 150℃. The materials $v_f = 0.61$ and the thermoplastic resin is reported to have a $T_g = 143°\text{C}$ and melt temperature $T_m = 343°\text{C}$. Crystallinity is not reported. Gradual reductions of S_u by 20 %–25 % are measured up to T_g, but then strength remains about constant to 175℃. Similar trends, but with a reduction of about 10 % are seen for stiffness. Normalized S-N curves of both laminates show important reductions in the fatigue performances at even moderately high temperatures. An initial 25 % reduction of fatigue strength between 25℃ and 75℃ is reported for both laminates, but the rate of fatigue strength reduction then slows and the maximum measured degradation of fatigue strength is about 40 % at 150℃. Gradual strength degradation upon fatigue cycling was also observed, and the degradation rate increased with temperature. The authors also proposed a model — inspired by earlier work by Chamis and Sinclair (177)

but using the thermoplastic's T_m instead of its T_g — which is of the following form:

$$\frac{S_{\max}}{S_{u,0}} = \sqrt{\frac{T_m - T}{T_m - T_0}} - \frac{B}{S_{u,0}} \log N. \tag{1.80}$$

In equation 1.80, T_0 is the temperature of the reference fatigue data and B is a material parameter representing the materials fatigue sensitivity and which is considered temperature independent in the paper. The resulting log-linear S-N curves appear to provide only a very crude estimate of the experimental data, even for the reference temperature. Furthermore, the model does not capture the change in the slope or curvature of the experimental results.

Mivehchi and Varvani–Farahani (189) approached the problem of temperature effects on fatigue by changing the parameters of the classical power-law S-N curve with temperature according to empirical relationships. The model relies on a $S_u(T)$ relationship given by:

$$S_u(T) = S_u(T_0) \left[1 - \frac{\frac{S_u(0)}{S_u(T_0)} - 1}{\ln\left(1 - \frac{T_0}{T_m}\right)} \ln\left(\frac{1 - \frac{T}{T_m}}{1 - \frac{T_0}{T_m}} \right) \right], \tag{1.81}$$

yielding the following fatigue curve equation:

$$\sigma_{max} = A(T) N(T)^{m(T)}; \tag{1.82}$$

$$A(T) = A(T_0) \left[1 - \frac{\frac{A(0)}{A(T_0)}}{\ln\left(1 - \frac{T_0}{T_m}\right)} \ln\left(\frac{1 - \frac{T}{T_m}}{1 - \frac{T_0}{T_m}} \right) \right]; \tag{1.83}$$

$$m(T) = m(T_0) \frac{\ln\left(1 - \frac{T}{T_m}\right)}{\ln\left(1 - \frac{T_0}{T_m}\right)}. \tag{1.84}$$

In these equations, $A(T)$ is the temperature dependent intercept of the S-N curve, $A(0)$ is the intercept at 0 K and $m(T)$ is the slope parameter. Temperatures T_0, T and T_m respectively represent the reference (usually ambient), analysis and matrix melt temper-

atures, given in Kelvin. This model, however, appears to suffer from a few weaknesses, namely:

- The parameter $A(T)$ is developed on the hypothesis that m is T independent, while it is explicitly dependent on T in the rest of the model.
- It is documented that the best fit power-law seldom converges to S_u (see e.g. Sutherland (120)). Yet, the assumption that it does is used in determining the parameters. This results in apparent bias in many of the predictions.
- The model $S_u(T)$ dependence (equation 1.81) is a strictly decreasing function, despite the expected plateau past the glass transition. Furthermore, negative strengths can be predicted below T_m.
- The model relies on the polymer's melt temperature as an input, a requirement that seems incompatible with its use for thermoset matrix composites. Yet, the model is benchmarked on thermoset composites without further explanations.

In the early 1990's Miyano et al. (190) studied the time and temperature effects on the static and fatigue bending behaviour of eight-harness satin carbon-epoxy composites with a $T_g = 236$℃ and $v_f = 0.66$. Tests were done in three-points bending within a temperature range of 25℃ to 230℃. Static tests were performed at a crosshead rate of 0.2 mm min^{-1} and of 200 mm min^{-1}.Fatigue tests were done at $R = 0.05$ and at frequencies of 0.02 Hz and 2 Hz. Results showed time-temperature interactions in both the static and fatigue regimes. They showed that a master curve of the static strength as a function of time and temperature could be built through the TTSP and that Arrhenius type relationships were adequate for representing the shift factors. As the S-N curves appeared to be well represented by a log-linear model converging to the static strength and as their slope was temperature independent, it was proposed that time and temperature effects on the fatigue life could be modelled through the use of the strength master curve. The relation, accounting for the relationship $N = ft_f$ where N is failure cycle count at frequency f

and t_f is the time to failure, is given by:

$$\sigma_{\max}(T, t_f, f) = S_u(T, t = 1/f) - m \log t_f - m \log f. \tag{1.85}$$

Over the next two decades, Miyano and his co-workers (191; 192; 193) further developed the approach and devised a methodology for predicting the influence of temperature on the long-term life (creep and fatigue) of carbon-reinforced composites. In its latest iteration, the advanced accelerated testing methodology (ATM-2), the method relies on master curves for creep, static strength and fatigue and uses time-temperature shift factors to model temperature effects. It is expected to function over a broad range of conditions by being able to deal with the viscoelastic nature of carbon fibre laminates and with failure probabilities. On the other hand, it is experimentally expensive since it requires creep, static and fatigue tests at multiple temperatures. Moreover, it relies on Miner's sum to deal with variable amplitude loading, an approach that, as was already discussed, is known to be unreliable for composites. It is therefore unlikely to fare well outside of CAF loading. The resulting basic equation is:

$$\begin{aligned} \log \sigma_f = & \log \sigma_0(t_0', T_0) + \frac{1}{\alpha} \log \Big[-\ln (1 - P_f) \Big] - n_r \log \left[\frac{S^*(t', T_0)}{S_c(t_0', T_0)} \right] \\ & - \frac{1 - R}{2} n_f \log (2N) + n_f^* \log (1 - k_D). \end{aligned} \tag{1.86}$$

In equation 1.86, σ_f is the failure stress, $\sigma_0(t_0', T_0)$ is the Weibull scale parameter of the static strength at the reference reduced time to failure t_0' and reference temperature T_0, α is the Weibull shape parameter of static strength and P_f is the desired probability of failure. Viscoelastic parameter $S^*(t', T_0)$ is based on linear viscoelasticity (BSI) and matrix compliance $S_c(t_0', T_0)$, while n_r is a failure mode dependent material parameter. The parameter n_f and n_f^* are material properties and k_D is the accumulation index from Miner's sum. Finally, R is the usual fatigue stress ratio and N is the number of cycles at failure. Guedes (194) has compared the CEM-SEI approach to ATM and showed that their predictions were similar in CAF, but differed in VAF. The difference was attributed

to the linear damage accumulation in the ATM approach, which is deemed to be too simplistic.

A probabilistic formulation for a CLD that includes temperature effects was proposed by Kawai, Matsuda and Yoshimura (96). The constant life diagram is based on two piecewise-non-linear functions respectively describing the tension and compression dominated fatigue regimes. Their formulation accounts for the asymmetry by imposing that the two segments meet at what they call the critical stress ratio $\chi = S_u^- / S_u^+$, where S_u^- and S_u^+ respectively stand for the static strength in compression and tension. The temperature dependence of their model comes from the static strength dependence on T, which is modelled through a modified hyperbolic function.

In a recent paper, Song et al. (195) studied the static and fatigue performance of 2.5D woven carbon preforms in a thermosetting bismaleimide resin with a T_g of 256℃ and $v_f = 0.52$. Tests were conducted at a frequency of 10 Hz and at temperatures of 25℃ and 180℃. Residual stiffness measurements were taken during fatigue tests. Results show that ambient temperature, the stiffness degradation is initially rapid, but stabilizes after the first few cycles (≈ 0.1). Conversely, at high temperature the stiffness degradation is initially slower, but continues at a constant rate. Strain accumulation is also evidenced at high temperature, probably due to damage accumulation and possibly viscoelasticity. It is interesting to note that a residual strength test performed after cycling at high temperature showed higher strength and stiffness than the average static specimen at 180℃, but still less than at room temperature. This was attributed to fibre realignment under the fatigue load, but could also result from residual cure. A fatigue model — similar to that of Chamis and Sinclair (equation 1.73), but where the square root is replaced by an arbitrary power and T_g is replaced by an arbitrary temperature parameter T_r — was proposed.

$$\frac{S_{\max}}{S_{u,0}} = a \left(\frac{T_r - T}{T_r - T_0} \right)^b - c \log N. \tag{1.87}$$

In equation 1.87, a, b, c and T_r are all empirical fitting parameters. The model appears to provide a good fit to experimental data. A stiffness degradation model with six empirical parameters is also proposed, but won't be discussed here.

The problem of temperature and time dependence of composite fatigue is sometimes looked at through the lens of creep-fatigue interaction. Crowther, Wyatt and Phillips (196) have shown that for certain materials, at low frequency, the fatigue process is dominated by creep and failure is time rather than cycle dependent. However, at higher frequency, fatigue becomes cycle dominated. This behaviour was corroborated by results from Eftekhari and Fatemi (166; 197), who studied the fatigue behaviour of neat, talc-filled and short fibre reinforced thermoplastics. They also used Epaarachchi and Clausen's (146) fatigue model in conjunction with a Larson-Miller type relationship to adequately model the effects of high temperature and high frequencies.

Samborski, Mandell and Miller (198) have recently studied the creep-fatigue interactions in $\pm 45^{\circ}$ glass fabric-epoxy laminates under tension ($R = 0.1$), reversed ($R = -1$) and compression ($R = -10$) loadings. Under tension and compression fatigue, significant cyclic strain accumulation was observed, while reversed fatigue loading produced no notable strain increase. Tensile loads produced higher creep strains than compression. The fatigue strain ranges did not change in compression fatigue, indicating that the stiffness remained constant. However, in tension and reversed loadings, the strain range increased towards the end of the fatigue life, indicating that the stiffness was degraded. This would mean that for compression, the strain accumulation is purely due to creep, while in tension a combination of creep and damage accumulation interact. Strain controlled fatigue tests, which would simulate the presence of much stiffer unidirectional plies along the load direction, show that stress relaxation can also occur in the off-axis plies. This results in some compressive stress accumulation upon unloading, which is also accompanied by a stiffness reduction. Strain-controlled tests resulted in higher lifetimes than stress-controlled experiments at similar initial load levels. Another interesting finding is that the cumulative time to reach 50% of the ultimate strain ϵ_u is comparable for creep

and fatigue, in both tension and compression. This value may thus prove to be an interesting damage metric. Finally, tests on a few specimens with approximately 20% of fibres added in the load direction showed greatly reduces the creep rates, but since the $\pm 45^{\circ}$ plies still initially support an important part of the load, their stiffness reduction due to viscoelastic effects tends to overload the UD plies and premature failure. The limited number of experiments suggest about a decade difference between load controlled tests and strain controlled tests at the same initial strain levels (shorter life in load control).

Sayyidmousavi et al. (199; 200) have devised a micromechanics model, which allows the evaluation of the three plane stress components in a unit cell of unidirectional fibre based on the applied strains. Those strains are evaluated as the sum of time-dependent strains obtained through Shapery's integral formulation and of the cycle dependent strains resulting from fatigue damage (stiffness degradation). The resulting stresses are then compared to a fatigue failure criterion similar to that of Hashin and Rotem (107). The resulting S-N curve at any fibre angle can then be obtained from the knowledge of the fatigue behaviour in the principal directions at the desired temperature. A good fit was obtained when the model was used to predict the behaviour of $[\pm 75]_{2S}$ carbon-epoxy tested at 10 Hz and at 25℃ and 114℃ by Rotem and Nelson (175). An interesting ability of their model is that of discriminating between the effect of creep and fatigue strains. It is thus shown that even if creep is much accelerated at high temperature, the fact that the time to failure is reduced means that fatigue damage effects may still dominate.

It is worth mentioning that under fatigue loading, a constant frequency does not result in a constant strain rate for all mean stresses and stress amplitudes. However, the physical parameter that is related to viscoelastic behaviour of a material is strain rate rather than frequency. Thus, it could be argued that fatigue experiments meant to validate models accounting for frequency effects should be performed at a constant strain rate rather than constant frequency. During the Upwind project, discussions were undertaken on the topic and Dr O. Krause (201) suggested that the dissipated strain energy rate is kept

constant for all fatigue experiment, leading to the following relationship:

$$f_2 = f_1 \frac{{\epsilon_1}^2}{{\epsilon_2}^2}. \tag{1.88}$$

Although this method does not provide a constant strain rate in all experiments, it has the benefit of minimizing the confounding side effect of specimen hysteretic heating at higher frequency. It does so by having all tests performed under a constant dissipated energy rate (assuming a constant loss factor).

1.6 Analysis

In the foregoing literature review, the nature and behaviour of composite materials were discussed both at the constituent, the lamina and the laminate levels. It was first shown that the basic physical nature of temperature and strain rate effects on the matrix materials are still not well understood. As a result, both physicists and engineers still mainly rely on empirical or phenomenological relationships to describe the thermomechanical and viscoelastic responses of polymers. Since many properties of fibre reinforced polymer matrix composites are matrix dominated, it is evident that their thermomechanics and viscoelastic responses share the same complexities as those of neat polymers, although somewhat complicated by the heterogeneous nature of composites.

It was then shown that due to its diffuse nature, the damage initiation and progression as well as failure in fibre reinforced composites submitted to fatigue is not fully understood. Thus, despite the evident advantages that a mechanistic approach to fatigue modelling would present, empirical and phenomenological models still prevail.

Given the review of frequency and temperature effects on the fatigue response of composites, it is clear that the study of the latter cannot be dissociated from the subjects of polymer thermomechanics and viscoelasticity. However, because of the relative immaturity of all these fields, it appears that we are still quite far from a purely physical or mechanistic model based solely on the individual response of constituents.

The current work will then focus on the more readily attainable objective of clarifying the interrelations and synergies that exist between the fatigue of composites, thermo-mechanics and viscoelasticity. On the basis of those findings, it is believed that some simplified empirical and phenomenological approaches can be devised and that a more basic understanding can be reached by relying on those regularities.

CHAPTER 2

TEMPERATURE AND FREQUENCY EFFECTS ON THE FATIGUE PROPERTIES OF UNIDIRECTIONAL GLASS FIBER-EPOXY COMPOSITES

Laurent Cormier[1], Rogier P. L. Nijssen[2], Sibrand Raijmaekers[2]

[1] Department of automated manufacturing engineering, École de Technologie Supérieure,
1100 Notre-Dame Ouest, Montreal, Quebec, Canada H3C 1K3
[2] Knowledge Center Wind Turbine Materials and Constructions (WMC), Kluisgat 5, 1771 MV Wieringerwerf, The Netherlands,
Presented at the 53rd AIAA/ASME/ASCE/AHS/ASC Structures, Structural Dynamics, and Materials Conference, Honolulu (Hawaii) on April's 24th 2012. Paper number: AIAA-2012-1574

Abstract

As wind turbines are likely to be installed in a wide variety of environments, knowledge of their materials mechanical properties under extreme environments is needed. The project presented herein aims at evaluating the effects of temperatures of -40℃, 23℃, and 60℃ on the static properties and fatigue lives of unidirectional glass-epoxy composites as found in wind turbine blades load bearing structures. Tensile and compressive static properties, as well as fatigue lives under $R = 0.1$ and $R = -1$ loading are evaluated. Moreover, in an attempt to reduce future tests time by using the highest frequency possible, efforts are spent in evaluating the effects of loading frequency on specimen fatigue lives. Frequencies ranging from 1 Hz to 24 Hz are studied. Results show that even if the static strength of the composite is much improved at low temperature, this does not translate to improved fatigue performances and may actually cause a reduction of fatigue lives. On the other hand, static strength degradation at higher temperatures does equate to a significant reduction in fatigue life. This is particularly true for fully reversed fatigue loading. It is also shown that higher loading frequencies are rapidly deleterious at room and elevated temperatures. However, considering the limited effect of low temperatures on fatigue

performances, it is believed that cooling could be coupled to higher frequencies in order to accelerate fatigue testing.

2.1 Introduction

Composite materials fatigue performance characterisation is resource intensive due to long test durations and large number of tests required. To optimize fatigue data collection in the *OPTIMAT* program, the fatigue test frequencies were related to load level following a strain range related rule. During tests at higher frequencies, it was observed that lower lifetimes were obtained. These were mainly attributed to internal heating of the laminate through visco-elastic effects and friction. These effects, combined with the poor heat conductivity of glass-epoxy laminates led to excessive heating of the specimens and reduced lives. Nevertheless, at the time it was not in the scope of the *OPTIMAT* project to de-couple the alleged effects of temperature and frequency on fatigue life. Still, accelerated and reliable fatigue testing of composite is desirable and using the highest possible frequency without deteriorating the performance of the material is a constant challenge for material scientists. Moreover, there are growing concerns about fatigue behavior of composite materials under extreme environmental conditions. One can then easily see the possible interactions between the environment (temperature, moisture or other atmospheric parameters) and test frequency.

This paper describes results from a test program carried out within the European *UPWIND* project. The former aims at providing data for better understanding of temperature and frequency effects on composite materials fatigue durability. As such, it consists of a dedicated test program that was elaborated in order to qualify and quantify the effects of temperature and frequency on fatigue life of unidirectional (UD) E glass-epoxy.

After a brief literature review on the frequency and temperature effects, the methodology and results from the aforementioned test program are presented and discussed.

2.2 State of the art

A brief review of relevant literature is presented here. First, published works on the effects of temperature on static strength of polymer matrix composites are presented. The state of the art relating to temperature and frequency effects on the fatigue behavior of composite materials is then discussed. Note that this literature review focuses on results for thermoset matrix composite systems.

2.2.1 Temperature effects on static properties

Effects of high temperatures on polymer matrix composite material properties have been the subject of several researches since the early days of advanced composites. However, study of the effects of low, but non-cryogenic temperatures on the mechanical properties of laminates and bonded joints enjoyed much less attention. A paper from Liu and Kharbari suggests that the need for further research in the area of hygrothermal effects, including cold temperature, are significant before composites can be widely used in common structures. As a result, it is suggested that this topic be further investigated (202).

Nevertheless, it is known that temperature can affect composite material properties at several scales. Therefore, thermal effects on static properties are first discussed with a focus on the micro-structural or constituent level behavior. Then considerations for laminate scale and macroscopic scale are presented.

2.2.1.1 Constituent scale effects

Although most inorganic fibers are not very sensitive to the range of temperatures applicable to polymer composites, the matrix is sensitive to thermal conditions. In general, a thermoset polymer system is in a glassy (stiff and brittle) state if its temperature is below a threshold usually known as the glass transition temperature (T_g). If the temperature approaches this threshold, the polymer's stiffness rapidly declines and its internal damping increases until the material reaches a state where viscous effects are dominant.

This condition is known as the rubbery state. It is however worth noting that some polymers also show an increase in internal damping at specific low temperatures. These transition temperatures are usually referred to as T_β and T_γ. These changes in material behavior are believed to be the results of molecular chains re-arrangements. At elevated temperatures, dilatations allow for increased chain mobility, resulting in a loss of modulus and increase in internal damping. On the other hand, low temperature reduces chain mobility, thus resulting in increased stiffness, strength and brittleness. Causes of transitions T_β and T_γ are not very well understood but are also believed to be due to chain rearrangement (39; 75).

Early in the polymer composite history, empirical relations modelled after tests on epoxy resin systems were proposed by Chamis to evaluate mechanical properties of polymers under the influence of temperature lower than T_g and absorbed moisture (85; 86). Chamis' relation suggests a change in polymer mechanical properties proportional to the square root of the difference between T_{gw}, the moisture degraded glass transition temperature of the matrix, and T, the actual temperature. This is in relatively good agreement with literature suggesting that while close to T_g, properties vary abruptly between an upper and a lower threshold, outside these bounds, mechanical properties are expected to display a slower variation, possibly almost linear (75). This relation may be used for determining composite material properties through the rules of mixture (RoM) and used as input for the classical laminate theory (CLT).

Like all other materials, composite constituents undergo dimensional changes when exposed to a temperature increase or decrease. However, composite materials themselves are heterogeneous and all phases may not react the same way to the thermal loading. Moreover, these phases are usually solidly bonded together and must remain under dimensional equilibrium. Therefore, internal strains will arise from temperature changes in composites. These are in addition to any pre-existing strains due to matrix shrinkage during polymerization or to external loads. Usually, fibers can be expected to have a coefficient of thermal expansion (CTE) about an order of magnitude lower than matrices.

Some fibers, like carbon and aramid, may also have anisotropic behavior and/or negative CTEs (75).

Lord and Dutta, have proposed a micromechanics model to evaluate the fiber and matrix axial stresses due to temperature changes. According to this model, constituent stresses are a function of their respective modulus (E), CTE, fiber volume fraction (v_f) and temperature difference from the reference (thermal stress free) temperature. It is suggested that this reference temperature should be close to T_g. This is because during the polymerization process and later cool down, it is assumed that the matrix can relieve thermal stresses until T_g is reached (76).

According to Lord and Dutta's relation, a temperature rise would induce compressive longitudinal stress in the matrix and tensile longitudinal stress in the fibers while a cool down would induce tensile stress in the matrix and compressive stress in the fibers. This last remarks then brings the concern that, being slender columns, fibers may buckle if a sufficiently low temperature is reached. In the event of thermally induced buckling of the fibers, compressive properties of the composite may be significantly degraded. Tensile matrix stress could also lead to cracking of the material.

2.2.1.2 Laminate scale effects

At the laminate scale, changes in matrix properties should result in changes of laminate properties. As, previously mentioned, modified matrix properties from Chamis' equations may be used in the RoM and CLT to estimate the material properties. However, Cormier and Joncas suggested that applying Chamis' relations to the RoM and CLT may not provide adequate evaluation of unidirectional (UD) laminate properties at low temperatures. In this research, tensile, compressive and short beam shear tests were performed at room and -40℃ and an increase in strength was noted at low temperatures, while tensile modulus stayed unaltered. In most cases the changes were shown to be higher than what Chamis equations and the CLT suggested (84).

The literature review presented in Cormier and Joncas' work also shows that there is important variability in the conclusions from researches on the effect of low temperatures on mechanical properties of composites. Different authors conclusions range from suggesting a slight degradation of the material to stating that there is a significant performance improvement. This is thought to be the result of the large number of material constituents, architectures and conditions that are studied (84).

Macroscopic effects of high temperatures on the mechanical properties of UD glass-epoxy laminates ($v_f = 65$ %) under static loading were studied by Aktas and Karakuzu (203). They performed tensile and compressive tests, both in the longitudinal and transverse fiber directions, as well as interlaminar and intralaminar shear properties measurements. Test temperatures ranged from 20℃ to 100℃ in 20℃ increments. Their work showed unidirectional composites lose strength and stiffness as temperature increases. More specifically, in the fiber direction, modulus remains quite constant up to 60℃ after which temperature, it drop significantly until halved at 100℃. On the other hand, transverse and shear modulus decrease gradually from 20℃ to 100℃, temperature where they are more than halved. Poisson's ratio seems to remain unaltered by increasing temperature. Longitudinal tensile and compressive strength as well as transverse compressive strength also gradually decrease as temperature increases. Both inter and intralaminar shear strengths showed a strong negative dependence on temperature, with significantly reduced performance from 40 ℃. Transverse tensile strength seems unaffected by a temperature increase.

Kinsella et al. also present test results for S glass-epoxy composites tested between -55℃ and 80℃ (204). Quasi-static tensile and compressive tests on 0°, ±45° and 90° laminates were performed. These results show that tensile and compressive modulus remained relatively unaltered by temperature changes between -55℃ to 80℃. On the other hand, shear modulus was increased by about 20 % at cold temperature and reduced by almost 30 % at 80 ℃. In terms of strength, at -55℃, tensile strength was improved by about 10 %. Compressive and shear strengths improved by a slightly higher proportion, more

in the 15 % range. At 80℃, tensile and compressive strengths were reduced by a similar amount whereas shear strength was reduced by close to 25 %.

2.2.2 Temperature and frequency effects on fatigue behavior

The topic of environmental effects on fatigue behavior of composite materials is still not fully addressed. For example, Kharbari et. al suggests that the study of hygrothermal effects on composite materials should focus on adhesive joint and fatigue properties (205). However, fatigue testing of composites is time consuming due to frequency limitations imposed by hysteretic heating. A short review on the individual and combined effects of temperature and frequency on fatigue properties of polymer composites is therefore presented.

Hygrothermal effects on fatigue life behavior of polymer composites was studied by Tang et al. (181). In this paper, a model for predicting the fatigue life of fiber-reinforced polymeric composites was established and verified. Fatigue experiments were made on a glass fiber-vinyl ester composite exposed to air, fresh water and salt water at 30 ℃. Experiments were conducted in a tension-tension mode at a stress ratio of $R = 0.1$ and maximum applied load ranging from 35 % to 70 % of ultimate tensile strength. Test frequency was set at 10 Hz for studying temperature effects. Tests were conducted at three temperatures: 4℃, 30℃ and 60℃. Results from these tests show that for this particular material, the fatigue life at 60℃ is about the same as that at 30℃, but the fatigue life at 4℃ is significantly longer than that at 30℃. However, even though fatigue life at 30℃ and 60℃ are said to be similar, the authors remark that the slope of the S-N curve is steeper at higher temperatures.

In Megnis et al. (206) a short elaboration is given about research on the fatigue life of UD material at room temperature and 60℃. In the $R = 0.1$ fatigue conditions they studied, the material did not show obvious difference in fatigue life between the two temperatures. All the data of fatigue life for extreme conditions are within confidence

limits of the reference data set. However the data of fatigue life at 60℃ are consistently below the regression line of the reference conditions.

Effects of cold temperatures on the fatigue behavior of polymer matrix composite is very scarcely documented. Work from Bureau and Denault focused on the effect of temperatures of -40℃ to 50℃ on the $R = 0.1$ flexural fatigue behavior of two composite materials (184). The first composite is a 2-2 glass tweed [sic, twill] in a polyester matrix and the second laminate is a biaxial glass fabric in polypropylene resin. Both laminates were of 60 % fiber weight fraction. Tests were ran at 5 Hz. According to their results, when normalized by the static strength at their respective temperatures, S-N curves for the glass-polyester were superimposed, while those of the polypropylene matrix composite showed a small improvement in fatigue life.

The possibility of using high-frequency loading for accelerating fatigue tests of polymer composite materials is discussed by R. Apinis(163). The results of this research are compared with those found in conventional low-frequency loadings. Results are given for an LM-L1 UD glass-fiber plastic in loadings at $R = -1$ with frequencies of 17 and 400 Hz. Apinis confirms that it is possible to accelerate the fatigue testing of polymer composite material by considerably increasing the loading frequency. The necessary condition for using this method is an intense cooling of specimens to prevent them from vibration heating. For achieving the same temperature modes of testing during high-frequency loading, the specimens were cooled by water jets. To prevent the material from the action of moisture, the surface of specimens was covered with a thin layer of wax.

The relation between frequency and fatigue life was also studied by Kharrazi and Sarkani (174). According to their work on fatigue of thirty plies woven glass-vinyl ester composites as cross-plies and [±45 °] laminates, frequency effects result from two different behaviors. At first, under low frequency loading, effects are mainly the results of the visco-elastic nature of the constituents. Time-dependent phenomenon such as creep may dominate the failure mode and a frequency increase result in an fatigue life improvement due to

reduced time at load. If frequency is further increased, they suggest that the increase in hysteretic heating is faster than that of heat dissipation and the thermo-elastic behavior of the matrix comes to dominate the failure mode. In this regime, an increase in frequency reduces the fatigue life of the specimen. Results from their work also suggests that, if the specimen temperature stabilises during testing, the frequency is low enough to avoid damage due to overheating. They also demonstrated that a large part of the fatigue life reduction can be avoided if testing is performed at higher frequency but paused to let the specimen cool down before the temperature reaches that of the plateau seen at lower frequencies. Finally, as could be expected, frequency effects are stronger in matrix dominated laminates (*i.e.* [$\pm$ 45 °]) than for fiber dominated architectures (*i.e.* [0 °/90 °]).

Hahn and Turkgenc summarized the results of different researches considering the effect of frequency on the fatigue behaviour as follows: "At low frequency ranges where there is negligible heat dissipation, as the load frequency increases, cycles to failure increase also. As higher frequency ranges are considered this increase is at a slower rate. When there is excessive heat dissipation however, a reverse trend can be observed" (165).

Mandell and Meier studied tension load frequency effects for cross-ply E glass-epoxy laminates. Test were carried at low frequencies of 0.01, 0.1 and 1 Hz to prevent any hysteretic heating and the specimens were subject to square and spike loadings. The authors observed that the number of cycles to failure increased at higher loading frequencies (122).

Mishnaevsky and Brøndsted proposed an analytical model for evaluation of fatigue damage that include frequency effects and that is applicable to the case when neither dynamic effects nor heat dissipation influence the damage growth in the materials (207). According to their work, the lifetime of a specimen under constant load is dependent on applied stress and temperature. Apparently, if considering a more complex case of multi-step loading, a failure of a material is not a step-wise event after a lapse of time, but a continuous process of the defect accumulation and degradation at the lower scale level. The

residual lifetime of a specimen under loading decreases due to the formation of defects. However, such multi-step loading can lead to the failure as well as one long step loading.

Considering fatigue, the cyclic tension-tension loading curve can be represented as a multi-step loading. A half-cycle curve can be discretized into several steps, and the damage increase for each step can then be determined. In this analytical approach it is stated that: "the total time to failure is constant, the frequency of loading does not affect the total time to failure". This means that the number of cycles to failure increases with increasing the loading frequency. On the other hand, the damage growth per cycle decreases with increasing loading frequency. Therefore, a decreasing correlation would exists between the damage growth rate in each cycle and the frequency of loading. Results were compared to the experiments by Mandell and Meier (122), to verify the analytical kinetic model of fatigue damage.

During the *OPTIMAT* blade project, Krause suggested an energy based method relating frequency to strain. He suggested that for constant amplitude loading the relation described in equation 1.88 can be used to determine frequency (f) at a given strain amplitude (ϵ) if an initial condition is known (201; 208).

$$f_2 = f_1 \frac{\epsilon_1^2}{\epsilon_2^2} \qquad \text{(equation 1.88 revisited)}$$

However, for this method to work, an initial reference frequency-strain amplitude must still be determined experimentally.

After observations made during the *OPTIMAT* blade project that tests at higher frequencies led to lower lives, work was performed in the European *UPWIND* project in order to establish the link between temperature and frequency effects in fatigue loading. Preliminary results were presented in papers by Nijssen (87; 209) and detailed in the project's final report (95).

2.3 Methodology

In order to evaluate the effects of frequency and temperature on the fatigue life of composites, an extensive test program was undergone. Static tests at different temperatures were first performed, followed by fatigue tests at several frequencies, load level combinations and at three temperatures. Details of the test program are given in Table 2.1.

Table 2.1 Test program description

Loading type	Conditions	Target N @ P	$S_{equivalent}$	$\dot{\epsilon}$ or f
Static tension	-40°C, ambient (23°C), 60°C	1/2 @ ultimate	–	1 mm/min
Static compression	-40°C, ambient (23°C), 60°C	1/2 @ ultimate	–	1 mm/min
$R = 0.1$ fatigue	-40°C, ambient (23°C)	10^4 @ 32 kN	525 MPa	2, 8, 24 Hz
		10^6 @ 20 kN	330 MPa	6, 8, 24 Hz
	60°C	10^4 @ 32 kN	525 MPa	2 Hz
		10^6 @ 20 kN	330 MPa	6 Hz
$R = -1$ fatigue	-40°C, ambient (23°C)	10^4 @ 24 kN	400 MPa	1, 24 Hz
		10^6 @ 14 kN	230 MPa	3, 24 Hz
	60°C	10^4 @ 24 kN	400 MPa	1 Hz
		10^6 @ 14 kN	230 MPa	3 Hz

The material tested was UD glass-epoxy composite. Fibers were Saertex® E glass unidirectional fabric of an areal weight of 963 g/m^2. Even though it is called unidirectional, the fabric contains about 5 % transverse reinforcements that are stitched to the main rovings. As a result, the fabric is not balanced and this was accounted for in the lamination by ensuring a symmetric lay-up which could be described as $[90/0_2/90]_s$. The matrix was Hexion® L135i epoxy with 134i-137i hardener. Laminates were vacuum infused between two rigid plates. The resulting laminate had a v_f around 55 %. All laminates were postcured for 10 hours at 70°C. The composite's T_g averaged 81.6°C.

In order to avoid differences due to geometric effects between tensile and compressive fatigue, the specimen geometry was the same for all tests. A straight sided and tabbed specimen of 130 mm in length, 20 mm in width and 3 mm in thickness was used. Bonded

tabs were made of 1 mm thick $[\pm 45]_s$ glass fiber-epoxy laminates. The specimen gage section length was 20 mm. Strain gages were mounted on both the longitudinal and transverse directions and on both faces of the samples. In addition, a thermocouple was glued to the lower right side to monitor specimen temperature during the tests.

Static tests are performed on at least six specimens at each temperature level. Axial load, displacement and strains are measured while stresses are calculated based on the average cross-section in the middle of each specimen and tensile modulus is calculated from the slope of the stress-strain curve between ± 500 $\mu\epsilon$ and ± 2500 $\mu\epsilon$. A minimum of six specimens were also tested for most conditions of the fatigue tests described in table 2.1.

Tests were performed at the Knowledge Center Wind turbine Materials and Constructions, in the Netherlands. Two servo-hydraulic test benches were used in this program, a 220 kN Zwick/Roel test frame and a custom-built 100 kN test frame. Temperature control was provided by a climate chamber annexed to the test frames and piped to an isolated box surrounding the grips and specimen. Conditioned air was circulated through the system, and the settings of the external climate chamber were adjusted based on temperature measurements in the test area. Relative humidity was never controlled. The room temperature tests were typically not carried out in the climate chamber but only under laboratory conditions. For low and high temperature tests, specimens were left to stabilize at the desired temperature for at least 15 minutes, or until measured specimen temperature was within one degree centigrade of the target environment. Static tests were carried out in displacement control and fatigue tests were load controlled.

2.4 Results

A summary of test results is presented here. Static tension results are first discussed, followed by static compression, and tensile and reversed fatigue results. Detailed information about the results for individual specimens are available in the *UPWIND* tab

of the *OPTIDAT* database (132). Results are also discussed in an *UPWIND* project report (95).

2.4.1 Influence of temperature on static tensile properties

Statistics on the strength and modulus obtained from static tension tests are presented in table 2.2 and table 2.3. According to these results, a temperature of 60℃ induces a significant reduction of the laminate tensile strength and modulus at -19.4 % and -8.1 % respectively. At -40℃ the tensile strength is improved by 13.4 %, while the tensile modulus appears to remain quite constant.

Table 2.2 Tensile strength

T ℃	$\overline{s}_L^+$ Pa	σs_L^+ MPa	$CV\, s_L^+$ %	δs_L^+ %
-40	1038	35	3.4	13.4
23 (ambient)	915	44	4.8	0
60	737	20	2.7	-19.4

Table 2.3 Tensile modulus

T ℃	$\overline{E}_L^+$ GPa	σE_L^+ GPa	$CV\, E_L^+$ %	δE_L^+ %
-40	37.0	0.60	1.62	-3.1
23 (ambient)	38.2	1.20	3.15	0
60	35.1	0.59	1.69	-8.1

2.4.2 Influence of temperature on static compressive properties

Statistics on compressive strength results are presented in table 2.4 while moduli are presented in table 2.5. These results show that compressive properties are strongly

affected by temperature conditions. At 60℃, strength is reduced by more than 30 % while a 7 % decrease in modulus is noted. At -40℃, strength is improved by about 30 % however, modulus is not significantly affected.

Table 2.4 Compressive strength

T °C	$\overline{s}_L^-$ MPa	σs_L^- MPa	$CV\, s_L^-$ %	δs_L^- %
-40	-719	48	-6.6	32.7
23 (ambient)	-542	50	-9.1	0
60	-372	32	-8.5	-31.3

Table 2.5 Compressive modulus

T °C	$\overline{E}_L^-$ GPa	σE_L^- GPa	$CV\, E_L^-$ %	δE_L^- %
-40	37.4	1.1	2.8	-0.2
23 (ambient)	37.4	0.8	2.1	0
60	34.8	0.4	1.3	-7.0

It is believed that the changes in mechanical properties are mainly the result of matrix property changes. At low temperatures, the improved performances of the composite may be due to strengthening and stiffening of the matrix material, while its weakening at higher temperature can explain the poor performances of the composite. Comparing the tensile and compressive strengths, one sees that the material shows a lower tolerance to compressive loading and that temperature has a greater effect on compressive strength than on tensile strength.

2.4.3 Influence of temperature on fatigue life

In order to allow for analysis of the extreme temperature fatigue behavior of the composite, results are presented in stress-life (S-N) diagrams. The assumption that the fatigue behavior varies linearly in the log-log stress-life space is made for modelling purposes. S-N curves and their respective 95 % confidence interval on the median line are calculated as per ASTM E 739 (152).

Figure 2.1 shows the fatigue life curves of tests performed at $R = 0.1$. In the upcoming S-N diagrams, solid lines are the 50 % survival curves while interrupted lines are 95 % confidence bounds on these curves. According to these results, a temperature of -40°C appears to result in a steeper slope of the S-N curve. Low temperature fatigue tests also show very good scatter characteristics. The curve for tests performed at 60°C are shown to have an average fatigue life about a decade shorter than that of a similar specimen loaded at ambient temperature. The slope of the fatigue curve at high temperature however, seems to remain unchanged. Scatter is also much increased at high temperature.

The S-N curves and 95 % confidence bounds for fully reversed loading fatigue at the same temperatures are plotted in Figure 2.2. At first, as for tensile fatigue, the effects of a temperature of -40°C seems to be a steeper slope of the S-N curve, suggesting increased fatigue sensitivity. However, closer inspection shows that within the data range, the curves for ambient and low temperatures fall within the same confidence intervals. Therefore, due to the important scatter seen at ambient temperature and elevated loads, differences between the curve for this condition and that of the low temperature may not be significant. Nonetheless, since both curves ($R = 0.1$ and $R = -1$) show an increase in slope at -40°C, this may suggest that even though in the latter case changes are not statistically significant for the current data set, the increase in S-N slope may still be real. Test data at low temperature again seem to show improved scatter characteristics compared to those obtained at higher temperature.

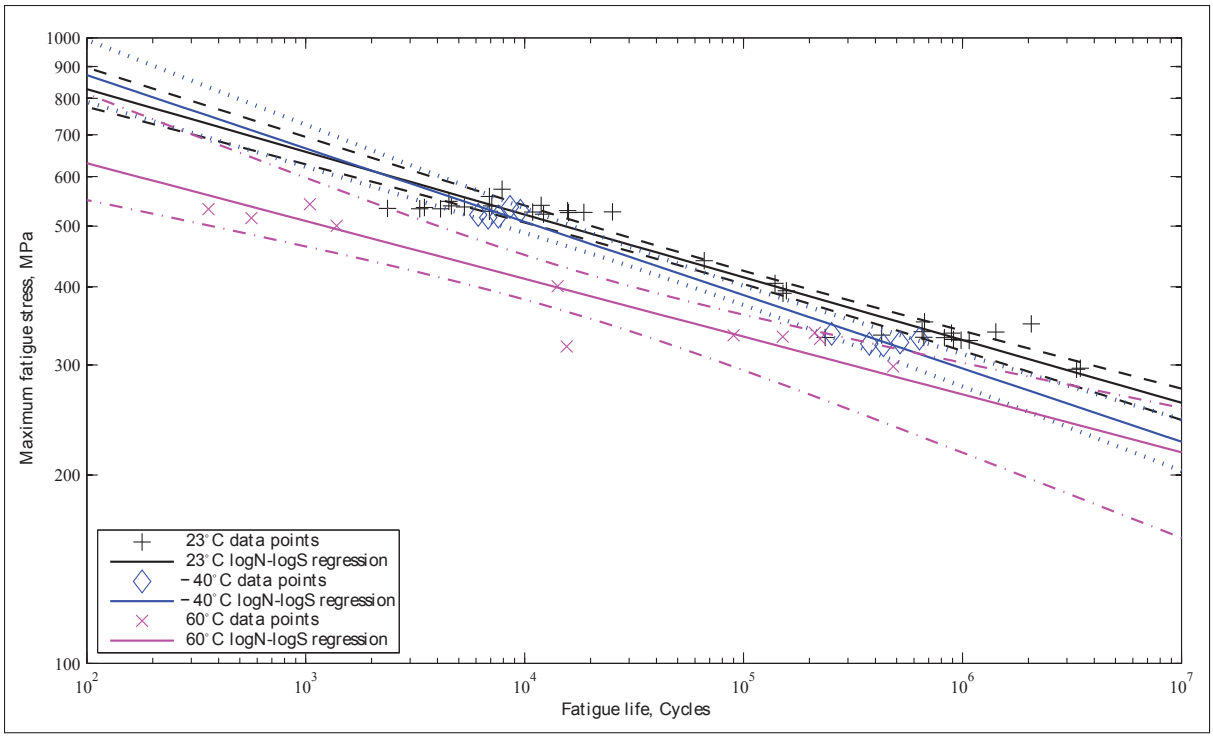

Figure 2.1 S-N diagrams for $R = 0.1$ fatigue at -40℃, 23℃, and 60℃

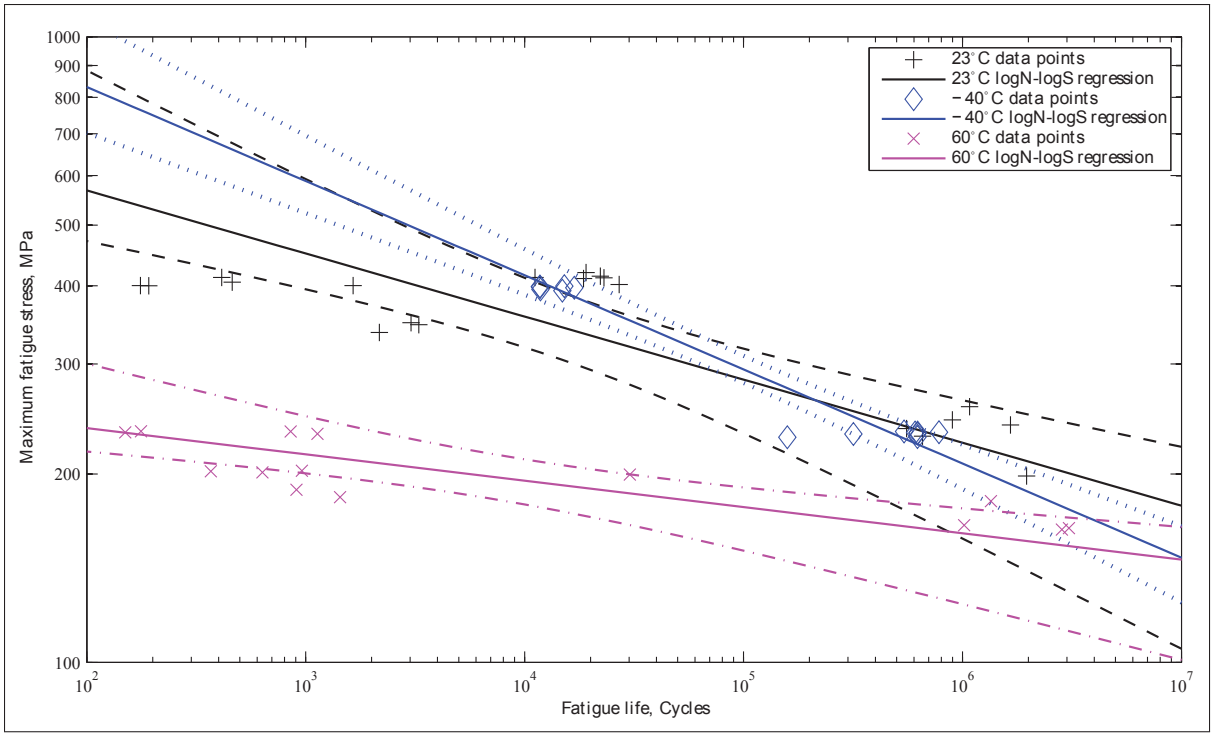

Figure 2.2 S-N diagrams for $R = -1$ fatigue at -40℃, 23℃, and 60℃

On the other hand, results from tests performed at 60℃ show a reduction in life of about three decades for a 230 MPa reversed loading and the specimen was unable to withstand fatigue loading at the planned 400 MPa load level. Therefore, it seems that under a fully reversed fatigue loading, a temperature of 60℃ is highly detrimental to the fatigue behaviour of the laminate under examination. Moreover, the slope of the $R = -1$ at 60℃ curve is reduced compared to that of the ambient temperature condition. Therefore, the life is also much more sensitive to small variations in load level.

The fatigue lives of specimens are also plotted against temperature for the low and high reference loads at $R = 0.1$ and $R = -1$. Figure 2.3 illustrates the behavior of the tension-tension fatigue test specimens while Figure 2.4 describes that of the fully reversed tension-compression fatigue.

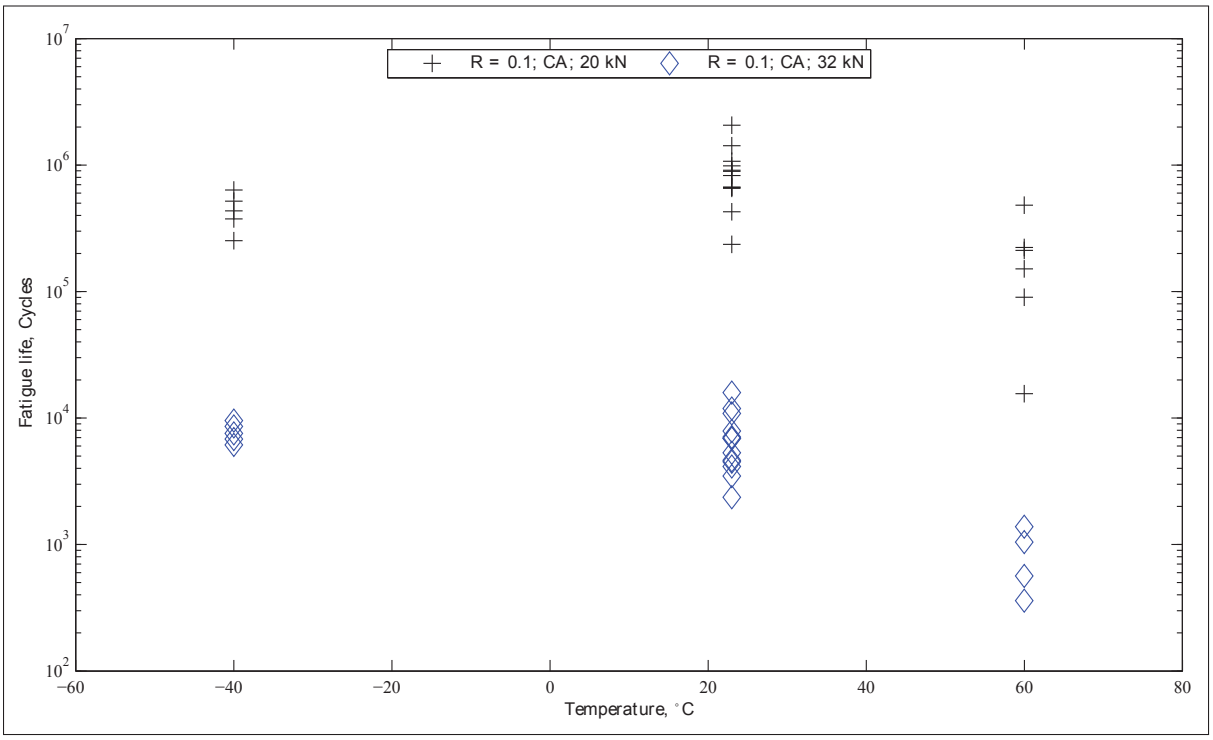

Figure 2.3 Life-temperature diagram for $R = 0.1$ fatigue

Results shown in Figure 2.3 illustrate again that the tension-tension fatigue strength of the E glass-epoxy laminate under study is degraded at a temperature of 60℃. At this temperature, specimen life is reduced by about an order of magnitude independently from the load level. At -40℃, although the average specimen life is similar to that at room temperature, scatter seems to be somewhat lower and there is a slight tendency for shorter lives at low loads.

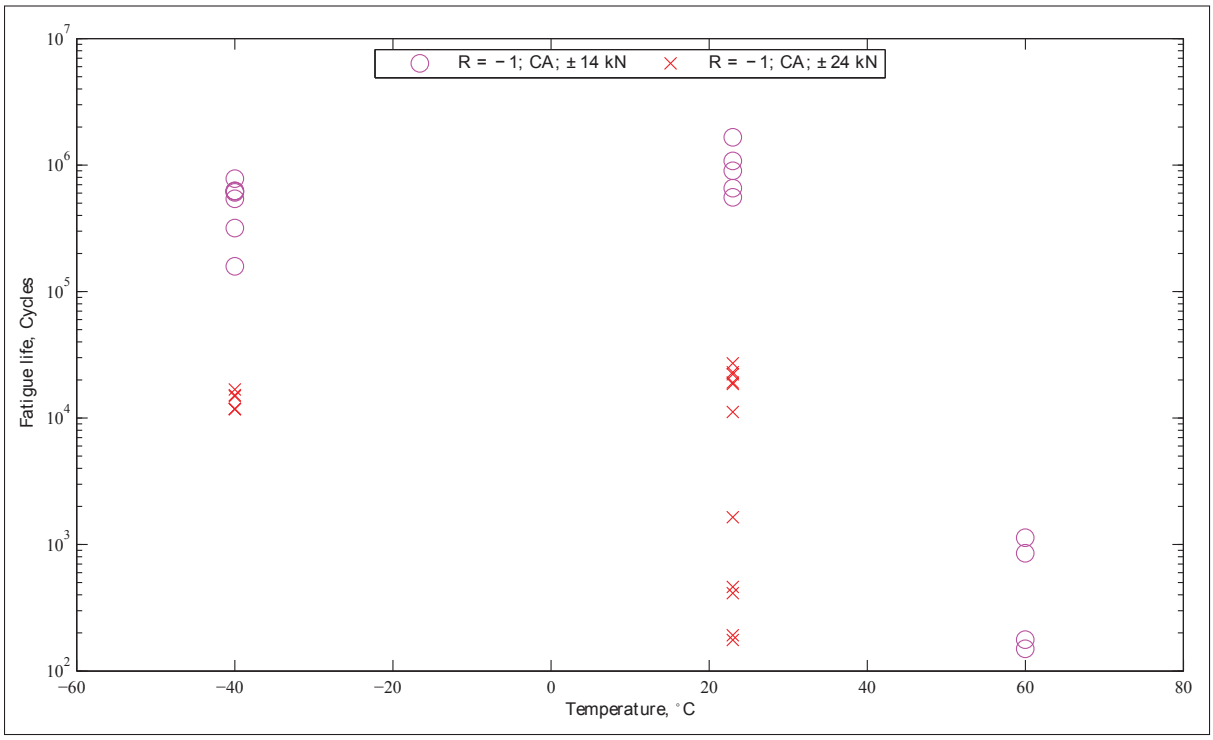

Figure 2.4 Life-temperature diagram for $R = -1$ fatigue

From Figure 2.4, the effect of high temperature on the $R = -1$ fatigue life of the laminate is also very clear. For example, it is evident that at 60℃, fatigue strength was reduced in such a way that specimens from the lower load level (±14 kN) only showed lives equivalent to those of the weakest specimens tested at room temperature, but at a higher load (±24 kN). Moreover, at 60℃, the specimens were weakened in such a way that fatigue tests at this higher load level could not be reliably performed. For tests at -40℃, results from Figure 2.4 suggest that life of the specimens seem to be similar to those at

room temperature. Nonetheless, at high loads, lives obtained for cold temperature tests are grouped above the room temperature average while at lower loads, the opposite is seen.

2.4.4 Influence of frequency on fatigue life

The effect of test frequency on the fatigue life of the laminate is studied at ambient and -40°C. For the reference condition (CA) the test frequency is related to the actual load applied on the specimen as per equation 1.88. For intermediate frequency (CAM), the tests are conducted at 8 Hz and are only performed at $R = 0.1$. Elevated frequency (CAH) tests are made at 24 Hz for both $R = 0.1$ and $R = -1$. CAM and CAH test frequencies are not related to the load level but are limited to test frame capacity. As a result, strain rates at elevated loads reach much higher levels in CAM and CAH tests. Resulting load rates calculated based on a laminate modulus of 38 GPa, a specimen cross-section of 61 mm^2 and a gage length of 20 mm are presented in Table 2.6.

Table 2.6 Strain rates summary

Loading type	P_{max} kN	f Hz	Mean $\dot{P}$ kN/s	Mean $\dot{\epsilon}$ s^{-1}	Mean $\dot{d}$ mm/s
Static	Failure	–	116	0.050	1
$R = 0.1$ fatigue	20	6	216	0.0932	1.86
	32	2	115	0.0497	0.994
	20	8	288	0.124	2.48
	32	8	461	0.199	3.98
	20	24	864	0.373	7.45
	32	24	1382	0.596	11.9
$R = -1$ fatigue	14	3	168	0.0725	1.45
	24	1	96	0.0414	0.828
	14	24	1344	0.580	11.5
	24	24	2304	0.994	19.9

Comparison of the S-N curves for $R = 0.1$ at reference and intermediate frequencies are presented in figure 2.5 and figure 2.6 while comparison with those at elevated frequencies are shown in figure 2.7 and figure 2.8.

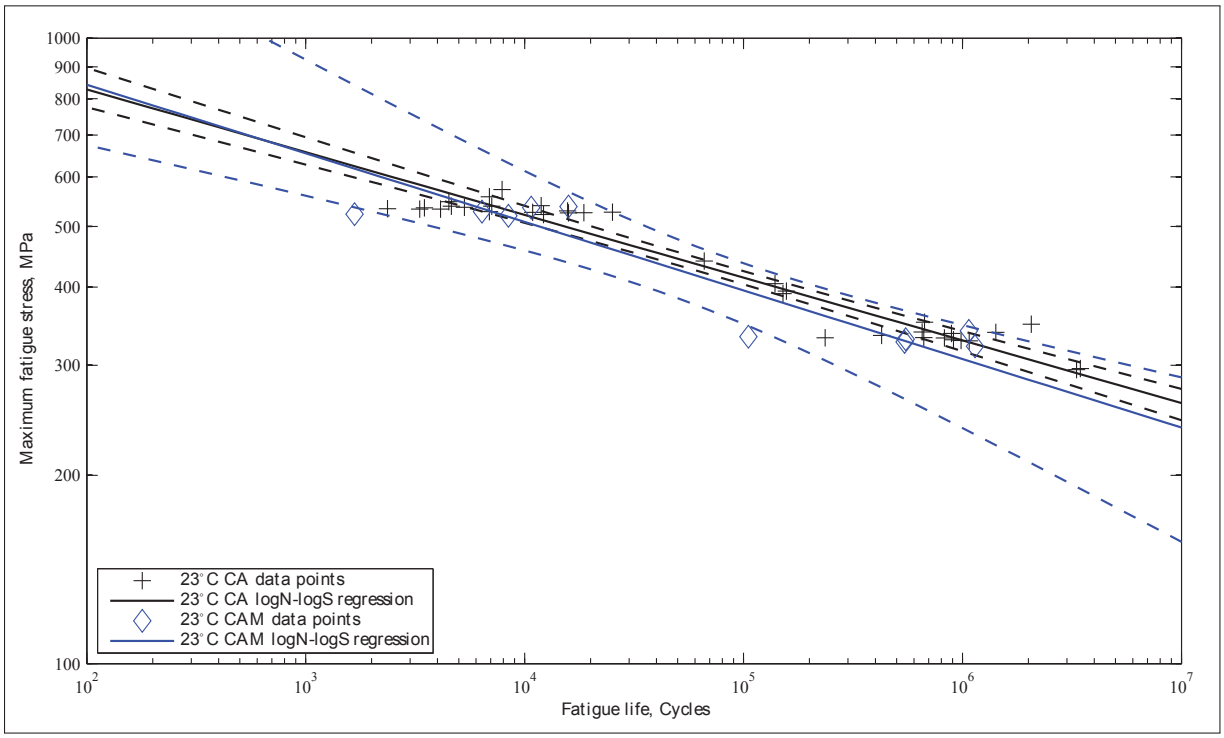

Figure 2.5 S-N diagrams for $R = 0.1$ fatigue at ambient temperature, intermediate (CAM), and low (CA) frequencies

From the results shown in Figure 2.5 and Figure 2.6, most data points for tests at intermediate frequency fall well within the dispersion of the baseline frequency test, although on the lower side. This suggests that for the unidirectional laminate being studied, a frequency of 8 Hz does not seem to significantly affect fatigue life of the specimen tested at room or at low temperature. Analysis of confidence bounds within the data range confirms that lives at moderate frequencies are comparable to those obtained at low frequencies for the same temperature.

In tensile fatigue, if the load frequency is increased to 24 Hz, lives of specimens tested at room temperature are reduced by almost a decade (figure 2.7) but the slope of the

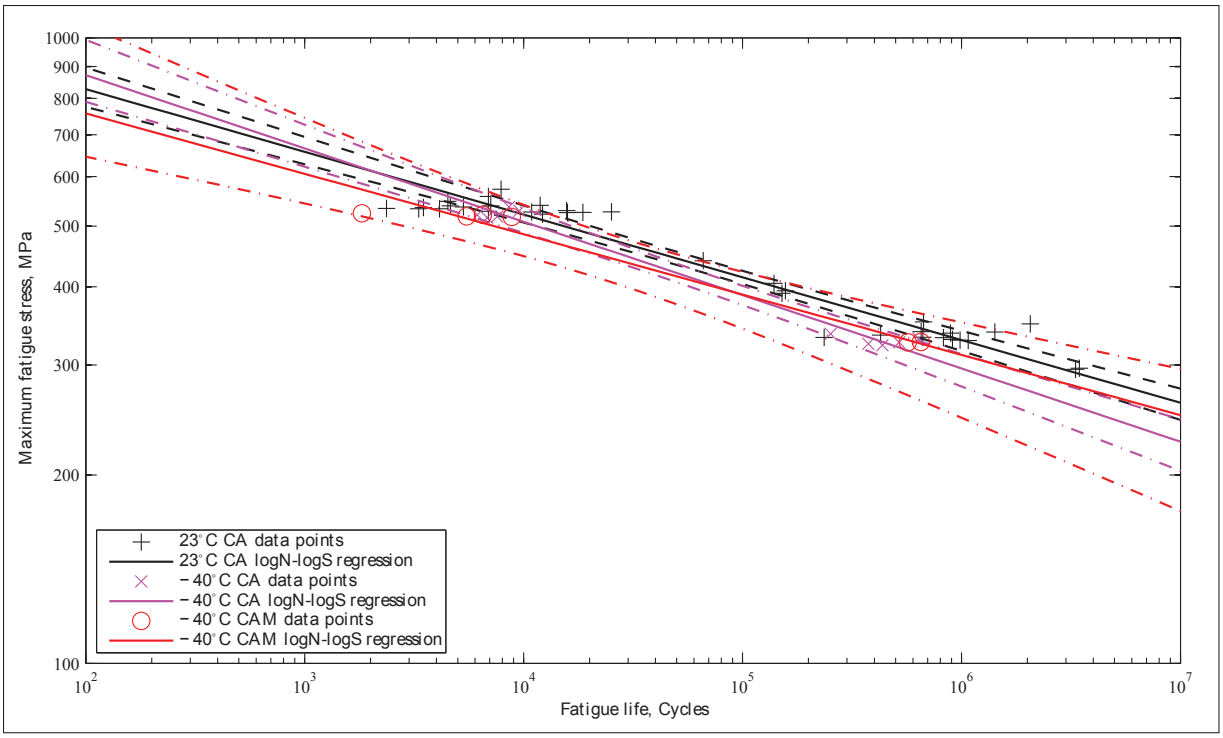

Figure 2.6 S-N diagrams for $R = 0.1$ fatigue at -40℃ intermediate (CAM) and low (CA) frequencies and 23℃ low frequency (CA)

S-N curve is not influenced. When tests are conducted at -40℃, the frequency effect appears to be reduced (figure 2.8). Low temperature CA and CAH curves have a slightly different slope and the CAH median curve appears to fall slightly out of the CA confidence bounds for a good part of the data range. Therefore, a S-N curve slope reduction at low temperature and high frequency cannot be ruled out. When compared to that of ambient temperature CA tests, the S-N curve of -40℃ CAH tests seems to be slightly shifted left, suggesting a small reduction of fatigue performance at higher frequency, even under intense cooling. Therefore either tests at -40℃ do not provide sufficient cooling to dissipate the additional internal heat generation due to the frequency (i.e. strain rate) increase, or the life reduction at higher frequencies is also affected by other factors. The fact that the slope difference between ambient and low temperature CA curves is similar to that between curves for CA and CAH at -40℃ also brings up the possibility that

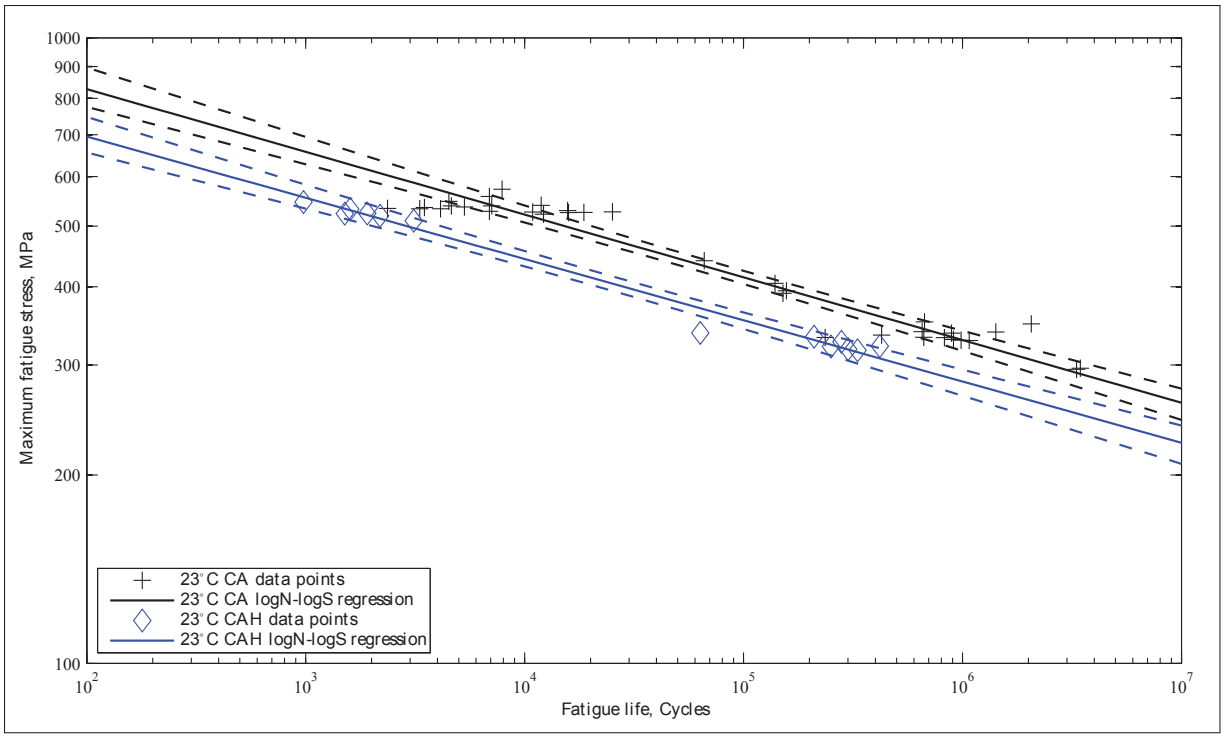

Figure 2.7 S-N diagrams for $R = 0.1$ fatigue at 23°C high (CAH) and low (CA) frequencies

even the low frequency used for ambient temperature testing is high enough to affect the results.

S-N curves for high frequency tests performed at $R = -1$ are presented in figure 2.9 and figure 2.10. These show that the general trends are the same as for tests conducted at a load ratio of $R = 0.1$. However, scatter is much more important for fully reversed fatigue.

From figure 2.9, the trend line of the fatigue life at ambient temperature and high frequency is about an order of magnitude lower than for low frequencies. Analysis of confidence bounds for these curves indicates that it is impossible to fit a single curve passing through both intervals within the data range so it can confidently be stated that the higher frequency results in a significant leftward shift of the S-N curve.

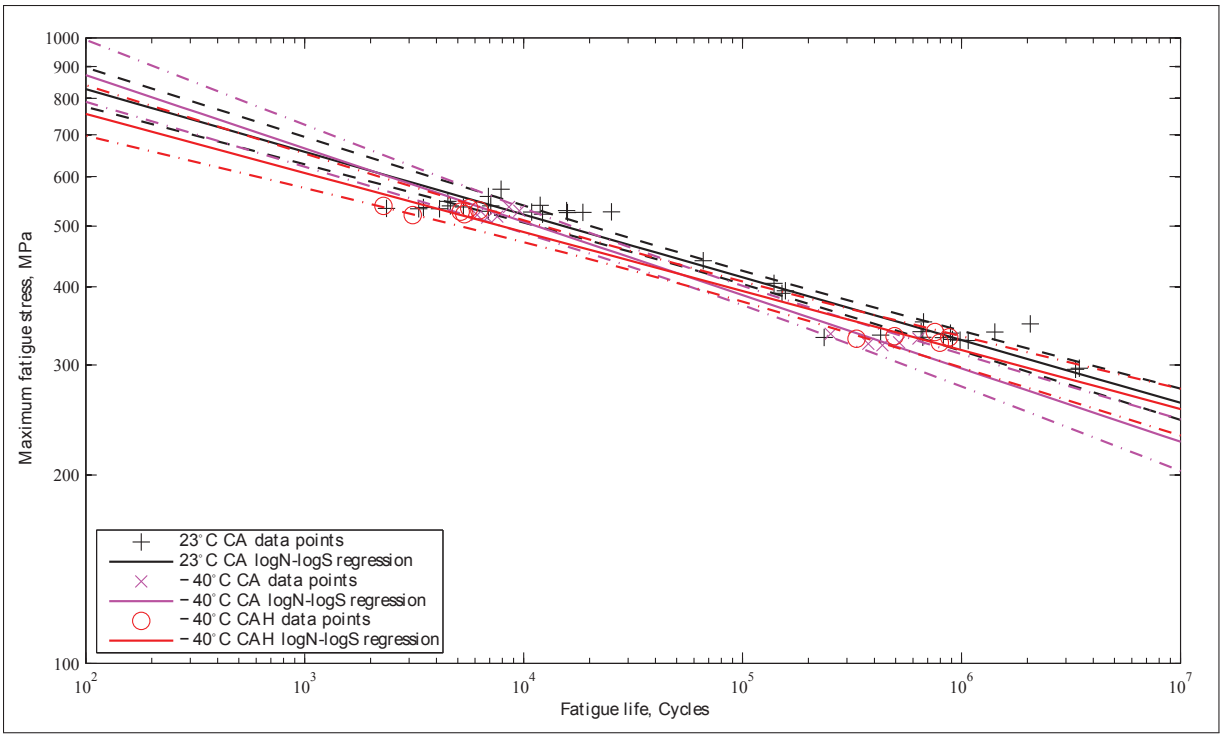

Figure 2.8 S-N diagrams for $R = 0.1$ fatigue at high (CAH) and low (CA) frequencies at -40℃ and low frequency (CA) at 23℃

Results from the -40℃ tests, shown in figure 2.10, prove that an increase in frequency induces a strong reduction of fatigue resistance at higher load levels, leading to an important reduction of the S-N curve slope. Consequently, average lives a decade lower are observed at the higher loads while similar lives are obtained at the lower end of the load range. This may be explained by the significant increase in strain rate for CAH tests at high load level. Therefore, an increase of frequency to 24 Hz for evaluation of fatigue performance at a temperature of -40℃ is to high.

Comparing CAH results at -40℃ to those from ambient CA, it is seen that the curve from the formers falls slightly outside the confidence bounds of the ambient CA condition on part of the data range, but that their confidence bounds have a considerable overlap. Therefore, the suggestion that for $R = -1$ fatigue of UD glass-epoxy composites, increasing test frequency while providing adequate cooling may produce similar results to those from ambient low frequency tests seems reasonable.

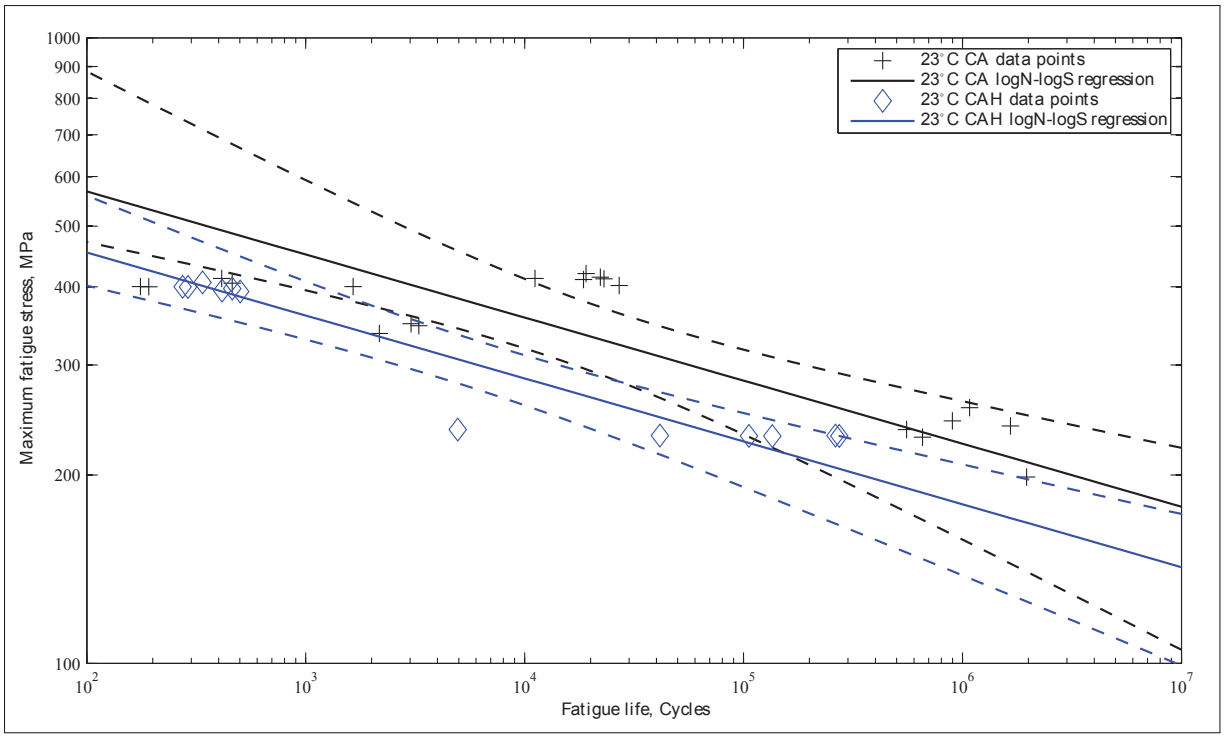

Figure 2.9 S-N diagrams for $R = -1$ fatigue at 23℃ high (CAH) and low (CA) frequencies

In order to relate effect of frequency on the fatigue life of the specimens, data points may also be plotted in a life-frequency diagram. In such a diagram, the fatigue life of each data point from a specific load level is plotted against the loading frequency. In this manner, frequency effects may be isolated. Figure 2.11 and Figure 2.12 respectively show the life-frequency plots for $R = 0.1$ and $R = -1$ tests.

The data presented in Figure 2.11 supports observations made from the S-N curves at $R = 0.1$. This is to say that at a given constant amplitude tension-tension loading, frequency up to 24 Hz result in a reduction of the composite fatigue life.

In the case of fully reversed fatigue, frequency effect seems to be more important than for tension-tension loading. For the ambient temperature tests performed at 24 Hz, lives are generally shorter than the low frequency average. At a temperature of -40℃, observations from the life-frequency diagram suggest that there is a load-temperature-frequency

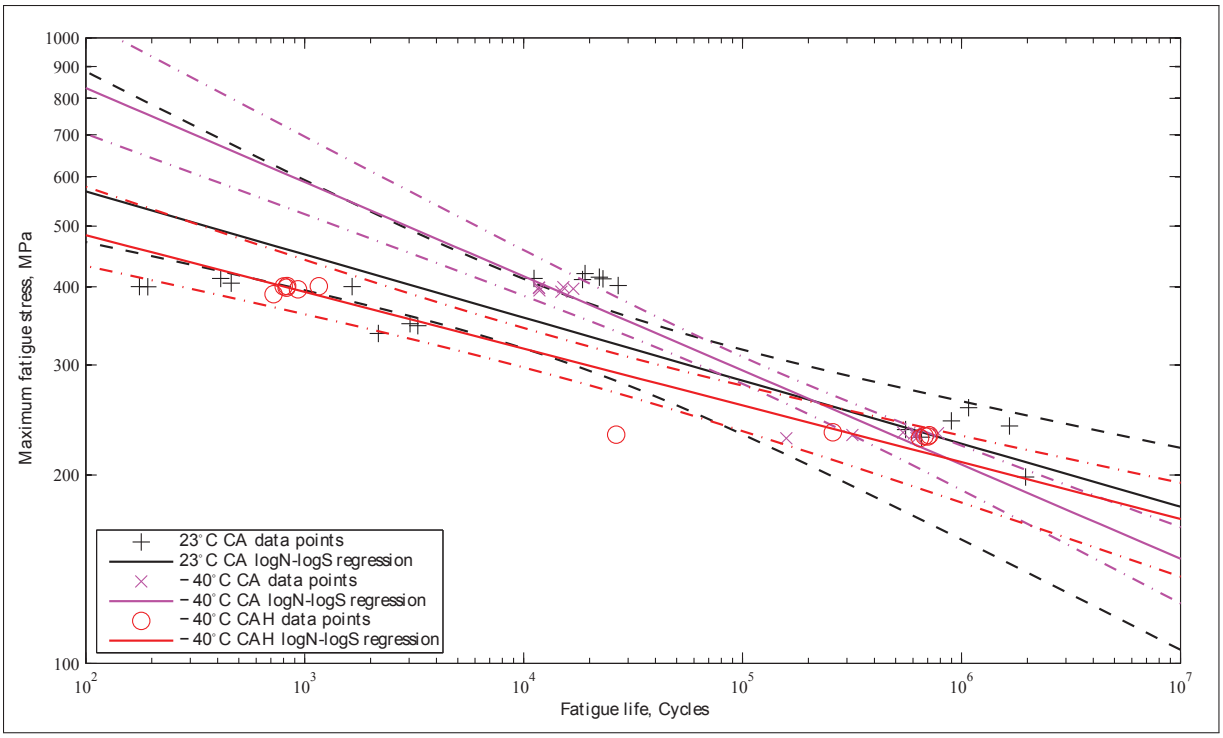

Figure 2.10 S-N diagrams for $R = -1$ fatigue at -40℃ high (CAH) and low (CA) frequencies and at 23℃, low frequency (CA)

interrelation. For high loads at low temperatures, there is a significant reduction of observed lives at 24 Hz. This is however not the case at lower loads were measured lives are quite similar independently of loading frequency. This could be attributed to the much higher strain rate at ±24 kN than at ±14 kN and supports the idea that, for the study of fatigue in composites, strain rate or strain energy rate should be accounted for instead frequency.

2.5 Conclusion

An extensive test program was carried out in an attempt evaluate consequences of testing at different temperatures on static properties of UD E glass-epoxy composites and to de-couple the effects of testing frequency and temperature on its fatigue performances. Therefore, the results shown in this report are a useful description of static and fatigue behaviour at $R = 0.1$ and $R = -1$ for temperatures of -40℃, 23℃ and 60℃.

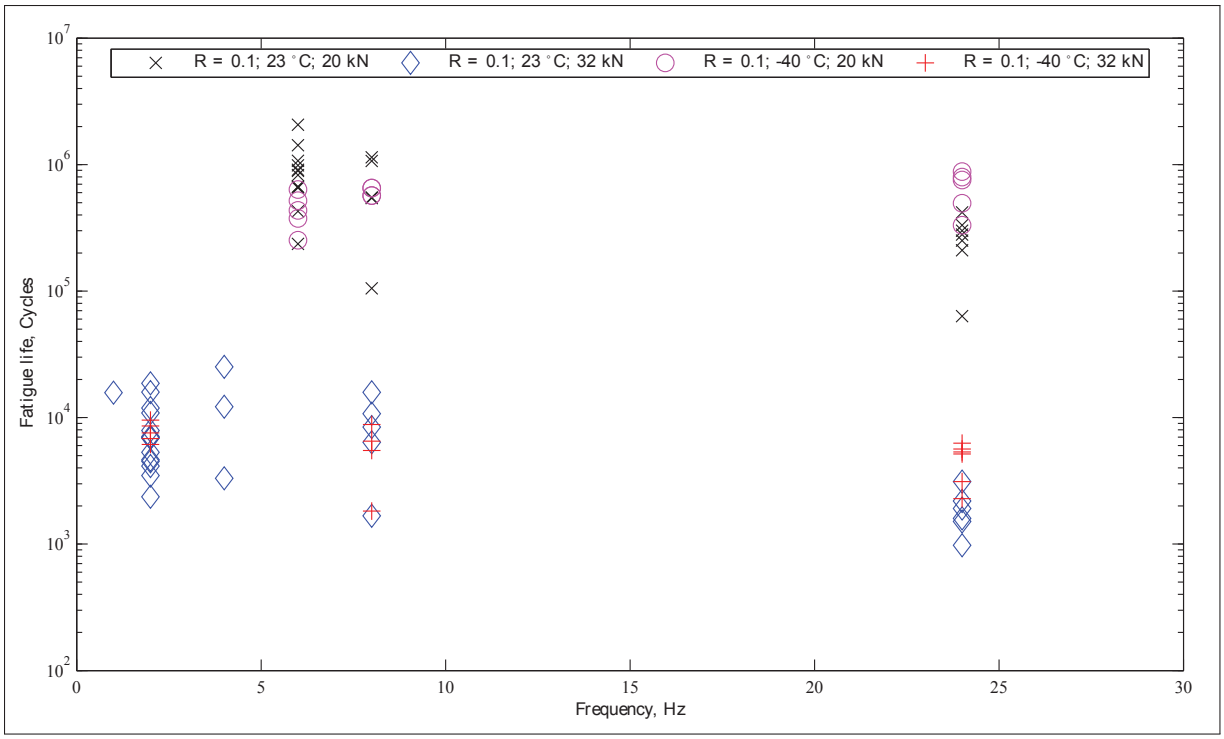

Figure 2.11 Life vs. test frequency for $R = 0.1$ fatigue

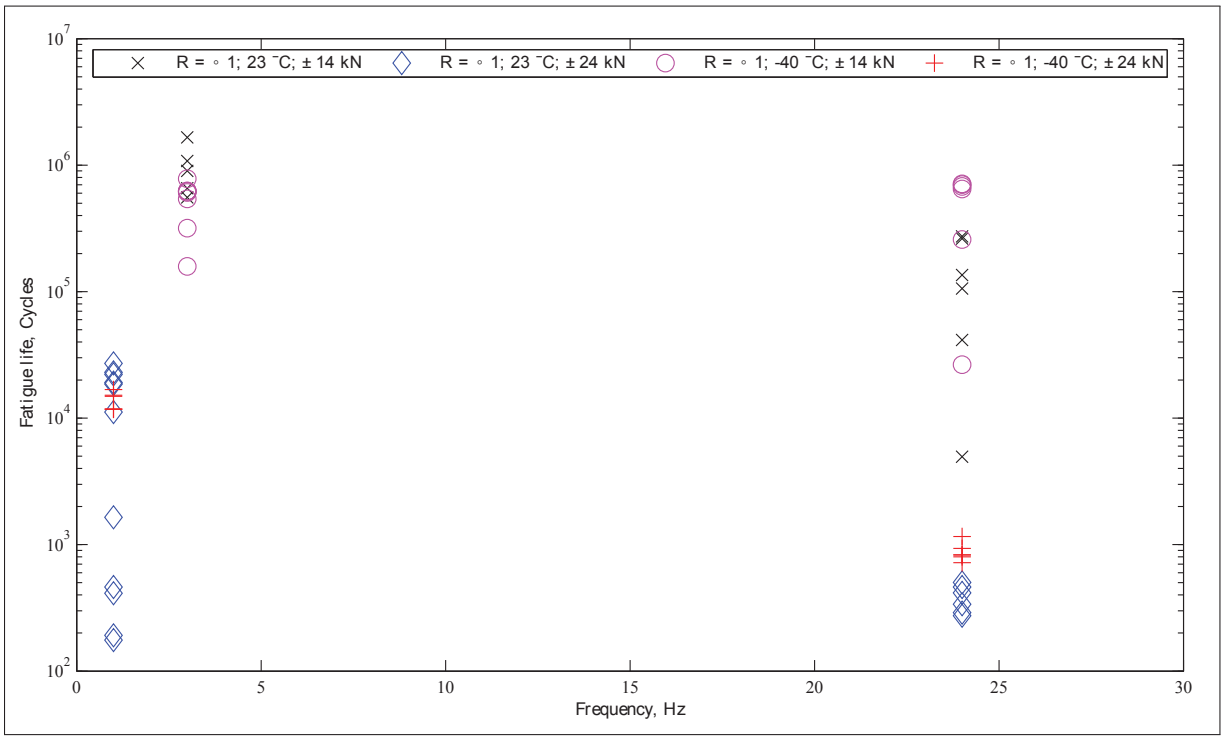

Figure 2.12 Life vs. frequency for $R = -1$ fatigue

These results show that static tensile and compressive strengths are significantly improved at -40℃, with gains of 13 % and 33 % respectively, while moduli remain unchanged. It is also observed that a temperature of 60℃ reduces these same strengths by 19 % and 31 %, while moduli are reduced by 7 % and 8 %. Therefore, under static loading, compressive properties are shown to be more sensitive to temperature than tensile ones.

Fatigue test results show that both temperature and frequency may significantly affect fatigue lives. It is demonstrated that the decrease of static properties at high temperature is reflected in fatigue. A temperature of 60℃ reduces fatigue life by about a decade for $R = 0.1$ loading while, with a three decades leftward shift of the S-N curve, it proves to reduce $R = -1$ fatigue strength to the point where it is almost impossible to test at the desired loads. However, the improvement in static strength due to cold temperature does not translate in a comparable improvement of fatigue performance. Lowering the temperature to -40℃ results in an increase of the S-N curve slope. In the case of $R = 0.1$ fatigue, lives are generally reduced while for $R = -1$ loading, lives may be slightly improved at high loads while they are reduced for lower loading.

Moderate frequencies (8 Hz) are shown to have very little effect on fatigue performance of UD glass-epoxy laminates. However, for a frequency of 24 Hz at ambient temperature, life reductions of a decade are obtained for both $R = 0.1$ and $R = -1$ loadings. At -40℃, S-N curves for high frequency tests appear to have a slightly lower slope than at low frequency. This may be the result of excessively high strain rates for elevated frequencies and loads leading to hysteretic heating of the specimen. Therefore, even though strong cooling is provided during fatigue testing at -40℃, the use of a 24 Hz frequency may be too high for evaluation of cold temperature fatigue performance.

Even in the scope of using high frequency and low temperature to reduce testing time for general fatigue performance evaluation, it appears that a temperature of -40℃ may not provide sufficient cooling for testing at 24 Hz under $R = 0.1$ loading. This assertion is supported by the lower fatigue lives obtained at -40℃ and 24 Hz compared to those for

the ambient temperature low frequency tests. On the other hand, the same temperature makes $R = -1$ elevated frequency results quite similar to those from 23℃ low frequency tests. This gives room for speculation on the possibility of accelerated testing, although a more thorough study of the fatigue failure mechanism should be pursued.

Finally, even if it is shown that there is a load-frequency-fatigue life interaction, it is suggested that strain rate or strain energy rate may provide a better indicator than frequency in order to model fatigue life.

Acknowledgments

The authors would like to acknowledge that work reported here was partially carried out in the framework of the EU-FP6 funded Upwind project, contract number SES6-019945. The authors also recognize the financial support of the Wind Energy Strategic Network (WESNet) of the Natural Sciences and Engineering Research Council of Canada (NSERC) for funding L. Cormier's international research visit and the KC-WMC for hosting this stay.

CHAPTER 3

EFFECTS OF LOW TEMPERATURE ON THE MECHANICAL PROPERTIES OF GLASS FIBRE–EPOXY COMPOSITES: STATIC TENSION, COMPRESSION, $R = 0.1$ AND $R = -1$ FATIGUE OF $\pm 45°$ LAMINATES

Laurent Cormier[1], Simon Joncas[1], Rogier P. L. Nijssen[2]

[1] Department of automated manufacturing engineering, École de Technologie Supérieure,
1100 Notre-Dame Ouest, Montreal, Quebec, Canada H3C 1K3
[2] Knowledge Center Wind Turbine Materials and Constructions (WMC), Kluisgat 5,
1771 MV Wieringerwerf, The Netherlands,

The following is the accepted version of the published article:

L. Cormier, S. Joncas and R. Nijssen, "Effects of low temperature on the mechanical properties of glass fibre-epoxy composites: Static tension, compression, $R = 0.1$ and $R = -1$ fatigue of $\pm 45°$ laminates", *Wind Energy*, vol. 19, pp. 1023-1041, June 2016, DOI:10.1002/we.1880.

Article available at http://onlinelibrary.wiley.com/doi/10.1002/we.1880/abstract

Abstract

Effects of cold climate exposure on composite material structures are scarcely documented. As a result, even if exceptional wind conditions prevail in some cold regions, uncertainties related to composite materials durability at low temperatures may hinder development of wind energy projects in those regions. Therefore, as part of the Wind Energy Strategic Network (WESNet) of the Natural Sciences and Engineering Research Council (NSERC) of Canada, efforts were made to evaluate the effects of cold climate exposure on the mechanical properties of glass–epoxy composites. Tensile and compressive quasi-static tests as well as tensile ($R = 0.1$) and fully-reversed ($R = -1$) fatigue tests were performed on vacuum-infused $[\pm 45]_{2s}$ glass–epoxy composites at -40℃ and 23℃. Results for quasi-static tests show an increase of tensile, compressive and shear strengths and moduli at low temperatures. It is also demonstrated that for the stress range under scrutiny, fatigue performance is improved at -40℃ for both the $R = 0.1$ and $R = -1$ loading cases. Moreover, the failure mode for $R = -1$ fatigue changed from

compressive failure due to buckling of delaminated plies to tensile failure, suggesting a more efficient use of the material. However, if $R = -1$ fatigue results at low temperature are extrapolated towards the very low stresses that are also part of wind turbine blades fatigue load spectrum, fatigue life may be degraded compared to that at ambient temperature. Finally, evidence of visco-elastic behaviour leading to changes in S-N curve slope parameter are reported.

3.1 Background

With the increased desire for harvesting resources from the world northernmost regions, questions arise regarding the performance and durability of equipments and structures exposed to the harsh environments prevailing there. Often, very limited information exists for operation under such severe conditions and reliability of equipments may have a major influence on projects costs, even more so considering the remoteness of the sites.

A good example of an industry facing challenges for harvesting resources from the North is the wind energy sector. Some northern regions have shown exceptional wind energy potential (210), but the financial risks associated with operation of a wind plant in those regions are sometimes very high. This risk is due in part to the uncertainties surrounding wind turbines' reliability and unavailability (e.g. due to shut down in case of weather conditions outside their design envelope) or failures. The report from the International Energy Agency (IEA) Task 19 expert group on wind energy in cold climate, provides several examples of the challenges facing the wind energy industry in cold regions (211).

Among the components that may undergo accelerated failure due to the harsh northern environment, one that could have a major impact on wind plant reliability is the turbine blade. As the blades are some of the most expensive components of utility scale wind turbines (212), their early failure might have a critical impact on a plant's cost of energy.

In their review of the challenges facing the composite materials industry in civil engineering applications, Kharbari and his colleagues suggested that future research on the topic of environmental effects on composites should concentrate on bonded joints and fatigue (205). More recently, in their review of material degradation in wind turbines, McGowan et al. concluded that the main degradation mechanisms of wind turbine blades were fatigue and creep and that a fundamental understanding of these mechanisms still lacked (9). McGowan also noted that for large wind turbine blades where inertial efforts are important, the exceptionally long fatigue life required – over $10^8 - 10^9$ cycles – meant that creep may become the dominant failure mode. In the concluding remarks of this review, the authors state that understanding the implications of service conditions such as moisture and temperature on the fatigue and creep performance of wind turbine blades composites is a necessity.

Figure 3.1 and Figure 3.2 respectively provide a description of typical loads on a utility scale wind turbine and of the geometry and material architecture of wind turbine blades. More detailed descriptions of wind turbine loads or blade structural design can be found in Hau (213), Brønsted et al. (12), Buckney et al. (214) or Griffin (215).

Figure 3.1 shows that wind turbine blades are essentially cantilever beams subjected to large flapwise bending aerodynamic loads, coupled to lesser chordwise bending and torsional aerodynamic loads. In addition to the aerodynamic loads depicted in Figure 3.1, inertial and gravitational loads are present although not illustrated as their value change greatly depending on the blade azimuth and acceleration. It is important to realize that all of these loads vary with time, leading to a very complex fatigue load spectrum. It is also worth noting that for multi-megawatt wind turbines, the gravitational loads and associated edgewise bending may become the structural design driver instead of the aerodynamic loads and flapwise bending (216).

As shown in Figure 3.2, the loads result in the blade upper surface being loaded in compression and the lower surface being under tensile stress. It is also seen that unidirectional

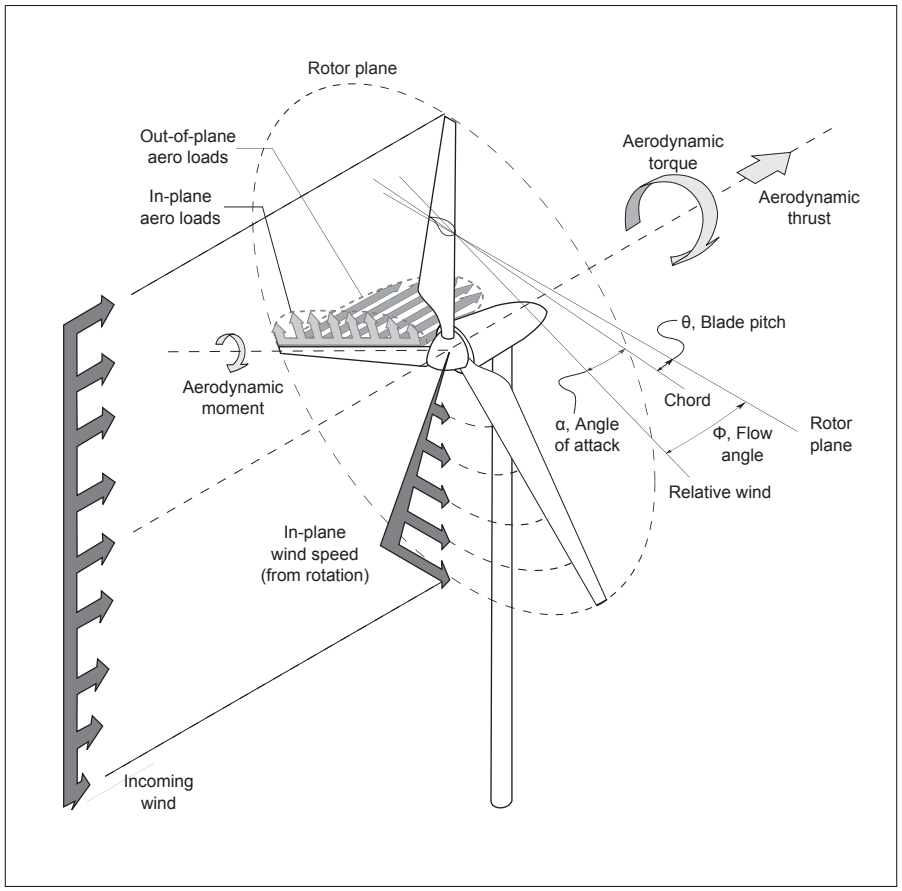

Figure 3.1 Schematics of simplified aerodynamic loading
for a typical utility scale wind turbine

and ±45° are the two major lamina configurations used in wind turbine blades load bearing structures. It is important to realize that failure of off-axis laminates like ±45° is likely to be dominated by matrix properties. As the latter are notoriously affected by temperature and moisture, it is evident that environmental conditions must also affect the mechanical performance of the composite. The adverse effects of high temperatures have been demonstrated in the past, but little efforts were devoted to identify effects of exposure to low temperatures.

A literature survey by Cormier and Joncas showed an important variability in the conclusions of past research on the effects of low temperature on the static properties of composites (84). For example, effects of temperature from 200 K to 422 K (-73℃ to

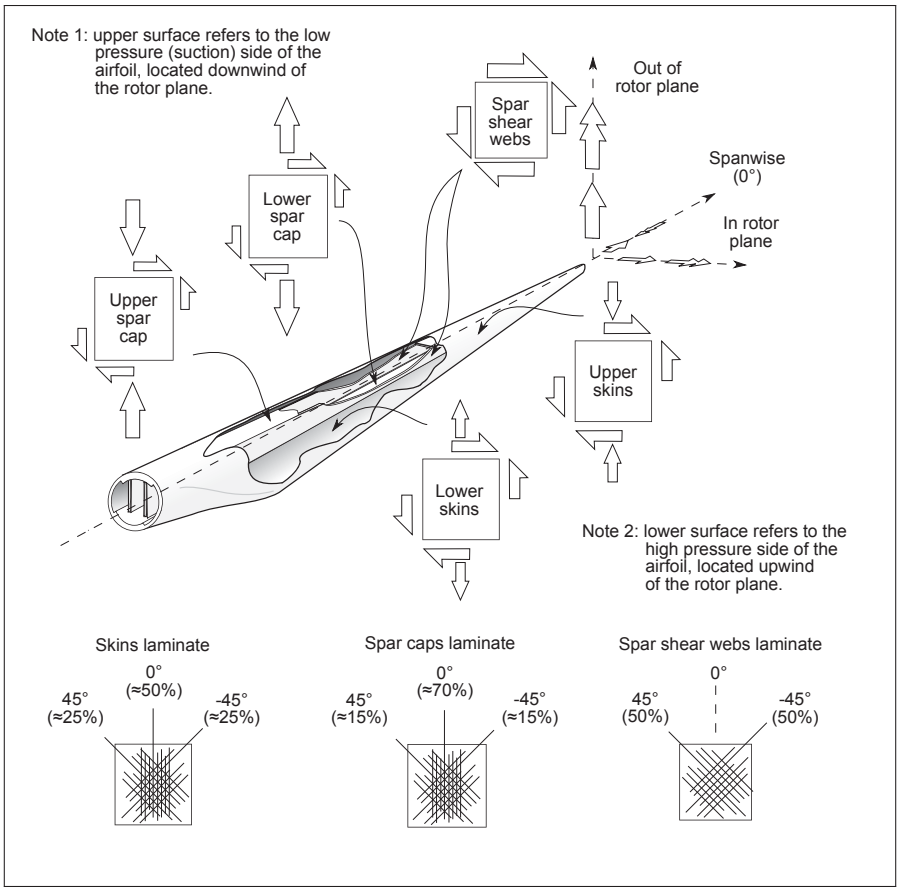

Figure 3.2 Typical utility scale wind turbine blade materials and loads

149℃) on static properties of carbon reinforced epoxy composites have been studied by Shen and Springer (217; 218). They concluded that low temperatures had little effects on tensile strength and modulus in the fibre direction, but that it could lower the tensile strength of some laminates with off-axis fibres. Bulmanis et al. reported reductions of strengths in carbon-epoxy, small reduction of wound glass–epoxy strength and no effects on [0/90] wound glass–epoxy (219). Dutta also reported results for temperatures ranging between -60℃ and 23℃. Low temperature produced compressive strength increase for pultruded glass–polyester, no effects on tensile strength of $\pm 45°$ S_2 glass–epoxy and decreasing tensile strength with increasing 0° fibre content for other S_2 glass–epoxy laminates (77; 103; 220). Cormier and Joncas reported large tensile and interlaminar shear

strength increase for unidirectional E glass–epoxy (fibre volume fraction, $v_f \approx 0.55$) at -40℃, but changes in modulus were not significant (84). A comparable tensile strength increase, as well as an increase in compressive strength, were also reported by Nijssen and Cormier (95) and Cormier et al. (221) for another unidirectional glass–epoxy with $v_f \approx 0.48$ tested at -40℃.

Early work on the topic of low temperature fatigue of glass–epoxy composites by Toth et al. (93) showed that cryogenic temperatures (20 K, -253℃) led to an increase in static tensile strength and $R = -1$ fatigue lives in triaxial $[-45/0_3/45/0_3/\pm 45/0_3/45/0_3/-45]$ laminates. However, they were unable to quantify the increase in static strength as their test frame was not strong enough to break the cold specimens. Furthermore, all their tests resulted in lives shorter than 100 000 cycles at loads less than 20 % of the laminate ultimate tensile stress at 300 K (27℃). Therefore, it is expected that improvements in glass fibre sizing and coupling agents as well as modern resin formulations may lead to modified behaviours. Moreover, the very long life expected from wind turbine blades would require extrapolation of results beyond reason.

A report by Sys also provides some $R = 0.1$ and $R = -1$ fatigue test data on $\pm 10°$ glass–unsaturated polyester composite with $v_f = 0.5$ tested at -20℃, 20℃ and 50℃ (180). Although very little analysis is provided with the data, results suggest that on a strain basis, the low temperature had little effects on fatigue performance.

Another example of work on low temperature fatigue is found in research from Bureau and Denault (184). They studied the effect of temperatures ranging from -40 ℃ to 50 ℃ on the $R = 0.1$ flexural fatigue of two composite materials. The first laminate was a 2-2 glass twill–polyester construction and the second was a biaxial glass fabric–polypropylene stacking. Both laminates were of $v_f = 0.6$. According to their results, when normalized by the static strength at their respective temperatures, stress-life (S-N) curves for the glass–polyester were superimposed, while those of the glass–polypropylene matrix composite showed a small improvement in fatigue life.

Tang et al. (181; 182) also showed that tensile fatigue of pultruded multi-axial E glass–vinyl ester laminates with $v_f = 0.36$ (about 0.24 random mat and 0.12 unidirectional roving in the principal direction) was influenced by temperatures in the range of 4℃ to 60℃. They suggested that the slope parameter of their S-N equation would decrease with an increase of temperature (clockwise rotation of the S-N curve). They also suggested that when plotting with stresses normalized by the static strength at the test temperature, the S-N curves would rotate about a point situated at $S = 2S_{ut}/3$ and $N = 1000$ cycles. However, their tests were run at 10 Hz, which is relatively high and might result in hysteretic heating of the specimen and interfere with interpreting the results. Moreover, their lowest test temperature was limited to 4℃.

Work from Nijssen and Cormier, conducted as part of the European Upwind project, also provides some results for tensile and reversed fatigue on unidirectional E glass–epoxy laminates ($v_f \approx 0.48\%$) at varying frequencies and temperatures (95; 221). Their results showed that at low frequencies, a temperature of -40℃ has minor negative to negligible impact on both tensile and reversed fatigue performance whereas a temperature of 60℃ proved very detrimental. The laminate glass transition temperature (T_g) was measured to be around 75℃.

Kujawski and Ellyin have shown that in $\pm 45^\circ$ glass–epoxy laminates, viscous effects play an important role in the dynamic response of the material (172). They observed that under cyclic loading, an accumulation of creep induced strains takes place and showed that the test frequency influences the cyclic creep rate. As dynamic thermal mechanical analyses under shear loading by Adams and Singh (39) have shown that epoxy resins and composites undergo a low-temperature transition (around $T = -40$℃) that is associated to a marked increase of loss factor, it is possible that low temperatures have deleterious effects on fatigue performance of $\pm 45^\circ$ glass–epoxy composites.

Understanding the effects of low temperatures on glass–epoxy composites response to fatigue loading is required to allow for the safe exploitation of the wind energy potential

in cold regions. In order to help bridging this knowledge gap, an important material testing campaign was included in the Wind Energy Strategic Network (WESNet) of the Natural Sciences and Engineering Research Council (NSERC) of Canada. This paper presents parts of the results from WESNet on the topic of cold climate durability of composite materials for wind turbines. It focuses on the results of the static tensile and compressive tests results as well as tensile and fully reversed fatigue test campaign on biaxial ($\pm 45°$) glass–epoxy composites.

3.2 Experimental

3.2.1 Material description

Test results presented herein are for glass–epoxy laminates of $[\mp 45]_{2s}$ configuration. The material had a $v_f = 0.47$ with standard deviation $\sigma = 0.01$ as measured by matrix burn-off on a single specimen of 25 mm by 25 mm taken from a random location on each of ten different 320 mm by 300 mm plates manufactured for specimen fabrication. The reinforcements are SAERTEX® multiaxial non-crimp fabrics. Each pair of $\mp 45°$ plies were pre-stitched fabrics of 831 g/m^2 total areal weight. Each of these stitched plies were constituted of a layer of 600 TEX E–glass strands oriented at -45° and good for 401 g/m^2 followed by 21 g/m^2 of 68 TEX E–glass strands at 90° and another 401 g/m^2 ply at +45°. These sub-plies were all stitched together with 6 g/m^2 worth of polyethersulfone (PES) thread running in the 0° and 90° directions. The matrix is Momentive Epikote™ MGS RIMR 135 epoxy resin cured with a 20/80 part mixture of Momentive Epikure™ MGS RIMH 134 and MGS RIMH 137 curing agents. Based on the resin manufacturer material data sheet, the cured neat resin's $T_g = 84.7°$C at the onset of the storage modulus drop, as measured by dynamic thermal mechanical analysis.

Laminates were manufactured at the Knowledge Center Wind Turbine Materials and Constructions (WMC) by vacuum assisted resin transfer moulding between two rigid aluminium plates that are bolted together. In order to provide a good control and

repeatability of laminates v_f and thickness, shims were inserted between the mould plates to ensure the predetermined spacing based on the target v_f and the areal weight of the fabric were respected. The tooling and resin were preheated to 30℃ prior to infusion. The infusion process was performed at 30℃. After infusion, the temperature was increased to 50℃ at a rate of 1℃/minute. Temperature was then kept at 50℃ for three hours. After the first temperature dwell period, temperature was raised to 70℃ at a rate of 1℃/minute where it remained for ten hours. The final cooling phase was uncontrolled. After fibre wetting under vacuum, the curing of the laminate is performed at atmospheric pressure to minimize void volume. Specimens were cut using a water-cooled diamond coated saw.

3.2.2 Test methods

Static and fatigue experiments were conducted on servo-hydraulic test frames either at École de technologie supérieure's (ETS) department of mechanical engineering material testing laboratory or at WMC. The air temperature around the specimen, the load and the displacement were monitored during the tests. An environmental chamber with temperature and humidity control was connected to the test chamber through a forced air system. The temperature control was on the environmental chamber and the temperature setpoint was adjusted so that the test chamber temperature matched the test temperature within ±1℃. In order to ensure that the temperature was uniform within the specimens, they were left at the test temperature for at least 15 minutes prior to testing. Tests were run at a temperature of -40℃ and 23℃. The test was interrupted if the air temperature within the test chamber was outside of a ±5℃ margin of the target temperature.

Tensile quasi-static experiments were performed in accordance to ISO 527 for off-axis laminates (222) and ISO 14129 for determination of shear properties (223). The compression tests are not standardized but the general requirements of ASTM D 3039 and ISO 527 were respected (except for the specimen geometry which is described later). Static test specimens were equipped with at least one longitudinal and one transverse

foil type strain gage with a grid resistance of 120 Ω (ETS) or 350 Ω (WMC) with respective excitation voltages of 2 V and 1 V. Low grid excitation voltages were used in order to minimize grid resistive heating. Tensile and compressive moduli are evaluated between 500 $\mu\epsilon$ and 2500 $\mu\epsilon$, while the shear chord modulus is evaluated between 1000 $\mu\epsilon$ and 5000 $\mu\epsilon$. Note that despite the extensive necking often encountered in $\pm 45^\circ$ laminates, failure stress are provided based on engineering strains, that is based on the nominal specimen cross-sectional area. At least five specimens were tested for each condition. It is important to realize that tensile testing of $\pm 45^\circ$ laminates allows for the characterization of both the tensile properties of the $\pm 45^\circ$ laminate as well as the shear properties of its constituent 0° unidirectional ply. However, it does not provide any information on shear performance of $\pm 45^\circ$ materials. The results, assuming limited constraint from the PES stitching and low amount of transverse fibres, are to be seen as a description of the shear behaviour of the UD laminates predominant in the spar caps and of the tensile behaviour of the $\pm 45^\circ$ laminates which form the major part of the skins and spars.

Fatigue experiments were load controlled and performed either at $R = 0.1$ or $R = -1$, with R being defined as the ratio of the minimum stress during the cycle (s_{min}) over the maximum cyclic stress (s_{max}) as per:

$$R = \frac{s_{min}}{s_{max}}. \tag{3.1}$$

Therefore, $R = 0.1$ makes for a pure tensile fatigue case and $R = -1$ implies a fully reversed fatigue cycle with an equal tensile and compressive stress magnitude.

All S-N curves and their equations are based on the maximum stress s_{max} or the maximum stress normalized by the static strength at the test temperature s_{max}/S_{ut}. Note that a capital S denotes a strength while a lower case s is used for stress. In practice, a maximum cyclic load P_{max} was defined and the stress was calculated according to:

$$s_1 = \frac{P}{A} \tag{3.2}$$

for tension or:

$$s_{12} = \frac{P}{2A} \tag{3.3}$$

for shear. In equation 3.2 and equation 3.3, P is the load and A is the specimen cross-sectional area. The subscripts 1, 2, 12 (as well as x, y, xy which will be used later) refer to material directions which are defined in Figure 3.3 c). Since the stress-strain relationship of the laminate is non-linear and since only a fraction of fatigue specimens were equipped with strain gauges, the analysis is limited to that based on stresses. A sinusoidal waveform was used for the load cycle. Low test frequencies (f) were also used in order to ensure that changes in behaviour at low temperature could not be attributed to a compensation of autogenous (hysteretic) heating (122; 181; 165; 174; 163). Moreover, the testing frequency was adjusted as a function of the maximum load in order to maintain an approximately constant strain energy rate as per equation 1.88, by Krause (201).

$$f_2 = f_1 \frac{\epsilon_1^2}{\epsilon_2^2} \qquad \text{(equation 1.88 revisited)}$$

Equation 1.88 is relative to a reference frequency-strain amplitude which must be determined experimentally. In the current work, the reference condition was based on surface temperature measurements near the grips at the higher fatigue load level. The acceptable threshold for temperature was set at 35℃ before failure. However, average temperatures during tests at room temperature were all below 27℃.

The use of equation 1.88 for determining test frequencies should make any internal heat generation due to viscous effects uniform over the range of experiments. Moreover, it ensures that if cyclic creep strain build-up occurs, it should also remain similar between experiments at different loads (172). Table 3.1 provides the description of the fatigue test matrix. Each of the S-N curves are obtained from a minimum of six specimens spread over a range of three load levels, allowing for a replication of 50% based on ASTM E 739 (152).

Table 3.1 List of fatigue specimens and associated test parameters

R -	Laboratory -	Specimen identifier -	T °C	f Hz	P_{max} N	A mm^2	s_{max} MPa
0.1	ETS	SI02I10	23	3.0	3400	72.9	47
		SU02I10	23	3.0	3825	64.8	59
		TA01I10	23	2.0	4250	64.9	66
		SO07I10	23	2.0	4250	66.8	64
		SU01I10	23	2.0	4250	64.2	66
		SI03I10	23	1.0	5100	73.1	70
		TA03I10	23	1.0	5100	65.7	78
		SR04I10	23	1.4	5950	68.6	87
		SY07i10	-40	2.0	4250	67.7	63
		SR01I10	-40	2.0	4250	66.1	64
		SO08I10	-40	1.4	5100	67.0	76
		SS10I10	-40	1.4	5100	65.0	79
		SY06I10	-40	1.4	5100	68.0	75
		SR05I10	-40	1.0	5950	69.4	86
		SU05I10	-40	1.0	5950	64.6	92
	WMC	SO02I10	23	4.0	4000	67.1	60
		SO03I10	23	4.0	4000	66.4	60
		SU10I10	23	4.0	4000	64.3	62
		SS04I10	23	4.0	4000	65.8	61
		SO04I10	23	2.0	6000	65.9	91
		SU06I10	23	2.0	6000	65.0	92
		SU09I10	23	2.0	6000	64.9	93
		TA08I10	23	2.0	6000	66.9	90
		SY04I10	-40	1.0	6000	67.9	88
		SY05I10	-40	2.0	6000	67.9	88
		SR06I10	-40	2.0	6000	69.4	86
		SR10I10	-40	2.0	5500	69.3	79
		SS03I10	-40	4.0	5250	66.0	80
		SH07I10	-40	4.0	5250	68.4	77
		SR08I10	-40	4.0	4000	69.6	58
		SI08I10	-40	4.0	5000	74.6	67
		SY03I10	-40	4.0	5000	66.1	76

Table 3.1 List of fatigue specimens and associated test parameters

R -	Laboratory -	Specimen identifier -	T °C	f Hz	P_{max} N	A mm^2	s_{max} MPa
-1	ETS	TB19R09	23	2.0	1750	53.2	33
		SN01R09	23	1.4	2100	52.8	40
		TB12R09	23	1.4	2100	54.1	39
		TB10R09	23	1.0	2450	54.1	45
		SN10R09	23	1.0	2450	53.8	46
		SV07R09	23	1.0	2750	51.7	53
		SN17R09	23	0.8	2800	53.8	52
		TB17R09	-40	1.4	2100	53.6	39
		SN02R09	-40	1.4	2100	53.3	39
		SN03R09	-40	1.0	2450	53.4	46
		SN20R09	-40	1.0	2450	53.9	46
		SV06R09	-40	0.8	2800	51.6	54
		TB03R09	-40	0.8	2800	54.8	51

3.2.3 Specimen description

The tensile specimen geometry is very similar to that of ASTM D3039 (224) and ISO 527 (222) for multi-axial laminates as well as that of ASTM D3518 (225) and ISO 14129 (223) for in-plane shear properties of ±45° laminates. This geometry also corresponds to the Optimat I10 specimen geometry (132). Figure 3.3 a) provides the general information on the specimen geometry. Note that according to the convention presented in Figure 3.3 c), the laminate that was used for in this project is $[\mp 45]_{2s}$. However, since in the context of this paper there is no difference between such a laminate and $[\pm 45]_{2s}$, no distinctions will be made from this point on. Although they are not required by the standards, straight tabs made of 2 mm thick ±45° glass–epoxy laminates bonded with epoxy adhesive were used. Tabs were used as, in addition to providing protection against mechanical damage due to gripping, they provide thermal insulation between the grips and the gage section.

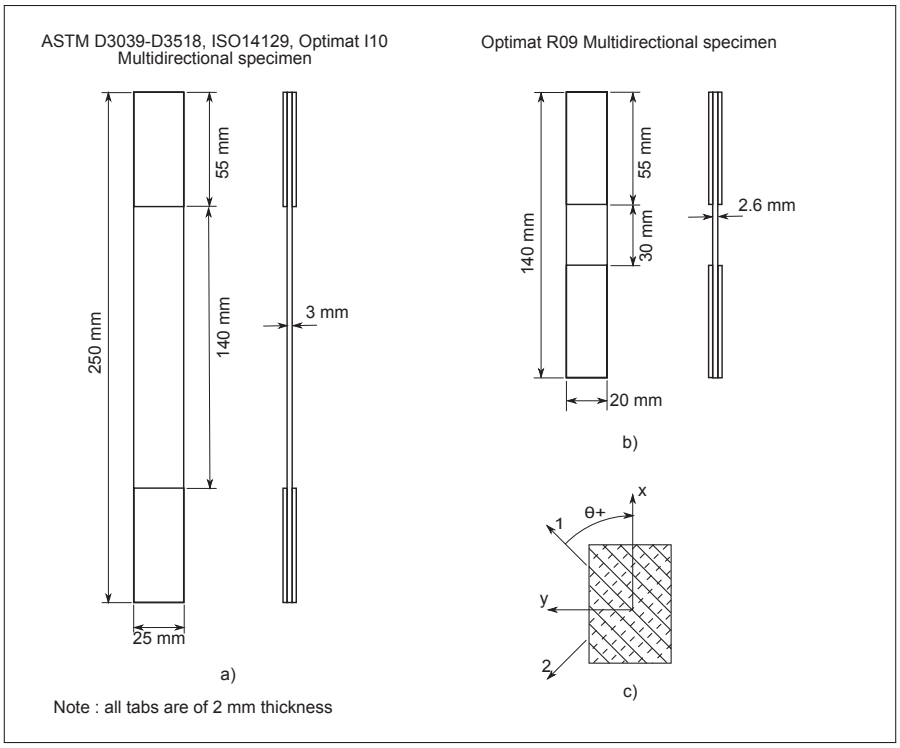

Figure 3.3 Specimen descriptions : a) ASTM D3039-D3518, ISO 527-14129, Optimat I10 Multidirectional specimen for tension and $R = 0.1$ fatigue tests, b) Optimat R09 Multidirectional specimen for compression and $R = -1$ fatigue tests, c) Specimen and fibre axes convention

Static compression and fully reversed fatigue specimens are of the Optimat R09 geometry. The R09 specimen is a general purpose geometry proposed in the Optimat project. It is a thick, short specimen designed to prevent buckling under compression and has a gage section longer than the specimen width to ensure that off-axis fibres do not run from one tabbed section to the other (132). A description of the R09 specimen geometry is provided in Figure 3.3 b).

It is worth noting that some of the materials and specimen peculiarities do not totally comply with the requirements of ISO 14129. First, the presence of stitching and transverse fibres will result in a constraint of the ply pairs reaction to shear. However, since

the stitching is non-structural and worth less than 1% of the fibre weight, it is believed that its effect will be limited. Similarly, the presence of 2.5% by weight of transverse glass fibres is expected to have limited effect on the material shear behaviour. Finally, the short length of the compression specimen is also likely to have a somewhat more complex stress distribution than a longer specimen, but the short length is a prerequisite to avoid buckling.

3.2.4 Determination of S-N parameters

Parameters of the S-N relationship and their statistics are estimated using the maximum likelihood (ML) estimation method. The ML method allows for the proper mathematical treatment of censored data (e.g. runouts or interrupted tests due to time constraints or technical reasons). A detailed description of the ML approach can be found in textbooks such as Nelson's (226) or Gijbels' paper (227). Applications to the fatigue problems are given in such papers as those from Nelson (156), Spindel and Haibach (228) and a specific application to fibrous composites is found in Sendeckyj (141).

Although the application of the ML estimation method is relatively complex, the concept itself is simple. The basic idea is to assume a relationship describing the phenomena being modelled and its underlying statistical distribution. Loosely speaking, the likelihood of a result is the probability of the datum point value being observed (or exceeded in the case of a runout) given the model and the statistical distribution. The likelihood of each data point is then evaluated as a function of the relationship parameters. The total likelihood of the relationship corresponds to the product of the likelihoods of each datum point. The solution of the problem is the set of relationship parameters that maximize the total likelihood and is found by optimization methods. It is interesting to note that the ML approach results in a weighting of the influence of a censored data point on the relationship parameter determination according to how far it lies from the average of the results. On the one hand, the farther a censored point is below the average, the more likely it is (i.e. its probability tends to unity) and the less impact it has on the total

likelihood. On the other hand, the farther a data point exceeds the average, the less likely it is (i.e. its probability tends to zero) and the more weight it has.

For the current project, a log-log linear relationship of the S-N curve as that of equation 3.4 is assumed.

$$\log(N) = \gamma_1 + \gamma_2 \log(s) \tag{3.4}$$

In equation 3.4, $\log(s)$ is the base 10 logarithm of the maximum cyclic stress (or normalized cyclic stress) and is the independent variable, $\log(N)$ is the base 10 logarithm of the life in cycles, while γ_1 is the intercept coefficient and γ_2 is the slope coefficient of the relationship. In order to assess the likelihood and as it is desirable that the model provides statistical information like confidence intervals on the S-N curve, an underlying statistical distribution is required. In the present work, it is assumed that the data has a lognormal distribution and that the log-standard deviation σ_L is constant for all stress levels. The ML estimation therefore also has to evaluate a third parameter $\gamma_3 = \sigma_L$. Confidence bounds are given by the approximate normal confidence interval approach. Parameters $\hat{\gamma}_1$, $\hat{\gamma}_2$ and $\hat{\gamma}_3 = \hat{\sigma}_L$ are the estimators that are provided by the ML method as approximate values of the true parameters γ_1, γ_2 and γ_3.

It is worth noting that the determiation of confidence bounds by the approximate normal confidence interval approach relies on the asymptotic theory and on the assumption of normal error distribution. However, in the context of fatigue in general, and particularly in part of the present work, a low number of test results preclude the robust verification of those underlying assumptions. Nevertheless, considering that the results of the present work are generally well behaved, the estimations should be acceptable.

3.3 Results and discussion

3.3.1 Strength and modulus of ±45° laminates

The tensile test on $[\pm 45]_{2s}$ laminates can either be regarded as providing off-axis strength and modulus of the laminate (S_x and E_x) or as an indicator of the shear properties of its cross-ply ($[0/90]_s$) 0° sub-laminate (S_{12} and G_{12}). The following analysis reflects these possibilities and results are provided for both cases.

3.3.1.1 Tensile properties

Results from the tensile experiments on $[\pm 45]_{2s}$ laminates are presented in Table 3.2 for both test temperatures. These results show that low temperatures leads to a significant increase of both tensile strength (S_x^+) and modulus (E_x^+) of ±45° laminates. S_x^+ increased by 33 % on passing from a temperature of 23℃ to a temperature of -40℃, while E_x^+ rose by 20 % for the same temperature drop. Inspection of the 95% normal confidence intervals on S_x^+ and E_x^+ shows that the differences in strength and modulus at the two test temperatures are statistically significant, while the change in standard deviation of these properties is not.

Table 3.2 Tensile properties of $[\pm 45]_{2s}$ glass–epoxy

T °C	Property -	S_x^+ MPa	$\sigma_{S_x^+}$ MPa	E_x^+ GPa	$\sigma_{E_x^+}$ GPa
23	Mean	130	4.38	11.8	0.444
	95% bounds	[127, 133]	[3.01, 7.99]	[11.5, 12.1]	[0.306, 0.811]
-40	Mean	173	6.34	14.2	0.861
	95% bounds	[165, 181]	[3.80, 18.31]	[13.2, 15.3]	[0.516, 2.49]

These changes are believed to be mostly due to increases in matrix mechanical properties, although the interphase (i.e. the transition region between the fibre surface and the bulk matrix) might also be affected by the temperature change. It appears that internal stresses due to the discrepancy between the matrix and fibre thermal expansion coefficient as well as the interlaminar thermal stress due to the lower temperature do not negatively impact the laminate strength.

3.3.1.2 Shear properties

Due to the importance of the shear stress component on ±45° laminates under tension loading, the test can also be considered as an indicator of the shear behaviour of UD or cross-ply laminates. Therefore, analysis of the tests from the shear perspective are also provided in Table 3.3.

Table 3.3 Shear properties of glass–epoxy 0° sub-plies

T °C	Property -	S_{12} MPa	$\sigma_{S_{12}}$ MPa	G_{12} GPa	$\sigma_{G_{12}}$ GPa
23	Mean	65.1	2.20	3.45	0.150
	95% bounds	[63.5, 66.7]	[1.51, 4.01]	[3.34, 3.56]	[0.103, 0.275]
-40	Mean	86.5	3.17	4.38	0.275
	95% bounds	[82.6, 90.5]	[1.90, 9.15]	[4.04, 4.72]	[0.165, 0.795]

As expected for matrix dominated properties, temperature effects are important. As could be anticipated from equation 3.2 and equation 3.3, when measured at a temperature of -40℃ the increase in S_{12} is 33 %, or the same as for tensile strength. However, the shear chord modulus (G_{12}) rises by 27 % in the same condition, which is more than what was observed for E_x. Again, the 95% normal confidence intervals show the statistical significance of the strength and stiffness increase at -40℃.

3.3.1.3 Compressive properties

A summary of results from compression experiments is given in Table 3.4.

Table 3.4 Compressive properties of $[\pm 45]_{2s}$ glass–epoxy

T °C	Property -	S_x^- MPa	$\sigma_{S_x^-}$ MPa	E_x^- GPa	$\sigma_{E_x^-}$ GPa
23	Mean	130	3.43	12.3	0.236
	95% bounds	[126, 134]	[2.14, 8.42]	[12.1, 12.5]	[0.148, 0.580]
-40	Mean	177	7.68	14.6	0.453
	95% bounds	[169, 185]	[4.79, 18.9]	[14.9, 15.0]	[0.283, 1.11]

Low temperatures result in a very significant increase of both S_x^- and E_x^- of $\pm 45°$ laminates. S_x^- increased by 36 % on passing from a temperature of 23℃ to a temperature of -40℃ while E_x^- rose by 24 % at low temperature. Based on the confidence intervals, the changes in strength and stiffness are statistically significant to the 5% level.

The fact that S_x^+ and S_x^- are very similar both nominally and at low temperature suggests that the R09 sample geometry was adequate to prevent buckling. It is also worth noting that the stitching may contribute to the good buckling resistance of the specimen as by being stitched in pairs plies are held together even if delamination occurs.

3.3.1.4 General considerations on static strength at low temperature

The current results show a globally improved performance of the $[\pm 45]_{2s}$ laminate at -40℃. These results are in contradiction to earlier work on off-axis composites by Shen and Springer (217; 218), Bulmanis et al. (219) and Dutta (77; 103; 220). However, more recent work on unidirectional glass-epoxy by Cormier and Joncas (84) as well as Nijssen and Cormier (95; 221) show improvements of mechanical properties at low temperatures. One of the possible causes for this discrepancy is the v_f, which are not stated in the

papers from Shen and Springer or Dutta, but that could have a significant effect on low temperature behaviour by influencing the stress distribution around fibres, increasing stress concentration with v_f. The specific thermo-mechanical properties of fibres — e.g. the negative coefficient of thermal expansion (CTE) of carbon fibres — may also have an important effect on thermal stresses occurring at low temperatures (28). The authors believe that changes in modern coupling agents and matrix formulations might also be involved as improvements to these parameters might allow a shift from a state where mechanical properties were limited by the interphase strength to a state where matrix properties govern failure in more modern laminates.

3.3.2 $R = 0.1$ tensile fatigue

A summary of individual specimen results for $R = 0.1$ fatigue tests is provided in Table 3.5.

The ML estimates of the fatigue curves parameters and their respective 95 % confidence bounds (based on absolute and normalized stresses) are given in Table 3.6 for both temperatures. The S-N curves based on absolute stresses are provided in Figure 3.4 while those based on normalized stresses are shown in Figure 3.5.

The following remarks can be formulated based on the results from Table 3.6 and Figure 3.4.

a. The change in slope of the S-N curves is small, but statistically significant (higher slope coefficient at -40℃).

b. The fatigue life at -40℃ is improved by more than an order of magnitude compared to that at 23℃.

c. The scatter of the results at low temperature seems to be lower.

Table 3.5 Results for $R = 0.1$ fatigue on $[\pm 45]_{2s}$ glass–epoxy

Laboratory	T °C	Specimen identifier -	s_{max} MPa	N^a Cycles
ETS	23	SI02I10	47	+10886752
		SU02I10	59	953283
		TA01I10	66	242181
		SO07I10	64	220179
		SU01I10	66	180607
		SI03I10	70	114619
		TA03I10	78	51655
		SR04I10	87	8824
	-40	SY07i10	63	3867128
		SR01I10	64	+1687988
		SO08I10	76	464906
		SS10I10	79	+79295
		SY06I10	75	752347
		SR05I10	86	258191
		SU05I10	92	70520
WMC	23	SO02I10	60	1670975
		SO03I10	60	1105538
		SO04I10	91	6392
		SS04I10	61	3180623
		SU06I10	92	2624
		SU10I10	62	459045
		SU09I10	93	1956
		TA08I10	90	4931
	-40	SY04I10	88	98133
		SY05I10	88	92502
		SR06I10	86	104809
		SR10I10	79	326375
		SS03I10	80	442294
		SH07I10	77	1047477
		SR08I10	58	+1677069
		SI08I10	67	+2008653
		SY03I10	76	+1004174

[a] Runouts indicated by a "+" sign before the cycle count.

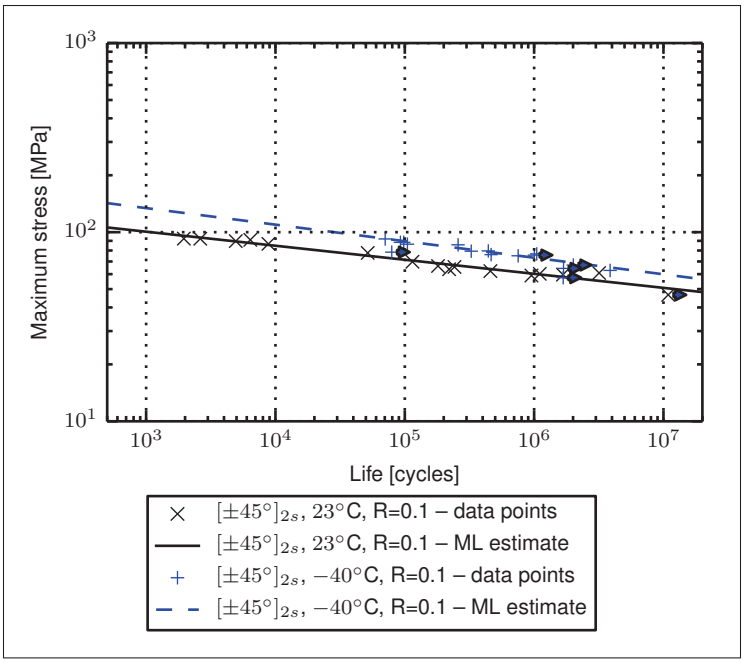

Figure 3.4 S-N curves for $R = 0.1$ fatigue on $[\pm 45]_{2s}$ glass–epoxy at 23℃ and -40℃ (solid arrows indicate runouts)

Table 3.6 Maximum likelihood estimators of S-N parameters for $R = 0.1$ fatigue on $[\pm 45]_{2s}$ glass–epoxy

Analysis type -	T °C	Property -	$\hat{\gamma_1}$ log(Cycles)	$\hat{\gamma_2}$ log(Cycles log(MPa)$^{-1}$)[a]	$\hat{\gamma_3} = \hat{\sigma}$ log(Cycles)
Absolute	23	Median	30.0	-13.5	0.215
		95 % bounds	[27.2, 33.0]	[-15.0, -11.9]	[0.146, 0.317]
	-40	Median	27.3	-11.4	0.148
		95 % bounds	[23.8, 31.4]	[-13.4, -9.4]	[0.093, 0.234]
Normalized	23	Median	1.49	-13.5	0.215
		95 % bounds	[1.13, 1.97]	[-15.0, -11.9]	[0.146, 0.317]
	-40	Median	1.73	-11.4	0.148
		95 % bounds	[1.17, 2.57]	[-13.4, -9.4]	[0.093, 0.234]

[a] log(Cycles) for normalized analysis

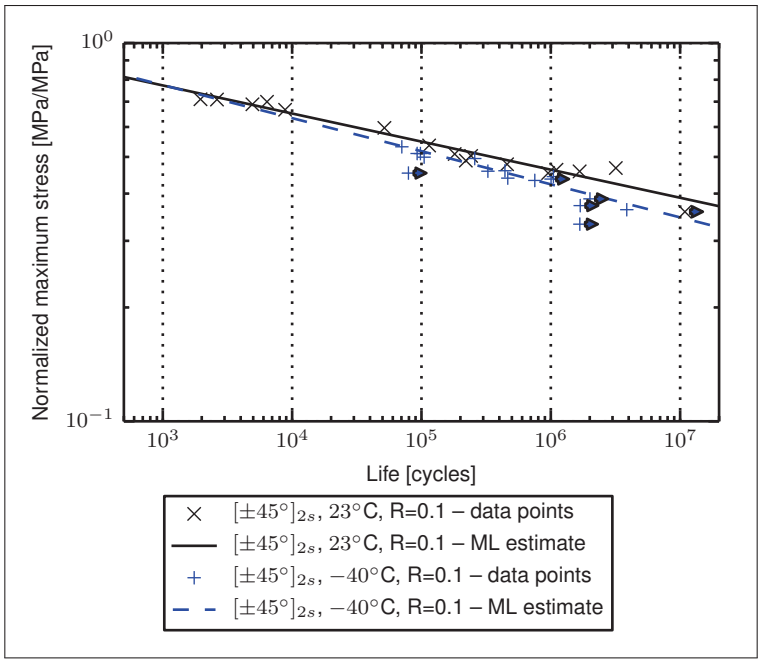

Figure 3.5 Normalized S-N curves for $R = 0.1$ fatigue on $[\pm 45]_{2s}$ glass–epoxy at 23℃ and -40℃ (solid arrows indicate runouts)

The first observation is supported by the fact that, although the damage evolution process is somewhat affected, the final failure mode seems to remain unchanged. Figure 3.6 illustrates the damage evolution for a room temperature test. The damage appears to initiate as matrix cracking between fibres. these cracks then grow along the fibre direction. Aided by the out-of-plane stress near the specimen edges, cracks emanating from each ply eventually coalesce, leading to ply separation near the edges. As these delaminations grow toward the centre of the specimen, the original cracks along the fibres also continue to grow and coalesce, creating additional delaminated regions. These damages continue to grow until final failure of individual plies along their fibre direction.

However, as evidenced by a much lower crack density outside the failure area on tests performed at -40℃, it appears that cracking, coalescence and delamination are delayed substantially at low temperature. In Figure 3.7, post-mortem photographs of specimens

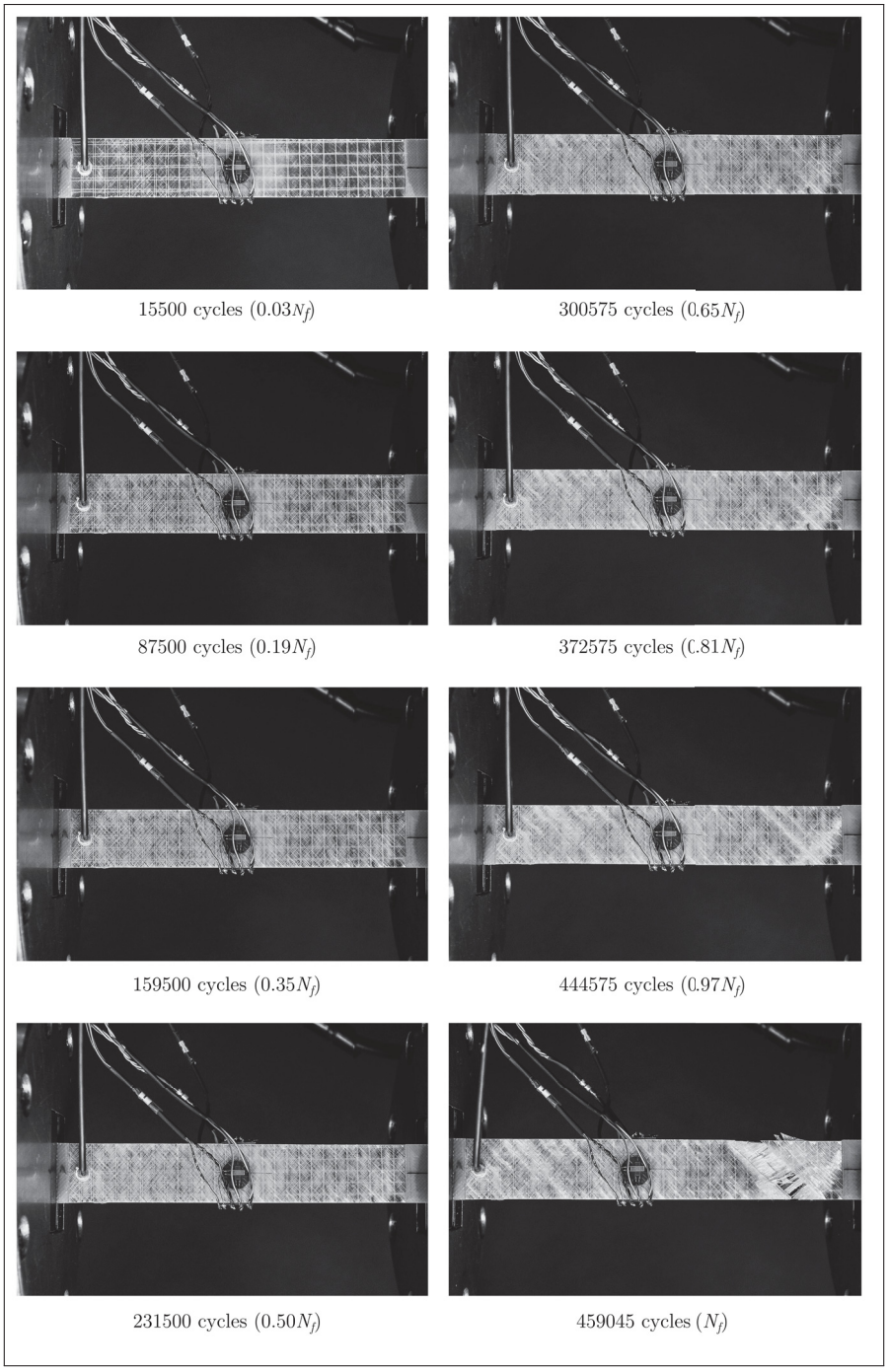

Figure 3.6 Damage progression for $R = 0.1$ fatigue on $[\pm 45]_{2s}$ glass–epoxy at 23°C (62 MPa, $\approx 0.5 S_x^+$)

from the two test temperatures after cyclic loading at 4250 N and 5950 N show the difference in damage distribution. At room temperature, the failure starts by the development

of multiple individual nucleation sites which interact together to form a broader network of damage ultimately leading to the specimen failure. In contrast, although cracking along the fibres also initiates randomly over the specimen subjected to low temperature, it seems that there is less interaction between damaged regions. The growth and coalescence phase is thus slowed down and a single region, which probably was initially weaker, collects most of the subsequent damage, leading to a rather localized failure. The reduced interaction between cracks may explain the lower scatter of -40℃ fatigue results.

This behaviour can be related to the work of Reifsnider and Case (229), where effects of matrix properties on failure and failure modes of UD composites were discussed. Their analysis led them to conclude that any temperature change could either provide an improvement or degradation of the composite's strength. This would be due to changes in stress redistribution around broken fibres and the descriptions of the phenomenon relies on the concept of ineffective length, which represents the distance required for the stress around the break to go back down to the average stress (Gao and Reifsnider (230), Subramanian, Reifsnider and Stinchcomb (231), Reifsnider and Case (229)). If the matrix is compliant, a large distance is required in order to redistribute the load around the broken fibre, while a stiff matrix can redistribute the load over a smaller distance. Clearly, the latter case results in a higher stress concentration around the break, which further leads to brittle failure. However, in the former case, accelerated failure is also possible due to increased interaction between fibre breaks. Therefore, optimal strength is obtained at an intermediate matrix compliance and changes of this matrix property due to moisture or temperature may result in either a positive or negative effect on strength. It is proposed here that for a $\pm 45^{\circ}$ laminate, a similar process may be active around matrix cracks and interply delaminations and that the stiffening of the matrix may reduce the length over which a stress concentration occurs close to the end of a matrix crack, reducing the potential for crack interactions.

It is believed that the changes in fracture mechanics at low temperature may also follow from a combination of additional factors. First, both the matrix tensile and shear

strengths are likely to be improved at low temperature, delaying the apparition of the initial cracks along the fibre direction. Second, changes in matrix and possibly interphase behaviour result in an increase of the interlaminar strength of glass–epoxy composites at low temperature. This was shown by short beam shear test results by Cormier and Joncas (84). Such an improvement in interlaminar strength would possibly delay the apparition and coalescence of interlaminar cracks that seem to have an important role in the failure process.

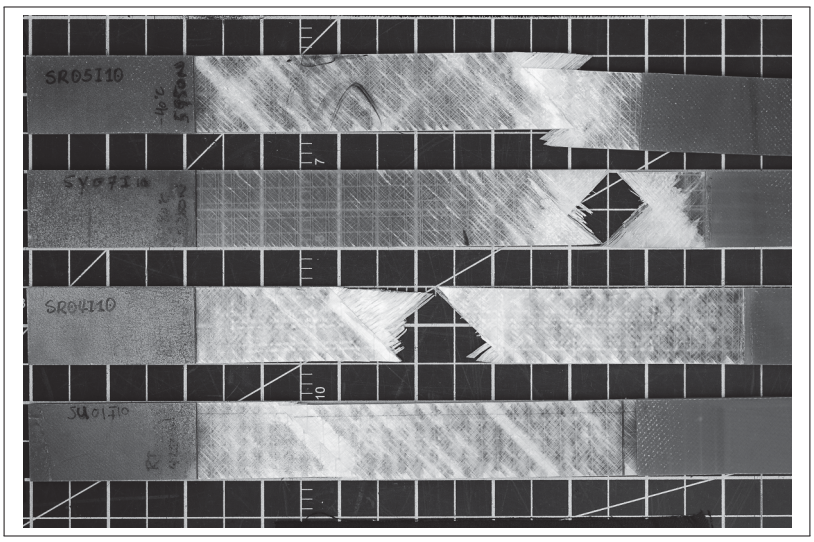

Figure 3.7 Typical failed $R = 0.1$ fatigue specimens. From top: -40°C, 5950 N (86 MPa); -40°C, 4250 N (63 MPa); 23°C, 5950 N (87 MPa) and 23°C, 4250 N (66 MPa)

The mechanisms described above appear to override the expected strength reduction resulting from internal tensile stresses developed in the matrix at low temperature as a consequence of the mismatch in fibres and matrix CTE. The micromechanics equations provided by Lord and Dutta (76) and given by equation 3.5 can be applied to estimate these internal tensile matrix stress due to a change in temperature T and specific moisture content M. In equation 3.5, the matrix properties, denoted by the subscript m, can be altered according to Chamis' empirical relations of equation 3.6 and equation 3.7 in order

to account for the influence of temperature and moisture content (85). In equation 3.5, E is the constituent Young's modulus, α is the CTE, β is the moisture swelling coefficient and T_g the glass transition temperature. F_m is the property reduction factor and can be applied to any matrix property. F_m is simply the ratio of X_m, any given matrix mechanical property, over its reference value X_{m0} and is correlated to the empirical relationship of equation 3.6. For equation 3.5 to equation 3.7, subscripts f, w and 0 respectively stand for fibres, wet and reference properties. Finally, in equation 3.5, the variable $T_{s=0}$ stands for the reference stress-free temperature. $T_{s=0}$ can be assumed to be close to T_g as during curing, chain mobility should allow relatively easy stress relaxation as long as $T \geq T_g$ (54) and that sufficient time is given for the visco-elastic relaxation to occur. Note that in the literature, the cure temperature (T_{cure}) has also been reported to be an indicator of $T_{s=0}$ (28). However, in the current context, T_g and T_{cure} are quite close and the definition of $T_{s=0}$ does not influence the reasoning. It should also be noted that, since the polymerization reaction is assumed to be complete, the chemical shrinkage is neglected in equation 3.5.

$$s_{1m}^{T+H} = \frac{E_m E_f v_f}{E_f v_f + E_m(1-v_f)} \Big[(\alpha_f - \alpha_m)(T - T_{s=0}) + (\beta_f M_f - \beta_m M_m)\Big] \tag{3.5}$$

$$F_m = \frac{X_m}{X_{m0}} = \left[\frac{T_{gw} - T}{T_{g0} - T_0}\right]^{1/2} \tag{3.6}$$

$$T_{gw} = (0.005 M_m^2 - 0.10 M_m + 1) T_{g0} \tag{3.7}$$

For example, if equation 3.5 is applied to a UD ply of anhydrous ($M = 0$) glass–epoxy with $v_f = 0.55$ and with E_m varying according to equation 3.6, the magnitude of matrix thermal stress due to a temperature drop to -40℃ is about 20 MPa. Such a stress is quite significant considering that the matrix strength at room temperature is around 70 MPa. Furthermore, as the matrix shrinkage in the direction of each ply principal fibre orientation is restrained, significant interlaminar stresses may be expected. Strengthening

processes such as those discussed earlier must therefore be active in order to counteract the negative effects of thermo-mechanical stresses.

Analysis of the normalized results from Figure 3.5 and Table 3.6 show further evidence of the slope change at low temperature and corroborate the existence of Tang et al. (181) "pivot point" around which the normalized S-N curve rotates for varying temperatures. However, Tang and his colleagues located it in the neighbourhood of 1000 cycles and $2S_{ut}/3$, while our results place it somewhat above $2S_{ut}/3$ on the stress axis. This difference might be explained by the higher test frequency in Tang's research leading to increased hysteretic heating and reduced lives at higher stresses. The fact that the normalized S-N curve for -40℃ is under that at 23℃ in the entire range of stress that was tested also suggests that the mechanisms improving static strength are not as effective in fatigue.

It is also believed that an increased cyclic creep strain build-up associated with a higher loss modulus at -40℃ might explain the reduction of the slope parameter and the resulting decrease in fatigue performance on a normalized stress basis. Indeed, Kujawski and Ellyin (172) demonstrated that, as a result of the visco-elastic nature of the polymer matrix, cyclic creep strain accumulation contributes to the fatigue failure of $\pm 45^{\circ}$ composites. For epoxy and glass–epoxy composites exposed to temperatures in the neighbourhood of -40℃, Adams and Singh's reported a peak of loss modulus (39). As loss modulus is an indicator of the viscous nature of a material, low temperatures should result in increased cyclic creep strain build-up and accelerated failure.

The cyclic creep strain accumulation hypothesis is further corroborated by the consistency of the fatigue results with Kujawski and Ellyin's remark that viscous effects are load dependent. In their work, increasing the test frequency resulted in increased cyclic creep strain rates under high loads whereas they were reduced at low loads. Put otherwise, an increase in frequency should translate into a counterclockwise rotation of the S-N curve. Accounting for the fact that temperature and frequency can be substituted one

to another for determining dynamic properties of polymers (39), it is possible to draw a parallel between frequency and temperature effects on cyclic creep build-up. However, it is important to realize that although a temperature decrease is usually assimilated to a lesser importance of the viscous behaviour and would normally be assimilated to a frequency increase, Adams and Singh results suggest otherwise. In fact, it becomes evident that the increased loss modulus at -40°C is equivalent to a frequency reduction. Improved performance at high loads and decreased performance at low loads, such as observed in the present case, are therefore coherent with the assumption of cyclic creep strain build-up.

Finally, as the normalization based on ultimate tensile strength appears to eliminate the shifting of the S-N curve towards the longer lives at low temperature, it is believed that this shift is essentially the result of the matrix strength improvement and reduction in interaction between damage sites. However, the change in slope is not affected by normalization, although the slope difference is visually emphasized on the normalized S-N curve. It is suggested that this change in slope parameter at low temperature might mainly results from increased viscous effects.

3.3.3 $R = -1$ fully reversed fatigue

Individual results for fatigue at $R = -1$ are provided in Table 3.7 for both 23°C and -40°C. The resulting ML parameters are given in Table 3.8. Figure 3.8 and Figure 3.9 provides a visualization of the S-N curves respectively based on absolute and normalized stresses.

On an absolute basis, the durability of glass–epoxy composites under $R = -1$ loading is strongly affected by a reduction of temperature from 23°C to -40°C. This is evidenced by an improvement in fatigue life of about one decade when compared to room temperature results. However, as opposed to the behaviour at $R = 0.1$, the slope parameter is strongly

Table 3.7 Results for $R = -1$ fatigue on $[\pm 45]_{2s}$ glass–epoxy

T °C	Specimen identifier -	s_{max} MPa	N^a Cycles
23	SV07R09	53	2888
	TB19R09	33	+2000000
	SN17R09	52	6387
	TB10R09	45	50200
	SN01R09	40	466964
	SN10R09	46	58368
	TB12R09	39	655993
-40	TB17R09	39	3166742
	SN03R09	46	1350723
	SV06R09	54	146550
	SN20R09	46	1385654
	TB03R09	51	364706
	SN02R09	39	2173327

[a] Runouts indicated by a "+" sign before the cycle count.

Table 3.8 Maximum likelihood estimators of S-N parameters for $R = -1$ fatigue on $[\pm 45]_{2s}$ glass–epoxy

Analysis type -	T °C	Property -	$\hat{\gamma}_1$ log(Cycles)	$\hat{\gamma}_2$ log(Cycles log(MPa)$^{-1}$)^a	$\hat{\gamma}_3 = \hat{\sigma}_L$ log(Cycles)
Absolute	23	Median	32.3	-16.7	0.068
		95 % bounds	[30.1, 34.7]	[-18.0, -15.3]	[0.032, 0.143]
	-40	Median	19.9	-8.4	0.139
		95 % bounds	[15.5, 25.6]	[-11.4, -5.4]	[0.062, 0.310]
Normalized	23	Median	-2.89	-16.7	0.068
		95 % bounds	[-3.59, -2.33]	[-18.0, -15.3]	[0.032, 0.143]
	-40	Median	1.02	-8.4	0.139
		95 % bounds	[0.18, 5.84]	[-11.4, -5.4]	[0.062, 0.310]

[a] log(Cycles) for normalized analysis

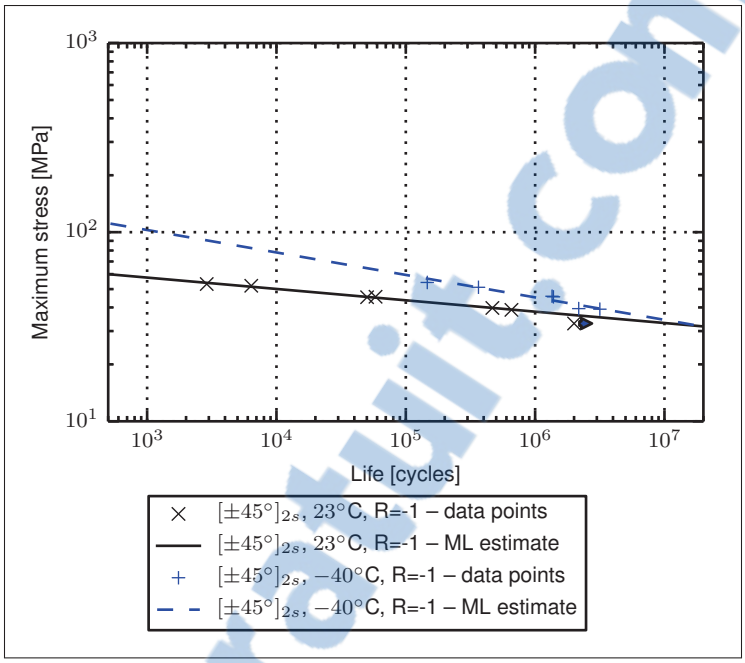

Figure 3.8 S-N curves for $R = -1$ fatigue on $[\pm 45]_{2s}$ glass–epoxy at 23℃ and -40℃ (solid arrows indicate runouts)

affected by temperature. This is consistent with the fact that a change in failure mode occurs between 23℃ and -40℃.

At room temperature, all specimens failed by ply buckling after extensive delamination whilst at -40℃, the load-displacement data indicates that all failures occurred in the tensile loading phase. This suggests that either or both of the following phenomenon occur:

a. The ply stiffness rises enough to bring the magnitude of critical buckling stress above that of the stress required to break the matrix.

b. The interlaminar shear strength increases sufficiently to mitigate the delamination growth.

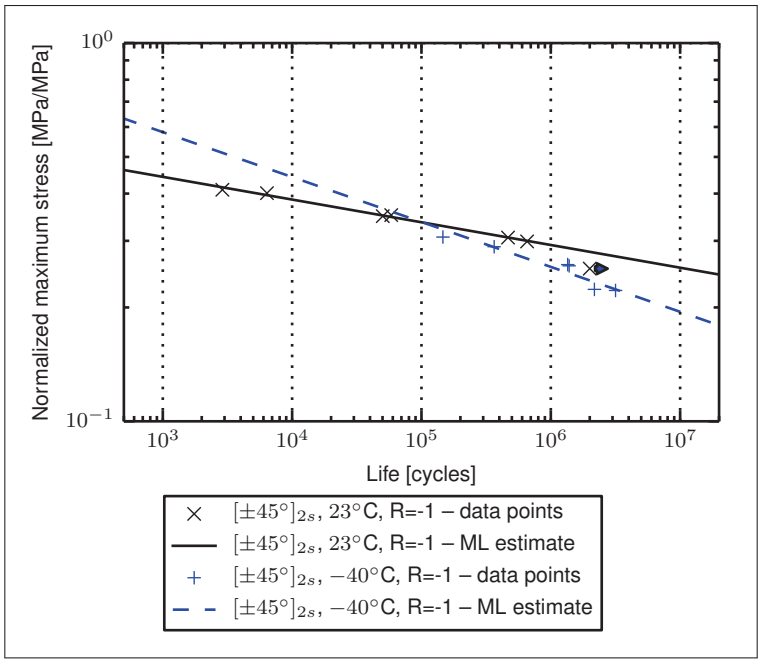

Figure 3.9 Normalized S-N curves for $R = -1$ fatigue on $[\pm 45]_{2s}$ glass–epoxy at 23℃ and -40℃ (solid arrows indicate runouts)

It appears that the mechanisms that lead to the retardation of damage growth and crack coalescence in tensile fatigue are also active in reversed fatigue. However, the added benefit of limited damage during the tensile cycles is that buckling of separated plies is eliminated.

However, even though the failure is tensile for $R = -1$ loading at -40℃, the $R = 0.1$ and $R = -1$ fatigue curves are not comparable. The reversed loading specimens fail much earlier and have a higher slope coefficient. This is easily seen by comparing $R = -1$ data in Figure 3.8 to $R = 0.1$ data from Figure 3.4. Nonetheless it is interesting to note that moving from a compressive failure due to buckling to a tensile failure is an indicator of more efficient material usage.

Note that although fully reversed fatigue lives are generally increased in the stress range measured in this study, wind turbines are designed for lower stresses and strains required to reach 10^8 to 10^9 cycles. If results are extrapolated to those low stresses, a temperature

of -40°C may result in lower lives as a crossover of the S-N curves is visible around 10^7 cycles.

When normalized with respect to the static strength, the improvement in low temperature fatigue resistance is less convincing. Figure 3.9 shows that for stress above $\approx 35\,\%$ of S_{ut}, fatigue lives are shorter at -40°C than at 20°C. Therefore, the mechanisms that improve static strength at low temperature appear to be less efficient for fatigue. The fatigue results for $R = -1$ loading are also in agreement with the cyclic creep strain accumulation hypothesis discussed in section 3.3.2 as the lives are shortened at low stresses while they are lengthened at higher loads.

3.4 Conclusions

The fatigue performance of glass–epoxy composites at low temperature is of interest for the wind turbine industry because huge wind energy potential exists in northern regions. However, turbine reliability is crucial in these remote regions and information on the durability of composites in cold climates is scarce. As a result, the WESNet research project included a broad material test program in order to study possible complications or gains related to the use of composites under cold climates and results for static and fatigue ±45° glass–epoxy are presented.

Results demonstrate that tension and compression strengths and moduli of the $[\pm 45]_{2s}$ laminate as well as the shear strength and modulus of its constituent plies are all significantly improved at low temperature. This is believed to result from increased mechanical properties of the matrix and interphase as well as from the reduced possibility for interaction between damage sites due to increased matrix stiffness. These effects appear to largely outweigh the internal intraply and interply stresses developed due to constrained thermal deformations.

On an absolute stress basis, results for constant amplitude fatigue at $R = 0.1$ showed that an approximately tenfold increase in fatigue life can be expected at -40°C when compared

to 23℃. Furthermore, the slope parameter was only slightly reduced under those conditions, resulting in improved lives at low stresses. Conversely, the slope parameter of the $R = -1$ fatigue S-N curve at -40℃ is decreased significantly. This reduction of the slope parameter is associated with the transition from compressive failure at 23℃ to tensile failure at -40℃. However, this change in slope parameter can result in shorter lives when the S-N curve is extrapolated towards the low stresses required to meet the extended lives expected in wind energy applications.

Nonetheless, when normalized by the static strength at a given temperature fatigue lives of $\pm 45°$ glass–epoxy composites are shorter in all situation apart for high stresses at $R = -1$, where the change in S-N slope parameter results in improved performance. It is believed that the behaviour exhibited by the normalized stress results is a consequence of the increased cyclic strain build-up due to a loss modulus increase at low temperature.

It was also demonstrated that the damage growth and distribution was affected by low temperatures. At room temperature, strong interactions between initial matrix cracks was observed. This led to multiple zones with comparable levels of damage just before the onset of failure. However, at low temperature, it appears that changes in matrix properties made cracks less likely to coalesce into larger damage and final failure is more localized.

Therefore, from a practical point of view, it seems that in absolute terms and within the stress ranges studied here the effects of low temperatures are mainly beneficial for the fatigue durability of $\pm 45°$ glass–epoxy composites. The main concern remaining for the wind energy industry in regard to the durability of the laminate is with potential degradation of fatigue strength at very low load, which was not studied in the current project but is relevant for the sector. Furthermore, it should be kept in mind that scaling and application to more complex laminates and structures are still scarcely documented in the literature.

CHAPTER 4

MODELLING THE EFFECT OF TEMPERATURE ON THE PROBABILISTIC STRESS–LIFE FATIGUE DIAGRAM OF GLASS FIBRE–POLYMER COMPOSITES LOADED IN TENSION ALONG THE FIBRE DIRECTION

Laurent Cormier[1], Simon Joncas[1]

[1] Department of automated manufacturing engineering, École de Technologie Supérieure,
1100 Notre-Dame Ouest, Montreal, Quebec, Canada H3C 1K3

The following is the accepted version of the published article:

L. Cormier and S. Joncas, "Modelling the effect of temperature on the probabilistic stress–life fatigue diagram of glass fibre–polymer composites loaded in tension along the fibre direction", *Journal of Composite Materials*, Available online, April 24, 2017, DOI:10.1177/0021998317704896.

Article available at http://journals.sagepub.com/doi/full/10.1177/0021998317704896

Abstract

Predicting the fatigue performance of composites has proven to be a challenge both conceptually, due to the inherent complexity of the phenomenon, and practically, because of the resource-intensive process of fatigue testing. Moreover, mechanical behaviour of polymer matrix composites exhibits a complicated temperature dependence, making the prediction of fatigue performance under different temperatures even more complex and resource intensive. The objective of this paper is to provide a method for the prediction of fatigue life of glass–polymer composites loaded in the fibre direction at various temperatures with minimal experimental efforts. This is achieved by using a static strength degradation approach to fatigue modelling, where only two parameters (including static strength) are temperature dependent, in conjunction with relationships for these two fatigue model parameters temperature dependence. The method relies on fatigue data at a single temperature and simple static tests at different temperatures to predict the effects of temperature on the material's fatigue behaviour. The model is validated on experimental data for two unidirectional (UD) and one woven glass–epoxy composites

and is found to accurately predict the effect of temperature on fatigue life of composites. A method to obtain probabilistic stress-life ($P-S-N$) fatigue diagrams including temperature effects is also discussed.

4.1 Introduction

Temperature effects on the fatigue performance of composite materials have been the subject of extensive research in the past decades. Yet, it appears that a definitive approach to modelling such temperature effects on material properties and durability is still not reached. This is certainly due to the fact that composites present themselves in a wide variety of reinforcement forms and constituent natures, while being used in a broadening range of structures subject to a wide range of external solicitations and environments. A universal model for fatigue thus has to reconcile the opposite requirements of accounting for an overwhelmingly large number of situations, yet remaining tractable and requiring a minimum of experimental efforts in order to establish the values of its input parameters.

Apart from all aspects of mechanical loading (e.g. load frequency, maximum stress, mean stress, stress amplitude, load sequence, ...), thermal loading is probably one of the most important factors in determining fatigue life of composite structures. However, most of the literature is focused on the effects of high temperatures on fatigue and very little information is available on the behaviour of composites at low atmospheric temperatures, or even cryogenic temperatures. Yet, as understanding the effects of temperature on the fatigue performance of composites is an important topic for many industries (e.g. civil infrastructure, transports, wind energy), multiple modelling approaches have been explored. Some of these, mostly those dealing with the widest possible temperature ranges, are discussed below.

Early work by Sims and Gladman (92) focused on the $R = 0.1$ fatigue of woven glass–epoxy composite loaded in the fibre direction for temperatures ranging from -150℃ to

150℃. Their results suggested that the stress–life (S–N) curves at different temperatures were superimposed when the maximum cyclic stress was normalized by the static strength (S_u) at the same temperature. Similar conclusions were also reached by Bureau and Denault (184) for bending fatigue of glass-polyester between −40℃ and 50℃, although it was not the case for glass-polypropylene under the same conditions. Bureau and Denault associated this result to the thermomechanical stability (e.g. lack of a structural transition such as vitrification, melting or low temperature transitions) of polyester within the experimental temperature range. However, even for thermosetting matrix composites, such a simple behaviour is not always borne out by experiment. For example, $R = 0.1$ fatigue results by Brassard (185) for UD glass–epoxy at −40℃ and 20℃ show a statistically significant downward shift of the normalized fatigue curve at low temperature and normalized fatigue curves at -40℃ and 23℃ for $\pm 45^\circ$ glass-epoxy at $R = 0.1$ obtained by Cormier et al. (232) show a statistically significant change in slope parameter with temperature.

Since Arrhenius type relationships have historically been successful in modelling the effect of temperature on chemical reactions and physical processes, it seems natural that it was applied to fatigue of composites. As such, Tang et al. (181) proposed an Arrhenius type relationship to be combined with their stiffness degradation model in order to predict effects of temperature on salt water saturated glass–vinylester cross-ply laminates. In practice, the model assumes that the slope parameter of the fatigue model follows an Arrhenius type behaviour. However, even though the model was in relatively good agreement with experiments run at 4℃, 30℃ and 65℃, the Arrhenius relationship is an empirical model that is fitted a posteriori. Thus, obtaining model parameters requires experimental fatigue data at multiple temperatures.

Rotem and Nelson (175) have proposed an approach for shifting fatigue curves to account for the effect of temperature. They used a combination of two shift factors respectively applying to S_u (or an artificial static strength given as the fatigue curve intercept with the stress axis) and to the slope of a log-linear S–N curve. In general, the shift factors would

need to be determined by experiments. However, for 65% volume fraction graphite–epoxy laminates, it is suggested that the slope factor would be unity if the artificial static strength was used instead of the actual S_u. For such a case, an empirical correlation between the artificial static strength shift factor and temperature was proposed. It is important to note that log-linear fatigue curves seldom fit well in both the low-cycle and high-cycle fatigue regime. In Rotem and Nelson's work, the curve was explicitly fitted to the high cycle regime.

Mivehchi and Varvani–Farahani (189) approached the problem of temperature effects on fatigue by changing the parameters of the classical power-law used to describe fatigue (log-log linear S–N curve) with temperature. However, even though it is documented that the best fit power-law seldom converges to S_u (see e.g. Sutherland (120)), the assumption that it does is used in determining one of the parameters. This results in evident bias in many of the resulting predictions. Also, the model S_u dependence on temperature is a strictly decreasing function, as opposed to the usual sigmoid behaviour. Finally, even though the model was benchmarked on thermoset polymers, it uses the polymer's melt temperature as an input. This requirement seems incompatible with such a use given that a thermoset matrix is chemically degraded before melting.

Miyano et al. (191; 192; 193) proposed an elaborated model for predicting the influence of temperature on the long-term life (creep and fatigue) of carbon-fibre composites. This model relies on a master curve approach based on experimental static, fatigue and creep results. It benefits from a broad range of applicability by being able to deal with the viscoelastic nature of carbon fibre laminates and by being able to deal with failure probabilities. However, it requires extensive material characterization in order to obtain model parameters.

Reifsnider's and his co-workers have also devised a thorough method, called the 'Critical Element Model'. This approach was developed over a period of more than twenty years, but has been synthesized by Reifsnider, Case and Duthoit (183). The model is able to

deal with the problem of fatigue at various temperatures as well as many other damage mechanisms such as creep and thermo-oxidation. The approach is based on kinetic theory and point-wise definition of stress and strength and appears to have the capacity to accurately model the evolution of strength and is possibly the closest we have been to a global solution to failure of composites under fatigue and other loading. However, it is achieved at the expense of an extremely detailed knowledge of material's properties and of their evolution (as well as the evolution of the stress-field) over time. Unfortunately, such detailed knowledge can only be gained through extensive experimental investigations.

Finally, the strength degradation model by Epaarachchi and Clausen (146) has provisions for dealing with temperature effects. However, the formulation of a function for modelling such effects was not provided and the special case of a constant parameter was developed in their paper.

An important aspect of the strength and stiffness of composites under combined thermal and mechanical loads is the time-dependence of the mechanical response. This in turns means that temperature and fatigue loading rates or frequency are possibly strongly interconnected and that creep-fatigue interactions are also likely.

Research on frequency effects mainly support the idea that if the temperature remains constant, an higher frequency leads to longer life. (122; 165; 166) However, since fibre reinforced polymers are often poor heat conductor, hysteretic heating can occur at relatively low frequencies (well below 10 Hz) (167; 169; 174). Sun and Chan (167) proposed a model based on crack propagation in visoelastic media to predict frequency effects on fatigue life, including the effect of temperature rise. In this context, Saff (169) and Hahn and Kim (170) proposed models for estimating the temperature rise from hysteretic heating based on viscoelasticity and heat transfer equations.

Creep fatigue interaction is another effect of the time dependence of mechanical response in polymers and their composites. Crowther, Wyatt and Phillips (196) have shown that for certain materials, at low frequency, the fatigue process is dominated by creep and

failure is time rather than cycle dependent. However, at higher frequency, fatigue becomes cycle dominated. This behaviour was corroborated by results from Eftekhari and Fatemi (166; 197). The accumulation of fatigue induced creep strains was also reported by Kujawski and Eyllin (172) for $[\pm 45]_{5s}$ glass-epoxy composites at room temperature. Evidence of viscoelastic behaviour was also reported in Cormier et al. (232) for $[\pm 45]_{2s}$ glass-epoxy at -40°C.

It is worth noting that fatigue models by Miyano et al. (191; 192; 193) and Reifsnider et al. (183) are meant to account for viscoelastic effects while the model by Epaarachchi and Clausen (146) includes the effect of frequency under the assumption of negligible hysteretic heating. However, Guedes (233) has suggested that the linear cumulative law employed by Myiano may not fare well for complex fatigue loads or long lifetimes. An alternative model based on the work of Reifsnider's (183) strength evolution integral concept is also shown to provide better life predictions when accounting for viscoelastic effects at low stresses (long fatigue life). Also, Eftekhari and Fatemi (166; 197) used Epaarachchi and Clausen's (146) fatigue model in conjunction with a Larson-Miller type relationship to adequately model the effects of high temperature and high frequencies on neat, talc filled and short glass fibres reinforced thermoplastics.

The state of the art just presented puts forward the main limitation of current methods for assessing effects of temperature on fatigue: a requirement for extensive fatigue and viscoelastic testing. An explicit objective of the work described here is to provide a methodology that minimizes the experimental burden required to obtain model parameters. The proposed method builds on Epaarachchi and Clausen's fatigue model and extends its abilities to the prediction of probabilistic tensile fatigue curves of glass fibre–epoxy composites loaded along the fibre direction at any temperature. The proposed approach lies on the following assumptions:

- Only S_u and one material parameter from the fatigue model are affected by temperature (T).

- A relationship between S_u and that material parameter exists.
- The evolution of S_u as a function of T can be modelled by a sigmoid function.
- Creep–fatigue interactions are negligible in the fibre direction.

This last assumption is perhaps the most important and warrants some additionnal discussion. It relies on Saff's work (169), which suggests that viscoelastic effects in fatigue mainly depend on matrix shear stresses. Considering that in the case of tensile loads applied in the fibre direction, this matrix shear stress is minimized, it is plausible that the effect of viscoelasticity will also be minimized. This idea is further supported by the results of Sullivan (51) and those of Brinson and Gates (55), that show creep to be mostly negligible in the fibre direction.

Together, these four assumptions allow for the prediction of fatigue curves at any temperature within a single structural transition (e.g. glass transition) provided that S_u is known for at least four temperatures and that fatigue results are available at one temperature.

4.2 Model description

As documented by Sendeckyj (115), Degrieck and Van Paepegem (116) or Nijssen (10), many formulations have been proposed to describe the S–N relationship of composites. The current work is based on a model by Epaarachchi and Clausen (146), which is presented in equations 4.1 and 4.2. This two parameter model relies on a strength degradation rule that describes the evolution of strength with cyclic loading and agrees with the two intuitive boundary conditions of $N = 1$ at $\sigma_{\max} = S_u$ and $N = \infty$ at $\sigma_{\max} = 0$.

$$D/\alpha = N^{\beta} - 1 \tag{4.1}$$

$$D = \left(\frac{S_u}{\sigma_{\max}} - 1\right)\left(\frac{S_u}{\sigma_{\max}}\right)^{0.6-\psi\sin\phi} \frac{f^{\beta}}{(1-\psi)^{1.6-\psi\sin\phi}} \tag{4.2}$$

In equation 4.1 and 4.2, α and β are material constants, $\sigma_{\max}$ is the maximum cyclic stress, f is the loading frequency, ϕ is the smallest angle between the fibre direction and the loading axis and ψ is defined as:

- $\psi = R$ for $-\infty < R < 1$ (tension or reversed loading),
- $\psi = \frac{1}{R}$ for $1 < R < \infty$ (compression).

Epaarachchi and Clausen stated that only α and S_u should be functions of temperature, but did not provide relationships for $\alpha(T)$ or $S_u(T)$. A goal of the current work is thus to provide such relationships. However, because of the temperature-sensitive creep–fatigue interactions present in off-axis composites (172; 199; 232) — which are not accounted for in the current modelling approach — the analysis is limited to tensile fatigue along the materials main fibre orientation. Therefore, equation 4.2 simplifies to:

$$D = \left(\frac{S_u}{\sigma_{\max}} - 1\right)\left(\frac{S_u}{\sigma_{\max}}\right)^{0.6} \frac{f^{\beta}}{(1-R)^{1.6}} \tag{4.3}$$

Then, it is seen that for a given set of f, S_u, $\sigma_{\max}$ and R, the relationship between $\sigma_{\max}$ and N only depends on α and β. A S–N curve can be obtained by plotting equation 4.4 over $\sigma_{\max}$.

$$N = \left(\frac{D}{\alpha} + 1\right)^{\frac{1}{\beta}} \tag{4.4}$$

Note that according to Epaarachchi and Clausen, α for a given material will differ for tests run at different temperatures. However, the model assumes that a single α, β pair, ideally obtained at $R = 0.1$, is required for $-\infty < R < 1$.

Thus, two requirements are identified for equation 4.4 to provide a complete description of the S–N relationship as a function of temperature. First, as S_u is an important model parameter and is affected by temperature, a methodology for providing a continuous description of $S_u(T)$ is needed. Second, another continuous relationship for $\alpha(T)$ is required. The proposed forms for these two relationships are discussed next.

4.2.1 $S_u(T)$ relationship

Several approaches for predicting temperature effects on S_u were proposed in the past, mainly to account for the influence of high temperatures. Possibly the best known is Chamis's (85) empirical relationship for estimating matrix properties as a function of temperature and absorbed moisture. Used in conjunction with micromechanics models, it can provide estimates of the effect of temperature on the mechanical properties of composites. However, as stated by Christensen (88), common micromechanical models such as the rules of mixtures are limited in precision. Experimental evidences by Cormier and Joncas (84) also suggest that this formulation does not accurately predict S_u at low temperature for UD glass–epoxy composites.

Mahieux et al. (100) demonstrated the ability of an earlier micromechanics model to predict temperature effects based on matrix properties and stress concentration around broken fibres. However, assumptions on stress transfer efficiency at the interface, fibre arrangement and load redistributions are required and the associated parameters are not easily obtained.

Cao et al. (91) suggested that for high temperatures, a modified hyperbolic tangent gave a good description of the change in ultimate strength for carbon reinforced polymer composites. However such a formulation suggests that the strength at low temperatures would be the same as that at room temperature, which is contrary to experimental evidence for glass–epoxy (95; 221; 84; 92; 93).

Kawai et al. (96) also used a scaled hyperbolic tangent for describing the tensile and compressive strength evolution as a function of temperature for their constant life diagram (CLD) formulation. In this specific formulation, the hyperbolic tangent was scaled so that it would present a strength plateau either at low or at high temperature. However, as the function is symmetric, it cannot simultaneously predict both the high and low temperature behaviour. It is therefore limited to relatively narrow temperature ranges.

As far as the authors know, few formulations have explicitly been proposed for estimation of tensile strength at low temperatures apart from the micromechanics model from Dutta (103). However, as noted in the original article, predicted and measured strengths differ by an order of magnitude. The model is also not expected to work at high temperatures because of the underlying assumption that compressive stresses due to matrix shrinkage promote fibre buckling.

Mahieux and Reifsnider (99) proposed a model based on the Weibull distribution survival function (SF) to describe the evolution of polymer modulus with temperature. The model is based on the assumption that this SF can describe the failure of secondary molecular bonds governing the polymer's stiffness. Although it was originally limited to describe the evolution of polymer stiffness as a function of temperature, Correia et al. (101) showed that the formulation also provides a relatively good fit on data for strength of composites as a function of temperature. However, Gibson et al. (90) suggest that Mahieux and Reifsnider's model tends to exhibit an excessively strong curvature in the low temperature region to accurately describe the actual strength or modulus behaviour.

Correia et al. (101) proposed an alternative to Mahieux and Reifsnider's model based on the Gompertz cumulative distribution function (CDF, with $\mathrm{CDF} = 1 - \mathrm{SF}$). However, since the Gompertz CDF has an even more abrupt initial transition than Weibull's SF, the problem noted by Gibson et al. (90) is not improved on. Moreover, since it uses the CDF, the physical explanations of Mahieux and Reifsnider are not applicable.

On the other hand, the SF of the Gompertz distribution (234; 235) provides a more gradual initial transition and, as a SF, is in agreement with Mahieux and Reifsnider's hypothesis. A new formulation of $S_u(T)$ based on the SF of the Gompertz distribution is thus proposed (equation 4.5) in an effort to improve on Mahieux and Reifsnider's concept.

Gompertz's SF is a monotonically decreasing function asymptotic to one and zero. However, a lower bound at $S_u = 0$ is not appropriate in the presence of fibres which will allow for some residual strength even for $T \gg T_g$ (91). Similarly, it is possible that low

temperature strength exceeds the strength at room temperature. Thence, the Gompertz SF needs to be scaled and shifted. The scaling is done through the addition of parameter A that multiplies the SF while the upwards shift is simply obtained by adding a constant S_u^*, the lower strength asymptote (remaining strength fraction at $T \gg \Theta$).

$$\frac{S_u}{S_{u,0}} = A \exp\{-\eta[\exp(-\gamma T_n) - 1]\} + S_u^*, \tag{4.5}$$

In equation 4.5, $S_u/S_{u,0}$ is the ratio of S_u at a given temperature T to $S_{u,0}$, the static strength at T_0, A is a global scaling parameter controlling the upper asymptote, η is the distribution shape parameter (an indicator of the structural transition temperature Θ), γ is the distribution scale parameter representative of the material temperature sensitivity. The model also relies on a normalized temperature T_n, defined as:

$$T_n = \frac{\Theta - T}{\Theta - T_0} \tag{4.6}$$

in which T_0 is the reference temperature, and Θ is the structural transition temperature. Note that T_0 could be any temperature, but for a matter of convenience it will in most cases be the standard laboratory temperature. The definition of T_n is based on two considerations. First, Θ should be representative of the structural transition temperature being considered (e.g. T_g) so that the inflection point of equation 4.5 lies close to Θ. Second, the condition that $S_u/S_{u,0} = 1$ at $T_n = 1$ (i.e. $T = T_0$) must be met. Based on this last condition, it is easily shown that:

$$A = \frac{1 - S_u^*}{\exp\{-\eta[\exp(-\gamma) - 1]\}}. \tag{4.7}$$

Thus, only three independent parameters (η, γ and S_u^*) remain. These parameters are obtained by fitting the model to S_u measurements at different temperatures over the range of interest and preferably spanning on each side of Θ.

Note that T_n is an inverse indicator of T when $\Theta > T_0$, meaning that $T_n < 0$ for $T > \Theta$ and vice versa. As this is likely to be the most common case (i.e. for analysis at $\Theta \approx T_g$), an explicit negative sign for the γ parameter is used in equation 4.5 and equation 4.7, ensuring that the Gompertz SF is an increasing function of T_n. However, when dealing with low temperature fatigue, it might become more practical to set a value of $\Theta < T_0$ allowing for reference experiments to be run at a temperature as close to ambient as possible despite the fact that Θ might be much lower. In such a case, the negative sign before γ in equations 4.5 and 4.7 would be omitted.

It is also worth noting that this formulation is limited to materials that exhibit a single structural transition around Θ. As an example, assuming that the region of interest is around $\Theta = T_g$, equation 4.5 cannot account for the additional relaxations at the melting temperature of thermoplastic resins, at the decomposition of thermosetting polymers or for the low temperature β or γ-transition of some matrices like those found by Sims and Gladman (92), Adams and Singh (39) or Robert and Benmokrane (94). However, even though equation 4.5 cannot continuously describe multiple transitions, separate application of the formula to each region is possible.

4.2.2 $\alpha(T)$ relationship

Based on results from two experimental investigations on the topic of temperature effects on fatigue life of UD glass–epoxy composites — the European Upwind (221; 95) project and the Canadian Wind Energy Strategic Network (WESNet) (84; 185) — it has been determined that there is a correlation between the effects of temperature on S_u and α. This correlation obeys equation 4.8 and is shown in Figure 4.1.

$$\left(\frac{S_u}{S_{u,0}}\right)^{T_n} = \frac{\alpha}{\alpha_0} \tag{4.8}$$

It is believed that the empirical relationship of equation 4.8 should remain valid as long as the following conditions are met. First, the specimen is not subject to excessive internal

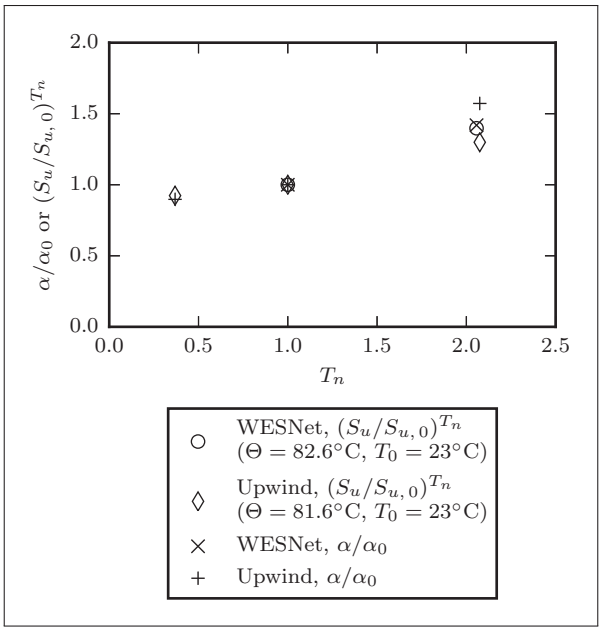

Figure 4.1 Correlation between α/α_0 and $(S_u/S_{u,0})^{T_n}$

heat generation due to hysteresis. Second, the failure modes for static and fatigue are and remain the same despite the temperature change. Third, the temperature change does not result in mechanical or chemical deterioration of the constituents due to internal stresses or thermo-oxidation.

Because of these requirements, it is desirable that quasi-static strength data are available beyond the temperature range of interest to ascertain the fact that a single transition is observed. In the case of multiple transitions, a full description of the material behaviour can still be obtained at the expense of fatigue tests at one temperature within each transition.

4.3 Materials and methods

The model predictions are compared to experimental results from four sources. The first two sources are recent and independent research programmes including quasi-static and fatigue test campaigns on UD glass–epoxy composites at different temperatures: the

European Upwind (221; 95) project and the Canadian WESNet programme (84; 185). The third source is an older data set by Sims and Gladman (92). The last is Cao et al.'s (91). The static relationship of equation 4.5 is validated on Upwind's, Sims and Gladman's and Cao et al.'s datasets. Fatigue predictions are compared to results from Upwind, WESNet and Sims and Gladman. These results are used because they cover a wide temperature range above and below ambient and include a variety of glass–fibre fabric types.

The data set by Sims and Gladman includes quasi-static and $R = 0.1$ fatigue data for 3.2 mm thick hot-pressed fine weave glass–epoxy laminates of $v_f = 0.45$. Tests were all performed along the main roving of the laminate. Quasi-static and cyclic tests were all performed under load control at a stress rate of 1250 $\mathrm{MPa\,s^{-1}}$. Tests were performed at temperatures of -150℃ to 150℃. However, as thermo-oxidation of the matrix was reported at 150℃, results at that temperature will not be considered here. It is also worth noting that Sims and Gladman only provide average fatigue lives at each load level and do not give information about the fatigue results dispersion. However, a 3% coefficient of variation is reported on S_u at all temperatures.

Cao et al.'s (91) provides S_u data at temperatures ranging from 20℃ to 120℃ for UD carbon-fibre composites with two different epoxy formulations, namely FR-E3P and SX-435 resins. These composites are later identified as CFRP1 for the composite using FR-E3P resin and CFRP2 for that using SX-435 resin.

Details of experimental procedures for Upwind and WESNet as well as computational approaches are given below.

4.3.1 Experimental

For Upwind and WESNet, load controlled fatigue experiments at $R = 0.1$ and displacement controlled quasi-static tests were performed. All experiments were carried out on

servo-hydraulic test frames. However, each test campaign had some peculiarities. Materials details for both programmes are given in Table 4.1.

Table 4.1 Description of materials

	Research programme	
Material property	Upwind	WESNet
Fibre form	963 g/m^2 stitched unidirectional E–glass	605 g/m^2 woven unidirectional E–glass
Warp roving	864 g/m^2, 2400 tex glass	594 g/m^2, 1100 tex E–glass
Primary fill	40 g/m^2, 200 tex glass	11 g/m^2 [a], 134 tex E–glass
Secondary fill	41 g/m^2, 61 tex glass	60 tex[b]
Stitching	18 g/m^2 polyethersulfone	None
Resin	Bisphenol A epichlorohydrin epoxy	Diglycidyl-ether of bisphenol-A epoxy
Hardener	Mixture of polyamines	Amine
Glass transition temperature	81.6℃[c]	82.6℃[d]
Fibre volume fraction (v_f)	0.48	0.55
Ply sequence	$[0_4]$[e]	$[0_3]$

[a] Combined primary and secondary fill areal weight

[b] Glass reinforced thermoplastic woven and fused to the warp fibres for every two primary fill rovings.

[c] As measured by differential scanning calorimetry on 12 specimens.

[d] Matrix property from resin manufacturer technical data sheet.

[e] As each ply is not balanced, fill fibres are alternatively placed facing out/in/in/out to ensure laminate symmetry and balance.

In the Upwind programme, tests were performed at −40℃, 23℃ and 60℃. At least six specimens were tested at each temperature for quasi-static evaluation. Fatigue experiments were conducted at two load levels with a minimum of five specimens tested at each level. The fatigue test frequency changed according to the load level in order to maintain an approximately constant strain energy rate as described in (221; 201; 208). This precaution ensured that if any internal heat generation or cyclic creep build-up occurred, it would remain relatively uniform over all test conditions, minimizing the risk that strain rate or hysteretic effects be confounded with temperature effects. Control

over the test temperature was achieved by circulating air from an external environmental chamber through the insulated test enclosure. Specimens were left standing in the test environment for a minimum of 15 minutes before the start of a test. The air and specimen surface temperature were both monitored during the tests.

A non-standard test specimen geometry was used. The geometry is taken from the OptiMAT Blade Project and the associated OptiDAT database (132), which used a common specimen geometry for tension and compression fatigue. This choice was made in order to eliminate potential uncertainties related to geometric effects. This geometry, referred to as R08, was used for Upwind in order to maintain consistency with results from the earlier OptiMAT Blade Project. The R08 specimen geometry is shown in Figure 4.2. End tabs are bonded with epoxy paste.

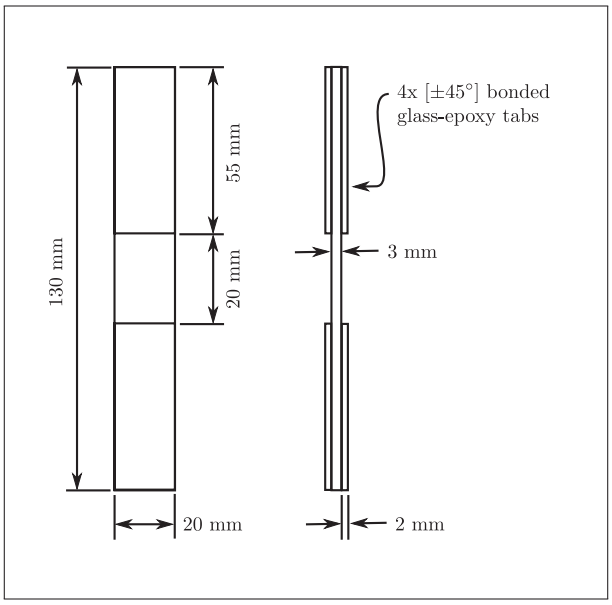

Figure 4.2 OptiMAT Blade Project
R08 specimen geometry

Laminates were manufactured at the Knowledge Centre Wind Turbine Materials and Constructions (WMC). They were vacuum infused under rigid tooling and cured at atmospheric pressure to minimize void volume. The lower and upper mould plates were

bolted together with shims inserted in between the plates to ensure a predetermined spacing based on the target v_f and the areal weight of the fabric. The tooling and resin were preheated to 30℃ prior to infusion. The infusion was performed at 30℃ under full vacuum. After infusion, the inlet and outlet were closed and the pressure set back to ambient. The temperature was then increased to 50℃ at a rate of 1℃/minute and kept at 50℃ for three hours. After the first temperature dwell period, the temperature was raised to 70℃ at a rate of 1℃/minute and remained at this temperature for ten hours. The final cooling phase was uncontrolled. Specimens were wet-cut using a circular diamond blade.

For the WESNet programme, quasi-static and fatigue tests were performed at −40℃ and 23℃ on specimens that were previously vacuum dried. Quasi-static tests were performed in accordance to ASTM D 3039 (224) on a minimum of five specimens per temperature condition. Fatigue tests under each temperature conditions were conducted on a minimum of six specimens distributed over three stress levels. Fatigue tests were performed at a constant frequency of 5 Hz which was verified to limit the specimen hysteretic heating to about two degrees Celsius as measured on the specimen surface. Room temperature tests were performed under laboratory ambient conditions while for tests at −40℃, the specimen was installed in a test chamber equipped with a liquid nitrogen cooling system. Air temperature around the specimen was monitored and controlled via a feedback loop controller.

For WESNet, the specimen geometry was as per ASTM D 3039 for UD composites. Bevelled tabs made of 2 mm thick ±45° glass–epoxy composites were bonded using epoxy paste adhesive. The test specimens were resin infused at full vacuum. However, once the laminate was fully impregnated with resin, the vacuum level was reduced to 3/4 bar for the duration of the consolidation. This last step was meant to reduce the thickness gradient along the plate length and to minimize the volume of any remaining entrapped gases. Specimens were machined on a numerically controlled milling machine

equipped with a polycrystalline diamond coated end mill and their edges were polished on water lubricated metallography polishing benches with abrasives up to 600 grit.

4.3.2 Computational approach

Model parameters for equation 4.5 are obtained by a non-linear regression using *Python 2 SciPy 0.17* package `optimize` module's `curve_fit` procedure. The regressions are performed on the mean strength, but the standard deviations are also provided to the `curve_fit` procedure for weighting purpose. Parameters for the $S_u(T)$ relationship are evaluated for materials from Upwind (95), Sims and Gladman (92) and Cao et al. (91) As the WESNet (84) material was only tested at two temperatures, the data are too scarce to fit the model.

In their paper, Epaarachchi and Clausen (146) used trial and error to fit their model. In the present study, parameters α and β from equation 4.1 are determined by using a script that symbolically solves for the slope parameter α and coefficient of determination r^2 as a function of β in a linear regression of $D(\beta, \sigma_{\max})$ on $N^\beta - 1$. A least square regression method is used and the regression line is forced to zero. The script then iterates over a range of β and evaluates the resulting α and r^2. The maximum value of r^2 is searched for and the associated α and β set is given as the solution. Values of coefficients α and β at reference temperature T_0 (denoted as α_0 and β_0) are first found using the aforementioned script. For all other temperatures, the condition $\beta = \beta_0$ is imposed and α is evaluated according to equation 4.8 (further identified as α_{model}).

The quality of fit of curves predicted using α_{model} and β_0 is evaluated using the coefficient of determination, further denoted as r^2_{model}. In order to provide a comparative basis, fatigue curves are also fitted on data at each temperature using the regression script with $\beta = \beta_0$. The output of those regression is further labelled as α_{reg} and r^2_{reg}.

For comparison purpose, the fatigue model is fitted using both the measured static strength ($S_{\text{u, measured}}$) and the modelled static strength ($S_{\text{u, model}}$). — predicted from

equation 4.5 — for all datasets except WESNet's. In this case experimental strength measurements are used.

Finally, in cases where the frequency used for fatigue tests under different load or temperature conditions is not constant, an average frequency is used in equation 4.4 and kept the same for all conditions. This is consistent with the approach used by Epaarachchi and Clausen (equation 4.1).

4.4 Results and discussion

4.4.1 $S_u(T)$ predictions for Cao et al.'s (91) material

As a demonstration of the ability of equation 4.5 to describe the evolution of $S_u(T)$, the model has been tested on data for two UD carbon fibre–epoxy composites from Cao et al. (91) For both fits, a reference temperature of $T_0 = 35°C$ was used. The structural transition temperature used was the midpoint of the reported T_g range. Thus, $\Theta = 49°C$ and $\Theta = 54°C$ are respectively used for modelling the behaviour of CFRP1 and CFRP2 materials.

Estimates of model parameters are $A = 0.1339$, $\eta = 0.99$, $\gamma = 1.53$ and $S_u^* = 0.71$ for CFRP1 and $A = 0.1841$, $\eta = 0.54$, $\gamma = 2.63$ and $S_u^* = 0.70$ for CFRP2. The model predictions and data are shown in Figure 4.3. It is seen that equation 4.5 provides a very good description of the effect of temperature on the strength of UD composites within the temperature range considered.

4.4.2 $S_u(T)$ and fatigue life predictions for Upwind's (95; 221) material

The static model (equation 4.5) is applied to data from Upwind at temperatures of −40℃, 23℃ and 60℃. In the following application, $T_0 = 23°C$ and the laminates $T_g = 81.6°C$ is taken for Θ. As S_u data are only available for two temperatures away from T_0, a further hypothesis is needed to fit equation 4.5. Based on results for UD carbon–epoxy tested

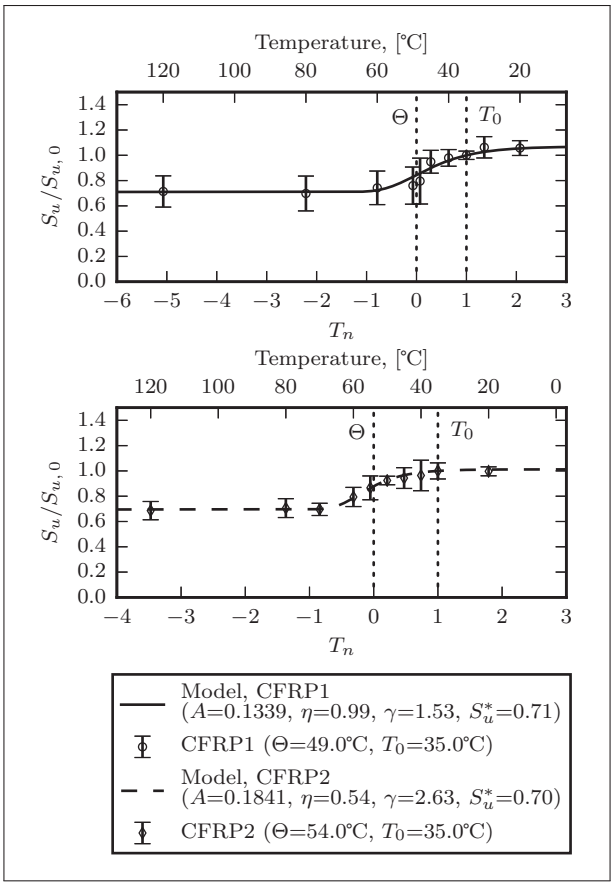

Figure 4.3 Prediction of strength as a function of temperature by equation 4.5 for Cao et al.'s (91) materials

above T_g published by Cao et al. (91) used previously, it is seen that a lower strength plateau is found around $2S_u/3$. It is thus assumed that for the composite system used for Upwind, a similar plateau is found, imposing $S_u^* = 2/3$. Other parameters are then found to be $A = 0.0364$, $\eta = 2.60$ and $\gamma = 1.88$. Figure 4.4 shows the resulting strength ratio as a function of temperature.

The fatigue model parameters as found by regression and as per equation 4.8 are given in Table 4.2. The resulting S–N curves are shown in Figure 4.5, where the solid line represents the curve at T_0 and the dashed lines are predicted using $S_{\mathrm{u,\,model}}$ and α_{model} for the relevant temperature.

It is worth stressing that in Figure 4.5 as well as in all further S–N curves provided, only the fatigue data at T_0 is used in the prediction while data points at other temperatures are only provided to illustrate the predictive capability of the proposed model.

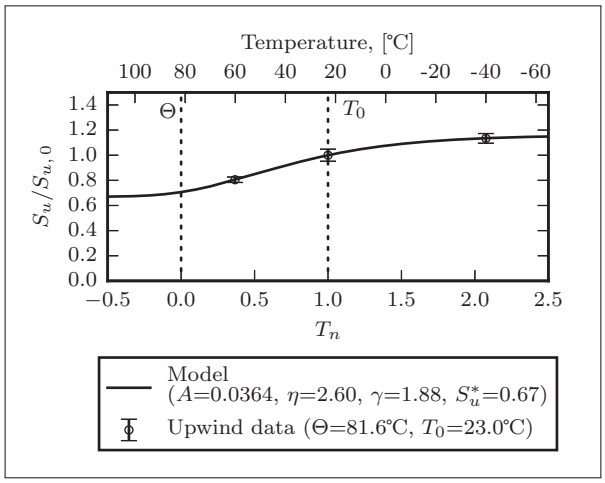

Figure 4.4 Prediction of strength as a function of temperature by equation 4.5 for Upwind's material

Table 4.2 Fatigue model parameters for Upwind's $R = 0.1$ data

Estimates based on measured static strength								
Temperature °C	T_n –	α_{reg} –	β –	r^2_{reg} –	$S_{\text{u, measured}}$ MPa	$(S_u/S_{u,0})^{T_n}$ –	α_{model} –	r^2_{model} –
-40	2.08	0.565	0.197	0.987	1038	1.299	0.456	0.925
23	1.00	0.351	0.197	0.966	915	1.000	0.351	0.966
60	0.37	0.325	0.197	0.934	737	0.924	0.324	0.933
Estimates based on modelled static strength								
Temperature °C	T_n –	α_{reg} –	β –	r^2_{reg} –	$S_{\text{u, model}}$ MPa	$(S_u/S_{u,0})^{T_n}$ –	α_{model} –	r^2_{model} –
-40	2.08	0.566	0.197	0.987	1039	1.302	0.457	0.924
23	1.00	0.351	0.197	0.966	915	1.000	0.351	0.966
60	0.37	0.323	0.197	0.934	735	0.922	0.324	0.934

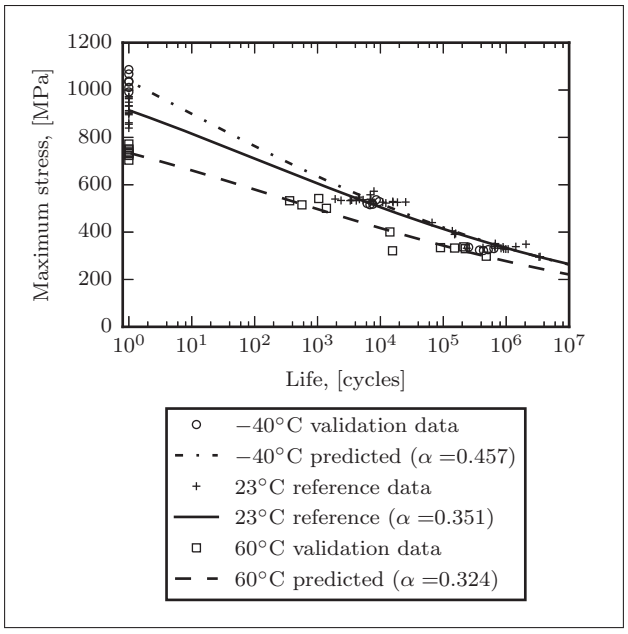

Figure 4.5 Predicted S–N curves at different temperatures for Upwind's material

As can be seen from Figure 4.5, the fit of the S–N curve is very good for all temperatures.

4.4.3 Fatigue life predictions for WESNet's (84; 185) material

Additional validation of the fatigue model is provided by comparing the predicted S–N curve against experimental data at -40℃ from the WESNet programme. The interest of this data set lies in the fact that — as was the case for Upwind — although quasi-static tests resulted in a substantial strength increase from 23℃ to −40℃, the fatigue life in the high cycle regime was not significantly affected. However, the fibre architecture of the WESNet and Upwind laminates were quite different. The ability of the model to deal with such behaviour is therefore tested and a comparison of the resulting model parameters will be possible.

The α and β parameters obtained by regression and with the proposed model are given in Table 4.3, while the baseline and predicted S–N curves are shown in Figure 4.6. This

figure shows that the baseline and predicted S–N curves are in acceptable agreement with the data. Nonetheless, it is seen that at 23℃, the S–N curve does not agree as well with the data as in previous cases. This is corroborated by the lower r^2 of 0.873. The broad scatter at low loads combined with the usual assumption of constant standard deviation used in the regression certainly contributed to the lesser fit. Yet, this latter assumption suggests that the curve should still be representative while the data could be biased at higher loads due to the low number of experiments. Considering these limitations of the WESNet data and the good fit of predictions at -40℃, the model results appear acceptable.

Table 4.3 Fatigue model parameters for WESNet's $R = 0.1$ data

Temperature ℃	T_n –	α_{reg} –	β –	r^2_{reg} –	S_u MPa	$(S_u/S_{u,0})^{T_n}$ –	α_{model} –	r^2_{model} –
-40	2.06	0.772	0.234	0.981	1232	1.398	0.761	0.979
23	1.00	0.544	0.234	0.873	1047	1.000	0.544	0.873

As noted earlier, although the fibre architecture used in WESNet and Upwind differed substantially, the same overall behaviour was observed in static and fatigue. The resulting model parameters are also comparable for both cases, although WESNet's material appears to be somewhat more fatigue sensitive as suggested by the stronger curvature of the S–N curves.

4.4.4 $S_u(T)$ and fatigue life predictions for Sims and Gladman's (92) material

In previous validation exercises, the model was tested against results for UD laminates within relatively narrow temperature ranges. It will now be tested against data from tests on woven laminates over a broader temperature range including two transition regions (as shown by the inversion of curvature around 25℃ in Figure 4.7). Application of both

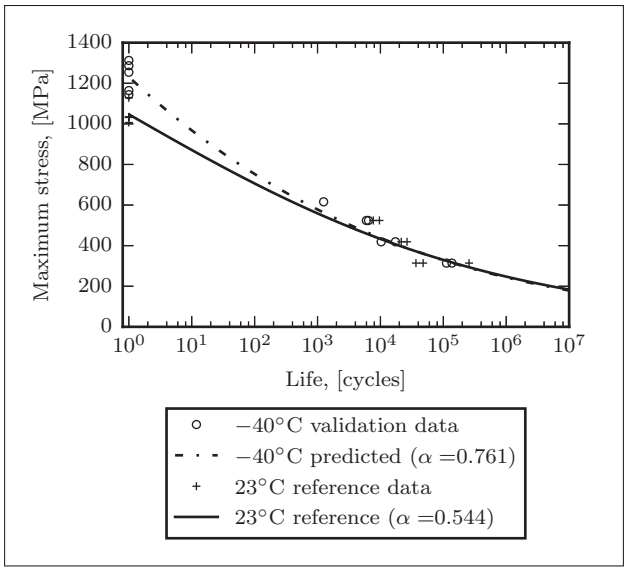

Figure 4.6 Predicted S–N curves at different temperatures for WESNet's material

the static and fatigue models to the two distinct regions is required and the predictive capacity within each transition region is verified.

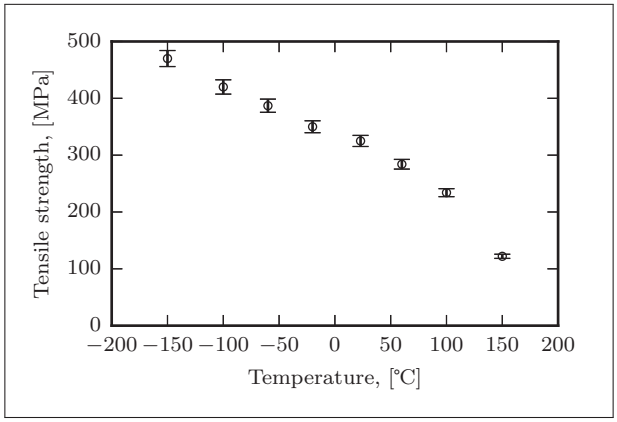

Figure 4.7 Tensile static strength as a function of temperature (Sims and Gladman (92))

In a first time, the ability of equation 4.5 to describe the evolution of S_u as a function of temperature within both regions is tested and the best fits obtained are shown in Figure 4.8. It is seen that within each transition, the model is very accurate, with the curve fitting easily within one standard deviation.

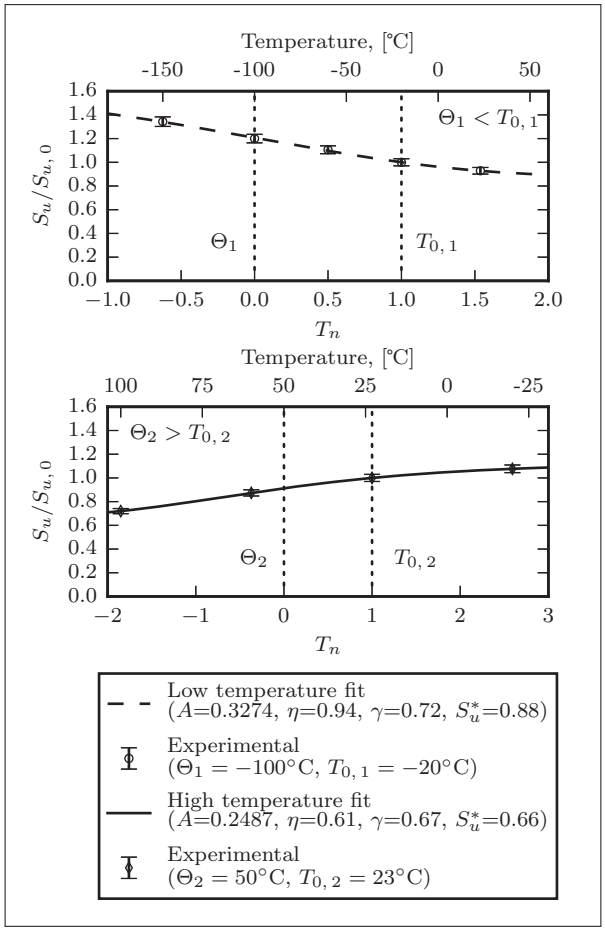

Figure 4.8 Prediction of strength as a function of temperature by equation 4.5 for Sims and Gladman's material

As a second test, the applicability of the empirical correlation of equation 4.8 for the prediction of α is verified. Two fits by equation 4.8 are required because the data spans two structural transitions. The correlation between α_{reg} and α_{model} is shown in Figure 4.9

for each of the two fits. The first fit uses $\Theta_1 = -100°\text{C}$ and $T_{0,1} = -20℃$ (low temperature transition) and the second is based on $\Theta_2 = 50°\text{C}$ and $T_{0,2} = 23℃$ (high temperature or glass transition). It is seen that the correlation is quite good within the glass transition range, but slightly lesser in the low temperature transition.

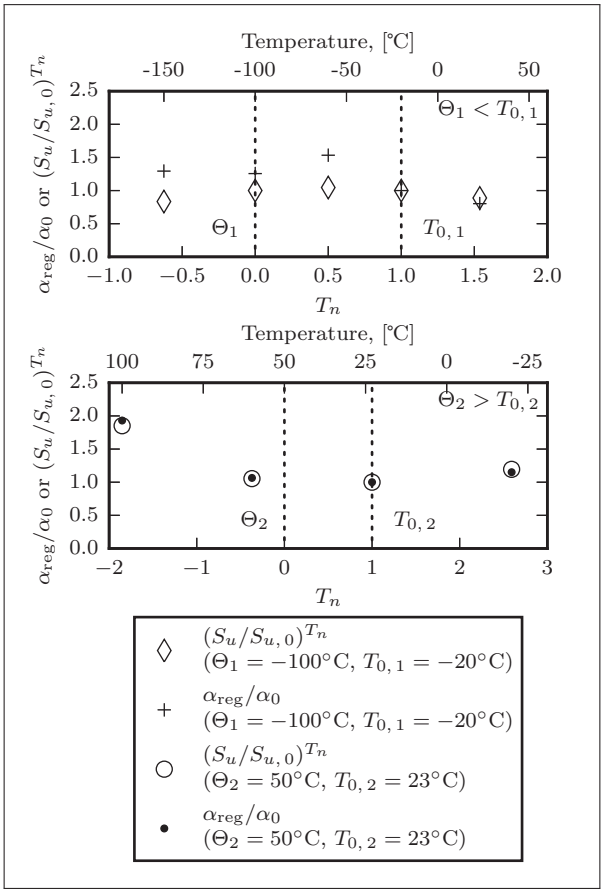

Figure 4.9 Correlation between α as found by regression and as predicted by Equation 4.8 for data by Sims and Gladman

Comparative values of α_{reg} and α_{model}, as well as other model parameters are given in Table 4.4 and 4.5 for both transition regions. S–N curves for the low temperature transition and within the glass transition region are respectively shown in Figure 4.10 and 4.11.

Table 4.4 Fatigue model parameters for Sims and Gladman's $R = 0.1$ data; low temperature transition ($\Theta_1 = -100°C$; $T_{0,1} = -20°C$)

Estimates based on measured static strength								
Temperature ℃	T_n –	α_{reg} –	β –	r^2_{reg} –	$S_{\text{u, measured}}$ MPa	$(S_u/S_{u,0})^{T_n}$ –	α_{model} –	r^2_{model} –
-150	-0.63	0.309	0.267	0.976	470	0.831	0.197	0.721
-100	0.00	0.295	0.267	0.985	420	1.000	0.237	0.924
-60	0.50	0.371	0.267	0.994	387	1.052	0.249	0.853
-20	1.00	0.237	0.267	1.000	350	1.000	0.237	1.000
23	1.54	0.191	0.267	0.992	325	0.895	0.212	0.980
Estimates based on modelled static strength								
Temperature	T_n	α_{reg}	β	r^2_{reg}	$S_{\text{u, model}}$	$(S_u/S_{u,0})^{T_n}$	α_{model}	r^2_{model}
-150	-0.63	0.308	0.267	0.976	469	0.834	0.199	0.737
-100	0.00	0.299	0.267	0.985	423	1.000	0.238	0.917
-60	0.50	0.365	0.267	0.994	384	1.046	0.249	0.865
-20	1.00	0.238	0.267	1.000	351	1.000	0.238	1.000
23	1.54	0.191	0.267	0.992	325	0.888	0.211	0.981

Results at low temperature presented in Figure 4.10 show a good agreement from room temperature down to $-100°C$. However, at $-150°C$, the S–N curve does not fit as well, particularly in the low cycle fatigue regime. It appears that at this very low temperature, the curvature of the fatigue curve would be required to increase significantly in order to provide a good fit. This suggests the current β estimate might not be as good at this temperature.

From Figure 4.11, it is seen that the agreement between the data and the S–N curves is quite good for temperatures ranging from 23℃ up to 100℃. Therefore, for this particular laminate the proposed method is even able to predict the fatigue performance above T_g. However, at $-20°C$ the predicted life is somewhat lower than the measured life, particularly for low cycle fatigue ($N < 1000$). This suggests that the room temperature β might not provide the best estimate of the material property at $-20°C$, a statement which is corroborated by the low temperature fit.

Table 4.5 Fatigue model parameters for Sims and Gladman's $R = 0.1$ data; high temperature transition ($\Theta_2 = 50°\text{C}$; $T_{0,2} = 23°\text{C}$)

Estimates based on measured static strength								
Temperature	T_n	α_{reg}	β	r^2_{reg}	$S_{\text{u, model}}$	$(S_u/S_{u,0})^{T_n}$	α_{model}	r^2_{model}
℃	–	–	–	–	MPa	–	–	–
-20	2.59	0.486	0.210	0.994	350	1.212	0.507	0.970
23	1.00	0.418	0.210	0.999	325	1.000	0.418	0.999
60	-0.37	0.451	0.210	0.997	284	1.051	0.439	0.993
100	-1.85	0.814	0.210	0.989	234	1.836	0.768	0.983
Estimates based on modelled static strength								
Temperature	T_n	α_{reg}	β	r^2_{reg}	$S_{\text{u, model}}$	$(S_u/S_{u,0})^{T_n}$	α_{model}	r^2_{model}
℃	–	–	–	–	MPa	–	–	–
-20	2.59	0.481	0.210	0.994	348	1.194	0.499	0.971
23	1.00	0.418	0.210	0.999	325	1.000	0.418	0.999
60	-0.37	0.445	0.210	0.999	282	1.047	0.438	0.991
100	-1.85	0.807	0.210	0.989	233	1.852	0.774	0.982

The generally good fit provided by the model validates the predictive ability of the proposed methodology for woven glass-epoxy composite loaded in tension along the fibre direction. It is also shown that in the case of materials exhibiting multiple structural transitions, minimal additional experimental efforts allow for the prediction of fatigue behaviour over very broad temperature ranges.

4.4.5 General discussion

As stated earlier, many models are available for describing the fatigue behaviour of composites. However, these are not all equal in terms of quality of fit. Although measures for goodness of fit are seldom provided in the fatigue literature, some documents do include r^2 values for S–N curves or CLDs (which can be seen as an extension of the S–N formulation over multiple load ratios R). For example, the 57 fits found in Boisseau et al. (236), Corum et al. (237) and Vassilopoulos et al. (129) have coefficients of determination in the range of $0.15 \leq r^2 \leq 0.99$ (mean $= 0.74$, median $= 0.83$, standard deviation $= 0.20$).

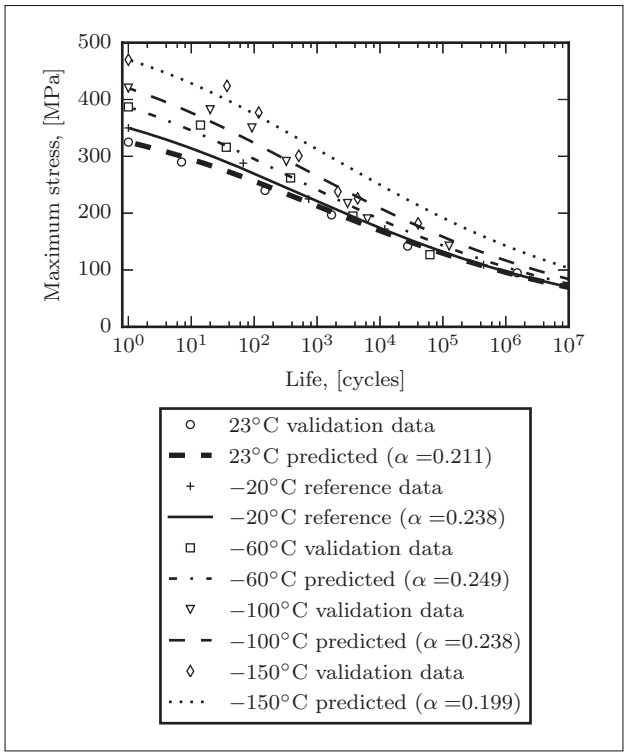

Figure 4.10 Predicted S–N curves at low temperatures for Sims and Gladman's material

From these results, it is seen that because of the inherent variability in the durability of composites subject to fatigue and because of small datasets usually used for fatigue research, relatively low coefficients of determinations may be expected.

In the current work, the model by Epaarachchi and Clausen was selected as a baseline for further development. With $r^2 \geq 0.999$ obtained for two out of the three baseline conditions and $r^2 = 0.873$ for the third, the goodness of fit for the baseline conditions compares favourably with results from the literature.

Also, based on the results summarized in Table 4.2, 4.4 and 4.5 the use of measured or modelled strength provides estimates of the fatigue model parameters that are very close. Values of r^2 for models based on measured and modelled strengths are mostly within a few tenths of a percent, with the worst difference being 1.6% for the fit at -150℃ on Sims

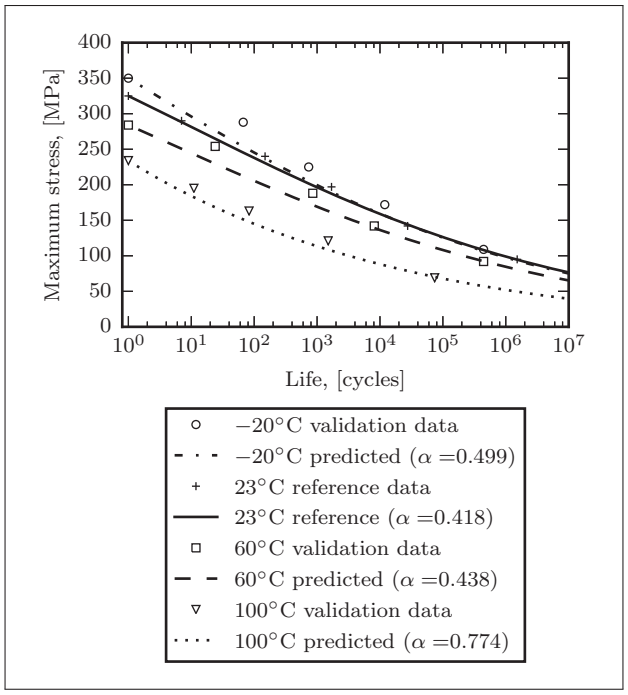

Figure 4.11 Predicted S–N curves at high temperatures for Sims and Gladman's material

and Gladman's data. Moreover, 12 out of the 14 curves fitted by regression using β_0 and the static strength model from equation 4.5 have a $r^2 > 0.95$ and 10 out of 14 even give $r^2 > 0.98$. Even the worst value of r^2 obtained, at 0.873 for WESNet's baseline condition, is above both the mean and median from the selected literature. It thus appears that the model by Epaarachchi and Clausen in conjunction with the proposed model for $S_u(T)$ is well suited to describe the behaviour of glass–polymer composites under tensile fatigue loading at any temperature.

Knowing that the baseline S–N curves are in good agreement with experiments, the fit of predicted curves can be evaluated. Nine out of the ten S–N curves predicted at various temperatures have $r^2 > 0.85$ and the lowest fit obtained is $r^2 = 0.737$ for woven laminates at -150℃. Thus, the goodness of fit for the proposed model also compares favourably with results from the literature and offers predictions that are at least as good as the average model from the literature which would have been fitted a posteriori to the data.

It is worth noting that predicted curves appear mostly conservative in their low-cycle fatigue life assessments. However, the prediction for the woven laminate at -150℃ is definitely biased towards longer lives in the high-cycle fatigue regime (Figure 4.10). Comparison of β between the two fits on Sims and Gladman's data as well as the behaviour of the curve at -150℃ suggest that as the temperature goes down, the value β could be expected to increase. This would be an indication that as the temperature is lowered, the difference between low-cycle and high-cycle fatigue behaviour gets more important.

The applicability of the proposed scheme is also corroborated by a comparison of r^2_{reg} and r^2_{model}. For most predicted curves, the fit is only slightly worse than that of the best fit obtained by regression on the data. Unexpectedly, it appears that predictions at low temperatures may be somewhat weaker than those for high temperatures, although still quite satisfying. This might be attributed to changes in failure modes or to shrinkage stresses effectively altering the fatigue stress ratio, two phenomenons that are not accounted for in the model.

As the value of r^2 alone may not be a sufficient indication of a model quality of fit, a plot of measured versus predicted lives for all test conditions is provided in Figure 4.12. In such a figure, points falling on the 45° line represent a perfect prediction from the model and the farther away from this diagonal a point is, the less accurate the prediction. In Figure 4.12, it is seen that of the 160 points used in the analysis, the model predicts a fatigue life within ± 1 decade of the measured one at a rate of 99.4% and within ± 0.5 decade for 96.9% of the data. An accuracy within ± 0.25 decade is even reached for 73.1% of the data. Considering the important scatter of fatigue data, such a level of accuracy in the prediction is very good.

The fit on results by Sims and Gladman (92) for which exact transition temperatures were unknown also suggest that both T_0 and Θ to be used in equation 4.6 can be chosen arbitrarily within a structural transition and the model should perform adequately. Thus,

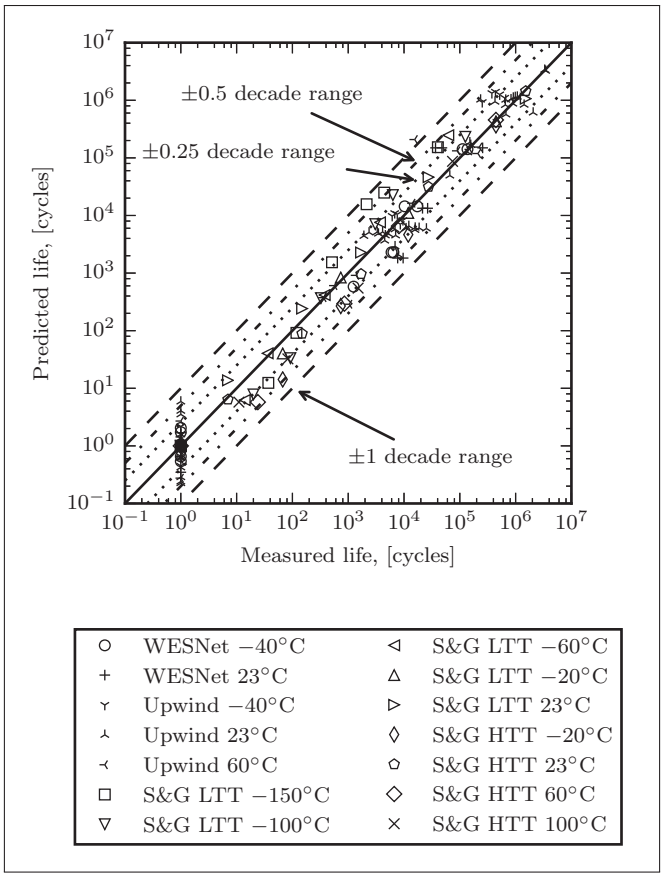

Figure 4.12 Measured versus predicted life diagram (S&G LTT and S&G HTT stand for Sims and Gladman low temperature transition and high temperature transition fits respectively)

although a transition temperature such as T_g seems like a natural candidate for Θ, it is not a requirement of the model.

Finally, Eftekhari and Fatemi (166; 197) have used the model by Epaarachchi and Clausen (146) — which is also the basis of the current work — in order to predict the effects of frequency and temperature on several neat, talc filled or short glass fibres reinforced thermoplastics. In these papers, they found that Epaarachchi and Clausen's model provides a good fit on experimental results and used a Larson-Miller type rela-

tionship to account for viscoelastic effects that were present at higher temperatures or lower load rates. A notable result from their research is that a single parameter set of $\alpha = 0.135$ and $\beta = 0.2$ was reported to provide a good fit for all the materials they tested. It is interesting to note that the values of β obtained in the current paper are close to that of Eftekhari and Fatemi. This suggests that in the absence of other information, a value of $\beta = 0.2$ might be useful for preliminary analysis or as a starting point in the optimization of model parameters. On the other hand, the use of a constant α does not appear to be a valid approach for long glass fibre reinforced thermosets as studied in the current paper. This is based on the fact that for all cases investigated here, α is shown to vary by more that 50% within a single transition region. Therefore, using a constant α would result in the use of an arbitrary value of the parameter (e.g. that from room temperature or an average over an arbitrarily chosen temperature range). For example, using the room temperature value of α for modelling the behaviour of Upwind's or Sims and Gladman's materials respectively reduces the resulting r^2 from 0.934 to 0.719 and from 0.982 to 0.652. Such reductions in the quality of fit are strong arguments against the use of a constant α in the case of long fibres reinforced thermosets, except as a very crude preliminary estimate.

4.4.6 Statistical considerations

Variability is an inherent property of the fatigue process in composites, thus the statistical treatment of fatigue data is of paramount importance. It is often the case with strength degradation fatigue models to assume a distribution of S_u and to relate the expected fatigue life to this distribution. This is done by finding the inverse function of the life N as a function of S_u and then obtaining the fatigue life distribution through a change of variable in the SF or CDF of S_u. Description of such a procedure is given in the work of Yang and Liu (138) or Sendeckyj (115).

However, the model by Epaarachchi and Clausen (146) — which is the basis of the current paper — happens to be of a high order and is thus not invertible analytically.

Nevertheless, since equation 4.4 is an increasing function of S_u over the range of interest ($N > 1$ and $\sigma_{\max} \leq S_u$), it has a unique inverse and the problem can be solved numerically. A general algorithm for obtaining the life N for a given maximum cyclic load $\sigma_{\max}$ and probability of survival is shown in Figure 4.13. A probabilistic stress-life (P–S–N) fatigue diagram can then be created by iterating the algorithm over a range of $\sigma_{\max}$.

In the current work, the distribution of S_u was assumed to be normal and the S–N curve was obtained with a least-square linear regression. The normal distribution was used for the sake of simplicity and because some data from the literature were only available as normal distribution means and standard deviations. Moreover, most sample sizes were too small to provide unbiased estimate of Weibull distribution's parameters.

A *Python 2.7.6* script was used to numerically solve the inversion problem. The `interp1d` method from the `scipy.interpolate` module (`scipy 0.17`) was used to invert the $N(S_u)$ relationship and the `cdf` method of the `norm` function from the `scipy.stats` module was used to recreate the transformed CDF. The method is applied to the Upwind reference data at 23℃ to demonstrate its functionality and the results are shown in Figure 4.14. The baseline S–N curve as well as those at 95 % and 99 % probability of survival are shown. Estimates at 50 % survival are also shown to demonstrate that they are equivalent to the baseline curve.

For establishing a P–S–N curve at other temperatures, one would only need to use parameters from the distribution of S_u at the desired temperature and the predicted fatigue model parameters (instead of running the linear regression). With this approach, it is possible to evaluate the S–N curve at any probability of survival and for any temperature given that the static life distribution parameters are known at those temperatures. However, the work of Christensen and Myiano (238) demonstrated both analytically and experimentally that scatter in fatigue life should not change with temperature. One could then estimate the fatigue life at any temperature and for any percentile of survival using the reference condition static strength distribution if no other information is available.

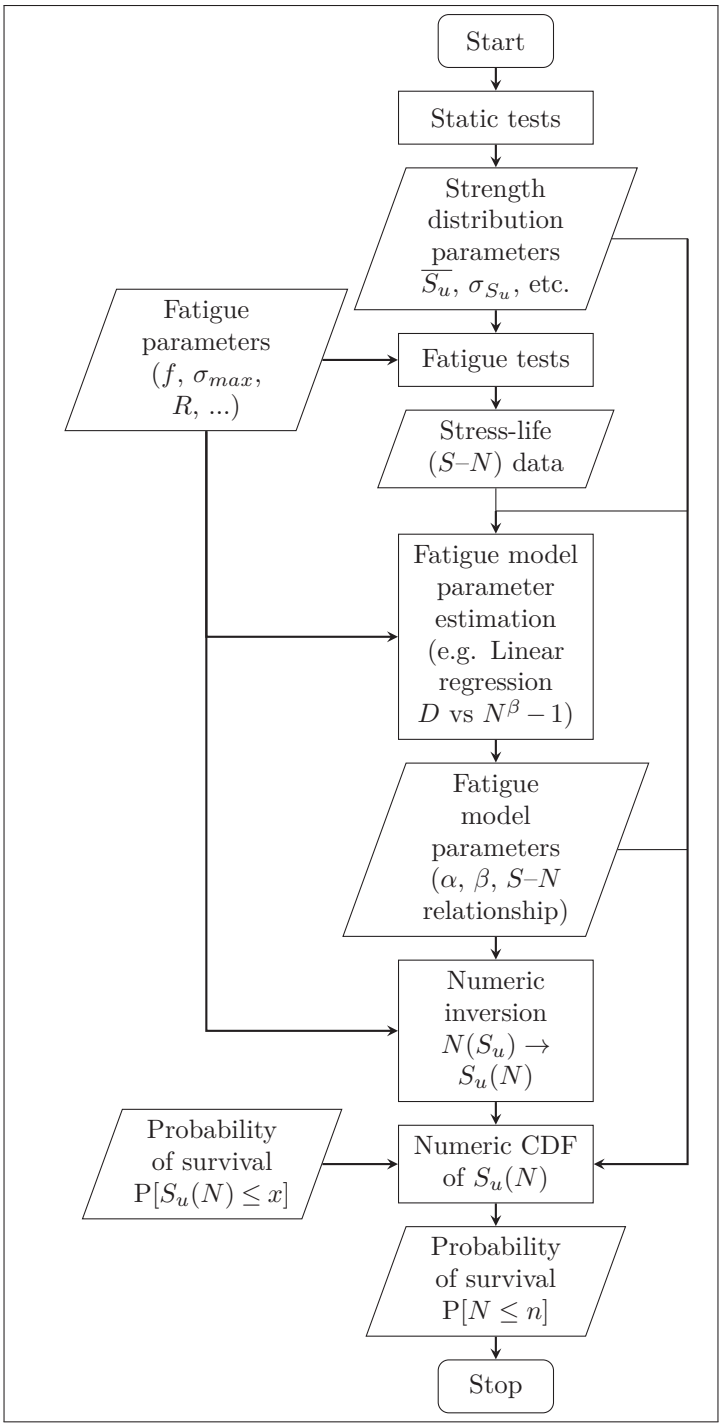

Figure 4.13 Numerical solution algorithm

Finally, despite the fact that a constant variance normal distribution was used to model S_u and to obtain fatigue model parameters through linear regression, this distribution

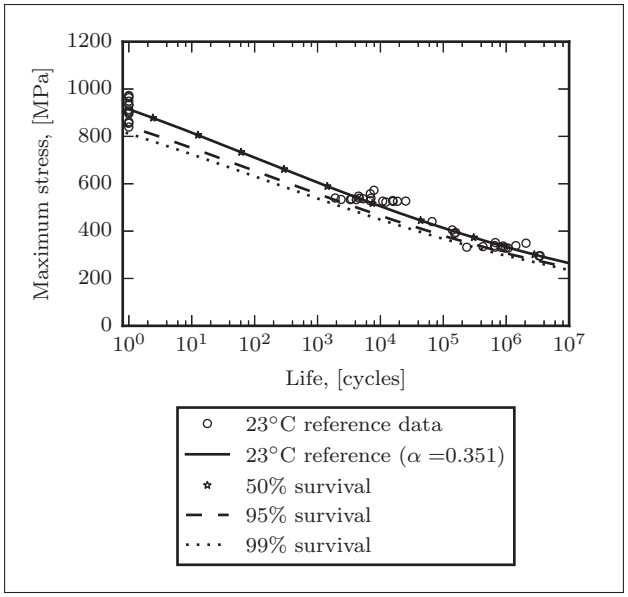

Figure 4.14 P–S–N curves for Upwind's material at 23℃

might not provide the best description of S_u and fatigue scatter. Although it is adequate in the current research context, applications where a given reliability is targeted would require validation of the distribution choice (e.g. log-Normal or Weibull) and analysis with the associated statistics on larger samples.

4.5 Conclusions

Prediction of fatigue life of composite materials has challenged material scientists for decades. Part of the difficulty lies in the combination of conflicting requirements of versatility, often translating into complex models, and that of minimal experimental efforts in order to determine model parameters. Although major advances have been made, challenges such as that of accounting for the influence of environmental factors on fatigue life remain.

The current work aims at providing a model for predicting fatigue life of glass fibre reinforced polymer composites loaded in tension along the fibre direction at any temperature,

while requiring only minimal experimental efforts. The procedure is based on two empirical formulations respectively describing the evolution of S_u and of a single fatigue model parameter with temperature. The experimental requirements for obtaining all of the parameters required by the method are limited to tensile strength tests at a minimum of four temperatures and fatigue data at one temperature.

It was shown that the proposed static strength model provides a very good description of that material property within a single structural transition (e.g. the glass transition) for the four materials on which the model was validated. Application of the fatigue model to results from three earlier independent research projects showed that the predicted S–N curves are in good to excellent agreement with experiments over a range of more than 100°C. It was also shown that for material exhibiting multiple structural transitions, the model could be applied separately within each transition and provide good results, at the expense of requiring additional fatigue data at one temperature within each transition. A method for obtaining probabilistic fatigue life estimates based on the static strength distribution is also provided.

However, as mentioned earlier, versatility is a desirable characteristic for a fatigue model. In this regard, the proposed model would still need to be validated for composites using different reinforcement materials and matrix systems. Moreover, it is likely that further adjustments would be required to generalize the model to other fibre orientations. Nonetheless, it is believed that the relative simplicity of the proposed method combined with its ability to predict fatigue life over a wide range of temperatures with minimal experimental efforts make it particularly attractive.

CHAPTER 5

A NEW APPROACH FOR ASSESSING THE STORAGE MODULUS, TRANSITION TEMPERATURES AND TIME–TEMPERATURE SUPERPOSITION CHARACTERISTICS OF EPOXIES AND THEIR COMPOSITES FROM DYNAMIC MECHANICAL TESTS

Laurent Cormier[1], Simon Joncas[1]

[1] Department of automated manufacturing engineering, École de Technologie Supérieure,
1100 Notre-Dame Ouest, Montreal, Quebec, Canada H3C 1K3
This is a pre-print (pre peer review version) of an article accepted for publication in the Journal of Thermal analysis and Calorimetry on October 16th, 2017.
The final authenticated version will be available online at: https://doi.org/10.1007/s10973-017-6774-6

Abstract

Epoxies are widely used as adhesives and matrix material for composites in civil infrastructure. As such structures are likely to be exposed to a wide variety of environmental conditions over long service lives, knowledge of their time-temperature sensitivity is desirable. The present study proposes a model describing the evolution of storage modulus for epoxies and their composites subject to forced dynamic excitations over wide temperature and frequency ranges. The model is tested against results for one epoxy and one carbon–epoxy composite. Results show a good agreement between the model and experiments, both in terms of temperature and frequency effects. Moreover, the model is shown to provide an unambiguous definition of the frequency dependent glass transition temperature, which is found to naturally follow the expected Arrhenius relationship with regards to frequency. Activation energies for the glass transition temperature evaluated by the new approach are in good agreement with results from the literature. It is also shown that when accounting for the effect of frequency on the glass transition, the evolution of the time-temperature shift factor is continuous across the glass transition.

5.1 Introduction

The use of polymers and polymer matrix composites for building and repairing large civil structures such as wind turbines, pipelines or bridges is increasing. However, such structures are inherently exposed to a large variety of environmental conditions, from hot and wet to cold and dry. In some regions like Canada, a single structure may experience temperatures ranging from close to -40℃ in winter to 20℃ or even 30℃ in summer, in addition to temperature gradients of about fifteen degrees over a single day (239). Combined with a great variability in external loads and the long expected lifetimes of civil infrastructure, these environmental conditions bring forward the requirement for a good knowledge of long-term properties of materials. However, polymers and polymer matrix composites are susceptible to viscoelastic behaviour even at room temperature or below. This means that in structural applications, creep or non-zero mean loading fatigue make polymers likely to fail earlier than could be expected on first account. This may be of particular concern for industries such as wind energy, where the laminate thicknesses are large, promoting hysteretic heat build-up at the laminate core (240).

Some of the most common tests for evaluating viscoelastic properties of materials are the creep, the relaxation and the dynamic mechanical analysis (DMA) tests. However, because of the physical limits of these experimental methods either in terms of duration (which cannot practically reach the lifetime of structures), loading rate/frequency or temperature range, the time–temperature superposition principle (TTSP) is often used for engineering purpose. This principle relies on the fact that many polymeric materials which are linear viscoelastic show the peculiarity that the shape of the curve representing their stiffness as a function of the logarithm of time under load (or loading frequency) remains constant for any temperature. Consequently, simply shifting the curves along the horizontal time/frequency axis (and possibly the vertical stiffness axis) should make it possible to superimposes curves obtained under different temperature conditions. Math-

ematically, this principle can be written as:

$$b_T M(a_T t, T) = M(t, T_0) \tag{5.1}$$

or recalling that frequency f is an inverse function of time ($f = 1/p$), with p the period in units of time:

$$b_T M\left(\frac{f}{a_T}, T\right) = M(f, T_0) \tag{5.2}$$

where M is the stiffness (e.g. the storage modulus E', loss modulus E'', complex modulus E^* or creep modulus E_c), b_T is the vertical shift factor, a_T the horizontal shift factor, T the temperature of interest and T_0 a reference temperature (Note that b_T is often close to unity and neglected in some applications (48)). Where this principle applies, the material is said to be thermorheologically simple. Because of the practical importance of this empirical principle, it has been the subject of extensive research since the middle of the 20th century, particularly for the study of material behaviour close to or across the glass transition.

One of the drawbacks of the method, apart from the difficult treatment of thermorheologically complex materials, is that obtaining the shift factor is an empirical process which may be somewhat subjective. Historically, plots were made on transparent paper and manually shifted to obtain a_T and b_T. In order to alleviate the problem, approaches for formally obtaining shift factors have been proposed. Examples of such methods are the least square method from Honerkamp and Weese (241) or the minimization of the distance between derivative by Naya et al.(242).

However, even with these objective approaches to obtaining the shift factors, the nature of the experiments is so that shift factors are only available over relatively narrow combinations of temperatures and frequencies. Moreover, at least two different fits are usually required, one below the glass transition temperature (T_g) and one above. Often, shift factors are fitted to an Arrhenius relationships if below T_g's range, or using the Williams-Landel-Ferry (WLF) (50) equation above T_g. Fulcher's (25) analogous equation (known

as the Vogel-Fulcher-Tamman or VFT relationship) is also used for modelling properties of amorphous materials and shift factors above T_g.

But the problem remains that T_g itself is not well defined and is a function of loading rate (or frequency) and of the thermomechanical loads history. It thus becomes unclear which formulation is best suited in some temperature ranges. In order to alleviate the latter problem, Brostow (243) proposed an equation for a_T based on free volume theory and the chain relaxation capability (CRC) concept. His equation was demonstrated to be usable across the glass transition. However, despite its apparent advantages, this method does not appear to have gained widespread acceptance or use.

Acknowledging the difficulty of identifying T_g independently of the loading rate or ageing characteristics, Li (244) used the TTSP to define the glass transition based on the maximum rate of change of the loss modulus E'' with frequency. Although this method does not solve the problem of identifying shift factors, it does partially address some difficulties with identifying a consistent value of T_g.

In a similar vein, Zhang et al. (245) also proposed a method for the measurement of T_g from damping peak at the resonance frequency of a free–free supported beam. The main objective of their approach was to provide a way of obtaining precise measurements of T_g at a fast rate so that the cure characteristics and absorbed moisture content would not change along the experiments. The novelty of their approach relied on an apparatus with a feedback loop circuit allowing to track the resonance frequency shift with temperature and a sample geometry and setup that minimized temperature gradients in the sample while allowing for rapid heating.

Molecular dynamic simulations have also been used to simulate the behaviour of polymers over temperature ranges. An example of such work is that of Sirk et al. (246), who simulated the dynamic behaviour of epoxy and obtained some correlation to experimental results. However, molecular dynamic models are still quite expensive computationally and cannot yet replace experimental efforts.

Similarly, temperature, load rate and heating rate effects on mechanical properties have been studied through the group interaction modelling (GIM) method which uses tabulated properties of molecular groups to infer properties of polymers. Such results are presented by Porter and Gould (247) but require a knowledge of the molecular structure of the polymer which is not always trivial to obtain.

In this paper, the TTSP concept is looked at from a new perspective by using continuous equations to explicitly describe the stiffness-frequency-temperature relationship, making the use of the time-temperature shift factors unnecessary. The proposed phenomenological equation is based on a statistical distribution of secondary molecular bonds breakage as a function of temperature, which is assumed to be related to the material stiffness. The result is an analytical expression providing information on the material stiffness at any frequency–temperature combination, based on a few easily performed DMA tests and without resorting to the TTSP nor to the evaluation of shift factors. Specifically, $E'(f)$ will be predicted based on measurements of $E'(T)$ at a few different frequencies. An unambiguously defined frequency dependent T_g — located at the inflection point of the stiffness–temperature curve — is also provided by the method.

In a first time, the modelling approach and model assumptions are presented. The model is then validated on experimental results from the literature for two different materials. Finally, implications of the results are discussed and a brief comparison with the TTSP is provided.

5.2 Model description

In Mahieux and Reifsnider (99), it is suggested that the Weibull distribution survival function (SF) could provide a better description of polymer modulus evolution as a function of temperature than the Arrhenius type relationship and its underlying Boltzmann distribution. The hypothesis was that the Weibull distribution could better describe the evolution of the remaining secondary bonds as a function of temperature and the result-

ing increase in molecular mobility across structural transitions. It was also proposed that a sum of such Weibull distributions could describe the behaviour of materials exhibiting multiple transitions. The resulting formulation is given by:

$$E(T) = \sum_{i=1}^{N} H_i \exp\left[-(T/T_{ref,i})^{k_i}\right], \tag{5.3}$$

where $E(T)$ is the polymer modulus, H_i is the magnitude of the i^{th} transition, T is the temperature, $T_{ref,i}$ represents the i^{th} transition temperature (or characteristic temperature) and k_i is the Weibull shape parameter of the i^{th} transition. It is easily seen that H_i would in most cases simply be equal to the difference of static moduli at the upper and lower stiffness plateaus (i.e. $E_i - E_{i+1}$).

However, given the desire to model the modulus of polymers and their composites, the work of Mahieux and Reifsnider suffers from a few limitations. First, the model converges to zero at very high temperature. While this is consistent with the original intent of modelling polymer stiffness, it is not if the model is extended to describe the stiffness of continuous fibre reinforced polymer composites.

A second shortcoming arises from the attractive yet problematic statement from Mahieux and Reifsnider (99) that the modulus is not imposed at any temperature and that the characteristic temperature $T_{ref,i}$ corresponds to the inflection point of the modulus curve. Upon inspection of the model, it appears that this statement is misleading since the value of the modulus at $T_{ref,i}$ is fixed, for a single given relaxation, by equation 5.3 which imposes $E(T = T_{ref,i}) = H_i \exp(-1) \approx 0.368 H_i$.

Furthermore, remembering that the inflection point of the curve would be found at $\mathrm{d}^2 SF_{Weibull}(T)/\mathrm{d}T^2 = 0$, one realizes that fixing the inflection at $T_{ref,i}$ in equation 5.3 equates to fixing the value of the Weibull exponent at $k = 0.5$ or $k = \infty$, therefore losing all of the model's adjustability. Thus, in Mahieux and Reifsnider's model, the modulus at $T_{ref,i}$ is actually fixed whilst the position of the inflection point is not.

From this discussion, it is evident that the reference temperature of Mahieux and Reifsnider is to the lower right of the transition. Therefore, unless the Weibull exponent is quite high, the use of conventional temperatures, such as the glass transition temperature (T_g) or the melt temperature (T_m), might not be suitable since these usually refer to temperatures closer to the beginning of the transition.

According to Gibson et al. (90), a third weakness of the model by Mahieux and Reifsnider is that the upper part of the transition tends to be too abrupt to accurately fit experimental results.

As an alternative, Correia et al. (101) proposed an adaptation of the Gompertz distribution to describe the evolution of composite materials properties as a function of temperature. However, by using the Gompertz cumulative distribution function (CDF) instead of the distribution's SF, the model by Correia and his colleagues shows a stronger curvature at low temperatures as compared to that at high temperatures. This is contrary to observations suggesting that higher temperatures have an increasingly strong effect on mechanical properties of polymers and their composites (see Chamis (85) for example). Furthermore, the use of the CDF deprives the model from the theoretical reasoning used by Mahieux and Reifsnider, which relies on the distribution SF. In order to solve these two problems and to improve on the formulation by Mahieux and Reifsnider, a new model based on the Gompertz SF is proposed here.

The Gompertz distribution originates from the work of Benjamin Gompertz (234) on tables of human mortality. It has been widely used to describe the evolution of the population as a function of age and also many life science phenomenons such as fertility and tumour growth (235; 248). Although the Gompertz distribution is usually used for describing time-dependent behaviours, it is proposed that its SF would also be a good candidate to model polymeric material properties evolution as a function of temperature. In the current work, the form of the Gompertz distribution used is based on that described by Garg et al. (235), which was transformed so that its supports lie within

$0 \leq T < \infty$ instead of $-\infty < T < \infty$. This form is particularly well suited for dealing with thermodynamic temperature units such as Kelvins. The general form of the Gompertz SF, which results in a monotonically decreasing sigmoid curve, is given by:

$$SF(T) = \exp\{-(b/c)[\exp(cT) - 1]\}, \tag{5.4}$$

where b is a scaling parameter and c is the slope parameter. It is interesting to note that behind its apparent complexity compared to the Weibull distribution, the Gompertz distribution is based on a quite simple hazard function (HF) — i.e. instantaneous failure rate — as illustrated by equation 5.5. As a reminder, the Weibull HF is provided in equation 5.6.

$$HF(T) = b\exp(cT) \tag{5.5}$$

$$HF_{Weibull}(T) = \frac{k}{T_{ref}}\left(\frac{T}{T_{ref}}\right)^{k-1} \tag{5.6}$$

From equation 5.5 and equation 5.6, it is seen that the natural logarithm of the Gompertz HF is a linear function of T, while the Weibull distribution's HF varies according to a power of T — in other words, the logarithm of Weibull's HF varies linearly with the logarithm of T. Realizing that the HF uniquely determines the probability density function (PDF) and therefore the CDF and SF (see Garg et al. (235) for example), it becomes clear that the HF constitutes the foundation on which the underlying hypothesis of Mahieux and Reifsnider's approach ultimately relies. Therefore, it could be argued that in terms of failure rate Gompertz's distribution is somewhat simpler than Weibull's and would be the most desirable given an equal quality of fit.

Interestingly, given positive values of b and c, the Gompertz HF has a monotonically increasing HF. This results in the desirable property that the Gompertz SF has a shallower curvature at the left of its inflection point. The corollary to this being that the temperature has an increasingly important effect on SF as it rises, which has the potential of

solving the initial curvature problem reported by Gibson et al. (90) that was discussed earlier.

On the hypothesis that the Gompertz SF is representative of the proportion of surviving secondary bonds in the polymer at a given temperature, the following conditions would need to be met in the case of the stiffness of pure polymers exhibiting a single relaxation:

$$SF(0) = 1, \tag{5.7}$$

$$SF(\infty) = 0, \tag{5.8}$$

$$\frac{\mathrm{d}SF(T)}{\mathrm{d}T} \leq 0. \tag{5.9}$$

However, extending the distribution to multiple transitions and to the prediction of composite properties requires four main modifications. First, the behaviour of the material needs to be modelled as a sum of N transitions. Second, controlling the magnitude of these transitions requires the introduction of a scaling parameter $(a_i - a_{i+1})$, which is directly related to the magnitude of each relaxation step. Third, a lower asymptote (a_{N+1}) needs to be added in order to represent the possibility of a residual property above the melt or decomposition temperature of the matrix, mostly necessary for the case of polymers reinforced by continuous fibres. Fourth, in order to locate the transition, the temperature is to be normalized by the reference transition temperature $T_{ref,i}$ (The introduction of the reference temperature parameter at the Gompertz HF level is detailed in Appendix A). Applying all these changes results in the form given by:

$$P(T) = a_{N+1} + \sum_{i=1}^{N} (a_i - a_{i+1}) \exp\left\{ -\left(\frac{b_i T_{ref,i}}{c_i}\right)\left[\exp\left(c_i \frac{T}{T_{ref,i}}\right) - 1\right]\right\}, \tag{5.10}$$

where $P(T)$ stands for the desired mechanical property.

Normalization by $T_{ref,i}$ has two main consequences. In a first time, it controls the influence of each of the N transitions on the global behaviour. That is, for $T \ll T_{ref,i}$,

the ratio $T/T_{ref,i} \to 0$, thus each exponential tends to unity and the contribution of the term to the global behaviour becomes that of an upper asymptote. Conversely, when $T \gg T_{ref,i}$, $T/T_{ref,i}$ becomes large, the outer exponential power becomes a negative number of great magnitude and the exponential itself gets very small. This gives the model an intrinsic ability to account for interactions between different relaxation modes.

In a second time, $T_{ref,i}$ contributes to the location of each transition. Two possibilities are considered here:

a. $T_{ref,i}$ is located at the inflection point of equation 5.4 (i.e. $\mathrm{d}^2SF(T)/\mathrm{d}T^2 = 0$).

b. $T_{ref,i}$ is located at the point of maximum curvature to the left of the inflection point of equation 5.4 (i.e. $\mathrm{d}^3SF(T)/\mathrm{d}T^3 = 0$).

In the context of DMA, T_g is conventionally given according to several definitions (see Figure 5.1). A first definition, usually referred to as $T_{g,onset}$ is located at the intersection of a straight line passing through the upper stiffness plateau and a tangent to the point of maximum slope of the $E'(T)$ curve. A second definition places the transition temperature at the peak of the loss tangent ($\tan\delta$) and is usually given the name $T_{g,peak}$. A third definition of T_g, which is rarely reported, is that given at the peak of loss modulus (E'') and here identified as $T_{g,loss}$. Although $T_{g,loss}$ is not used frequently, some consider it to be the best indicator of T_g obtained by thermomechanometry (e.g. Rieger (249)) as it is a direct measure of dissipated energy and will show each constituent T_g in polymer blends. It is also worth noting that the peak of $\tan\delta$ often occurs within a few degrees of the peak of E''. Furthermore, the measure of T_g obtained by another common method — differential thermal analysis — and $T_{g,loss}$ should agree closely (249).

It then appears that if one is to relate the values of T_g (or any other transition temperature) found using common methods to $T_{ref,i}$, any of the two proposed definitions for $T_{ref,i}$ could lead to good results. Yet, it is likely that locating $T_{ref,i}$ at the inflection point (closely corresponding to $T_{g,loss}$ or $T_{g,peak}$) might provide more flexibility in the

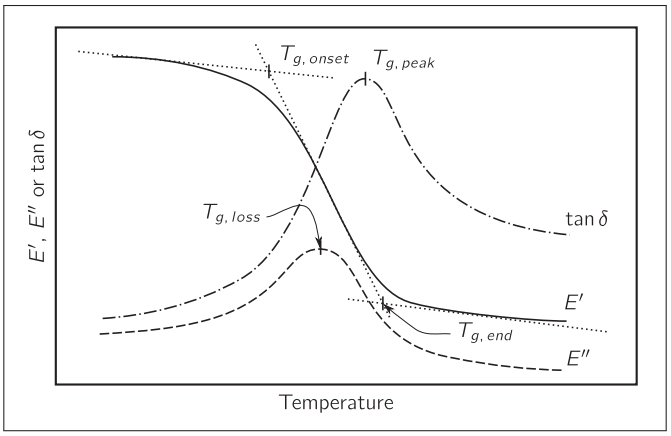

Figure 5.1 Conventional definitions of T_g based on measurements by dynamic mechanical thermal analysis

case of low transition slopes than the use of $T_{g,onset}$ and $T_{ref,i}$ at the point of greatest curvature. This first approach will then be further developed here and used for fitting the model to data from the literature (see Appendix B for the development of the second approach). Thus, posing:

$$\frac{\mathrm{d}^2 P(T)}{\mathrm{d}T^2} = 0, \tag{5.11}$$

then, assuming all transitions to be distinct:

$$T = \frac{T_{ref,i}}{c_i} \ln\left(\frac{c_i}{b_i T_{ref,i}}\right). \tag{5.12}$$

Or in other terms, at $T = T_{ref,i}$:

$$b_i = \frac{c_i}{T_{ref,i}} \exp\left(-c_i\right). \tag{5.13}$$

Putting equation 5.13 into equation 5.10, the latter simplifies to:

$$P(T) = a_{N+1} + \sum_{i=1}^{N} (a_i - a_{i+1}) \exp\left\{-\exp\left(-c_i\right)\left[\exp\left(\frac{c_i T}{T_{ref,i}}\right) - 1\right]\right\}. \tag{5.14}$$

Therefore, the proposed model requires $3N+1$ independent parameters as an input, with N being the number of transitions.

Equation 5.14 gives a general form for the stiffness–temperature relationship, including the possibility to account for any number of structural transitions. However, it is not yet related to frequency (or time at load). From the literature, it is known that T_g is related to frequency by an Arrhenius relationship (33) such that:

$$T_g = \frac{E_a}{R \ln (f_0/f)} \tag{5.15}$$

where E_a is the glass transition activation energy, R is the ideal gas constant, f_0 is the pre-exponential frequency factor. Thus, given T_g at some frequencies, E_a and f_0 can be obtained from the slope and intercept of the best fit straight line from the $\ln f$ vs $1/T_g$ plot. For the glass transition region, equation 5.15 is thus substituted to T_{ref} in equation 5.14 to get the explicit frequency dependence of the stiffness. Barral et al. (32) also showed that an Arrhenius relationship is adequate for modelling the β-transition in the epoxy system consisting of a diglycidyl ether of bisphenol A (DGEBA) resin cured with 1,3-bisaminomethylcyclohexane (1,3-BAC) hardener. Therefore it is postulated that a generalized form of equation 5.15 can be substituted to $T_{ref,i}$ in equation 5.14 for any transition.

Note that the Arrhenius T_g relationship here performs two functions. First, it is used as a validation tool by verifying that the T_g obtained from equation 5.14 at different frequencies indeed follows an Arrhenius type behaviour. Second, once it is demonstrated that the model captures this behaviour of the material, it allows for the inclusion of frequency effects by substituting the Arrhenius relationship to T_{ref}.

Finally, experience has shown that sometimes, the slope parameters c_i and the upper asymptotic modulus a_i also are functions of f. It will be shown later that a simple log-log linear relationship (equation 5.16 and 5.17) provides an adequate prediction of the

evolution of c_i and a_i with frequency if needed.

$$\ln c_i = m_{ci} \ln f + \gamma_{ci} \Rightarrow c_i = f^{m_{ci}} \exp(\gamma_{ci}) \tag{5.16}$$

$$\ln a_i = m_{ai} \ln f + \gamma_{ai} \Rightarrow a_i = f^{m_{ai}} \exp(\gamma_{ai}) \tag{5.17}$$

In equations 5.16 and 5.17, m and γ are respectively the slope and intercept of the log-log $c(f)$ or $a(f)$ relationships.

5.3 Materials and methods

To demonstrate the ability of the proposed model to provide a continuous description of the storage modulus of polymer or polymer matrix composite over a wide range of temperature and frequency, the model is validated on experimental results from the literature.

First, the model is tested on DMA data for 5% liquid rubber toughened epoxy from Li (244) over a frequency range of 0.1 Hz $> f >$ 100 Hz and temperatures from approximately 300 K to 390 K. Such a system is representative of many industrial adhesive.

A second dataset used for validating the model is that from Goertzen and Kessler (34) for room temperature cured carbon–epoxy composites, a potential candidate material for ageing pipeline repairs and reconditioning. The material is made of biaxial woven carbon fibre fabric hand laid up with a DGEBA resin cured with an aliphatic amine hardener.

Note that the data points are extracted from the continuous curves in the original articles. Therefore, they are representative of the material behaviour, but may not coincide exactly with actual measurement points.

5.3.1 Computational approach

In a first time, equation 5.14 is fitted to the data at each frequency using a standard non-linear least square. Specifically, a *Python* 2.7.6 script running the `curve_fit` method from the `optimize` module of `scipy`'s package version 0.17.0 is used. This first step provides the 'best-fit' parameters for the model.

From these 'best-fit' parameters, linear regressions are performed to obtain parameters of the Arrhenius relationship for $T_{ref,i}$ (equation 5.15) and log-log relationships for the c_is (equation 5.16) and a_is (equation 5.17). These regression are performed using the `linregress` method from `scipy`'s `stats` module. These relationships are then substituted to $T_{ref,i}$s, c_is and a_is in equation 5.14 to obtain the $E'(f,T)$ model, which is compared to experimental data both in the temperature and frequency domain.

As data by Li (244) spans a single transition, the corresponding shift factors (a_T) were obtained from the proposed model.

Finally, the quality of fit for the proposed method is evaluated by the coefficient of determination r^2 and the p-value of linear model parameters against the null hypothesis of a zero slope. The 5% significance level for the p-value is used unless otherwise specified.

5.4 Results

5.4.1 Rubber toughened epoxy storage modulus

The model was used to obtain materials parameters for rubber toughened epoxy at multiple frequency. Since the T_g of rubber is much lower than the temperature range of the test, this material exhibits a single transition phase over the range of temperatures considered here. Best-fit model parameters for equation 5.14 are obtained at each frequency. These parameters are summarized in Table 5.1. Note that for this material, $T_g = T_{ref,1}$.

Table 5.1 Model parameters from non-linear least square regression for rubber toughened epoxy

f Hz	$T_{ref,1} = T_g$ K	c_1 –	a_1 MPa	a_2 MPa
0.1	349.0	28.77	2794	12.0
0.5	353.1	30.11	2716	12.0
1.0	354.8	29.63	2709	12.0
5.0	358.3	28.35	2674	12.0
10.0	358.9	26.97	2716	12.0
50.0	362.8	26.95	2699	12.0
100.0	364.6	26.37	2686	12.0

From these, the Arrhenius and $c(f)$ parameters are obtained. For equation 5.15, values of $E_a = 480$ kJ/mol and $f_0 = 5.97 \times 10^{70}$ Hz are obtained. The coefficient of determination for this regression is $r^2 = 0.993$ and a p-value $= 2 \times 10^{-5}$ on the slope.

Parameters $m_{c1} = -0.0161$ and $\gamma_{c1} = 3.36$ are obtained for equation 5.16. However, in this case, r^2 is only 0.602 because of the important dispersion of the c parameter. Also worth noting is that the p-value of the slope is only 0.070, meaning that the hypothesis of a zero slope cannot be ruled out based on the basis of a 5% significance level. Yet, based on other evidence and on the decreasing value of c with f (as opposed to $\ln c$–$\ln f$), it is chosen to maintain the hypothesis of frequency sensitivity.

The log-log relationship on a_1 is also tested for and parameters $m_{a1} = -0.0047$ and $\gamma_{a1} = 7.91$ are obtained as best-fit estimates, with an $r^2 = 0.507$ and a p-value of 0.112. Given the low r^2 and p-value as well as the fact that the upper asymptote of the modulus was undistinguishable in the original plot, it is decided that the average value of a_1 should be used for further analysis.

The Arrhenius relationship of $T_g(f)$ as well as the $a(f)$ and $c(f)$ regression curves are shown in Figure 5.2, 5.3 and 5.4 respectively.

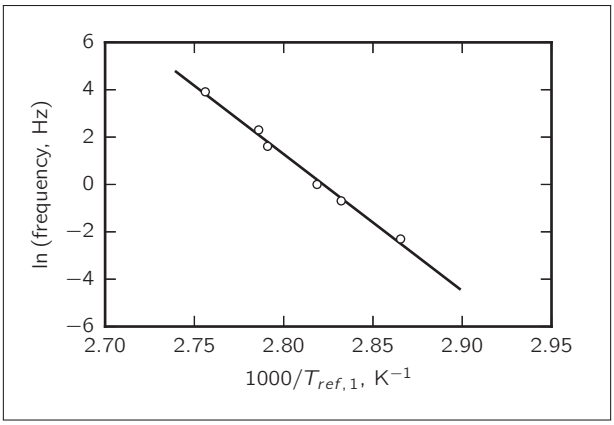

Figure 5.2 Transition temperature $T_{ref,1}(f) = T_g(f)$ Arrhenius relationship for rubber toughened epoxy

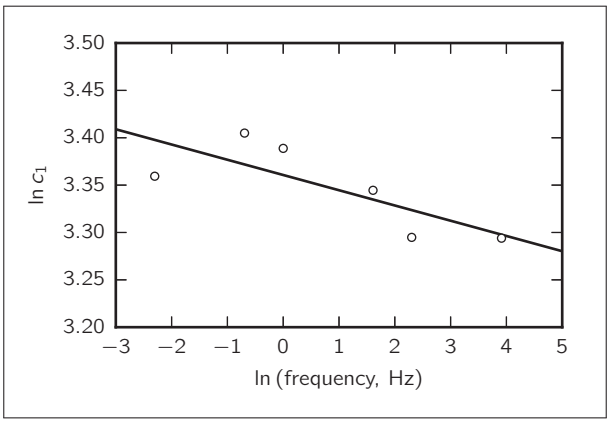

Figure 5.3 Slope–frequency relationship for rubber toughened epoxy

Figure 5.5 shows $E'(T)$ curves at different frequencies for temperatures across the glass transition. These curves are plotted from equation 5.14 in which $T_{ref,1}$ and c_1 were respectively substituted by equations 5.15 and 5.16.

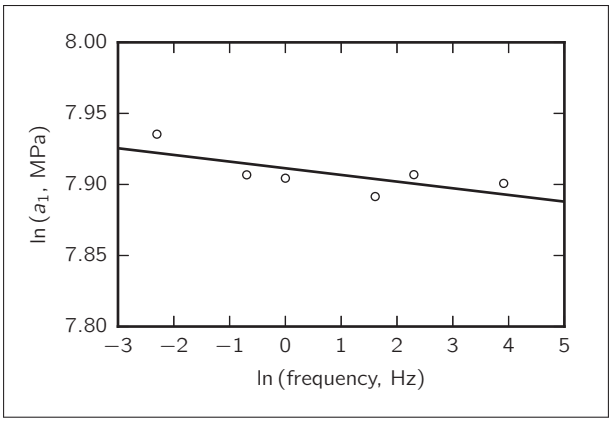

Figure 5.4 Asymptotic modulus $a_1(f)$ frequency dependence for rubber toughened epoxy

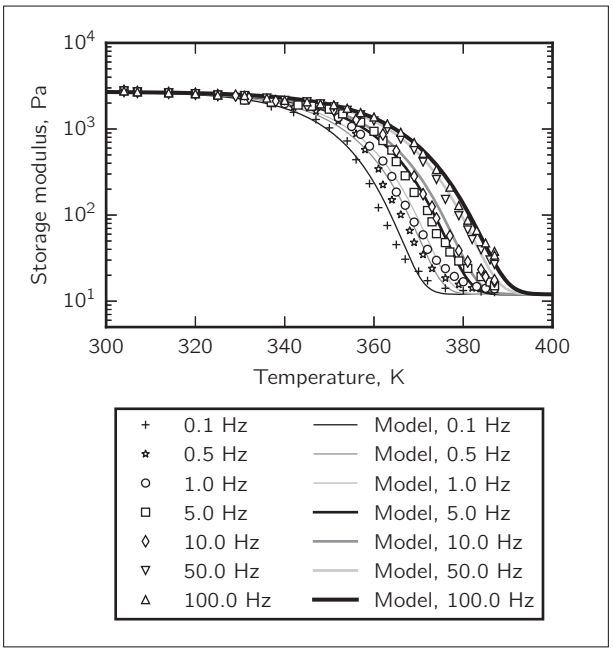

Figure 5.5 Storage modulus as a function temperature at various frequencies for rubber toughened epoxy

From this equation, $E'(f)$ can easily be obtained. Such a representation is given in Figure 5.6, where experimental data are compared to the model.

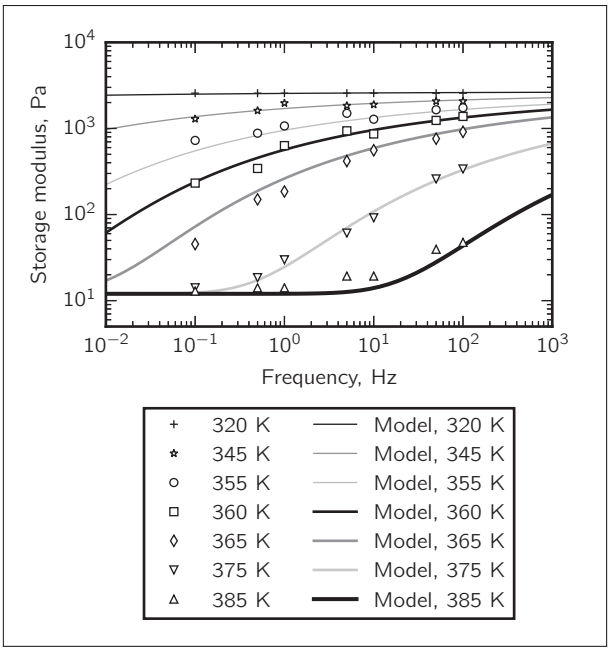

Figure 5.6 Storage modulus as a function of frequency at various temperatures for rubber toughened epoxy

Although they are not required with the current approach, horizontal shift factors a_T are obtained from equation 5.2. Figure 5.7 shows such a_T factors as a function of temperature at four frequencies and based on a reference temperature $T_0 = 423$ K. It is seen that curves do not superimpose, implying some degree of thermorheological complexity.

5.4.2 Carbon–epoxy composite storage modulus

The DMA data for carbon–epoxy from Goertzen and Kessler (34) shows more than one transition. This is due to the fact that the material is cured at room temperature and that a residual cure results from heating during the DMA experiments. The model is thus fitted accounting for two transitions, one representing the baseline epoxy, and one for the cure effects. Optimal parameters for the model are provided in Table 5.2. These results show that while $T_{ref,2}$, a_1, a_2 and a_3 show a definite increasing trend with f, c_2 decreases with increasing f, while $T_{ref,1}$ and c_1 show no clear trend.

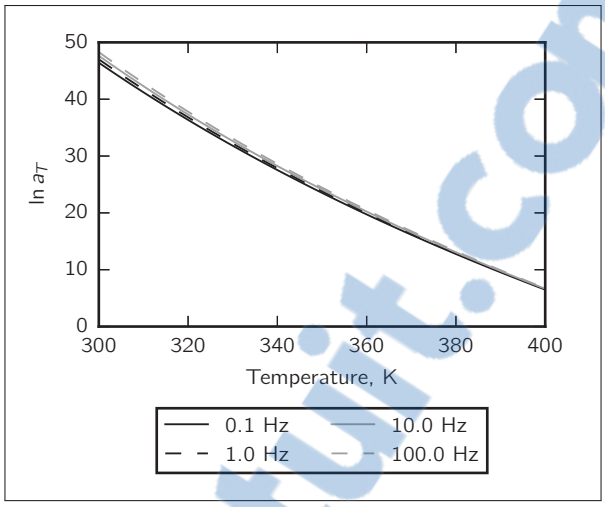

Figure 5.7 Storage modulus shift factors a_T for rubber toughened epoxy ($T_0 = 423$ K)

Table 5.2 Model parameters from non-linear least square regression for carbon–epoxy composite

f Hz	$T_{ref,1}$ K	$T_{ref,2} = T_g$ K	c_1 –	c_2 –	a_1 GPa	a_2 GPa	a_3 GPa
0.316	330.2	334.8	271.0	101.0	37.9	20.9	0.779
1.00	330.7	336.6	220.9	86.92	38.1	25.0	0.807
3.16	331.7	338.8	152.8	75.92	38.2	27.5	0.825
10.0	331.3	340.9	206.8	59.96	38.6	33.1	0.849
31.6	330.6	343.6	390.2	49.93	38.8	36.3	0.905

The transition temperatures-frequency relationships are shown in Figure 5.8. For this material, the lowest transition temperature ($T_{ref,1}$) only varied by about 1.5 K over the frequency range and no clear trend was observable for that parameter. This is reflected by a low $r^2 = 0.169$ and a p-value of only 0.492, suggesting that the parameter is very weakly correlated to frequency and that the hypothesis of a constant value cannot be rejected. This is consistent with the fact that the temperature at which the residual cure starts is not expected to have a strong dependence on f. The average of all measured

values, $T_{ref,1} = 330.9$ K, was thus used for modelling purpose independently of the loading frequency.

On the other hand, the glass transition temperature $T_{ref,2} = T_g$ closely followed the Arrhenius relationship of equation 5.15, with an activation energy of $Ea = 496.8$ kJ/mol and a pre-exponential factor $f_0 = 1.18 \times 10^{77}$ Hz. The coefficient of determination for this regression is $r^2 = 0.996$ and the p-value is 1×10^{-4}.

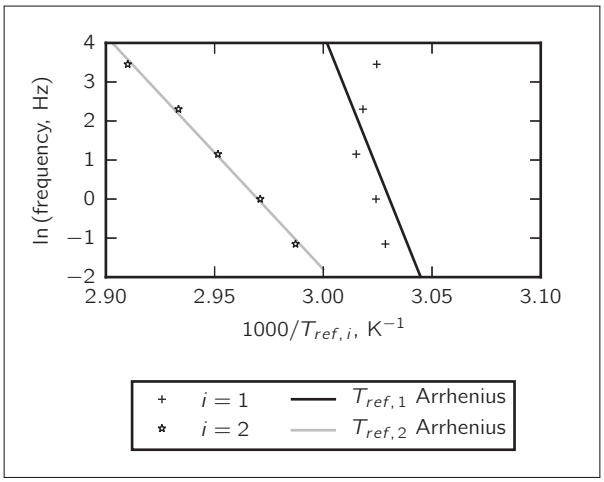

Figure 5.8 Transition temperatures $T_{ref,1}(f)$ and $T_{ref,2}(f) = T_g(f)$ Arrhenius relationship for carbon–epoxy

The effect of frequency on the slope parameters c_1 and c_2 is shown in Figure 5.9. The slope parameters for the transitions are obtained for equations 5.16 and 5.17. For the first transition, parameters $m_{c1} = 0.0576$ and $\gamma_{c1} = 5.40$ were obtained. However, an $r^2 = 0.091$ and a p-value of 0.622 show that over this range of frequency, assuming a zero slope would yield comparable results. The average value of $c_1 = 248.3$ was thus used instead of the linear model. This is again consistent with the assumption that a residual cure should not be strongly correlated to frequency.

For the slope parameter c_2, the regression provides parameters of $m_{c2} = -0.155$ and $\gamma_{c2} = 4.46$, with an $r^2 = 0.990$ and a p-value of 4×10^{-4}, suggesting an excellent fit.

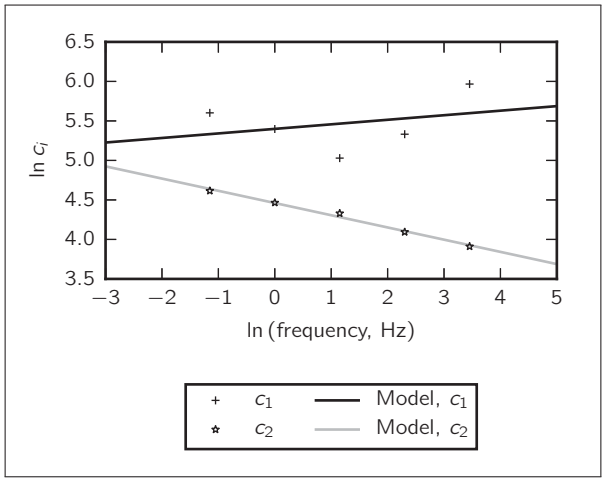

Figure 5.9 Slope parameters $c_1(f)$ and $c_2(f)$ relationships for carbon–epoxy

Finally, the asymptotic moduli a_1 and a_2 also vary with frequency and they are shown in Figure 5.10. The log-log fit between these moduli and the frequency is quite good. A slope parameter $m_{a1} = 0.121$ and intercept $\gamma_{a1} = 23.9$ ($r^2 = 0.988$, p-value $= 6 \times 10^{-4}$) are obtained for the first transition, while for the second transition $m_{a2} = 5.39 \times 10^{-3}$ and $\gamma_{a2} = 24.4$ ($r^2 = 0.989$, p-value $= 5 \times 10^{-4}$).

The model fit for $E'(T)$ is shown in Figure 5.11, where it is seen that a good agreement is obtained. The resulting $E'(f)$ prediction can then be obtained from the analytic model. This prediction is compared to experimental results in Figure 5.12.

5.5 Discussion

The validation exercises, performed on the two materials, show good agreement of the model with experimental results. Figures 5.5 and 5.11 demonstrate the fit between experimental values of $E'(T)$ and the combination of equations 5.14, 5.15, 5.17 and 5.16.

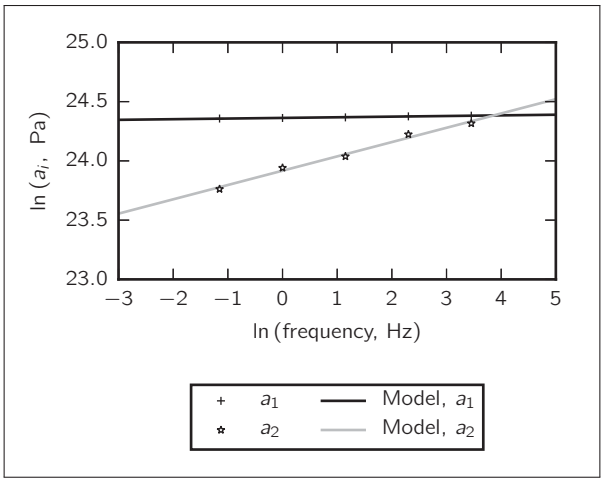

Figure 5.10 Asymptotic moduli $a_1(f)$ and $a_2(f)$ frequency dependence for carbon–epoxy

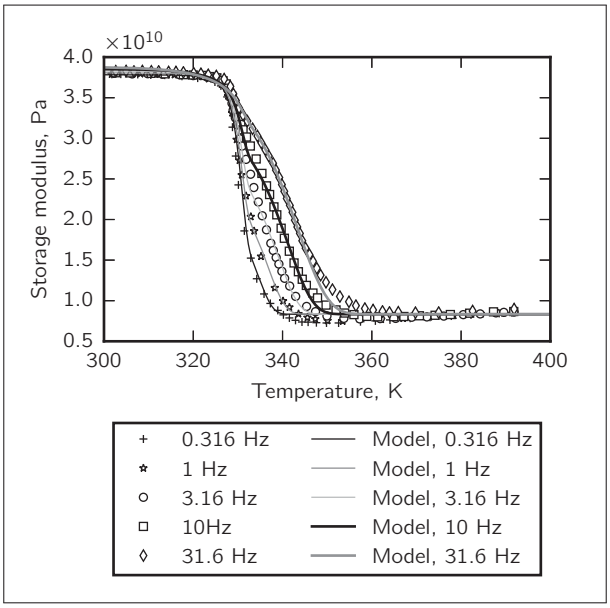

Figure 5.11 Storage modulus as a function of temperature at various frequencies for carbon–epoxy

The validity and usefulness of these equations are also supported by the good predictions of $E'(f)$ they provide from the analysis of $E'(T)$ measurements at a few frequencies.

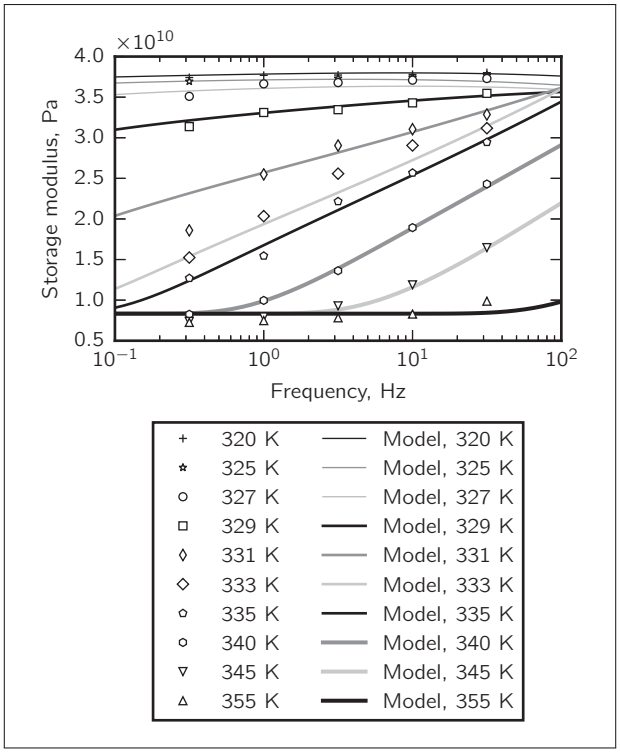

Figure 5.12 Storage modulus as a function of frequency at various temperatures for carbon–epoxy

These $E'(f)$ predictions, shown in Figure 5.6 and 5.12, provide a good fit even within the glass transition region where there is a strong stiffness gradient and marked frequency effects. This provides good confidence on the model applicability.

Moreover, the model appears to have a natural ability to capture the Arrhenius relationship of $T_g(f)$. This is demonstrated by the very good fit of the Arrhenius relationship with $r^2 = 0.993$ for toughened epoxy and $r^2 = 0.996$ for carbon-epoxy composites. The fact that this empirically observed behaviour of the material is reproduced by the model supports its validity.

The activation energies obtained based on T_g assessment for rubber toughened epoxy by Li (33) are $536.3\,\mathrm{kJ\,mol^{-1}}$, $479.9\,\mathrm{kJ\,mol^{-1}}$ and $384.9\,\mathrm{kJ\,mol^{-1}}$ respectively based on

$T_{g,\ onset}$, $T_{g,\ loss}$ and $T_{g,\ peak}$. These activation energies, particularly that for $T_{g,\ loss}$, are in good agreement with that obtained with the proposed model ($E_a = 480\,\mathrm{kJ\,mol^{-1}}$).

The estimated activation energy obtained by the current approach ($E_a = 496.8\ \mathrm{kJ\,mol^{-1}}$) based on DMA results by Goertzen and Kessler (34) is, however, somewhat higher than reported in the original article at $E_a = 331\ \mathrm{kJ\,mol^{-1}}$ based on $T_{g,\ peak}$ or $E_a = 384\,\mathrm{kJ\,mol^{-1}}$ based on $T_{g,\ loss}$. It is believed that the discrepancy between our estimate and previous assessments follows from our model's ability to discriminate between the effect of the residual cure and that of the actual glass transition. Values of E_a obtained from the application of the proposed model are also comparable to those obtained based on $T_{g,\ peak}$ by Li, Lee-Sullivan and Thring (33) for Novolac epoxy ($498.9\ \mathrm{kJ\,mol^{-1}} \leq E_a \leq 537.3\ \mathrm{kJ\,mol^{-1}}$), by Barral et al. for DGEBA epoxy cured with 1,3-BAC ($E_a = 345\ \mathrm{kJ\,mol^{-1}}$) or by Karbhari and Wang (250) for wet conditioned glass–vinylester composites ($283.7\ \mathrm{kJ\,mol^{-1}} \leq E_a \leq 346.4\ \mathrm{kJ\,mol^{-1}}$).

Two interesting trends challenging accepted ideas about the TTSP are also shown in Figure 5.7. The first trend is the continuous nature of a_T shift factors across T_g when frequency effects on T_g itself and on the slope parameter c are accounted for. This suggests that the hypothesis of a discontinuity in the behaviour outside and within the glass transition region may after all only be an artefact of the failure to account for T_g's own frequency sensitivity. Thus, the generally accepted idea that a_T is described by an Arrhenius relationship well above and below T_g and by the WLF or VTF equation around T_g might in fact originate from neglecting to clearly define T_g and excluding the frequency effect on that particular parameter. The shape of the a_T curve is, however, qualitatively comparable to that of the WLF model, that is it shows some upward concavity.

This result is particularly interesting in the light of the work of Liu et al. (24) who, by plotting $\log a_T$ against $T' = T_g/(T - 0.77T_g)$ (with $0.77T_g$ originating from Adam and Gibbs theory (52)), were able to obtain a single linear Arrhenius relationship of $\log a_T$ valid for a wide range of polymers across the glass transition ($1.1 < T/T_g < 1.77$ or

$1 < T' < 3$) and into the melt regime. As would be expected, between $T' \approx 2$ and $T' \approx 3$, the predicted curve would indeed be linear. Note, however, that because of the high crosslink density of epoxy, a_T becomes negligible for $T' \leq 2$, which is $T \geq 1.27T_g$, or into the rubbery plateau.

The second trend follows from accepting that there may be a change in the slope parameter c of the $E'(T)$ curve with frequency, which implies that a_T is somewhat sensitive to frequency. In the current case, this results in a series of $\ln a_T(T)$ curves that converge to unity at $T = T_0$, but do not superimpose at lower temperatures. The proposed method can therefore deal with $E'(f)$ curves that change shape with temperature, which is to say that it can represent the behaviour of materials that exhibit some level of thermorheological complexity.

Finally, the application of the model to Goertzen's data shows that the model is even able to capture some of the effects of residual cure as a second transition where the rate of secondary bonds failure is reduced compared to the initial state.

5.6 Conclusion

In this paper, an alternative to the TTSP is provided for predicting the evolution of epoxy resins and composites storage modulus as a function of temperature and frequency. The proposed model has the advantage of accounting for the variation of T_g with f and can also deal with a limited level of thermorheological complexity. Moreover, it provides a wider range for estimates than conventional methods because, as opposed to the Arrhenius, WLF or VTF equations, it is not limited to only one side of the glass transition.

Furthermore, although the focus of this paper is on epoxies and their composites, it appears that the rationale behind the approach is likely to work for other polymer systems. Considering this potential and the possibility of an analogous model for E'' (which is un-

der development), the potential of the method can be very interesting from an engineering point of view.

CHAPTER 6

LINKING THE STORAGE MODULUS, LOSS MODULUS AND LOSS FACTOR OF POLYMERS THROUGH STATISTICAL DISTRIBUTIONS

6.1 Introduction

In Chapter 5, it was proposed that the Gompertz distribution's survival function (SF) could be used to model the effects of temperature on the storage modulus (E') of polymers and polymer composites. It was then hypothesized that as temperature rises, secondary molecular bounds within the polymer would fail and be responsible for the change in modulus. It was further suggested that the SF would describe the proportion of secondary atomic bonds remaining at a given temperature. Consequently, it could be used to describe the materials modulus. By extension, it was suggested that a similar train of thought could justify the use of the model for describing the material strength.

As a corollary to the model presented in Chapter 5, the Gompertz distribution's cumulative density function (CDF) sharing the same parameters as those found for the SF represents the proportion of failed bounds at a given temperature. It then follows that the Gompertz probability density function (PDF) could be associated with the relative probability that a bond becomes mobile at a given temperature. Put otherwise, the PDF could be seen as the fraction of bonds just becoming mobile at that temperature. It is further hypothesized that through their increased mobility the molecules around these failed bonds would be responsible for the energy dissipation which is measured as the loss modulus (E'') in dynamic mechanical thermal analysis (DMTA).

In the present chapter, the theory and hypotheses related to the proposed model will first be discussed. The applicability of the model will then be demonstrated through the application to data from the literature.

6.2 Theory

In dynamic mechanical thermal analysis, the storage modulus (E') — which is a measure of a viscoelastic material restitutive ability — usually show a trace that is a monotonous decreasing function of temperature (T) with multiple transitions occurring at various temperatures. Conversely, the loss modulus (E'') — which is a measure of the dissipative character of a viscoelastic solid — takes the form of an asymmetric bell shaped curve. Recalling that the definitions of E' and E'' are:

$$E' = \frac{\sigma_0}{\epsilon_0} \cos \delta \tag{6.1}$$

and:

$$E'' = \frac{\sigma_0}{\epsilon_0} \sin \delta, \tag{6.2}$$

and further recalling that $\cos(\delta) = \sin(\delta - \pi/2)$, it is easily seen that given that $\delta(T)$ would be the same in both equation 6.1 and equation 6.2 at a given T, the inflection point of E' ($\mathrm{d}^2E'(T)/\mathrm{d}T^2 = 0$) should occur at the peak of E'' ($\mathrm{d}E''(T)/\mathrm{d}T = 0$).

As demonstrated in Chapter 5, the Gompertz SF proves to describe the multiple transitions of a polymer's E' particularly well. Here, by analogy, it is proposed that the E'' behaviour can be modelled by the product of a sum of normal distributions PDFs and of the Gompertz PDF, an approach believed to be compatible with Adam and Gibbs ((52), p.142) demonstration that:

> (...) the overwhelming majority of transitions are undergone by regions whose size differs negligibly from the smallest size z^* that permits a transition at all.

In this context, the Normal PDF represents the distribution of dissipative energy per unit volume as a function of temperature for individual relaxation modes, whilst the Gompertz PDF would represent the distribution of dissipative sites and is responsible for the asymmetry of the E'' trace.

This viewpoint would also be in accordance with the energy landscape paradigm of Stillinger and Weber (251; 252), according to which the molecules of the polymer are trapped in a given energetic state imposed by the molecular arrangement of the glassy solid. Under this paradigm, a change in temperature allows the structure to visit neighbouring energetic configurations by providing enough energy to allow molecules to skip from one configuration (called an energy basin) to the other. In the current context, the normal PDF could be seen as a representation of the energy dissipated in changing the configuration of the most mobile units, the existence of which is represented by Gompertz's PDF.

By definition, all functions from a statistical distribution can be obtained from its hazard function HF. In the case of the Gompertz distribution (with the added localization parameter of Chapter 3), the HF is given by:

$$HF(T) = b\exp\left(cT/T_{ref}\right); \qquad \text{(5.5 revisited)}$$

while the SF is obtained by:

$$\begin{aligned} SF(T) &= \exp\left\{-\int_0^T HF(u)\mathrm{d}(u)\right\} \\ &= \exp\left\{-\left(\frac{bT_{ref}}{c}\right)\left[\exp\left(\frac{cT}{T_{ref}}\right)-1\right]\right\}. \end{aligned} \qquad \text{(5.4 revisited)}$$

Using the additional definition that $PDF = HF\,SF$:

$$PDF(T) = b\exp\left(\frac{cT}{T_{ref}}\right)\exp\left\{-\left(\frac{bT_{ref}}{c}\right)\left[\exp\left(\frac{cT}{T_{ref}}\right)-1\right]\right\}. \qquad (6.3)$$

Finally, knowing that $SF = 1 - CDF$, the Gompertz's CDF is:

$$CDF(T) = 1 - \exp\left\{-\left(\frac{bT_{ref}}{c}\right)\left[\exp\left(\frac{cT}{T_{ref}}\right) - 1\right]\right\}. \tag{6.4}$$

In the current work, the hypothesis is that around a given transition temperature, the Gompertz SF would describe the proportion of surviving secondary bounds and the CDF the proportion of failed secondary bounds. This entails that the Gompertz PDF would then describe the relative probability of bounds to be broken (i.e. to become mobile) at a given temperature and that would actively participate in the energy dissipation associated with the failure of secondary bonds. However, as stated before the failure of secondary bonds is not the only factor that affects E''. Rather, the amount of loss per broken bond also needs to be accounted for.

In accordance to the energy landscape paradigm, different molecular configurations can be explored at different energy levels. At low temperature, the system may be trapped in a deep energy meta-basin with high energy barriers to overcome in order to change its state. A meta-basin would be a deep energy basin itself constituted of multiple smaller basins, each of which corresponding to a specific molecular arrangement. As the temperature increases, the energy provided might allow the system to explore some basins of slightly higher energy that constitute the meta-basin without overcoming the global energy barriers. As the temperature increases, more and more of the sub-basins are available and ultimately, the meta-basin is escaped and another level is reached where the scheme recommences. Here, given the very large number of basins — i.e. molecular arrangements — being possible, it is hypothesized that the breadth of configurations (and associated energy dissipation characteristics) can be modelled by a sum of normal distributions of mean T_{ref} and of standard deviation σ_i, each of which would represent the various mobility modes (e.g. segmental mobility, side branches rotation, intermolecular mobility, etc.) of the molecules that were rendered mobile by the increased temperature.

Recalling that the Normal distribution PDF is:

$$PDF_{Normal} = \frac{1}{\sigma\sqrt{2\pi}} \exp\left(\frac{-(T-\mu)^2}{2\sigma^2}\right), \tag{6.5}$$

it ensues that the following formulation is proposed for the evolution of E'' in the case of a single transition.

$$E''(T) = \epsilon_0 + b \exp\left(\frac{cT}{T_{ref}}\right) \exp\left[-\exp(-c)\left(\exp\left(\frac{cT}{T_{ref}}\right) - 1\right)\right] \sum_{j=1}^{M} \zeta_j(T) \tag{6.6}$$

and

$$\zeta_j(T) = \frac{\epsilon_j}{\sigma_j\sqrt{2\pi}} \exp\left(\frac{-(T-T_{ref})^2}{2\sigma_j^2}\right). \tag{6.7}$$

In equation 6.6, ζ_j is the damping function and ϵ_j is the energy dissipation term per unit volume and σ_j is the standard deviation of the dissipative terms of the j^{th} of M relaxation mode. T_{ref} is the reference temperature (e.g. the glass transition temperature T_g or the melt temperature T_m), which acts as the means of the normal PDFs and locate the Gompertz PDF. The c coefficient would be the same parameter as obtained for the Gompertz fit on E' as per Chapter 3. Note that in equation 6.6, the location of T_{ref} has been imposed at the inflection point of the SF (or peak of the PDF) for reasons discussed in Chapter 3. Therefore, the parameter b has been found to be $c/T_0 \exp(-c)$ (equation 5.13).

Equation 6.6 is easily generalized to the following form to cover an arbitrary number (N) of transitions.

$$E''(T) = \epsilon_0 + \sum_{i=1}^{N} b_i \exp\left(\frac{c_i T}{T_{ref\,i}}\right) \exp\left[-\exp(-c_i)\left(\exp\left(\frac{c_i T}{T_{ref\,i}}\right) - 1\right)\right] \sum_{j=1}^{M} \zeta_{ij}(T), \tag{6.8}$$

where:

$$\zeta_{ij}(T) = \frac{\epsilon_{ij}}{\sigma_{ij}\sqrt{2\pi}} \exp\left(\frac{-(T-T_{ref\,i})^2}{2\sigma_{ij}^2}\right).$$

Note that in equation 6.6 and equation 6.8, the term ϵ_0 is the baseline dissipative term and should be accounted for by the sum of the effects of the rightmost transitions. However, to account for the possibility that some relaxation information at higher temperatures is incomplete, the term is left in the model.

It is interesting to remember that the loss factor ($\tan\delta$) is given by:

$$\tan\delta = E''/E'. \tag{6.9}$$

In the case of resonant methods, the damping coefficient δ is also given by the relationship:

$$\delta = E''\pi/E', \tag{6.10}$$

Therefore, given equation 5.14 and equation 6.8, the damping parameter $\delta(T)$ is fully characterized.

Recalling that E'' is the product of the Normal PDF and the Gompertz PDF, while E' is based on the Gompertz SF, one sees that $\tan\delta$ therefore implies the ratio of the Gompertz PDF to the Gompertz SF, which is the definition of the Gompertz HF, the simple expression of equation 5.5. However, this simplification is mostly relevant in the case of the modelling of a single transition as there are interactions between each region in the case of multiple transitions.

Up to now, the model exclusively has descriptive capabilities. However, it is interesting to note that some of the model parameters can be related to structural material properties either through direct analytical modelling or, at least, through statistical correlations with structural properties. For example Foreman et al. (253) have proposed an Arrhenius type relationship to predict the β-transition temperature and the Group Interaction Modelling (GIM) theory has been used by Gumen et al. (254) to predict the T_g of epoxy resins. Foreman et al. also propose expressions for the cumulative loss tangent ($\int_0^T \tan\delta(T)\mathrm{d}T$) that could be useful for evaluating the dissipative terms of equation 6.8.

The amplitude of the relaxation steps and the slope parameter, however, remain harder to relate to analytical formulations. Nevertheless, there are strong indications that they could be related to the molecular weight and cross-link density of polymers as these properties tend to have important effects on the evolution of the modulus with temperature (see e.g. Nielsen (30)). Ultimately, such formulations could be used to reduce the model reliance on experimental data.

6.3 Results and discussion

The proposed model is tested against results from the literature. A first dataset for epoxy Ciba-Geigy 913 at low temperature is found in Adams and Singh (39). The model fit for this data is shown in Figure 6.1. Parameter estimators are provided in Table 6.1.

Table 6.1 Model estimators for epoxy resin Ciba-Geigy 913, experimental data by Adams and Singh (39)

Parameter	Unit	Estimate
$T_{ref,1}$	K	212
a_1	MPa	3070
a_2	MPa	1480
c_1	-	3.6
ϵ_0	MPa	2000
ϵ_{11}	MPa	245×10^3
ϵ_{12}	MPa	1.4×10^6
σ_{11}	K	18
σ_{12}	K	135

Figure 6.1 shows that the model is in very good agreement with the experimental data. From this application, it appears that the model performs very well in describing the

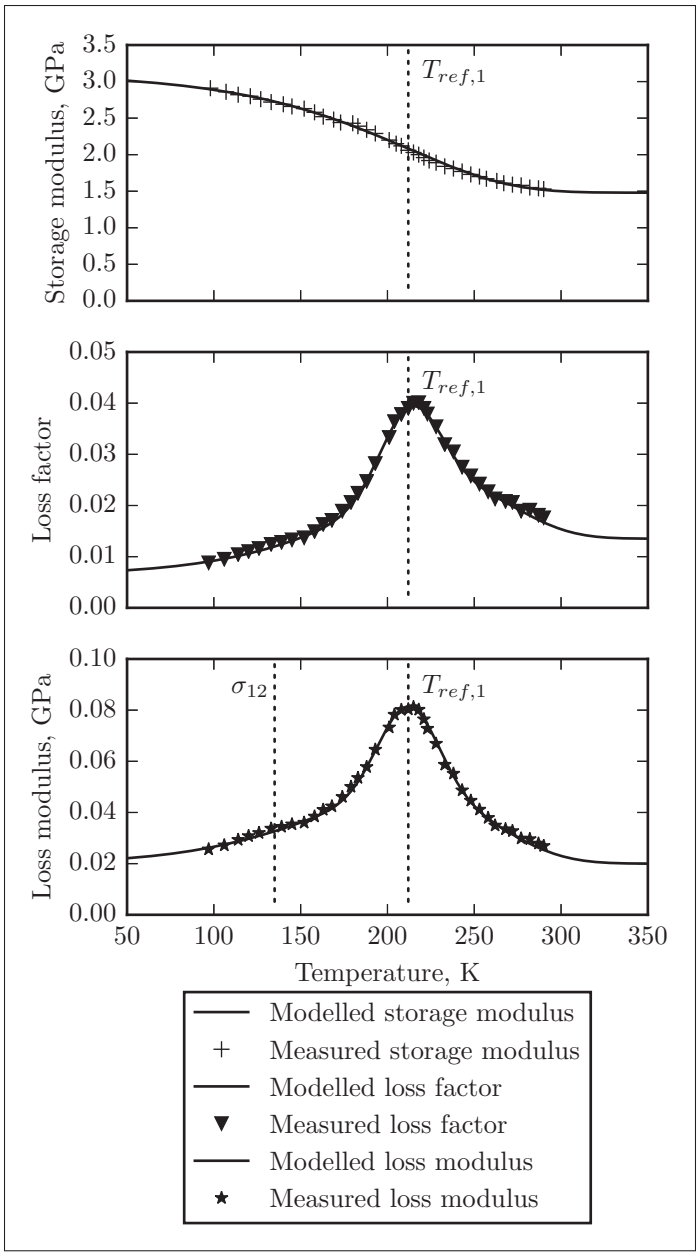

Figure 6.1 Dynamic properties of epoxy Ciba-Geigy 913, experimental data from Adams and Singh (39)

behaviour around a low temperature transition. However, this application does not give any information on the suitability of the model in the case of multiple transitions.

For the case of multiple transitions, a second validation dataset is found in Lewis and Nielsen (255). Lewis and Nielsen's results are for Epon 828 epoxy over a wide range of

temperatures covering three transitions, one of which may be attributed to the addition of a diluent. The model estimators for Lewis and Nielsen's data are provided in Table 6.2 while the resulting fit is shown in Figure 6.2.

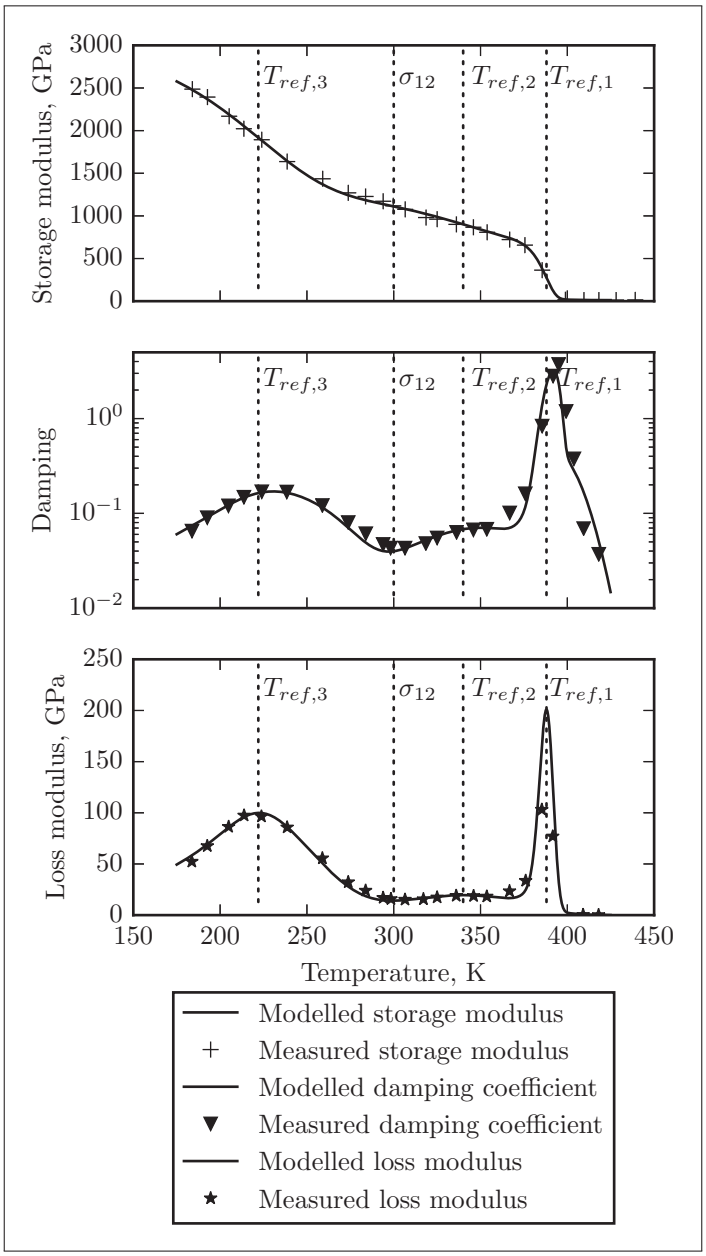

Figure 6.2 Dynamic shear properties of epoxy Epon 828, experimental data from Lewis and Nielsen (255)

Table 6.2 Model estimators for epoxy resin Epon 828, experimental data by Lewis and Nielsen (255)

Parameter	Unit	Estimate
$T_{ref,1}$	K	222
$T_{ref,2}$	K	340
$T_{ref,3}$	K	388
a_1	MPa	3050
a_2	MPa	1300
a_3	MPa	670
a_4	MPa	12
c_1	-	5.5
c_2	-	8.7
c_3	-	68
ϵ_0	MPa	0
ϵ_{11}	MPa	0.1×10^6
ϵ_{12}	MPa	6.5×10^6
ϵ_{21}	MPa	0.65×10^6
ϵ_{31}	MPa	30×10^3
ϵ_{32}	MPa	80×10^3
σ_{11}	K	19
σ_{12}	K	300
σ_{21}	K	125
σ_{31}	K	5
σ_{32}	K	50

Once again, the model is shown to provide a good agreement with the experimental data. However, because of the presence of a second viscoelastic phase (rubber) and diluent, additional damping parameters are required.

6.4 Conclusions

In this section, an extension to the model of chapter 3 has been proposed. The model, again based on the Gompertz statistical distribution, allows for the description of the storage and loss modulus as well as of the damping coefficient of polymers and reinforced polymers as a function of temperature.

Validation through the application of the model to data from the literature has shown that the proposed formulation provides a good fit to experimental data over a particularly wide range of temperature, a quality that is often found lacking in competing formulations.

Nonetheless, first principle formulations for the storage and damping parameters as well as for the transition temperatures are yet to be provided. Therefore, the model still relies on substantial experimental data.

CHAPTER 7

MODELLING THE EFFECTS OF TEMPERATURE ON THE INSTANTANEOUS STRENGTH OF POLYMER COMPOSITES ACROSS MULTIPLE TRANSITIONS

7.1 Introduction

In Chapter 4, it was shown that the Gompertz distribution's SF provides a good description of the $S_u(T)$ relationship within a single physical transition when using a normalized temperature. While the use of such a normalized temperature was useful in the context of fatigue modelling, it had the side effect of limiting the model to a single transition.

In Chapter 5, the same Gompertz SF was also shown to provide a good description of the storage modulus over multiple transition regions.

In the current section, it will be shown that the use of the Gompertz SF, modified as in Chapter 5 can also be used to describe the evolution of instantaneous static strength. In its final form, the model from Chapter 5 is given in equation 5.14, which is also given below as a reminder.

$$P(T) = a_{N+1} + \sum_{i=1}^{N} (a_i - a_{i+1}) \exp\left\{ -\exp(-c_i) \left[\exp\left(\frac{c_i T}{T_{ref,i}} \right) - 1 \right] \right\}. \quad \text{(5.14 revisited)}$$

The only modification is that here, the a_is would stand for strength scale factors instead of stiffness scale factors. Example applications are shown below, accompanied by a short discussion on the model effectiveness.

7.2 Materials and methods

To demonstrate the ability of the proposed model to provide a continuous description of the strength and modulus of polymer composites over a wide range of temperature,

the model predictions are compared to experimental results from two datasets from the literature.

Cao et al. (91) provide static strength data at temperatures ranging from 20℃ to 120℃ for unidirectional carbon-fibre composites with two different epoxy formulations, namely FR-E3P and SX-435 resins. These composites are later identified as CFRP1 for the composite using FR-E3P resin and CFRP2 for that using SX-435 resin. Validation of the model for strength of carbon–epoxy composites and modulus of neat epoxy over a single transition is done with those data.

Finally, Robert and Benmokrane's (94) tensile and bending strength data for glass-vinylester cover temperatures from -100℃ to 325℃ and will be used to demonstrate the capability of the model to represent multiple transitions.

7.2.1 Computational approach

In all cases, the model is fitted using a standard non-linear least square regression procedure for a single variable and multiple model parameters. Specifically, a *Python* script running the `curve_fit` method from the `optimize` module of the `scipy` package version 0.15.1 is used.

For data by Cao et al. (91), all available data points are plotted and the normal 95%confidence intervals on model parameters are provided. In the case of static results by Robert and Benmokrane, only the mean and coefficient of variation of the data were available. Therefore, statistics on the model parameters are not provided. However, the standard deviations of the data at each temperature were used as weighting parameters for each of the points used in the regression.

7.3 Results and discussion

In the data by Cao et al. (91), a single relaxation phase around T_g is observed for 0° carbon-epoxy laminates made with both resin formulations. Cao and his colleagues evaluated that the transition ranged from $T_{g,onset} = 42$℃ to $T_{g,end} = 56$℃ (315 K to 329 K) for the FR-E3P epoxy, where $T_{g,end}$ is defined as the intersection of the lower asymptote and the tangent to the inflection point of the DMTA curve. For the second resin formulation (SX-435), the transition ranged from $T_{g,onset} = 45$℃ to $T_{g,end} = 63$℃ (318 K to 336 K).

Table 7.1 Model estimators for tensile strength of carbon-epoxy composites (data by Cao et al. (91))

Carbon – FR-E3P epoxy			
Parameter	Unit	Estimate	95% confidence interval
$T_{ref,1}$	K	320	[318, 322]
a_1	MPa	4088	[3921, 4262]
a_2	MPa	2800	[2634, 2977]
c_1	-	85.8	[42.0, 175.3]
Carbon – SX-435 epoxy			
Parameter	Unit	Estimate	95% confidence interval
$T_{ref,1}$	K	332	[329, 336]
a_1	MPa	4339	[4140, 4549]
a_2	MPa	3012	[2866, 3167]
c_1	-	42.1	[21.5, 81.8]

Table 7.1 gives the predicted T_g based on the application of the model to tensile strength results as 320 K for the FR-E3P resin and 332 K for the SX-435 formulation. Both of these estimates, as well as the limits for their respective 95% normal confidence intervals, therefore lie within the T_g range measured by the original authors.

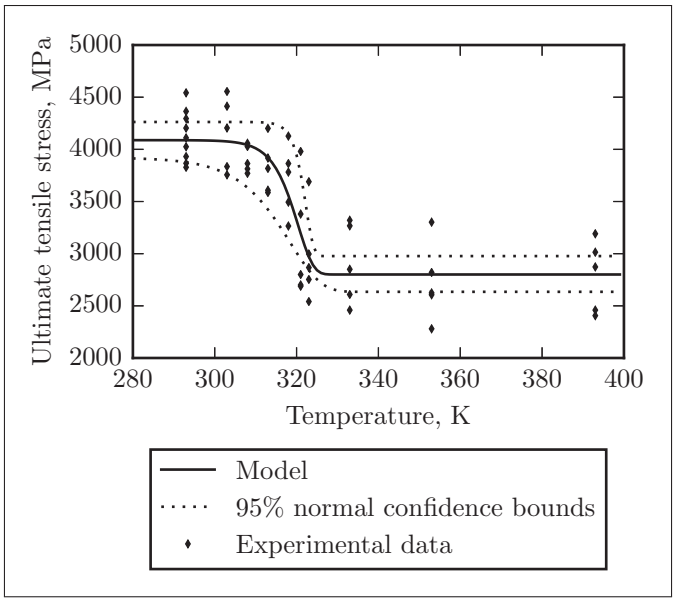

Figure 7.1 Tensile strength as a function of temperature for carbon–FR-E3P epoxy (experimental data by Cao et al. (91))

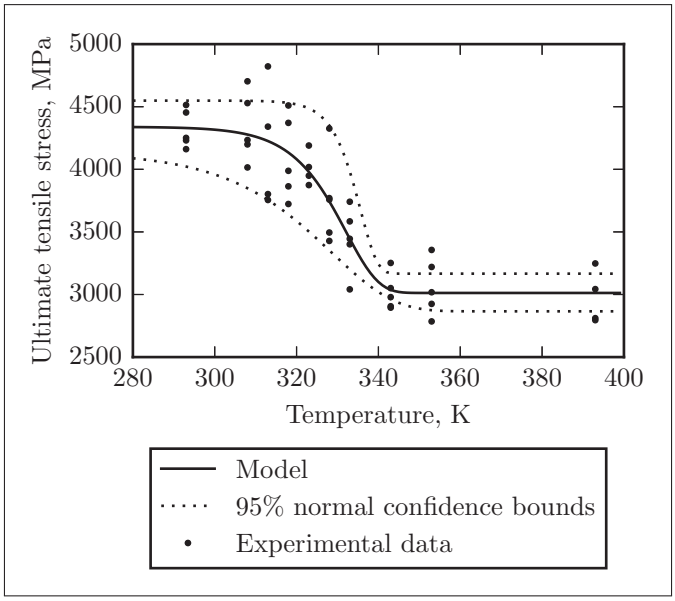

Figure 7.2 Tensile strength as a function of temperature for carbon–SX-435 epoxy (experimental data by Cao et al. (91))

Figures 7.1 and 7.2 show that the fit between the data and the model is quite good for both of the composites S_u across the whole temperature range.

Results from Robert and Benmokrane (94) for glass-vinylester composite are spread over a broader temperature range — from 173 K to 598 K — and exhibit three definite relaxation phases. However, the first relaxation is only partially described by the data and appears to range down to a lower temperature than that for which data are available. Similarly, the high temperature transition is not fully covered by experimental data.

Parameter estimates obtained from fitting the model to the experimental data are provided in Table 7.2 for tension and bending loads. Figures 7.3 to 7.4 show those results graphically.

Table 7.2 Model estimates for strength of glass–vinylester composites (data from Robert and Benmokrane (94))

		Tensile	Bending
Parameter	Unit	Estimate	
$T_{ref,1}$	K	114	213
$T_{ref,2}$	K	396	406
$T_{ref,3}$	K	656	525
a_1	MPa	1904	2274
a_2	MPa	777	1097
a_3	MPa	526	177
a_4	MPa	0	64
c_1	-	1.7	4.3
c_2	-	11.9	19.8
c_3	-	10.5	10.2

Robert and Benmokrane had reported that $T_g \approx 385$ K as obtained by Differential Scanning Calorimetry (DSC). Therefore, at 396 K and 406 K respectively, the estimates of

T_g given by the model are in acceptable agreement (within about 5% of the measured value) for the tensile and bending loading modes.

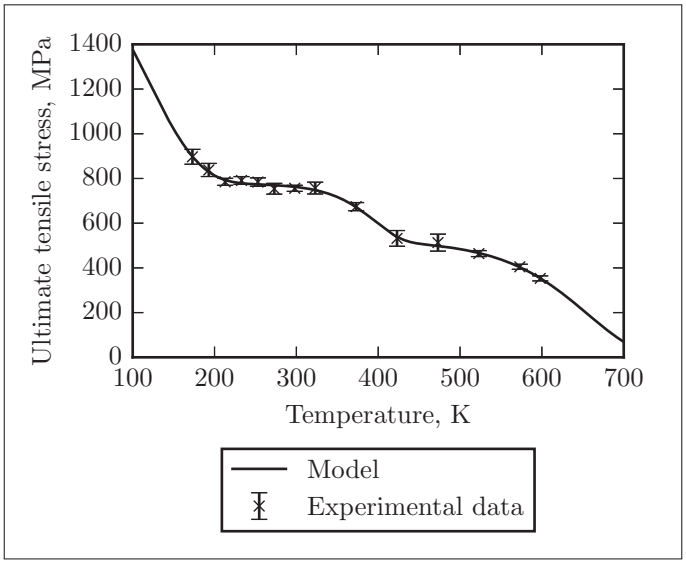

Figure 7.3 Tensile strength as a function of temperature for glass–vinylester (experimental data by Robert and Benmokrane (94))

From Figures 7.3 and 7.4 it is seen that the model shows a very good fit to the data and remains mostly within the standard deviation of experimental data across the whole temperature range. Comparing parameters obtained for the two loading modes, it appears that a single set of parameters would likely be insufficient to describe all the failures. However, the slope parameters for each transition are of the same order of magnitude.

The preceding paragraphs have demonstrated the ability of the model to describe the evolution of S_u as a function of temperature. However, a few limitations of the model need to be discussed.

First, the model is static and cannot capture the time dependence of strength often characteristic of polymers and their composites. The capacity to predict instantaneous

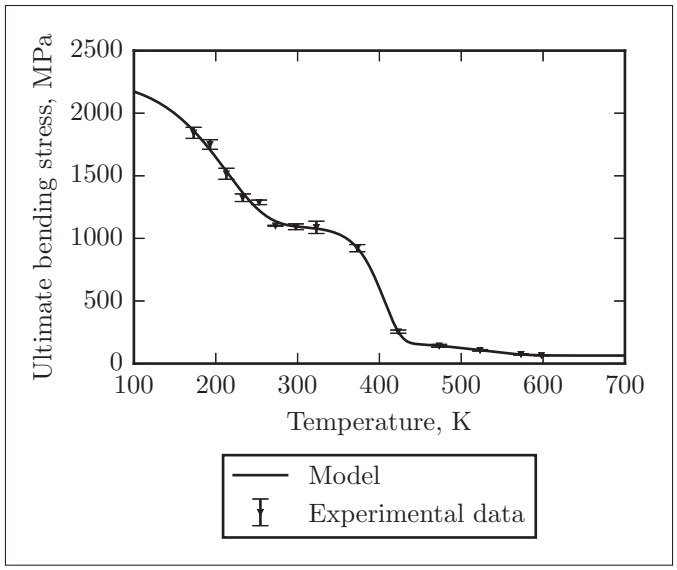

Figure 7.4 Bending strength as a function of temperature for glass–vinylester (experimental data by Robert and Benmokrane (94))

performances of the composite should not be confused with prediction of creep behaviour that might be required, mostly at elevated temperatures.

Second, to the author's knowledge, the question of the influence of temperature on the scatter of composites mechanical properties is unresolved. For example, the data from the literature that was used herein show that the distribution of strength as a function of temperature is possibly not homoscedastic and most results reproduced here appear to have larger scatter around transition regions. Static and fatigue data on carbon fibre reinforced polymers from the aeronautic industry suggests that scatter of strength properties may be influenced by temperature (155). However, Christensen and Miyano (238) have analytically and empirically demonstrated that temperature should not influence the scatter characteristics of strength.

It could also be debated that the apparent scatter in strength at a given temperature within a transition is to be partially attributed to the scatter in T_g rather than solely in the scatter of the strength itself. Although such inconsistent scatter behaviour does not

infringe the model hypotheses, many standard estimates of model parameters confidence bounds or percentiles that are likely to be used with such a model rely on the hypothesis of homoscedasticity. Therefore, one should carefully consider the implications of the scatter properties when using this model.

In the current work, it was hypothesized that the strength at a given temperature is normally distributed. This choice was made both for convenience and because the original papers from which the data are taken used the Normal distribution. However, if one is interested in obtaining specific percentiles or a prerequisite reliability level, it would be advisable to consider other strength distributions — such as the often preferred Weibull distribution — and to recourse to maximum likelihood methods instead of non-linear regressions and its underlying normal distribution.

7.4 Conclusions

The influence of temperature on the instantaneous static strength of fibre reinforced polymer composites is of great importance to the civil and transportation industry. In the current chapter, a model based on the Gompertz distribution has been proposed to describe the evolution of strength of polymer composites as a function of temperature.

When compared to data from the literature, the model has shown to provide a good description of the evolution of a composite strength with temperature. It also has shown its ability to deal with an arbitrary number of relaxation phases.

However, the physical description of the relationship between secondary bond failure and material properties is not yet clearly defined. Therefore, in most cases, the model still needs to rely on extensive experimental data to obtain estimates of the model parameters.

CONCLUSION AND RECOMMENDATIONS

In order to properly estimate the durability of structures, a good knowledge of their constituent materials response to mechanical and environmental loads is required. This is particularly true of structures that are installed in remote areas where inspection and maintenance are hard, sometimes even impossible, over certain periods such as winter. In the case of composite materials, such knowledge is still quite incomplete. This lack of knowledge originates from the many complexities of their behaviour, of which a few are listed below:

- inhomogeneous and anisotropic nature;
- large range of constituent materials, both organic and inorganic;
- time-dependent response (viscoelasticity, ageing, thermal or chemical degradation, crystallization, residual cure, moisture or solvent uptake);
- processing parameters sensitivity (cure conditions, voids, crystallinity, fibre waviness).

Moreover, the broad spectrum of applications (medical, nuclear, aerospace, wind energy, sports, transports, ...) for which they are used — and have excessively different requirements with regards to cost, environment, durability, reliability or legal framework among other things — also contributes to this lack of knowledge by making research results hard to transfer from one domain to another.

The work presented in this thesis is intended to partially address this lack of knowledge. This goal is reached by characterizing and modelling the temperature effects on the mechanical behaviour of representative wind turbine blade materials. Because of the Canadian context, a particular attention is given to the effects of low temperature.

Although the prime motivation of the project is to reduce uncertainties related to the operation of wind turbines in northern climates, an effort has been made to make most of the results as generalizable as possible. The main research question was thus divided into sub-problems dealing with different laminate lay ups and loading conditions and for which a simplified analysis was proposed. The outcome of the research is as follows.

First, the response of unidirectional laminates to static and fatigue loading at different load rates and temperatures was analysed. It was demonstrated that even for fibre dominated laminates, both high and low temperatures had a significant effect on the quasi-static tensile and compressive strengths. On the one hand, the strength rose at low temperature and decreased at high temperatures, with the changes in compression being almost twice as large as those in tension. On the other hand, the stiffness changed only by a couple percent at low temperature, but decreased significantly at high temperature. On the fatigue side, high temperatures resulted in a large reduction of fatigue lives, mostly through a shift of the room temperature S-N curve. The reduction was about one decade at $R = 0.1$, but reached a dramatic three decades at $R = -1$. Conversely, low temperature curves have shown better low cycle fatigue performance, but an increased slope meant that high and very high cycle fatigue lives are adversely affected. The difference in both the magnitude of the S-N curve shift and slope change is greater for $R = -1$ fatigue than for $R = 0.1$.

The study of frequency effects showed that below 8 Hz, all results were comparable, but that higher frequency data points tended to be located at the lower edge of the confidence bounds. Tests at 24 Hz did show a marked reduction in lifetime, with both $R = 0.1$ and $R = -1$ curves being shifted by at least a decade, while their slope parameters remained comparable. Tests performed at 24 Hz, but at low temperature (-40°C) show slightly lower lives and potentially increased slopes when compared to baseline data, but the changes

are barely statistically significant. The difference between low and high frequency at low temperature is significant, however, with the high-frequency tests showing a shallower slope.

Second, the effect of low temperature on the tensile and compressive static and fatigue properties of $\pm 45^{\circ}$ laminates at room and low temperatures were studied. As such results are extremely scarce in the literature, the experimental results in themselves are worthwhile. However, some important analysis was also provided. Results for quasi-static tests show an increase of tensile, compressive and shear strengths and moduli at low temperatures (-40℃) in the range of 30 % and 20 % respectively, when compared to room temperature tests. It is also found that for the stress range studied and when looking in absolute maximum stress, fatigue performance is improved at low temperatures for both the $R = 0.1$ and $R = -1$ fatigues. However, the slope of S-N curves is steeper at low temperature, with the effect being more pronounced at $R = -1$ than at $R = 0.1$. The very large difference between ambient and low temperatures test results at $R = -1$ is partially attributed to a change in the failure mode. Specifically, failure resulted from the buckling of delaminated plies in the compressive part of the cycle at room temperature to tensile failure at low temperature. This suggests a more efficient use of the material at low temperature. However, if $R = -1$ fatigue results at low temperature are extrapolated towards the very low stresses that represent a large part of wind turbine blades loading, life may still be degraded compared to that at ambient temperature. Evidence of viscoelastic behaviour, resulting in changes of the S-N curve slope parameter were also found at both stress ratios.

Third, given that the viscoelastic behaviour should be minimized under tensile loading in the fibre direction, a method for predicting the influence of temperature and strain rate on the fatigue life of composites is proposed. In the objective of minimizing the

experimental burden required to obtain model parameters, a strength degradation model was adopted, for which relationships expressing temperature effects on static strength and on one other temperature dependent model parameter are proposed. The model's predictions were shown to provide very good correlation with measured fatigue lives over wide temperature ranges. Given the importance of reliability in fatigue analysis, a method to obtain probabilistic S-N curves with the model is also discussed.

As discussed in the literature review, the understanding of the physics behind the glass transition (as well as other low temperature transitions) in amorphous materials used as matrices in polymer composites is still quite incomplete, as are the related fields of thermomechanics and viscoelasticity. The same could be said of the understanding of the physics behind the fatigue damage and failure in composite materials. Furthermore, the fatigue failure of composites and the problems of thermomechanics and viscoelasticity are closely intertwined. Thus, although the development of a purely mechanistic model based on constituent properties could be seen as the ultimate goal of researchers in the field of composite fatigue, it might still be too early to hope for a modelling approach that is purely based on physical grounds.

Given this reality, phenomenological approaches are relevant since they are a first step in linking the physics of a phenomenon to its outcome. In this respect, three additional phenomenological models were provided as building blocks for future work.

Therefore, based on the survival function of Gompertz distribution, a first model to represent the effect of temperature on the failure of secondary molecular bonds in a polymer was elaborated. The model describes the evolution of the storage modulus — assumed to be proportional to the amount of remaining secondary bonds in the polymer — as a function of both time and frequency and allows for an unambiguous definition of the glass transition temperature. Load rate effects on the glass transition are also

modelled. The advantage of this model compared to the classical time-temperature superposition is that it does not rely on empirical shift factors. However, using this model, it was demonstrated that by accounting for the frequency dependent glass transition temperature, the shift factors across the transition would be represented by a unique monotonic function, as opposed to the usual requirement of multiple fit above, within and below the glass transition.

A second model was proposed, this time for the description temperature effects on the loss modulus. It assumes that the loss modulus can be represented by the product of distribution of dissipated energy per breaking secondary bonds (the normal distribution probability density function) to the number of such secondary bonds breaking (the Gompertz probability density function). The model was shown to be in very good agreement with experimental results from the literature and can easily be related to the storage modulus model.

Also, based on the known similarity between the shape of the modulus as a function of temperature curve and that of instantaneous strength as a function of temperature, a descriptive model of strength as a function of temperature was proposed based on the Gompertz survival function. The model proved to be fit data over multiple transition regions.

The research described within this dissertation is thus successful in improving the understanding of temperature and strain rate effects on the thermomechanical and viscoelastic behaviour of polymers and composites. It is also valuable by relating the new knowledge to the fatigue performance of glass fibre reinforced polymers subjected to tensile loading along the main fibre direction. By providing a tool for the probabilistic assessment of fatigue life under concurrent temperature and fatigue loading with minimal experimental burden, it is reckoned that the uncertainties regarding the durability of wind

turbine blades in the Canadian climate are at least partially mitigated. It is believed that the proposed methodologies will be useful for practitioners in the field of composite structures, as well as provide significant leads to further research in the fields of polymer thermomechanics and fatigue of composites.

Among the research that still needs to be undertaken, the most notable short term objective would be to adapt the fatigue model to account for viscoelastic effects that are present when the fatigue load includes a compression component or when no fibres are aligned with the main load. It is believed that this could be dealt with through a change in the slope parameter of the fatigue model. However, it is also believed that the most promising approach might be to include the effect of creep and fatigue damage directly in the residual stress model. This would have the advantage of a greater generality of the solution. Alternatively, the proposed formulation for storage and loss moduli might be incorporated in multi-scale modelling approaches so that a mechanistic solution is more closely approached.

However, beyond the specific knowledge gaps that still prevent us from solving the problems related to predicting the fatigue behaviour of composite materials, this study evidenced some problematic practices that are not congruent with the current knowledge and that need to be addressed. Foremost, despite the fact that composite materials exhibit high scatter in their properties and in their physical response to external stimulus, this scatter is seldom accounted for in the published research. Among other things, the quality of fit for proposed models is scarcely analysed with a quantitative approach. For example, in the specific field of fatigue, the effects of modelling assumptions may result in significant bias in specific fatigue regimes (low, high and very high cycle fatigue), but this is seldom discussed.

It also appears that the confounding variable of strain rate is usually not adequately accounted for since most fatigue research is performed at constant frequency, while the loads are varied. This means that the response is influenced by more than one conditions and that the adequate interpretation of results may be hindered. This may be even more problematic as the frequencies used still tend to be high enough to result in specimen hysteretic heating. It might thus be advisable to favour a constant maximum strain rate over a constant frequency, while ensuring that specimen temperature is monitored. This latter recommendation may be of particular relevance now that thermoplastic matrices and woven preforms, which are known to exhibit relatively high viscoelasticity and which may also be more sensitive to ageing, are gaining popularity.

In the light of this study, it is evident that an overwhelming gap still separates the engineers and researchers from the objective of modelling the fatigue damage of composites from first principles. Empirical research is still quite necessary and in practice, full scale testing of composite structures is likely to be a necessity in the foreseeable future. Yet, it is also evident that many practical solutions can be developed and that if properly designed, these solutions can significantly reduce the burden of these tests.

APPENDIX I

MAXIMUM LIKELIHOOD ESTIMATION OF FATIGUE CURVES INCLUDING RUNOUT DATA

1. Classical analysis of fatigue data

Fatigue of materials is a complex phenomenon requiring a broad palette of tools and methods for the analysis of fatigue data. The most frequent type of analysis for fatigue data is the Wöhler curve, more commonly known as the Stress-Life or $S-N$ curve. Here, the term stress may be seen more in the general sense of mechanical sollicitation and is usually expressed in terms of stress or strain. In elaborating the experiments and formulating the definition of the curve, it is important to consider the loading and failure mechanisms in order to ensure that the data are representative of the actual case to be analyzed. For example, low cycle ($N < 10^3$ cycles) fatigue failure mechanisms of metals are related to local strain and plasticity and a strain controlled experiment and representation is better suited. For high cycle ($10^3 < N < 10^8$) fatigue, stress based definition is adequate, but for some application a strain based approach may still be better suited.

The $S-N$ curve provides a quick view of the general material expected life under various levels of constant amplitude variable loading. Some peculiarities of the $S-N$ diagram are that:

- The definition of a fatigue curve is only complete when, in addition to the stress and life axes, an indication of the stress variability is provided (*i.e.* R ratio).
- The independent variable is the stress S but, against usual conventions, it is shown on the ordinate.
- The life N is the dependent random variable and is usually counted in cycles and shown on a base 10 logarithmic scale.

- The basic form of the fatigue curve represents the median life of the data.

The following paragraphs provide additional information on these peculiarities. First the definitions of the stress level and variability are discussed, followed by considerations on the modeling of the stress-life relation and the mathematical definition of the $S-N$ curve usign the least-square regression method is provided. Note that methodologies for $S-N$ curve computation are provided in ASTM E739 (152) and ASTM STP No.313 (121).

1.1 Definition of stresses and ratios

By definition, the fatigue process implies a variable sollicitation of the material through changes in loads or in strains. Therefore life data obtained for a given loading sequence are specific to this particular sequence. Fatigue curves then need to include a description of the fatigue loading parameters in order to be complete. In its simplest form, the fatigue load has a constant amplitude as illustrated in figure I-1. The most frequent descriptions of this type of loading is either by a reference stress s and the stress ratio R or by the mean stress s_m and the stress amplitude s_a (equations 3.1, A I-1 and A I-2). The reference stress may be any one of the minimum s_{min}, maximum s_{max} or average s_m described as shown in figure I-1.

$$R = \frac{s_{min}}{s_{max}} \qquad \text{(equation 3.1 revisited)}$$

$$s_m = \frac{s_{max} + s_{min}}{2} \qquad \text{(A I-1)}$$

$$s_a = \frac{s_{max} - s_{min}}{2} \qquad \text{(A I-2)}$$

For composite fatigue, some information on the frequency of the load should also be included because of the influence that loading rate may have on the life of the component. This equation states that when the sum of n_i (the number of cycles at stress level i) over N_i (the expected life at stress i) reaches unity, the part will fail.

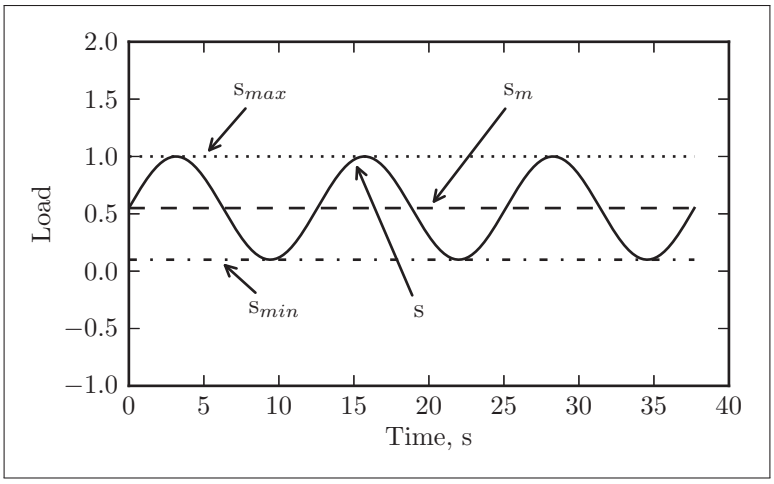

Figure-A I-1 Definition of fatigue stresses

Finally, a more complex fatigue spectra may be binned to simpler CA fatigue data by methods such as rainflow counting combined with a damage rule such as Miner's sum (equation A I-3).

$$\sum_{i=1}^{k} \frac{n_i}{N_i} = 1 \qquad \text{(A I-3)}$$

1.2 Modeling and general assumptions

Often overlooked are the underlying hypotheses accompaying the $S-N$ diagram. The curve defines the median life of a sample of the population of material. Therefore, a statistical distribution must be chosen in order to evaluate this median. Because it provides for solid, relatively simple and easily tractable statistical treatment, the usual assumption is that of a Normal or Lognormal distribution of the data. The data for each stress level is then defined by a pair of constants, the mean μ and the standard deviation σ. However, any other distribution may be (or should be) used if the Normal distribution does not fit the data adequately.

The distribution parameters are required in order to establish other percentiles of survival as would most likely be required in a design process where a 50% survival would obviously be inadequate. A curve at a probability other than 50% is usually refered to as a $P-S-N$ curve, where the P stands for the probability of failure. These are usually computed

as single sided limits of the distribution since in reliability analysis, only failures before a defined time limit are deemed to be problematic.

1.2.1 Normal distribution

The standard Normal distribution is a continuous distribution of a random variable which is symmetric about zero and that has the following probability density function (PDF) $\phi(y)$:

$$\phi(y) = \frac{1}{\sqrt{2\pi}} \exp\left(-\frac{1}{2}y^2\right). \tag{A I-4}$$

Knowing that the cumulative density function (CDF) $\Phi(y)$ is the integral of the PDF and must be equal to unity at $y = \infty$, then:

$$\begin{aligned} \Phi(y) &= \int_{-\infty}^{y} \phi(x)\,\mathrm{d}x; \\ \Phi(y) &= \frac{1}{\sqrt{2\pi}} \int_{-\infty}^{y} \exp\left[-\frac{1}{2}x^2\right] \mathrm{d}x. \end{aligned} \tag{A I-5}$$

The standard Normal distribution has a mean of zero, with variance of one. In order to generalise the distribution, the PDF is scaled by a factor of $1/\sigma$ and the mean is translated by a factor μ. Therefore, the general Normal distribution is defined by the following PDF:

$$\begin{aligned} f(y) &= \frac{1}{\sigma}\phi\left(\frac{y-\mu}{\sigma}\right); \\ f(y) &= \frac{1}{\sqrt{2\pi}\sigma} \exp\left[-\frac{1}{2}\left(\frac{y-\mu}{\sigma}\right)^2\right] \end{aligned} \tag{A I-6}$$

and CDF:

$$\begin{aligned} F(y) &= \int_{-\infty}^{y} f(x)\,\mathrm{d}x; \\ F(y) &= \frac{1}{\sqrt{2\pi}\sigma} \int_{-\infty}^{y} \exp\left[-\frac{1}{2}\left(\frac{x-\mu}{\sigma}\right)^2\right] \mathrm{d}x; \\ -\infty &< y < \infty. \end{aligned} \tag{A I-7}$$

In equations A I-6 and A I-7, μ is the population mean, while σ is the population standard deviation. It is important to note that while the mean (given in the same unit as y) can take any value, the standard deviation (also given in the same unit as y) must be positive. The Normal cumulative density function integral of equation A I-7 is also often provided in its standard form $\Phi(z)$ of mean $\mu = 0$ and standard deviation $\sigma = 1$, and scaled by the standardised normal deviate z:

$$\begin{aligned} F(y) &= \Phi(z); \\ z &= \frac{y-\mu}{\sigma}; \\ -\infty &< y < \infty. \end{aligned}$$

The Normal distribution also corresponds to a wear-out model, because of its ever increasing hazard (HF) and cumulative hazard functions (CHF) $h(x)$ and $H(x)$. Figure I-2 shows the PDF, CDF, HF and CHF for the standard normal distribution.

$$\begin{aligned} H(x) &= \int_{-\infty}^{x} h(x)\,\mathrm{d}x; \\ h(x) &= \frac{f(x)}{1-F(x)}; H(x) \quad = -\ln\left(1-F(x)\right). \end{aligned} \tag{A I-8}$$

Finally, the $100p\%$ percentile of the normal distribution is given by:

$$\eta_p = \mu + z_p\sigma, \tag{A I-9}$$

where z_p is the standard normal percentile. This can be found by solving equation A I-7 for $F(y) = p$, but common values of p are usually found in tables. Table I-1 provides some of the most frequent standard normal percentiles. Note that the population mean μ of a normal distribution is equal to $\eta_{0.50}$, the median of the population, since $z_{0.50} = 0$.

Table-A I-1 Common standard normal percentiles

$100p\%$	0.1	1.0	5.0	50.0	95.0	99.0	99.9
z_p	-3.090	-2.326	-1.645	0.000	1.645	2.326	3.090

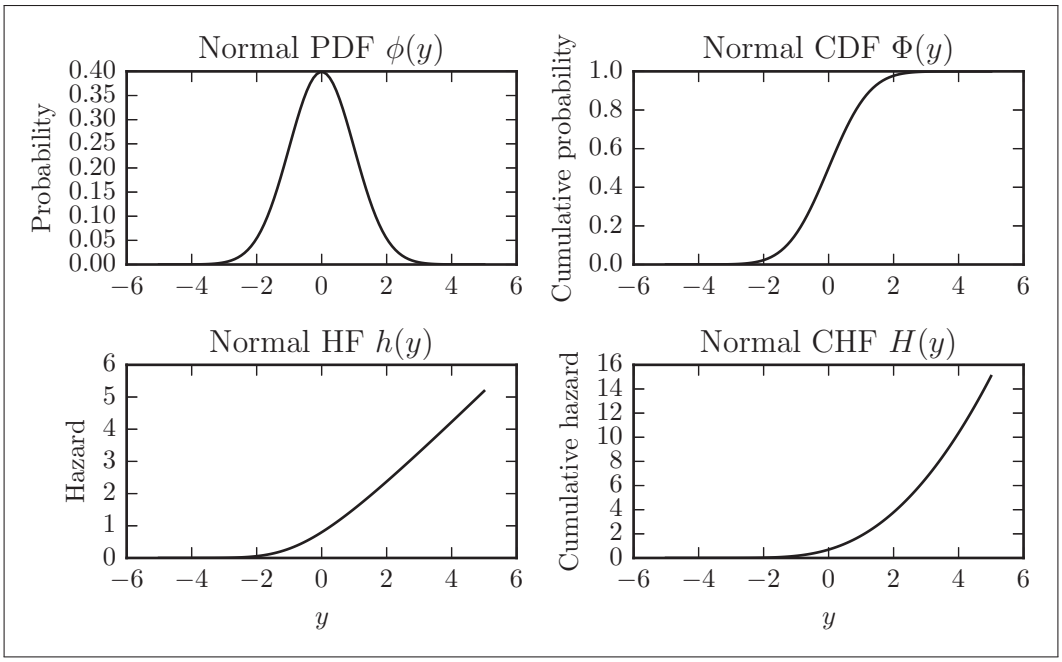

Figure-A I-2 Standard normal distribution functions

1.2.2 Lognormal distribution

The Lognormal distribution is closely related to the Normal distribution, with the main difference being that the logarithm of the random variable is normally distributed. Put otherwise, the logarithm of the variable has a Normal distribution of mean μ and standard deviation σ. Therefore, the random variable must now be positive and μ is the mean of the logarithm of the variable (called log mean of the distribution) while σ is the standard deviation of the logarithm of the variable (called log standard deviation). Also note that while $-\infty < \mu < \infty$ and $\sigma > 0$ as in the Normal distribution, they no longer share the units of the variable but are now unitless.Assuming a base 10 for the logarithm leads to the following definition of the Lognormal PDF:

$$f(t) = \frac{1}{\ln(10)\sqrt{2\pi}t\sigma} \exp\left[-\frac{1}{2}\left(\frac{\log(t) - \mu}{\sigma}\right)^2\right] \qquad \text{(A I-10)}$$

and Lognormal CDF:

$$F(t) = \Phi(z);$$
$$z = \frac{\log(t) - \mu}{\sigma}; \quad \text{(A I-11)}$$
$$y > 0. \quad \text{(A I-12)}$$

For the Lognormal distribution, the median $\tau_{0.50}$ is given by 10^{μ}. This defination of the Lognormal distribution results in μ acting as a scale parameter and σ acting as a shape parameter. Therefore, remembering that, as per equation A I-8, $h(t) = f(t)/(1 - F(t))$, the shape of the Lognormal HF is also influenced by these two parameters. This is illustrated in figure I-3.

As seen in figure I-3, the Lognormal HF shows some peculiarities. First of all, for small values of σ (*e.g.* $\sigma \leq 0.2$) $h(t)$ increases progressively, much like for the Normal distribution, but eventually decreases for high values of t. Therefore, the Lognormal PDF and CDF also behave similarly to that of the normal distribution. Then, for $\sigma = 0.5$, $h(t)$ varies very little over the distribution. Finally, high values of σ (*eg.* $\sigma \geq 0.8$), result in a rapid initial increase of $h(t)$ followed by a slow decrease as t increases. This added flexibility makes the Lognormal distribution quite useful for modeling the life of components. However, one must be aware of the fact that $h(0) = 0$ and that $h(t) \to 0$ for very high values of t. These two properties are seldom seen in life data analysis but are not a problem unless one is interested in the most extreme percentiles of the distribution.

1.2.3 Stress-life model

The modeling of the fatigue behaviour represented by the $S - N$ curve usually rests on the additional assumption that for the range of interest, the stress-life relation is linear either in the log-linear space (eq. A I-13) or log-log space (A I-14). However, any other

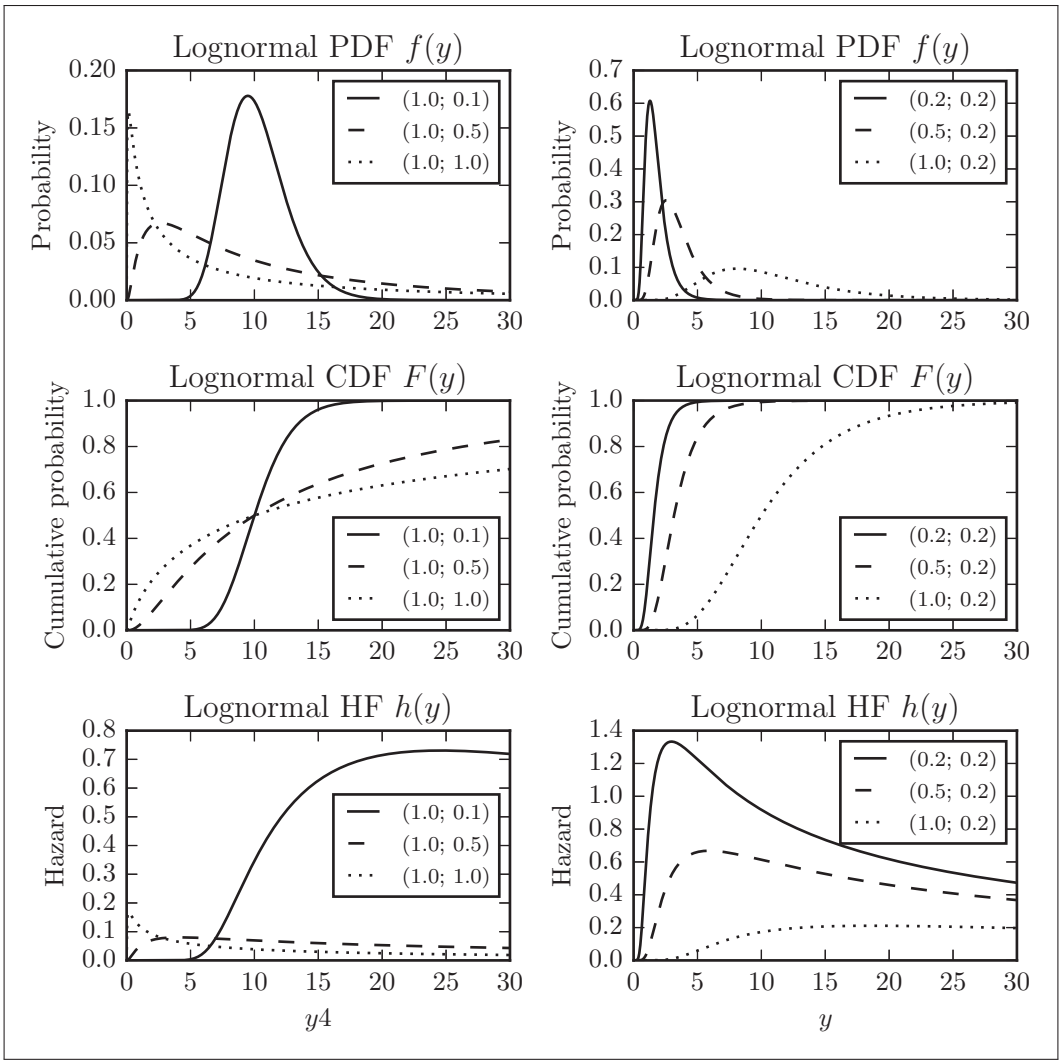

Figure-A I-3 Lognormal distribution functions for different (μ; σ) pairs

form may be used in order to correctly represent the data.

$$\log N = a + bS \tag{A I-13}$$

$$\log N = c + d \log S \tag{A I-14}$$

An additional assumption is that the data points are independent and identically distributed (iid) according to the chosen statistical distribution that was chosen. The classic method used for determining the values of the model parameters is the least square re-

gression and this method further assumes a constant sample standard deviation (or its logarithm).

2. Types of life data

The most simple type of life data encountered is called complete data. In such a situation, all specimens are subjected to a definite stress until failure is recorded. For this type of data, the least square regression can be applied with good confidence on the resulting parameters estimate as long as the model is adequate and the sample is large enough, iid and representative of the actual population.

However, it is not always possible or desireable to test all specimens to failure. Moreover, many different situation may render some data useless or unavailable. These incomplete data may then fall in different categories, the most important ones being: censored data, missing data and truncated data. Moreover, censoring may take many forms. The problem of incomplete data has many implications. For example, the LSQ method has no provision for effectively dealing with censored data. If the datum from an interrupted test is discarded, an important amount of upstream efforts is just lost, the sample size is reduced and the iid assumption may be violated. Nonetheless, including the datum as a failure is not legitimate either since it will bias the parameters estimate in an undetermined way, reducing confidence in the process.

Censoring happens when the observation of an event for a specific specimen is not allowed but partial information still is available. This may be the result of various circumstances leading to different censoring schemes. Missing data is simply a more extreme case where no information is available for a given specimen or the information available is known to be erroneous. In truncated data information is only partially available, however this is due to the fact that only a random fraction of the population may be observable. Therefore, although similar to censored data, truncated data should not be confused with the former for the choice of an analysis method (227).

Since censored data are of particular interest to fatigue testing, more details are provided on censoring schemes.

2.1 Censoring

Assuming that both the model and data are valid, censored data is of course, less informative than complete data. Nonetheless, it still provides valuable information and the loss of accuracy may often be more than compensated for by the added flexibility and reduced resources requirements. However, in addition to the more involved statistical analysis required for the treatment of censored data, censoring also requires some supplementary precautions to ensure the validity of the results. In other words, when dealing with censored data, one must first be careful in identifying whether the censoring process may violate some modeling assumption or hide other information and whether the censoring process is independent of the process under scrutiny.

Some of the most common types of censored data are : type I, type II, right censored, left censored, interval censored and double censored. Moreover, for each of these categories the censoring processes may be random (noninformative) or nonrandom (informative) and may be either singly censored or multiply censored.

In a random (or non-informative) censoring process, the censoring is independent from the process of interest. This is preferable to a non-random censoring, where there is a relation between censoring time and failure time. Random censoring allows for the use of simpler modeling and solutions available for data analysis. For example, removing a fatigue specimen because it looks like it is about to break is not recommanded because the censoring is then dependent on the failure process itself.

In singly censored data, all subjects are run concurrently until a predefined censoring trigger is reached. A multiply censored data set allows for different start times and censoring triggers for each specimen.

In type I censoring, the experiment is started at the same time for all specimens and the experiment is stopped at a predetermined time (*i.e.* singly time censored). For specimens that did not fail within the censoring time t_c, the only information available is that $t \geq t_c$. Note that t_c is fixed and therefore not a random variable in type I censoring. Then, the censoring process may not be a non-informative one. A variant of this censoring scheme allows for restart of part of the remaining subject until a new censoring time is reached and so on. Such a test would be refered to as a multiply time censored type I program.

In type II censoring, the experiment is again started at the same time for all specimens. However, the experiment is stopped after a certain portion x of the n initial specimens have failed (*i.e.* singly failure censored). Then, for the unfailed specimens at the time of failure t_f, one only knows that $t \geq t_f$. It is again obvious that type II censoring is not independent of the failure process and may therefore not be qualified as random censoring. A variant of this censoring scheme allows for restart of a fraction of the remaining subject until a new failure ratio is reached and so on. Such a test would be then be refered to as multiply failure censored type II program.

Right censored data are more general than type I and type II in that they suppose that the experiment start time is known but must not be equal for all subjects and that, if failure is not recorded at the end of the experiment, an individual censoring time t_{c_i} is known. Then, for unfailed specimens, one only knows that $t_i \geq t_{c_i}$. If the reason for censoring (*e.g.* stopping the experiment) is not related to the failure process, the right censoring may be assumed to be random (or non-informative).

Left censoring implies that the event of interest happened before the first attempt of observing the event of interest. In such a case, the only information available is that $t \leq t_c$. In such a case, the independence of the censoring and the event may also lead to a random censoring. Although unlikely to happen in fatigue experiments, this type of censoring may happen, among other reasons, in case of measurement equipement

malfunction. For example, failure of the specimen happened but cycling (and cycle counting) comtinued until manually interrupted.

Double censoring happens when each subject is associated with both a left censoring time t_{cl} and a right censoring time t_{cr}, but is continually monitired between these two. The possible informations available from a specimen is either $t \leq t_{cl}$, $t = t_f$ or $t \geq t_{cr}$.

Interval censoring happens when a subject is only periodically monitored instead of continually monitored. Therefore, one only knows that failure happened between two inspection time. Therefore, observation of a failure at the i^{th} inspection time t_i indicates that $t_{i-1} \leq t \leq t_i$.

Depending on their specifics, left, right and doubly censored data may fall in any of the random, nonrandom, singly or multiply censored categories. The censoring scheme will influence the statistical methods used for fitting the model.

3. Fitting the model parameters

Once the stress–life model has been established, it must be fitted to the data through the selection of the most representative values for the model parameters. Many possibilities exist for attaining this goal, but the nature of the data itself may preclude certain types of analyses. Examples of fitting methods include graphical estimation of the parameters, least square regression (LSQ) and maximum likelihood estimation (MLE).

The following section provides a method for estimating the model parameters for a complete data set. This is achieved with the LSQ method. After that, a description of the MLE method, which is suitable for estimating model parameters of datasets that include censored data, is detailed.

3.1 Complete data and least square regression analysis for log-log linear stress-life relationship and lognormal life distribution (226)

First, lets assume a test program is constituted of j stress levels ($j = 1,2,3,\ldots,J$) containing i specimens ($i = 1,2,3,\ldots,n_j$). Then, for a random process, the log of a specimen failure time is of the form:

$$y_{ij} = \mu(x_j) + e_{ij}. \tag{A I-15}$$

That is the log of the life (y) of specimen i, tested at stress level j, is equal to the sum of the mean log of life at stress $\mu(x_j)$ (where x_j is the log of stress) and of a random error e_{ij} on the log of life (y_{ij}).

Further assuming a linear relationship of the average life in the log-log space, the mean life is described by:

$$\mu(x_j) = \gamma_0 + \gamma_1 x_j. \tag{A I-16}$$

In order to estimate the coefficients of equation A I-16, average stresses and lives as well as the standard deviation for the data set need to be evaluated. The average loglife $\bar{y_j}$ and standard deviation s_j for a given stress level are given by:

$$\bar{y_j} = \frac{\sum_{i=1}^{n_j} y_{ij}}{n_j}; \tag{A I-17}$$

$$s_j = \sqrt{\frac{\sum_{i=1}^{n_j} (y_{ij} - \bar{y}_j)^2}{(n_j - 1)}}. \tag{A I-18}$$

Note that s_j has $n_j - 1$ degrees of freedom (ν_j) and that if $n_j = 1$, s_j cannot be evaluated. The $\bar{x_j}$ are the log of the stress at level j.

The grand averages of all data are further given by:

$$\bar{x} = \frac{\sum_{j=1}^{J}(n_i \bar{x_i})}{n}; \tag{A I-19}$$

$$\bar{y} = \frac{\sum_{j=1}^{J}(n_j \bar{y_j})}{n}. \tag{A I-20}$$

Now that these preliminary statistics have been calculated, the sums of squares are obtained through:

$$S_{xx} = \sum_{j=1}^{J} n_j (x_j - \bar{x})^2; \tag{A I-21}$$

$$S_{yy} = \sum_{j=1}^{J} \sum_{i=1}^{n_j} (y_{ij} - \bar{y})^2; \tag{A I-22}$$

$$S_{xy} = \sum_{j=1}^{J} n_j (x_j - \bar{x}) \bar{y}_j. \tag{A I-23}$$

If each (or most) specimens is tested at a different stress level, equations A I-20 to A I-23 must be run over all n specimens. This approach is used in ASTM standard for tensile testing of composites (224).

Finally, least square regression estimates of the coefficients γ_0 and γ_1, namely c_0 and c_1, are given by:

$$c_1 = \frac{S_{xy}}{S_{xx}}; \tag{A I-24}$$

$$c_0 = \bar{y} - c_1 \bar{x}. \tag{A I-25}$$

And the pooled estimate of the log-standard deviation (σ) based on lack of fit (which has $n-2$ degrees of freedom) is:

$$s' = \sqrt{\frac{S_{yy} - c_1 S_{xy}}{(n-2)}}. \tag{A I-26}$$

Therefore, according to the least square regression of the data, the estimate of the mean log of life at any given log-stress x_0 is:

$$\hat{\mu}(x_0) = c_0 + c_1 x_0. \tag{A I-27}$$

3.1.1 Confidence intervals of least square estimates

Of major interest in order to compare different fatigue curves are the confidence intervals of the mean and standard deviation of the least square estimates. The sample's standard deviation ($\sigma[\hat{\mu}(x_0)]$) is evaluated knowing that $\hat{\mu}(x_0)$, as a unbiased estimator of $\mu(x_0)$, has a normal sampling distribution with mean equal to the true population mean $\mu(x_0)$. The standard error of $\hat{\mu}(x_0)$ is then equal to the standard deviation of the sampling distribution:

$$\sigma[\hat{\mu}(x_0)] = \sigma\sqrt{\frac{1}{n} + \frac{(x_0 - \bar{x})^2}{S_{xx}}}. \tag{A I-28}$$

Using equation A I-26 in order to estimate σ provides us with the estimate of $\hat{\mu}(x_0)$ standard deviation with $\nu = n - 2$ degrees of freedom as:

$$s[\hat{\mu}(x_0)] = s'\sqrt{\frac{1}{n} + \frac{(x_0 - \bar{x})^2}{S_{xx}}}. \tag{A I-29}$$

Upper and lower $100\alpha\%$ confidence limits for the true value of the logmean life $\mu(x_0)$ are then given by:

$$\begin{aligned} \underline{\mu}(x_0) &= \hat{\mu}(x_0) - t(\alpha';\nu)s[\hat{\mu}(x_0)]; \\ \overline{\mu}(x_0) &= \hat{\mu}(x_0) + t(\alpha';\nu)s[\hat{\mu}(x_0)]. \end{aligned} \tag{A I-30}$$

In equations A I-30, (α', ν) is the student t-distribution percentile where α' is equal to the upper or lower tail $(\alpha/2)$ of the distribution and given by $\alpha' = (1+\alpha)/2$ while ν is the number of degrees of freedom of s'.

Similarly, upper and lower bounds for c_0 and c_1 are found by estimating their respective standard deviations by:

$$s(c_0) = s'\sqrt{\frac{1}{n} + \frac{\bar{x}^2}{S_{xx}}}; \tag{A I-31}$$

$$s(c_1) = s'\sqrt{\frac{1}{n} + \frac{1}{S_{xx}}}. \tag{A I-32}$$

And calculating bounds as:

$$\begin{aligned} \underline{\gamma_0} &= c_0 - t(\alpha';\nu)s(c_0); \\ \overline{\gamma_0} &= c_0 + t(\alpha';\nu)s(c_0); \end{aligned} \tag{A I-33}$$

$$\begin{aligned} \underline{\gamma_1} &= c_1 - t(\alpha';\nu)s(c_1); \\ \overline{\gamma_1} &= c_1 + t(\alpha';\nu)s(c_1). \end{aligned} \tag{A I-34}$$

Finally, a confidence interval on σ, the true log-standard deviation of the population, is evaluated by:

$$\begin{aligned} \underline{\sigma} &= s'\sqrt{\frac{\nu}{\chi^2[(1+\alpha)/2;\nu]}}; \\ \overline{\sigma} &= s'\sqrt{\frac{\nu}{\chi^2[(1-\alpha)/2;\nu]}}. \end{aligned} \tag{A I-35}$$

Where $\chi^2(\delta;\nu)$ is the $100\delta\%$ chi-square percentile with ν degrees of freedom.

3.1.2 Other percentiles

The previous analysis allowed for the determination of the parameters for the standard 50% survival fatigue curve. However, a curve for a higher surviving fraction is usually of more interest for design purpoise (a $S-N-P$ curve). Such a curve is simply obtained by shifting the curve by the use of the properties of the normal distribution as per equation A I-9. The $100p\%$ percentile of model $y_p(x_0)$ is then given by:

$$\begin{aligned} y_p(x_0) &= \hat{\mu}(x_0) + z_p s'; \\ y_p(x_0) &= \gamma_0 + \gamma_1 x_0 + z_p s'. \end{aligned} \tag{A I-36}$$

An estimate of the lower $100\gamma\%$ confidence bound on a percentile of the model is also provided by:

$$\eta_p(x_0) \approx y_p(x_0) - z_\gamma \sqrt{\frac{z_p^2}{2\nu} + \frac{1}{n} + \frac{x_0 - \bar{x}}{S_{xx}}} s'. \qquad \text{(A I-37)}$$

3.1.3 Limitation of the least square regression

The use of least square regression for evaluating fatigue curve parameters suffers from two major limitations (256):

- It only allows for proper evaluation of the parameters if the data is complete, *i.e.* contains only time to actual failure. It cannot account for interrupted tests (runouts).
- It only account for physical variability in the fatigue process but does not account for the statistical uncertainties associated to the evaluation of parameters.

The fact that runouts are not accounted for in the least square regression leads to either excluding runout data or considering runouts as failure. It is evident that neither of these solutions is good pratice since they either lead to inefficient testing or biased interpretation.

The second limitation is mostly important for relatively small samples, where statistical uncertainties may become comparable to physical uncertainties.

3.2 Censored data and the use of maximum likelihood estimation for log-log linear stress-life relationship and lognormal life distribution

As stated earlier, the least square regression method in itself has no provisions for adequately dealing with runouts. Therefore, a different approach must be used. In its general form, the maximum likelyhoood estimation can deal with all types of data presented earlier. However, the added complications of dealing with non-random censoring are not going to be dealt with here.

The basic concept of maximum likelihood estimation is first presentend, followed by the mathematical formulation of the MLE problem. A discusion on the optimization of the likelihood function will then be provided and further use of the MLE tools and results for assessing functions of the model and determining confidence intervals as well as other percentiles will complete the section.

3.2.1 Basic concept

The basic concept of maximum likelihood is actually quite simple. It relies on the idea that once a model and its underlying distributions and relationships are known or chosen, it is possible to write a function that would represent the likelihood of the data (including censored data points) with regards to all the model parameters or coefficients. The best estimate of these parameters and coefficients values would then correspond to those that maximize the likelihood function.

3.2.2 Mathematical formulation

This setion presents the essential principles and calculations associated with fitting the model parameters using the maximum likelihood method. The method presented herein is adequate for complete, random censored and interval data. The ML method is basically divided in three steps:

a. Formulation of the likelihood L, or more specifically of the logarithm of the likelihood $\pounds$, as a function of the data, of the data type and of the J model parameters and coefficients γ_j.

b. Derivation of $\partial\pounds/\partial\gamma_j$, the first partial derivative of the likelihood function according to its model parameters and solution of $\partial\pounds/\partial\gamma_j = 0$ to obtain the estimated parameters $\hat{\gamma}_j$ of all J parameters γ_j.

c. Construction of the $J \times J$ matrix of partial second derivatives $\partial^2 \pounds / \partial \gamma_j \gamma_j$ with respect to all model parameters γ_j and calculation of confidence limits for the model parameters and other estimates.

Along with the general formulation of the model, the development of a log-log linear two-parameter stress-life relationship with Lognormal life distribution will also be presented.

3.2.2.1 Data form and organisation.

The present formulation assumes that the data is structured in a matrix form. The data matrix includes, for each of the $i = [1; n]$ specimens, the dependent variable y_i, the independent variable x_i and the censoring indicator C_i if the data are of the censored or interval types. Note that interval data should have a pair of dependent variables $y_i; y_i'$, the lower and upper limits of the interval.

In the example case of a log-log linear stress-life relationship with right random censored data, the dependent variable y would be the base 10 log of the life, the independent variable x the base 10 log of the stress and the censoring indicator would be, for example $C = 0$ for an actual failure time measurement and $C = 1$ for a runout.

3.2.2.2 Model statistical distribution.

The model that is fitted to the data contains both a relationship between x and y and a statistical distribution for the dependent variable y.

The dependent variable y_i for each specimen is assumed to have a continuous statistical CDF with Q distribution parameters:

$$F_i(y_i; \theta_1, \theta_2, \ldots, \theta_Q). \qquad \text{(A I-38)}$$

Knowing that $f = dF/dy$ the PDF is expressed by:

$$f_i(y_i;\theta_1,\theta_2,\ldots,\theta_Q) = \frac{dF_i(y_i;\theta_1,\theta_2,\ldots,\theta_Q)}{dy}. \tag{A I-39}$$

However, in general the distribution is assumed to be the same for all y so equations A I-38 and A I-39 may be understood as:

$$F(y;\theta_1,\theta_2,\ldots,\theta_Q);$$
$$f(y;\theta_1,\theta_2,\ldots,\theta_Q) = \frac{dF(y;\theta_1,\theta_2,\ldots,\theta_Q)}{dy}.$$

In the example case of fatigue with an assumed Lognormal distribution of life (*i.e.* y is the base 10 log of life), the CDF and PDF would respectively be:

$$F(y;\mu,\sigma) = \Phi\left[\frac{y-\mu}{\sigma}\right];$$
$$f(y;\mu,\sigma) = \frac{1}{\ln(10)\sqrt{2\pi}y\sigma}\exp\left[-\frac{1}{2}\left(\frac{y-\mu}{\sigma}\right)^2\right].$$

Then according to the previous discussion, this would be a $Q = 2$ parameters distribution.

3.2.2.3 Distribution parameters relationships.

The relationship between the Q distribution parameters θ and the independent variable x is assumed to be expressed by a function of J independent variables x_1 to x_J and P model coefficients γ_1 to γ_P. Although each of the relationships can be a function of all coefficients, each of the latter usually appears in only one distribution parameter relationship. Nonetheless, the general formulation would be:

$$\begin{aligned}\theta_1 &= \theta_1(x_1,\ldots,x_J;\gamma_1,\ldots,\gamma_P),\\ &\vdots\\ \theta_Q &= \theta_Q(x_1,\ldots,x_J;\gamma_1,\ldots,\gamma_P).\end{aligned} \tag{A I-40}$$

Note that while the form of the relationships is assumed or known, the numerical values of the parameters remain unknown. Also note that these relationships are provided for each individual specimens, which means that for specimen i the formulation would be:

$$\begin{aligned} \theta_{1i} &= \theta_1(x_{1i}, \ldots, x_{Ji}; \gamma_1, \ldots, \gamma_P), \\ &\vdots \\ \theta_{Qi} &= \theta_Q(x_{1i}, \ldots, x_{Ji}; \gamma_1, \ldots, \gamma_P). \end{aligned} \tag{A I-41}$$

In the log-log linear fatigue life model previously described and assuming that x is the base 10 logarithm of the stress, the relationship would write down as:

$$\begin{aligned} \theta_1 &= \mu = \gamma_1 + \gamma_2 x, \\ \theta_2 &= \sigma = \gamma_3; \end{aligned}$$

or on a specimen specific basis:

$$\begin{aligned} \theta_{1i} &= \mu_i = \gamma_1 + \gamma_2 x_i, \\ \theta_{2i} &= \sigma_i = \sigma = \gamma_3; \end{aligned}$$

and would have $P = 3$ model coefficients.

3.2.2.4 Specimen likelihood

The likelihood of a single specimen L_i can be assimilated to the probability of the "observed" value of its dependent variable given the value of its independent variable, but remembering that the response variable may actually have an exactly observed, censored or interval value.

In the case of the exactly observed value of y_i for a given specimen, the specimen likelihood is given by the PDF of the assumed distribution at point (x_i, y_i):

$$L_i = f(y_i; \theta_{1i}, \ldots, \theta_{Qi}). \tag{A I-42}$$

This L_i can be regarded as the probability that failure occured at y_i given x_{1i} to x_{1J} and γ_1 to γ_P.

In the case of a right censored specimen, the likelihood that the specimen fails at a loglife higher than y_i is given by the reliability function of the assumed distribution.

$$L_i = 1 - F(y_i; \theta_{1i}, \ldots, \theta Qi) \tag{A I-43}$$

Then, for the case of left censored, the likelihood of a failure before y_i is given by the CDF of the assumed distribution.

$$L_i = F(y_i; \theta_{1i}, \ldots, \theta Qi) \tag{A I-44}$$

Finally, for an interval censored specimen, the likelihood is given by the difference of the CDF at y_i' and y_i, where $y_i < y_i'$.

$$L_i = F(y_i'; \theta_{1i}, \ldots, \theta Qi) - F(y_i; \theta_{1i}, \ldots, \theta Qi). \tag{A I-45}$$

Note that equation A I-45 reduces to equation A I-44 if the lower endpoint of the interval is $-\infty$ or zero and reduces to equation A I-43 if the upper endpoint is $+\infty$.

3.2.2.5 Sample likelihood

Remembering that each of the n specimens from a given sample are assumed to be iid, their respective response variable y_i should also show independent random variations.

Therefore, the likelihood of the sample L is the joint probability of the n dependent variable outcomes and given by the product of the individual specimens likelihoods L_i.

$$L \equiv \prod_{i=1}^{n} L_i. \tag{A I-46}$$

3.2.2.6 Log likelihood

As will be seen later, the estimation of the model parameters and confidence intervals requires first and second order partial derivatives of the sample likelihood. The use of the natural logarithm of the likelihood $\pounds$ will then make the solution easier by turning the product of specimen likelihoods into the sum of their logarithms. Therefore the specimen log likelihood is provided by:

$$\pounds_i \equiv \ln L_i \tag{A I-47}$$

and given the properties of logarithms, the sample log likelihood is given by:

$$\pounds \equiv \sum_{i=1}^{n} \pounds_i. \tag{A I-48}$$

3.2.3 Maximum likelihood estimates of model coefficients

The values of $\gamma_1, \ldots, \gamma_P$ that maximise the sample log likelihood are the maximum likelihood estimates of the coefficients $\hat{\gamma}_1, \ldots, \hat{\gamma}_P$. It may be possible to obtain these by solving the following system of partial differential equations:

$$\begin{aligned} \frac{\partial \pounds(\gamma_1, \gamma_2, \ldots, \gamma_P)}{\partial \gamma_1} &= 0, \\ \frac{\partial \pounds(\gamma_1, \gamma_2, \ldots, \gamma_P)}{\partial \gamma_2} &= 0, \\ &\vdots \\ \frac{\partial \pounds(\gamma_1, \gamma_2, \ldots, \gamma_P)}{\partial \gamma_P} &= 0. \end{aligned} \tag{A I-49}$$

It is nevertheless quite frequent that an analytical solution for the likelihood function maximization is not feasible. Therefore, the recourse to a numerical solution of equation A I-49 or numerical search is required. In the case of numerical optimization, convergence speed and accuracy can be improved by substracting a value close to the average from every independent variables in the formulation. It is also good practice to verify that solutions from the numerical optimization are global rather than local optimum. For simple formulations like that of fatigue this can be done graphically, but more complex forms may require more refined approaches. For example, (226) suggests that an optimum is found if all eigenvalues of the Fisher matrix evaluated locally (*i.e.* using the solution of the optimizer as values of the model parameters) are positive.

3.2.3.1 Local Fisher information matrix

Consisting of the $P \times P$ negative partial derivative of the log likelihood function arranged in a symmetric matrix, the Fisher local information matrix $\mathbf{F}$ is used in the estimation of the variance and covariance of the estimated function parameters $\hat{\gamma}_1, \ldots, \hat{\gamma}_P$ and as just mentioned, in the validation that the optimization results are at a global maximum.

$$\mathbf{F} = \begin{bmatrix} -\frac{\partial^2 \hat{\pounds}}{\partial \gamma_1^2} & -\frac{\partial^2 \hat{\pounds}}{\partial \gamma_1 \gamma_2} & \cdots & -\frac{\partial^2 \hat{\pounds}}{\partial \gamma_1 \gamma_P} \\ -\frac{\partial^2 \hat{\pounds}}{\partial \gamma_2 \gamma_1} & -\frac{\partial^2 \hat{\pounds}}{\partial \gamma_2^2} & \cdots & -\frac{\partial^2 \hat{\pounds}}{\partial \gamma_2 \gamma_P} \\ \vdots & \vdots & \ddots & \vdots \\ -\frac{\partial^2 \hat{\pounds}}{\partial \gamma_P \gamma_1} & -\frac{\partial^2 \hat{\pounds}}{\partial \gamma_P \gamma_2} & \cdots & -\frac{\partial^2 \hat{\pounds}}{\partial \gamma_P^2} \end{bmatrix}. \qquad \text{(A I-50)}$$

Note that $\mathbf{F}$ is a symetric matrix.

3.2.3.2 Covariance matrix and standard error of parameter estimates

A local estimate of the asymptotic covarience $\mathbf{V}$ for $\hat{\gamma}_1, \ldots, \hat{\gamma}_P$ is provided by the inverse of the local Fisher information matrix.

$$\mathbf{V} = \mathbf{F}^{-1} = \begin{bmatrix} \text{var}(\hat{\gamma}_1) & \text{cov}(\hat{\gamma}_1;\hat{\gamma}_2) & \ldots & \text{cov}(\hat{\gamma}_1;\hat{\gamma}_P) \\ \text{cov}(\hat{\gamma}_2;\hat{\gamma}_1) & \text{var}(\hat{\gamma}_2) & \ldots & \text{cov}(\hat{\gamma}_2;\hat{\gamma}_P) \\ \vdots & \vdots & \ddots & \vdots \\ \text{cov}(\hat{\gamma}_P;\hat{\gamma}_1) & \text{cov}(\hat{\gamma}_1;\hat{\gamma}_2) & \ldots & \text{var}(\hat{\gamma}_P) \end{bmatrix}. \quad \text{(A I-51)}$$

The positions of the variances and covariances in $\mathbf{V}$ are at the same positions as the corresponding second partial derivatives in matrix $\mathbf{F}$. An estimation of the standard error of $\hat{\gamma}_P$, $\sigma(\hat{\gamma}_P)$, is therefore given by:

$$\sigma(\hat{\gamma}_P) = \sqrt{\text{var}(\hat{\gamma}_P)}, \quad \text{(A I-52)}$$

which is used in the determination of approximate confidence intervals on the maximum likelihood estimate of the relationship.

3.2.4 Functions of the model

Apart from the initial relationship evaluated using the MLE method, additional functions of the model are of interest to the fatigue analyst. For example, the confidence intervals of the $S-N$ curve and a fatigue curve at other percentiles of the distribution are of interest. The general formulation of a function of the model is as follows. First, lets define h, the function of the model as $h = h(\gamma_1, \ldots, \gamma_P)$. Thus, the estimate of h is provided by:

$$\hat{h} = h(\hat{\gamma}_1, \ldots, \hat{\gamma}_P). \quad \text{(A I-53)}$$

The variance of $\hat{h}$ is required for the evaluation of approximate normal confidence intervals. The asymptotic estimate of this variance is provided by:

$$\mathrm{var}(\hat{h}) = \hat{\mathbf{H}}'\mathbf{V}\hat{\mathbf{H}}; \tag{A I-54}$$

where $\hat{\mathrm{H}}$ is the column vector of partial derivatives $\partial\hat{h}/\partial\gamma_P$

$$\hat{\mathbf{H}} = \begin{bmatrix} \partial\hat{h}/\partial\gamma_1 \\ \vdots \\ \partial\hat{h}/\partial\gamma_P \end{bmatrix}, \tag{A I-55}$$

$\mathbf{V}$ is the local estimate of the covariance matrix from equation A I-51 and $\hat{\mathbf{H}}'$ is the transpose of $\hat{\mathbf{H}}$ (equation A I-55).

Finally, the estimate of $s(\hat{h})$, the standard error of $\hat{h}$, is:

$$s(\hat{h}) = \sqrt{\mathrm{var}(\hat{h})}, \tag{A I-56}$$

and is used in the determination of confidence intervals on the true value of h.

3.3 Confidence intervals, single-sided limits and other percentiles

The estimation of the approximate normal $100\gamma\%$ confidence interval on the true value of the relationship or of its parameters is based on the previously stated method for describing functions of the model. That is to say that h would be either a parameter estimate (*i.e.* $\hat{\gamma}_1, \ldots, \hat{\gamma}_P$) or the relationship estimate itself (*e.g.* $y = \hat{\gamma}_1 + \hat{\gamma}_2 x$). However, the form of the interval will vary according to the value to which the bounds are either mathematically or physically limited. Put otherwise, the formulation of the confidence interval on h is unbounded ($-\infty < h < \infty$), positive ($h > 0$) or fractional ($0 < h < 1$) to ensure that the bounds are not outside the limits of h.

Note that the estimation of the confidence interval depends both on the confidence level γ and on the number of failures. This fact translates into poorer estimates for higher values of γ (*i.e.* higher confidence level) or a lower number of failures.

As for the formulation of the bounds themselves, assuming that $\hat{h}$ is the maximum likelihood estimate of the true value of h and that $s(\hat{h})$ is the estimate of the standard error on $\hat{h}$. The upper and lower $100\gamma\%$ bounds on $\hat{h}$ if the range of h is unbounded are given by:

$$\underline{h} = \hat{h} - K_\gamma s(\hat{h}); \tag{A I-57}$$

$$\overline{h} = \hat{h} + K_\gamma s(\hat{h}). \tag{A I-58}$$

In equation A I-57, since the limits are double sided, K_γ is the $100(1+\gamma)/2$th standard normal percentile as per table I-1.

In the case of positive limits, the upper and lower confidence bounds take the form of:

$$\underline{h} = \hat{h} \exp\left(\frac{-K_\gamma s(\hat{h})}{\hat{h}}\right); \tag{A I-59}$$

$$\overline{h} = \hat{h} \exp\left(\frac{K_\gamma s(\hat{h})}{\hat{h}}\right). \tag{A I-60}$$

This formulation would be required for the estimation of the bounds on the standard deviation ML estimate as it must be positive.

Finally, for limits with $[0,1]$ bounds such as fraction failing, the form of the bounds estimate is:

$$\underline{h} = \frac{\hat{h}}{\hat{h} + (1-\hat{h})\exp\left(\frac{K_\gamma s(\hat{h})}{\hat{h}(1-\hat{h})}\right)}; \tag{A I-61}$$

$$\overline{h} = \frac{\hat{h}}{\hat{h} + (1-\hat{h})\exp\left(\frac{-K_\gamma s(\hat{h})}{\hat{h}(1-\hat{h})}\right)}. \tag{A I-62}$$

In order to provide adequate estimates of the bounds, the number of failure must be sufficient to ensure that $\hat{h}$, $\ln(\hat{h})$ or $\ln(\hat{h}/(1-\hat{h})$ are respectively approximately normal for unbounded, positive and $[0,1]$ fractional limits. Single sided limits such as other percentiles are provided by replacing the value of K_γ by z_γ, the $100\gamma\%$ standard normal percentile, in equations A I-57 to A I-61.

4. Application and validation

An implementation of the maximum likelihood method for estimation of fatigue curve parameters with fatigue data including runout was made usign the Python programming language. The main function is the file `SN_MLE_MT.py` from which all subfunctions are called and the fatigue data is input in the file `SN_Data.py` in the form of a dictionary. `SN_MLE_MT.py` is able to process any number of $S-N$ curves and outputs the ML estimates of the relationship parameters, of the 95% normal confidence intervals on the curves and on its parameters and provides individual and combined plots of the $S-N$ curves.

Apart from the general assumptions required for the LSQ and MLE methods, additional assumptions used in the calculation are:

- log-log linear formulation of the fatigue relationship as per equation A I-14;

- γ_1, the intercept of the $S-N$ curve with the N axis is positve and its bounds are evaluated as per equation A I-59;
- γ_2, the slope of the $S-N$ curve can range from $-\infty$ to ∞ and its bounds are evaluated as per equation A I-57;
- γ_3, the log-standard deviation is positve and its bounds are evaluated as per equation A I-59;
- log-Normal distribution of life.

The basic steps of the $S-N$ curve calculation are as decribed in the following outline:

a. In `SN_MLE_MT.py`, identify the data sets from `SN_Data.py` to be used in the calculations as a list under the `usedata` variable name.

b. Run `SN_MLE_MT.py`.

    a. From `SN_Data.py`, import fatigue data for the sets defined in `usedata` to the `Data` and `Legends` dictionaries.

    b. Call of `LSQ_reg.LSQSN` function to perform least square estimation of the fatigue parameters for each data sets after removal of censored data points. The output is stored in the `Stats` dictionary.

    c. Construction of the log likelihood functions for each data sets by the `mLnL` method of the `likelihood.py` function and optimization of each data sets usign the Nelder-Mead (derivative free) optimization algorithm. Results for each data sets are stored in the `Results` dictionary.

    d. Call of the `Conf_int` method from `Statistics_MT.py` in order to calculate the Fisher and covariance matrices, the eigenvalues of the Fisher matrix as well as the 95% confidence intervals on the $S-N$ relationship and its parameters. This also requires the call of `likelihood_syms.py` function for the construction of

the symbolic form of the likelihood function. Results for each data sets are stored in the `Bounds_stats` dictionary.

e. Display results in the form individual and combined plots of $S-N$ curves, including confidence intervals on the 50th percentile.

Note that the `SN_MLE_MT.py` function explicitely calls multi-threaded calculation for the evaluation of the `Conf_int` method of `Statistics_MT.py` function. This is made in order to speed the processing by allowing for parallel evaluation of the symbolic calculations required in the the evaluation of the partial derivatives of the likelihood functions. An important improvement of the program would be to use the pre-evaluated derivatives instead of performing all the derivations as part of the MLE estimation process.

Also worth noting are some limitations of the algorithm. The first limitation is due to the fact that LSQ and MLE use $n-2$ degrees of freedom in some statisctics, meaning that at least three data points are required for each dataset in order to run without errors. Second, is that at the time of writing, the program can only manage complete and right censored data. Third, although substraction of the mean stress from each term of the likelihood function would be recommended in order to improve convergence caracteristics of the optimization, it was not done so in order to keep the standard definition of the $S-N$ curve. Finally, the confidence intervals are given by the normal approximation, which is known to provide poorer approximation than the likelihood ratio for small sample size. Nonetheless, the estimates given by the normal approximation are assumed to be sufficient for the current needs.

APPENDIX II

INTRODUCTION OF THE NORMALIZATION TEMPERATURE TO THE GOMPERTZ DISTRIBUTION SURVIVAL FUNCTION

All functions of a statistical distribution can be derived from the distribution's hazard function (HF). In the case of the Gompertz distribution normalized by an added localization parameter, the HF is given as:

$$HF(T) = b\exp(cT/T_{ref}). \tag{A II-1}$$

By definition the SF is:

$$SF(T) = \exp\left\{-\int_0^T HF(u)\mathrm{d}(u)\right\} \tag{A II-2}$$

$$= \exp\left\{-\left(\frac{bT_{ref}}{c}\right)\left[\exp\left(\frac{cT}{T_{ref}}\right)-1\right]\right\}. \tag{A II-3}$$

APPENDIX III

DEVELOPMENT OF EQUATION 5.10 BASED ON LOCATING T_G AT THE POINT OF MAXIMUM CURVATURE UPSTREAM OF THE INFLECTION POINT

Imposing that $T_{ref,i}$ occurs at the point of maximum curvature located to the left of the inflection point of the Gompertz SF, then:

$$\frac{\mathrm{d}^3 SF(T)}{\mathrm{d}T^3} = 0, \tag{A III-1}$$

and:

$$T = \frac{T_{ref}}{c} \ln\left[\frac{-c(\sqrt{5}-3)}{2bT_{ref}}\right]. \tag{A III-2}$$

Or in other terms, at $T = T_{ref}$:

$$b = \frac{-c(\sqrt{5}-3)}{2T_{ref}} \exp(-c), \tag{A III-3}$$

and then, equation 5.10 simplifies to:

$$P(T) = a_{N+1} + \sum_{i=1}^{N} (a_i - a_{i+1}) X_i(T) \tag{A III-4}$$

with:

$$X_i(T) = \exp\left\{\frac{\sqrt{5}-3}{2} \exp(-c_i)\left[\exp\left(\frac{c_i T}{T_{ref,i}}\right) - 1\right]\right\}. \tag{A III-5}$$

BIBLIOGRAPHY

[1] Government of Canada, "Canadian energy pricing trends 2000-2010 - energy facts." https://www.neb-one.gc.ca/nrg/ntgrtd/mrkt/archive/2011cndnnrgprcngtrndfct/cndnnrgprcngtrndfct-eng.pdf, Octobre 2011. Visited 2017-03-02.

[2] IPCC Core Writing Team, "Climate change 2007: Synthesis report. Contribution of working groups I, II and III to the fourth assessment report of the intergovernmental panel on climate change," tech. rep., Intergovernmental Panel on Climate Change (IPCC), 2007.

[3] IPCC Core Writing Team, "Climate change 2014: Synthesis report. Contribution of working groups I, II and III to the fifth assessment report of the intergovernmental panel on climate change," tech. rep., Intergovernmental Panel on Climate Change (IPCC), 2014.

[4] S. Ray, "U.S. electric generating capacity increase in 2016 was largest net change since 2011." http://www.eia.gov/todayinenergy/detail.php?id=30112, February 2017. Visited 2017-03-02.

[5] "Powering Canada's future." http://canwea.ca/wp-content/uploads/2016/02/Canada-Current-Installed-Capacity_e.pdf, Decembre 2015. Visited 2017-05-26.

[6] "Canadian wind energy association website." http://canwea.ca/wind-energy/installed-capacity/. Visited 2016-06-20.

[7] GWEC, "Global wind report 2015: Annual market update," tech. rep., Global Wind Energy Counsil (GWEC), 2016.

[8] D. Ancona and J. McVeigh, "Wind turbine – materials and manufacturing fact sheet," tech. rep., United-States Department of Energy, 2001.

[9] J. G. McGowan, R. W. Hyers, K. L. Sullivan, J. F. Manwell, S. V. Nair, B. McNiff, and B. C. Syrett, "A review of materials degradation in utility scale wind turbines," *Energy Materials*, vol. 2, no. 1, pp. 41–64, 2007.

[10] R. Nijssen, *Fatigue Life Prediction and Strength Degradation of Wind Turbine Rotor Blades*. PhD thesis, Delft University, 2006.

[11] A. R. Shah and C. C. Chamis, "Cyclic load frequency effects on fatigue reliability of polymer matrix composites," in *37th Structure, Structural Dynamics and Materials Conference*, no. AIAA-96-1559-CP, (Salt Lake City, UT, U.S.A.), pp. 2133–2143, American Institute of Aeronautics and Astronautics, April 1996.

[12] P. Brøndsted, H. Lilholt, and A. Lystrup, "Composite materials for wind power turbine blades," *Annual Review of Materials Research*, vol. 35, pp. 505–538, 2005.

[13] "Canadian atlas level 0." http://collaboration.cmc.ec.gc.ca/science/rpn/modcom/eole/CanadianAtlas0.html, Decembre 2000. Visited 2016-06-20.

[14] D. Elliott, C. Holladay, W. Barchet, H. Foote, and W. Sandusky, "Wind energy resource atlas of the United States." http://rredc.nrel.gov/wind/pubs/atlas/atlas_index.html, Octobre 1986. Visited 2017-02-28.

[15] "Wind energy in Canada," 2009. Visited 2016-06-20.

[16] S. Joncas, *Thermoplastic Composite Wind Turbine Blade*. PhD thesis, Delft University of Technology, 2010.

[17] L. C. E. Struik, *Physical Aging in Amorphous Polymers and Other Materials*. PhD thesis, Technische Hogeschool Delft, novembre 1977.

[18] T. S. Chow, "Molecular kinetic theory of the glass transition," *Polymer Engineering and Science*, vol. 24, p. 14, 1984.

[19] F. H. Stillinger and P. G. Debenedetti, "Glass transition thermodynamics and kinetics," *Annual Review of Condensed Matter Physics*, vol. 4, pp. 263–285, 2013.

[20] W. Kauzmann, "The nature of the glassy state and the behavior of liquids at low temperatures," *Chemical Reviews*, vol. 43, pp. 219–256, 1948.

[21] P. G. Debedenetti and F. H. Stillinger, "Supercooled liquids and the glass transition," *Nature*, vol. 410, pp. 259–267, 2001.

[22] S. L. Simon and G. B. McKenna, "Experimental evidence against the existence of an ideal glass transition," *Journal of Non-Crystalline Solids*, vol. 355, no. 10-12, pp. 672–675, 2009. Proceedings of the International Workshop on Glass and Entropy.

[23] J. H. Gibbs and E. A. DiMarzio, "Nature of the glass transition and the glassy state," *The Journal of Chemical Physics*, vol. 28, no. 3, pp. 373–383, 1958.

[24] C.-Y. Liu, J. He, R. Keunings, , and C. Bailly, "New linearized relation for the universal viscosity-temperature behavior of polymer melts," *Macromolecules*, vol. 39, no. 25, pp. 8867–8869, 2006.

[25] G. S. Fulcher, "Analysis of recent measurements of the viscosity of glasses," *Journal of the American Ceramic Society*, vol. 8, no. 6, pp. 339–355, 1925.

[26] R. P. White and J. E. G. Lipson, "Polymer free volume and its connection to the glass transition," *Macromolecules*, vol. 49, no. 11, pp. 3987–4007, 2016.

[27] T. G. Fox, Jr. and P. J. Flory, "Second-order transition temperatures and related properties of polystyrene: I influence of molecular weight," *Journal of Applied Physics*, pp. 581–591.

[28] S. White and H. Hahn, "Cure cycle optimization for the reduction of processing-induced residual stresses in composite materials," *Journal of Composite Materials*, vol. 27, no. 14, pp. 1352–1378, 1993.

[29] L. E. Nielsen, "Cross-linking-effect on physical properties of polymers," *Journal of Macromolecular Science Part C*, vol. 3, no. 1, pp. 69–103, 1969.

[30] L. E. Nielsen, *Mechanical Properties of Polymers and Composites*. Marcel Dekker inc., 1974.

[31] J. B. Enns and J. K. Gillham, "Time-temperature-transformation (TTT) cure diagram: Modeling the cure behavior of thermosets," *Journal of Applied Polymer Science*, vol. 28, no. 8, pp. 2567–2591, 1983.

[32] L. Barral, J. Cano, A. López, P. Nogueira, and C. Ramírez, "Determination of the activation energies for α and β transitions of a system containing a diglycidyl ether of bisphenol A (DGEBA) and 1,3-bisaminomethylcyclohexane (1,3-BAC)," *Journal of thermal analysis*, vol. 41, no. 6, pp. 1463–1467, 1994.

[33] G. Li, P. Lee-Sullivan, and R. W. Thring, "Determination of activation energy for glass transition of an epoxy adhesive using dynamic mechanical analysis," *Journal of Thermal Analysis and Calorimetry*, vol. 60, no. 2, pp. 377–390, 2000.

[34] W. Goertzen and M. Kessler, "Dynamic mechanical analysis of carbon/epoxy composites for structural pipeline repair," *Composites Part B: Engineering*, vol. 38, no. 1, pp. 1 – 9, 2007.

[35] Y. Bai and L. Jin, "Characterization of frequency-dependent glass transition temperature by Vogel-Fulcher relationship," *Journal of Physics D: Applied Physics*, vol. 41, no. 15, p. 152008, 2008.

[36] R. W. Hertzberg, *Deformation and Fracture Mechanics of Engineering Materials*. John Wiley & Sons, 4 ed., 1996.

[37] P. Badrinarayanan, W. Zheng, Q. Li, and S. L. Simon, "The glass transition temperature versus the fictive temperature," *Journal of Non-Crystalline Solids*, vol. 353, no. 26, pp. 2603 – 2612, 2007.

[38] M. Takayanagi, "Some structural factors in low temperature transtions of polymers," *Pure and applied chemestry*, vol. 23, pp. 151–182, January 1970.

[39] R. D. Adams and M. M. Singh, "Low temperature transitions in fibre reinforced polymers," *Composites Part A: Applied Science and Manufacturing*, vol. 32, no. 6, pp. 797–814, 2001.

[40] J. Vincent, *Structural Biopolymers*. Princeton University Press, 3 ed., 2012.

[41] D. Gutierrez-Lemini, *Engineering Viscoelasticity*. Springer, 2014.

[42] R. F. Gibson, *Principles of Composite Material Mechanics*. Mechanical Engineering, Boca-Raton, USA: CRC Press, 2 ed., 2007.

[43] R. Schapery, "Stress analysis of viscoelastic composite materials," *Journal of Composite Materials*, vol. 1, no. 3, pp. 228–267, 1967.

[44] H. F. Brinson and C. Brinson, *Polymer Engineering Science and Viscoelasticity: An Introduction*. Springer, 2 ed., 2015.

[45] R. Gibson, S. Hwang, and C. Sheppard, "Characterization of creep in polymer composites by the use of frequency-time transformations," *Journal of Composite Materials*, vol. 24, no. 4, pp. 441–453, 1990.

[46] J.-M. Parot and B. Duperray, "Exact computation of creep compliance and relaxation modulus from complex modulus measurement data," *Mechanics of Materials*, vol. 40, no. 7, pp. 575 – 585, 2008.

[47] R. M. Guedes, A. T. Marques, and A. Cardon, "Creep or relaxation master curves calculated from experimental dynamic viscoelastic function," *Science and Engineering of Composite Materials*, vol. 7, pp. 259–268, 1998.

[48] J. Dealy and D. Plazek, "Time-temperature superposition – a user guide," *Rheology Bulletin*, vol. 78, no. 2, pp. 16–31, 2009.

[49] E. Barbero, "Time-temperature-age superposition principle and its application to linear viscoelastic materials," in *Creep and fatigue in polymer matrix composites* (R. M. Guedes, ed.), ch. 2, pp. 48–68, Woodhead publishing, 2011.

[50] M. L. Williams, R. F. Landel, and J. D. Ferry, "The temperature dependence of relaxation mechanisms in amorphous polymers and other glass-forming liquids," *Journal of the American Chemical Society*, vol. 77, no. 14, pp. 3701–3707, 1955.

[51] J. L. Sullivan, "Creep and physical aging of composites," *Composite Science and Technology*, vol. 39, no. 3, pp. 207–232, 1990.

[52] G. Adam and J. H. Gibbs, "On the temperature dependence of cooperative relaxation properties in glass-forming liquids," *Journal of Chemical Physics*, vol. 43, pp. 139–146, July 1965.

[53] P. Wood-Adams and S. Costeux, "Thermorheological behavior of polyethylene: Effects of microstructure and long chain branching," *Macromolecules*, vol. 34, no. 18, pp. 6281–6290, 2001.

[54] G. M. Odegard and A. Bandyopadhyay, "Physical aging of epoxy polymers and their composites," *Journal of Polymer Science Part B: Polymer Physics*, vol. 49, no. 24, pp. 1695–1716, 2011.

[55] L. C. Brinson and T. S. Gates, "Effects of physical aging on long term creep of polymers and polymer matrix composites," *International Journal of Solids and Structures*, vol. 32, no. 6, pp. 827 – 846, 1995.

[56] R. Kohlrausch, "Theory of the electric residue in the leyden jar," *Philosophical Magazine Series 4*, vol. 7, no. 46, pp. 305–320, 1854. English translation of Kohlraush, Poggendorf Annalen der Physik und Chemie, vol 91, p.56 (1854).

[57] F. Kohlrausch, "Ueber die elastische nachwirkung bei der torsion," *Annalen der Physik und Chemie*, vol. 195, no. 7, pp. 337–368, 1863.

[58] M. Cardona, R. V. Chamberlin, and W. Marx, "The history of the stretched exponential function," *Annalen der Physik*, vol. 16, no. 12, pp. 842–845, 2007.

[59] M. Berberan-Santos, E. N. Bodunov, and B. Valeur, "History of the Kohlrausch (stretched exponential) function: Pioneering work in luminescence," *Annalen der Physik*, vol. 17, no. 7, pp. 460–461, 2008.

[60] G. Williams and D. C. Watts, "Non-symmetrical dielectric relaxation behaviour arising from a simple empirical decay function," *Transactions of the Faraday Society*, vol. 66, pp. 80–85, 1970.

[61] R. A. Schapery, *Irreversible Thermodynamics and Variational Principles with Applications to Viscoelasticity*. PhD thesis, 1962.

[62] R. A. Schapery, "On the characterization of nonlinear viscoelastic materials," *Polymer Engineering & Science*, vol. 9, no. 4, pp. 295–310, 1969.

[63] R. A. Schapery, "Correspondence principles and a generalized J integral for large deformation and fracture analysis of viscoelastic media," *International Journal of Fracture*, vol. 25, no. 3, pp. 195–223, 1984.

[64] R. Schapery, "Nonlinear viscoelastic and viscoplastic constitutive equations based on thermodynamics," *Mechanics of Time-Dependent Materials*, vol. 1, no. 2, pp. 209–240, 1997.

[65] Y. S. Urzhumtsev and R. D. Maksimov, "Time-stress superposition in nonlinear viscoelasticity," *Polymer Mechanics*, vol. 4, no. 2, pp. 318–320, 1968.

[66] W. L. Griffith, D. H. Morris, and H. F. Brinson, "Accelerated characterization of graphite/epoxy composites," 1980.

[67] V. V. Shcherbak and A. Y. Gol'dman, "Long-term strength of high-density polyethylene and its prediction," *Strength of Materials*, vol. 12, no. 6, pp. 731–736, 1980.

[68] F. R. Larson and J. Miller, "A time-temperature relationship for rupture and creep stresses," *Transactions of the American Society of Mechanical Engineers*, vol. 74, pp. 765–775, 1952.

[69] S. S. Manson and A. M. Haferd, "A linear time-temperature relation for extrapolation of creep and stress-rupture datas," Tech. Rep. NACA-TN-2890, NACA Lewis Flight Propulsion Laboratory, March 1953.

[70] S. N. Zhurkov, "Kinetic concept of the strength of solids," *International Journal of Fracture Mechanics*, vol. 1, 1965.

[71] W. I. Griffith, *The Accelerated Characterization of Viscoelastic Composite Materials*. PhD thesis, 1980.

[72] F. T. Wallenberger, J. C. Watson, and H. Li, "ASM handbook," in *Composites* (D. B. Miracle and S. L. Donaldson, eds.), vol. 21, ch. Glass fibres, pp. 28–34, ASM International, 2001.

[73] M. A. Boyle, C. J. Martin, and J. D. Neuner, "ASM handbook," in *Composites* (D. B. Miracle and S. L. Donaldson, eds.), vol. 21, ch. Epoxy resins, pp. 78–89, ASM International, 2001.

[74] T. Koufopoulos and P. S. Theocaris, "Shrinkage stresses in two-phase materials," *Journal of Composite Materials*, vol. 3, no. 2, pp. 308–320, 1969.

[75] P. K. Dutta, "Thermo-mechanical behavior of polymer composites.," in *Advanced multilayered and fibre-reinforced composites; Proceedings of the NATO Advanced Research Workshop*, (The Netherland), pp. 541–554, 1998.

[76] H. W. Lord and P. K. Dutta, "On the design of polymeric composite structures for cold regions applications," *Journal of Reinforced Plastics and Composites*, vol. 7, pp. 435–458, Sept. 1988.

[77] P. K. Dutta, "Structural fiber composite materials for cold regions," *Journal of Cold Regions Engineering*, vol. 2, no. 3, pp. 124–134, 1988.

[78] J. Halpin and N. Pagano, "Observations on linear anisotropic viscoelasticity," *Journal of Composite Materials*, vol. 2, no. 1, pp. 68–80, 1968.

[79] S. W. Beckwith, "Viscoelastic creep behavior of filament-wound case materials," *Journal of Spacecraft*, vol. 21, no. 6, pp. 546–552, 1982.

[80] D. A. Dillard, *Creep and creep Rupture of Laminated Graphite/Epoxy Composites*. PhD thesis, Virginia Polytechnic Institute and State University, March 1981.

[81] R. M. Guedes, "Time-dependent failure criteria for polymer matrix composites: A review," *Journal of Reinforced Plastics and Composites*, vol. 29, no. 20, pp. 3041–3047, 2010.

[82] E. Bosze, A. Alawar, O. Bertschger, Y.-I. Tsai, and S. Nutt, "High-temperature strength and storage modulus in unidirectional hybrid composites," *Composites Science and Technology*, vol. 66, no. 13, pp. 1963 – 1969, 2006.

[83] L. Cormier, "Effets du froid, de l'humidité et des cycles de gel et dégel sur les propriétés mécaniques des composites verre/époxy utilisés pour la fabrication de pales d'éoliennes," Master's thesis, École de technologie supérieure, 2009. Mémoire de maitrise.

[84] L. Cormier and S. Joncas, "Effects of cold temperature, moisture and freeze-thaw cycles on the mechanical properties of unidirectional glass fiber-epoxy composites," in *51st AIAA / ASME / ASCE / AHS / ASC Structures, Structural Dynamics and Materials Conference*, no. AIAA-2010-2823, (Orlando, FL, United-States), AIAA, 2010.

[85] C. C. Chamis, "Simplified composite micromechanics equations for hygral, thermal and mechanical properties," Tech. Rep. NAS 1.15:83320, NASA Glenn Research Center, 1983.

[86] C. C. Chamis, "Simplified composite micromechanics equations for strength, fracture toughness and environmental effects," Tech. Rep. NAS 1.15:83696, NASA Glenn Research Center, 1984.

[87] R. Nijssen, E. Stammes, and T. Westphal, "Material and subcomponent research for improved rotor blade design," in *2nd Technical Conference on Wind turbine Rotor Blades*, (Esssen, Germany), June 2010.

[88] R. M. Christensen, "A critical evaluation for a class of micro-mechanics models," *Journal of the Mechanics and Physics of Solids*, vol. 38, no. 3, pp. 379 – 404, 1990.

[89] L. Liu, J. Holmes, G. Kardomateas, and V. Birman, "Compressive response of composites under combined fire and compression loading," *Fire Technology*, vol. 47, no. 4, pp. 985–1016, 2011.

[90] A. G. Gibson, Y. S. Wu, J. T. Evans, and A. P. Mouritz, "Laminate theory analysis of composites under load in fire," *Journal of Composite Materials*, vol. 40, no. 7, pp. 639–658, 2006.

[91] S. Cao, X. Wang, and Z. Wu, "Evaluation and prediction of temperature-dependent tensile strength of unidirectional carbon fiber-reinforced polymer composites," *Journal of Reinforced Plastics and Composites*, vol. 30, no. 9, pp. 799–807, 2011.

[92] G. D. Sims and D. G. Gladman, "A framework for specifing the fatigue performance of glass fibre reinforced plastics," Tech. Rep. NPL Report DMA (A) 59, National Physical Laboratory, December 1982.

[93] J. M. Toth, W. J. Bailey, and D. A. Boyce, "Fiberglass epoxy laminate fatigue properties at 300 and 20 K," in *Fatigue at low temperature* (R. I. Stephens, ed.), no. ASTM STP 857, (Philadelphia), pp. 163–172, American Society for Testing and Materials, 1985.

[94] M. Robert and B. Benmokrane, "Behavior of GFRP reinforcing bars subjected to extreme temperatures," *Journal of Composites for Construction*, vol. 14, no. 4, pp. 353–360, 2010.

[95] R. Nijssen and L. Cormier, "Experiments and modelling of influence and interaction of temperature and frequency on fatigue life," Tech. Rep. Upwind Deliverable D 3.1.8/WMC-2010-94, Knowledge Centre Wind turbine Materials and Constructions, February 2011.

[96] M. Kawai, Y. Matsuda, and R. Yoshimura, "A general method for predicting temperature-dependent anisomorphic constant fatigue life diagram for a woven fabric carbon/epoxy laminate," *Composites Part A: Applied Science and Manufacturing*, vol. 43, no. 6, pp. 915 – 925, 2012.

[97] Y. Bai and T. Keller, "Modeling of strength degradation for fiber-reinforced polymer composites in fire," *Journal of Composite Materials*, vol. 43, no. 21, pp. 2371–2385, 2009.

[98] Y. Bai, T. Keller, and T. Vallée, "Modeling of stiffness of FRP composites under elevated and high temperatures," *Composites Science and Technology*, vol. 68, no. 15-16, pp. 3099 – 3106, 2008.

[99] C. Mahieux and K. Reifsnider, "Property modeling across transition temperatures in polymers: A robust stiffness-temperature model," *Polymer*, vol. 42, no. 7, pp. 3281 – 3291, 2001.

[100] C. Mahieux, K. Reifsnider, and S. Case, "Property modeling across transition temperatures in PMC's: Part I. tensile properties," *Applied Composite Materials*, vol. 8, no. 4, pp. 217–234, 2001.

[101] J. R. Correia, M. M. Gomes, J. M. Pires, and F. A. Branco, "Mechanical behaviour of pultruded glass fibre reinforced polymer composites at elevated temperature: Experiments and model assessment," *Composite Structures*, vol. 98, pp. 303 – 313, 2013.

[102] H. H. Abdelmohsen, "Simulation of tensile strength of anisotropic fibre-reinforced composites at low temperature," *Cryogenics*, vol. 31, pp. 399–404, 1991.

[103] P. K. Dutta, "Tensile strength of unidirectional fiber composites at low temperatures," in *Japan-U.S. Conference on Composite Materials*, pp. 782–792, 1993.

[104] C. Bathias, "An engineering point of view about fatigue of polymer matrix composite materials," *International journal of fatigue*, vol. 28, pp. 1094–1099, 2006.

[105] K. Reifsnider, "Fatigue bahavior of composite materials," *International Journal of Fracture*, vol. 16, pp. 563–583, 1980.

[106] K. L. Reifsnider, ed., *Fatigue of composites*, vol. 4 of *Composite Materials Series*. Elsevier, 1991.

[107] Z. Hashin and A. Rotem, "A fatigue failure criterion for fiber reinforced materials," *Journal of Composite Materials*, vol. 7, no. 4, pp. 448–464, 1973.

[108] J. E. Masters and K. L. Reifsnider, "An investigation of cumulative damage development in quasi-lsotropic graphite/epoxy laminates," in *Damage in Composite Materials: Basic Mechanisms, Accumulation, Tolerance and Characterization* (K. L. Reifsnider, ed.), no. ASTM STP 775, (Philadelphia), pp. 40 – 62, American Society for Testing and Materials, 1982.

[109] R. Talreja, "Damage analysis for structural integrity and durability of composite materials," *Fatigue & Fracture of Engineering Materials & Structures*, vol. 29, no. 7, pp. 481–506, 2006.

[110] T. Mesogitis, A. Skordos, and A. Long, "Uncertainty in the manufacturing of fibrous thermosetting composites: A review," *Composites Part A: Applied Science and Manufacturing*, vol. 57, no. 0, pp. 67 – 75, 2014.

[111] J. Mandell and J.-Y. Tsai, "Effects of porosity on delamination of resin-matrix composites," Tech. Rep. WRDC-TR-89-3032, Flight Dynamics Laboratory - Wright Research and Development Center, 1990. Final report for period June 1984 - June 1987.

[112] J. F. Mandell, D. D. Samborsky, and D. S. Cairns, "Fatigue of composite materials and substructures for wind turbine blades," Tech. Rep. SAND2002-0771, Sandia, 2002.

[113] A. Chambers, J. Earl, C. Squires, and M. Suhot, "The effect of voids on the flexural fatigue performance of unidirectional carbon fibre composites developed for wind turbine applications," *International Journal of Fatigue*, vol. 28, no. 10, pp. 1389 – 1398, 2006.

[114] J. Lambert, A. Chambers, I. Sinclair, and S. Spearing, "3d damage characterisation and the role of voids in the fatigue of wind turbine blade materials," *Composites Science and Technology*, vol. 72, no. 2, pp. 337 – 343, 2012.

[115] G. P. Sendeckyj, "Chapter 10 - life prediction for resin-matrix composite materials," in *Fatigue of Composite Materials* (K. Reifsnider, ed.), vol. 4 of *Composite Materials Series*, pp. 431 – 483, Elsevier, 1991.

[116] J. Degrieck and W. Van Paepegem, "Fatigue damage modeling of fibre-reinforced composite materials: Review," *Applied Mechanics Reviews*, vol. 54, pp. 279–300, july 2001.

[117] S. Wicaksono and G. B. Chai, "A review of advances in fatigue and life prediction of fiber-reinforced composites," *Proceedings of the Institution of Mechanical Engineers, Part L: Journal of Materials Design and Applications*, vol. 227, no. 3, pp. 179–195, 2013.

[118] E. Castillo, A. Fernández-Canteli, R. Koller, M. L. Ruiz-Ripoll, and A. García, "A statistical fatigue model covering the tension and compression Wöhler fields," *Probabilistic Engineering Mechanics*, vol. 24, pp. 199–209, Apr. 2009.

[119] C. Kassapoglou, "Fatigue life prediction of composite structures under constant amplitude loading," *Journal of Composite Materials*, vol. 41, no. 22, pp. 2737–2754, 2007.

[120] H. J. Sutherland, "A summary of the fatigue properties of wind turbine materials," *Wind Energy*, vol. 3, no. 1, pp. 1–34, 2000.

[121] ASTM Commitee E-11 on Quality Control and Materials, "ASTM manual on fitting straight lines," No. ASTM STP 313, (Philadelphia), American Society for Testing and Materials, 1962.

[122] J. F. Mandell and U. Meier, "Effects of stress ratio, frequency and loading time on the tensile fatigue of glass-reinforced epoxy, long-term behaviour of composites," in *Long-Term Behavior of Composites* (T. O'Brien, ed.), no. ASTM STP 813, (Philadelphia), pp. 55–77, American Society for Testing Material, 1983.

[123] H. El Kadi and F. Ellyin, "Effect of stress ratio on the fatigue of unidirectional glass fibre/epoxy composite laminae," *Composites*, vol. 25, no. 10, pp. 917–924, 1994.

[124] J. R. Schaff, "ASM handbook," in *Composites* (D. B. Miracle and S. L. Donaldson, eds.), vol. 21, ch. Fatigue and Life Prediction, pp. 252–258, ASM International, 2001.

[125] C. E. Demers, "Tension-tension axial fatigue of E-glass fiber-reinforced polymeric composites: fatigue life diagram," *Construction and Building Materials*, vol. 12, no. 5, pp. 303 – 310, 1998.

[126] G. Sendeckyj, "Constant life diagrams — a historical review," *International Journal of Fatigue*, vol. 23, no. 4, pp. 347 – 353, 2001.

[127] Det Norske Veritas, "Design and manufacture of wind turbine blades, offshore and onshore wind turbines," Standard DNV-OS-J102, Det Norske Veritas, October 2006.

[128] Germanisher Lloyd, "Guidelines for the certification of wind turbines," 2010. Germanischer Lloyd.

[129] A. P. Vassilopoulos, B. D. Manshadi, and T. Keller, "Influence of the constant life diagram formulation on the fatigue life prediction of composite materials," *International Journal of Fatigue*, vol. 32, no. 4, pp. 659 – 669, 2010.

[130] D. Flore and K. Wegener, "Modelling the mean stress effect on fatigue life of fibre reinforced plastics," *International Journal of Fatigue*, vol. 82, Part 3, pp. 689 – 699, 2016.

[131] Montana State University - Composite Technologies Research Group and Sandia National Laboratories (United States Department of Energy), "SNL/MSU/DOE Composite Materials Fatigue Database, Version 25.0," database. http://energy.sandia.gov/energy/renewable-energy/water-power/technology-development/advanced-materials/mhk-materials-database/. Visited 2017-05-30.

[132] Knowledge Center Wind turbine Materials and Constructions, "Optidat fatigue of wind turbine materials database," database, 10 2011. https://www.wmc.eu/optimatblades_optidat.php. Visited 2017-05-30.

[133] R. Talreja, "Fatigue of composite materials: Damage mechanisms and fatigue-life diagrams," *Proceedings of the Royal Society of London*, vol. A 378, pp. 461–475, 1981.

[134] R. Talreja, "Damage and fatigue in composites â€“ a personal account," *Composites Science and Technology*, vol. 68, no. 13, pp. 2585 – 2591, 2008.

[135] J. C. Halpin, T. J. Johnson, and M. E. Wadoups, "Kinetic fracture models and structural reliability," *International Journal of Fracture Mechanics*, vol. 8, 1972.

[136] L. J. Broutman and S. Sahu, "A new theory to predict cumulative fatigue damage in fiberglass reinforced plastics," in *Composite materials: Testing and design (Second conference)*, no. ASTM STP 497, (Philadelphia), pp. 170–188, American Society for Testing and Materials, 1972.

[137] H. Hahn and R. Kim, "Proof testing of composite materials," *Journal of Composite Materials*, vol. 9, no. 3, pp. 297–311, 1975.

[138] J. Yang and M. Liu, "Residual strength degradation model and theory of periodic proof tests for graphite/epoxy laminates," *Journal of Composite Materials*, vol. 11, no. 2, pp. 176–203, 1977.

[139] T. Philippidis and V. Passipoularidis, "Residual strength after fatigue in composites: Theory vs. experiment," *International Journal of Fatigue*, vol. 29, no. 12, pp. 2104 – 2116, 2007.

[140] J. Whitney, "Fatigue characterization of composite materials," in *Fatigue of fibrous composite materials* (K. N. Lauraitis, ed.), no. ASTM STP 723, (Philadelphia), American Society for Testing and Materials, 1981.

[141] G. P. Sendeckyj, "Fitting models to composite materials fatigue data," in *Test Methods and Design Allowables for Fibrous Composites* (C. C. Chamis, ed.), no. ASTM STP 734, (Philadelphia), pp. 245–260, American Society for Testing and Materials, 1981.

[142] K. L. Reifsnider and W. W. Stinchvomb, "A critical-element model of the residual strength and loife of fatigue-loaded composite coupons," in *Composite Materials: Fatigue and Fracture* (H. T. Hahn, ed.), no. ASTM STP 907, (Philadelphia), American Society for Testing and Materials, 1986.

[143] A. D'Amore, G. Caprino, P. Stupak, J. Zhou, and L. Nicolais, "Effect of stress ratio on the flexural fatigue behaviour of continuous strand mat reinforced plastics," vol. 5, pp. 1–8, 1996.

[144] G. Caprino, A. D'Amore, and F. Facciolo, "Fatigue sensitivity of random glass fibre reinforced plastics," *Journal of Composite Materials*, vol. 32, no. 12, pp. 1203–1220, 1998.

[145] G. Caprino and A. D'Amore, "Flexural fatigue behaviour of random continuous-fibre-reinforced thermoplastic composites," *Composites Science and Technology*, vol. 58, no. 6, pp. 957 – 965, 1998.

[146] J. A. Epaarachchi and P. D. Clausen, "An empirical model for fatigue behavior prediction of glass fibre-reinforced plastic composites for various stress ratios and test frequencies," *Composites Part A: Applied Science and Manufacturing*, vol. 34, no. 4, pp. 313 – 326, 2003.

[147] R. Nijssen and A. van Wingerde, "Shear strength of UD material at -40℃ Iosipescu test results at WMC," Tech. Rep. OB_TG3_R023 rev. 000, Knowledge Centre Wind turbine Materials and Constructions, 2005. Optimat Blade Project.

[148] V. Passipoularidis and T. Philippidis, "Strength degradation due to fatigue in fiber dominated glass/epoxy composites: A statistical approach," *Journal of Composite Materials*, vol. 43, no. 9, pp. 997–1013, 2009.

[149] A. D'Amore, M. Giorgio, and L. Grassia, "Modeling the residual strength of carbon fiber reinforced composites subjected to cyclic loading," *International Journal of Fatigue*, vol. 78, pp. 31 – 37, Sept. 2015.

[150] A. D'Amore and L. Grassia, "Constitutive law describing the strength degradation kinetics of fibre-reinforced composites subjected to constant amplitude cyclic loading," *Mechanics of Time-Dependent Materials*, vol. 20, no. 1, pp. 1–12, 2016.

[151] Y. Ma, Y. Zhang, T. Sugahara, S. Jin, Y. Yang, and H. Hamada, "Off-axis tensile fatigue assessment based on residual strength for the unidirectional 45Â° carbon fiber-reinforced composite at room temperature," *Composites Part A: Applied Science and Manufacturing*, vol. 90, pp. 711 – 723, 2016.

[152] ASTM subcommitee E08.04, "Standard Practice for Statistical Analysis of Linear and Linearized Stress-Life (S-N) and strain-Life (ϵ-N) Fatigue," Standard E 739, ASTM Committee E08 on Fatigue and Fracture, West Conshohocken, PA, USA, 2004.

[153] H. Sutherland and P. Veers, "The development of confidence limits for fatigue strength data," in *2000 ASME Wind Energy Symposium*, Aerospace Sciences Meetings, American Institute of Aeronautics and Astronautics, 2000.

[154] K. O. Ronold and A. T. Echtermeyer, "Estimation of fatigue curves for design of composite laminates," *Composites Part A: Applied Science and Manufacturing*, vol. 27, no. 6, pp. 485 – 491, 1996.

[155] J. Tomblin and W. Seneviratne, "Determining the fatigue life of composite aircraft structures using life and load-enhancement factors," Tech. Rep. DOT/FAA/AR-10/6, Federal Aviation Administration, June 2011.

[156] W. Nelson, "Fitting of fatigue curves with nonconstant standard deviations to data with runouts," *Journal of Testing and Evaluation*, vol. 12, no. 2, pp. 69–77, 1984.

[157] C. B. King, Y. Hong, S. P. Dehart, P. A. Defeo, and R. Pan, "Planning fatigue tests for polymer composites," *Journal of Quality Technology*, vol. 48, pp. 227–245, July 2016.

[158] ASTM subcommitee D30.04, "Standard test method for tension-tension fatigue of polymer matrix composite materials," Standard D3479/D3479M-12, ASTM subcommity D30.04 on Lamina and Laminate Test Methods, West Conshohocken, PA, USA.

[159] H. Kotik and J. P. Ipiña, "Frequency effect in short-beam shear fatigue of a glass fiber reinforced polyester composite," *International Journal of Fatigue*, vol. 90, pp. 116 – 124, 2016.

[160] P. Bailey, C. Hoehl, P. Jamshidi, C. Cowan, S. Squires, and A. Smith, "Enhanced fatigue testing of composites," in *19th International Conference on Composite Materials*, International Conference on Composite Materials, 2013.

[161] P. B. Bailey, "Use of IR temperature measurement and thermography for control and monitoring of fatigue tests," in *Evaluation of Existing and New Sensor Technologies for Fatigue, Fracture and Mechanical Testing* (J. Kang, D. Jablonski, and D. Dudzinski, eds.), no. ASTM STP 1584, pp. 169–185, ASTM International, 2015. West Conshohocken, PA 2015.

[162] T. J. Adam and P. Horst, "Very high cycle fatigue of fibre-reinforced composites: an alternative experimental approach," in *19th Conference on composite materials*, 2013.

[163] R. Apinis, "Acceleration of fatigue tests of polymer composite materials by using high-frequency loadings," *Mechanics of Composite Materials*, vol. 40, pp. 107–118, 2004.

[164] A. Kahirdeh, M. Naderi, and M. Khonsari, "On the role of cooling on fatigue failure of a woven glass/epoxy laminate," *Journal of Composite Materials*, vol. 47, no. 15, pp. 1803–1815, 2013.

[165] H. T. Hahn and O. Turkgenc, "The effect of loading parameters on fatigue of composite laminates: Part IV information systems," resreport DOT/FAA/AR-00/48, U.S. Department of Transportation, Federal Aviation Administration , Office of Aviation Research, December 2000.

[166] M. Eftekhari and A. Fatemi, "On the strengthening effect of increasing cycling frequency on fatigue behavior of some polymers and their composites: Experiments and modeling," *International Journal of Fatigue*, vol. 87, pp. 153 – 166, 2016.

[167] C. T. Sun and W. S. Chan, "Frequency effect on the fatigue life of a laminated composite," in *Composite Materials :Testing and Design (Fifth Conference)* (S. W. Tsai, ed.), no. ASTM STP 674, pp. 418–430, American Society for Testing and Materials, 1979.

[168] C. T. Sun and E. S. Chim, "Fatigue retardation due to creep in a fibrous composite," in *Fatigue of Fobrous Composite Materials* (K. N. Lauraitis, ed.), no. ASTM STP 723, (Philadelphia), pp. 233–242, America Society for Testing and Materials, 1981.

[169] C. R. Saff, "Effect of load frequency and lay-up on fatigue life of composites," in *Long-Term Behavior of Composites* (T. K. O'Brien, ed.), no. ASTM STP 813, (Philadelphia), pp. 78–91, American Society for Testing and Materials, 1983.

[170] H. T. Hahn and R. Y. Kim, "Fatigue behavior of composite laminate," *Journal of Composite Materials*, vol. 10, no. 2, pp. 156–180, 1976.

[171] A. Katunin, W. Hufenbach, P. Kstka, and K. Holeczek, "Frequency dependence of the self-heating effect in polymer-based composites," *Journal of achievements in materials and manufacturing engineering*, vol. 41, pp. 9–15, 2010.

[172] D. Kujawski and F. Ellyin, "Rate/frequency-dependent behaviour of fibreglass/epoxy laminates in tensile and cyclic loading," *Composites*, vol. 26, no. 10, pp. 719–723, 1995.

[173] S. Lin, C. b. Ma, N. Tai, S. Wu, J. Wu, and J. Lin, "Effect of frequency on the fatigue behavior of $[\pm 45]_{4s}$ laminate of carbon fiber reinforced polyetheretherketone (PEEK) composites under tension-tension loading," *Journal of Polymer Research*, vol. 2, no. 3, pp. 171–178, 1995.

[174] M. R. Kharrazi and S. Sarkani, "Frequency-dependent fatigue damage accumulation in fiber-reinforced plastics," *Journal of Composite Materials*, vol. 35, no. 21, pp. 1924–1953, 2001.

[175] A. Rotem and H. Nelson, "Fatigue behavior of graphite-epoxy laminates at elevated temperatures," in *Fatigue of Fibrous Composite Materials* (K. N. Lauraitis, ed.), no. ASTM STP 723, (Philadelphia), pp. 152–173, American Society for Testing and Materials, 1981.

[176] X. R. Xiao, "Modeling of load frequency effect on fatigue life of thermoplastic composites," *Journal of Composite Materials*, vol. 33, no. 12, pp. 1141–1158, 1999.

[177] C. C. Chamis and J. H. Sinclair, "Durability/life of fiber composites in hygrothermomechanical environments," in *Composite Materials: Testing and Design* (J. M. Daniels, ed.), no. ASTM STP 787, (Philadelphia), pp. 498–512, American Society for Testing and Materials, 1982.

[178] G. H. and.S. Knaak, "Fibre-epoxy composites at low temperatures," *Cryogenics*, vol. 24, no. 11, pp. 639 – 647, 1984.

[179] J. W. Weeton, D. M. Peters, and K. L. Thomas, eds., *Engineer's Guide to Composite Materals*. American Society for Metals, 1987.

[180] W. Sys, *RUG Investigations of GL-UP Materials*, ch. 2, pp. 120–130. No. EUR 16684 EN, European Commission - Directorate General XIII, Telecommunications, Information Market and Exploitation of Research, 1996.

[181] H. C. Tang, T. Nguyen, T. J. Chuang, J. W. Chin, H. F. Wu, and J. Lesko, "Temperature effects on fatigue of polymer composites," in *Composites Engineering, 7th Annual International Conference. ICCE/7.* (D. Hui, ed.), pp. 861–862, Composites Engineering and College of Engineering, University of New Orleans., July 2000.

[182] H. C. Tang, T. Nguyen, T. J. Chuang, J. W. Chin, J. Lesko, and H. F. Wu, "Fatigue model for fiber-reinforced polymeric composites," *Journal of Materials in Civil Engineering*, vol. 12, pp. 97–104, May 2000.

[183] K. Reifsnider, S. Case, and J. Duthoit, "The mechanics of composite strength evolution," *Composites Science and Technology*, vol. 60, no. 12-13, pp. 2539–2546, 2000.

[184] M. N. Bureau and J. Denault, "Fatigue resistance of continuous glass fiber/polypropylene composites: Temperature dependance," *Polymer Composites*, vol. 25, pp. 622–629, 2004.

[185] D. Brassard, "Étude des effets du climat nordique sur la durée de vie en fatigue en tension des composites unidirectionnels de fibres de verre et d'époxy," Master's thesis, École de technologie supérieure, Montréal, 2014.

[186] S. Kumagai, Y. Shindo, and A. Inamoto, "Tensionâ€"tension fatigue behavior of GFRP woven laminates at low temperatures," *Cryogenics*, vol. 45, no. 2, pp. 123 – 128, 2005.

[187] Y. Shindo, S. Takano, K. Horiguchi, and T. Sato, "Cryogenic fatigue behavior of plain weave glass/epoxy composite laminates under tension-tension cycling," *Cryogenics*, vol. 46, no. 11, pp. 794 – 798, 2006.

[188] M.-H. R. Jen, Y.-C. Tseng, H.-K. Kung, and J. Huang, "Fatigue response of APC-2 composite laminates at elevated temperatures," *Composites Part B: Engineering*, vol. 39, no. 7â€"8, pp. 1142 – 1146, 2008.

[189] H. Mivehchi and A. Varvani-Farahani, "Erratum to: Temperature dependence of stress–fatigue life data of FRP composites," *Mechanics of Composite Materials*, vol. 47, no. 3, pp. 369–376, 2011.

[190] Y. Miyano, M. K. McMurray, J. Enyama, and M. Nakada, "Loading rate and temperature dependence on flexural fatigue behavior of a satin woven CFRP laminate," *Journal of Composite Materials*, vol. 28, no. 13, pp. 1250–1260, 1994.

[191] Y. Miyano, M. Nakada, H. Kudoh, and R. Muki, "Prediction of tensile fatigue life under temperature environment for unidirectional CFRP," *Advanced Composite Materials*, vol. 8, no. 3, pp. 235–246, 1999.

[192] Y. Miyano, M. Nakada, and H. Cai, "Formulation of long-term creep and fatigue strengths of polymer composites based on accelerated testing methodology," *Journal of Composite Materials*, vol. 42, no. 18, pp. 1897–1919, 2008.

[193] M. Nakada and Y. Miyano, "Advanced accelerated testing methodology for long-term life prediction of CFRP laminates," *Journal of Composite Materials*, 2013. DOI:10.1177/0021998313515019.

[194] R. Guedes, "Creep and fatigue lifetime prediction of polymer matrix composites based on simple cumulative damage laws," *Composites Part A: Applied Science and Manufacturing*, vol. 39, no. 11, pp. 1716 – 1725, 2008.

[195] J. Song, W. Wen, and H. Cui, "Fatigue behaviors of 2.5D woven composites at ambient and un-ambient temperatures," *Composite Structures*, vol. 166, pp. 77 – 86, 2017.

[196] M. Crowther, R. Wyatt, and M. Phillips, "Creep-fatigue interactions in glass fibre/polyester composites," *Composites Science and Technology*, vol. 36, pp. 191–210, 1989.

[197] M. Eftekhari and A. Fatemi, "Fatigue behaviour and modelling of talc-filled and short glass fibre reinforced thermoplastics, including temperature and mean stress effects," *Fatigue & Fracture of Engineering Materials & Structures*, 2016. DOI:10.1111/ffe.12497.

[198] D. D. Samborsky, J. F. Mandell, and D. A. Miller, "Creep/fatigue behavior of resin infused biaxial glass fabric laminates," in *AIAA SDM Wind Energy Session*, 2013.

[199] A. Sayyidmousavi, H. Bougherara, and Z. Fawaz, "The role of viscoelasticity on the fatigue of angle-ply polymer matrix composites at high and room temperatures- a micromechanical approach," *Applied Composite Materials*, vol. 22, no. 3, pp. 307–321, 2014.

[200] A. Sayyidmousavi, H. Bougherara, and Z. Fawaz, "A micromechanical approach for the fatigue failure prediction of unidirectional polymer matrix composites in off-axis loading including the effect of viscoelasticity," *Advanced Composite Materials*, vol. 24, no. sup1, pp. 65–77, 2015.

[201] O. Krause, "Testing frequency for dynamic tests," Tech. Rep. OB_TC_N003_-DLR, Deutsches Zentrum für Luft- und Raumfahrt, DLR, December 2002. Optimat Blade Project.

[202] J. J. Liu and V. M. Karbhari, "Performance and design of fibre-reinforced polymer composites at cold temperatures : current status and future needs," *International Journal of Materials and Product Technology*, vol. 28, no. 1, pp. 1–7, 2007.

[203] M. Aktas and R. Karakuzu, "Determination of mechanical properties of glass-epoxy composites in high temperatures," *Polym Compos*, vol. 30, no. 10, pp. 1437–1441, 2009.

[204] M. Kinsella, D. Murray, D. Crane, J. Mancinelli, and M. Kranjc, "Mechanical properties of polymeric composites reinforced with high strength glass fibers," in *33rd International SAMPE Technical Conference*, (Seattle, WA, United states), pp. 1644 – 1657, 2001.

[205] V. M. Karbhari, J. W. Chin, D. Hunston, B. Benmokrane, T. Juska, R. Morgan, J. J. Lesko, U. Sorathia, and D. Reynaud, "Durability gap analysis for fiber-reinforced polymer composites in civil infrastructure," *Journal of Composites for Construction*, vol. 7, no. 3, pp. 238–247, 2003.

[206] M. Megnis, P. Brondsted, and K. Primdahl Eriksen, "Effects of extreme conditions on properties of the reference material," Tech. Rep. OB_TG3_R015, RISØ, 2005. Optimat Blade Project.

[207] L. Mishnaevsky jr. and P. Brøndsted, "Micromechanical modeling of strength and damage of fiber reinforced composites," Tech. Rep. Risø-R-1601(EN), Risø National Laboratory, March 2007.

[208] O. Krause and T. P. Philippidis, "General test specification," Tech. Rep. OB_-TC_R014 rev.005, Deutsches Zentrum fÃ¼r Luft- und Raumfahrt; DLR, 2005. Optimat Blade Project.

[209] R. Nijssen, T. Westphal, E. Stammes, and J. Sari, "Strength and fatigue of wind turbine rotor laminates and subcomponents," in *AIAA/ASME Wind Energy Symposium*, no. AIAA- 2010-1189, (Orlando, FL, United states), 2010.

[210] B. Ait-Idriss, F. Pelletier, and L. Robert, "Étude sur l'évaluation du potentiel éolien, de son prix de revient et des retombées économiques pouvant en découler au québec," Tech. Rep. R-3526-2004, 2004.

[211] I. Barig-Gould, R. Cattin, M. Durstewitz, M. Hulkkonen, A. Krenn, T. Laasko, A. Lacroix, E. Peltola, G. Ronsten, L. Tallhaug, and T. Wallenius, "Expert group study on recommended practice : Wind energy projects in cold climates," tech. rep., International Energy Agency, 2011.

[212] DOE, "Renewable energy technology characterizations," Tech. Rep. TR-109496, U.S. Department of Energy - Office of Utility Technologies, Energy Efficiency and Renewable Energy and Electric Power Research Institute, December 1997.

[213] E. Hau, *Wind Turbines: Fundamentals, Technologies, Application, Economics*. Luxembourg: Springer, 2013.

[214] N. Buckney, A. Pirrera, S. D. Green, and P. M. Weaver, "Structural efficiency of a wind turbine blade," *Thin-Walled Structures*, vol. 67, no. 0, pp. 144 – 154, 2013.

[215] D. A. Griffin, "Windpact turbine design scaling studies technical : Area 1 - composite blades for 80 to 120 meter rotor," Tech. Rep. NREL/SR-500-29492, National Renewable Energy Laboratory, 2001.

[216] P. C. Capponi, T. Ashuri, , G. J. van Bussel, and Kallesøe, "A non-linear upscaling approach for wind turbines blades based on stresses," in *Proceedings of the Eeuropean Wind Energy Association 2011 conference and exhibition, Brussels, Belgium, 14-17 March 2011*, European Wind Energy Association, 2011.

[217] C.-H. Shen and G. S. Springer, "Effects of moisture and temperature on the tensile strength of composite materials," *Journal of Composite Materials*, vol. 11, pp. 2–16, Jan. 1977.

[218] C.-H. Shen and G. S. Springer, "Environmental effects on the elastic moduli of composite materials," *Journal of Composite Materials*, vol. 11, pp. 250–64, 1977.

[219] V. N. Bulmanis, G. M. Gunyaev, V. V. Krivonos, G. P. Mashinskaya, V. M. Merkulova, G. I. Milyutin, A. A. Gerasimov, and S. A. Kuz'min, "Atmospheric durability of polymer-fiber composites in cold climates," *Mechanics of Composite Materials*, vol. 27, no. 6, pp. 698–705, 1991.

[220] P. K. Dutta, "Low-temperature compressive strength of glass-fiber-reinforced polymer composites," *Journal of Offshore Mechanics and Arctic Engineering, Transactions of the ASME*, vol. 116, no. 3, pp. 167–172, 1994.

[221] L. Cormier and R. Nijssen, "Temperature and frequency effects on the fatigue properties of unidirectional glass fiber-epoxy composites," in *53rd AIAA / ASME / ASCE / AHS / ASC Structures, Structural Dynamics and Materials Conference*, no. AIAA-2012-1574, (Honolulu, HI, United-States), AIAA, April 2012.

[222] ISO TC 61/SC 2, "Plastics - Determination of tensile properties, Parts 1 to 5," Standard ISO 527, Interrnational Organization for Standardization, Geneva, 1993.

[223] ISO TC 61/SC 13, "Fibre-reinforced plastic composites – Determination of the in-plane shear stress/shear strain response, including the in-plane shear modulus and strength, by the ±45° tension test method," Standard ISO 14129, Interrnational Organization for Standardization, Geneva, 1997.

[224] ASTM subcommitee D30.04, "Standard Test Method for Tensile Properties of Polymer Matrix Composite Materials," Standard D 3039/D 3039M - 08, ASTM subcommitee D30.04 on Lamina and Laminate Test Methods, West Conshohocken, PA, 2008.

[225] ASTM subcommitee D30.04, "Standard Test Method for In-Plane Shear Response of Polymer Matrix Composite Materials by Tensile Test of a ±45° Laminate," Standard D 3518/D 3518M-13, ASTM subcommitee D30.04, West Conshohocken, PA, 1994 (reapproved 2001).

[226] W. B. Nelson, *Accelerated Testing: Statistical Models, Test Plans and Data Analysis*. Wiley Series in Probability and Statistics, Wiley-Interscience, 2004.

[227] I. Gijbels, "Censored data," *Wiley Interdisciplinary Reviews: Computational Statistics*, vol. 2, no. 2, pp. 178–188, 2010.

[228] J. Spindel and E. Haibach, "The method of maximum likelihood applied to the statistical analysis of fatigue data," *International Journal of Fatigue*, vol. 1, no. 2, pp. 81 – 88, 1979.

[229] K. L. Reifsnider and S. Case, "Mechanics of temperature-driven long-term environmental degradation of polymer based composite systems," in *Proceedings of the ASME Material Division: Presented at the 1995 ASME International Mechanical Engineering Congress and Exposition*, vol. 1, pp. 225–230, ASME, november 1995.

[230] Z. Gao and K. L. Reifsnider, "Micromechanics of tensile strength in composite systems," in *Composite Materials: Fatigue and Fracture*, vol. 4, pp. 453–470, ASTM, 1993.

[231] S. Subramanian, K. L. Reifsnider, and W. W. Stinchcomb, "Tensile strength of unidirectional composites: The role of efficiency and strength of fiber-matrix interface," *Journal of Composites Technology & Research*, vol. 17, pp. 289–300, October 1995.

[232] L. Cormier, S. Joncas, and R. Nijssen, "Effects of low temperature on the mechanical properties of glass fibre-epoxy composites: Static tension, compression, $R = 0.1$ and $R = -1$ fatigue of $\pm 45°$ laminates," *Wind Energy*, vol. 19, pp. 1023–1041, June 2016.

[233] R. Guedes, "Durability of polymer matrix composites: Viscoelastic effect on static and fatigue loading," *Composites Science and Technology*, vol. 67, no. 11-12, pp. 2574–2583, 2007.

[234] B. Gompertz, "On the nature of the function expressive of the law of human mortality, and on a new mode of determining the value of life contingencies," in *Philosophical Transactions of the Royal Society of London*, vol. 115, pp. 513–583, 1825.

[235] M. L. Garg, B. Raja Rao, and C. K. Redmond, "Maximum-likelihood estimation of the parameters of the Gompertz survival function," *Journal of the Royal Statistical Society: Series C (Applied Statistics)*, vol. 19, no. 2, pp. 152–159, 1970.

[236] A. Boisseau, P. Davies, and F. Thiebaud, "Fatigue behaviour of glass fibre reinforced composites for ocean energy conversion systems," *Applied Composite Materials*, vol. 20, no. 2, pp. 145–155, 2012.

[237] J. Corum, R. Battiste, K. Liu, and M. Ruggles, "Basic properties of reference crossply carbon-fiber composite," Tech. Rep. ORNL/TM-2000/29, Oak Ridge National Laboratory, February 2000.

[238] R. Christensen and Y. Miyano, "Stress intensity controlled kinetic crack growth and stress history dependent life prediction with statistical variability," *International Journal of Fracture*, vol. 137, no. 1-4, pp. 77–87, 2006.

[239] "Canadian climate normals." http://climate.weather.gc.ca/climate_normals/index_e.html. Government of Canada, visited 2016/08/26.

[240] F. Lahuerta, R. Nijssen, F. van der Meer, and L. Sluys, "Experimental-computational study towards heat generation in thick laminates under fatigue loading," *International Journal of Fatigue*, vol. 80, pp. 121–127, 2015.

[241] J. Honerkamp and J. Weese, "A note on estimating mastercurves," *Rheologica Acta*, vol. 32, no. 1, pp. 57–64, 1993.

[242] S. Naya, A. Meneses, J. Tarrío-Saavedra, R. Artiaga, J. López-Beceiro, and C. Gracia-Fernández, "New method for estimating shift factors in time–temperature superposition models," *Journal of Thermal Analysis and Calorimetry*, vol. 113, no. 2, pp. 453–460, 2013.

[243] W. Brostow, "Temperature shift factor: Polymer mechanical properties above and below glass transition," *Materials Chemistry and Physics*, vol. 13, no. 1, pp. 47 – 57, 1985.

[244] R. Li, "Time-temperature superposition method for glass transition temperature of plastic materials," *Materials Science and Engineering:A*, vol. 278, no. 1-2, pp. 36–45, 2000.

[245] Y. Zhang, R. D. Adams, and L. F. M. da Silva, "A rapid method of measuring the glass transition temperature using a novel dynamic mechanical analysis method," *The Journal of Adhesion*, vol. 89, no. 10, pp. 785–806, 2013.

[246] T. W. Sirk, K. S. Khare, M. Karim, J. L. Lenhart, J. W. Andzelm, G. B. McKenna, and R. Khare, "High strain rate mechanical properties of a cross-linked epoxy across the glass transition," *Polymer*, vol. 54, no. 26, pp. 7048 – 7057, 2013.

[247] D. Porter and P. J. Gould, "Predictive nonlinear constitutive relations in polymers through loss history," *International Journal of Solids and Structures*, vol. 46, no. 9, pp. 1981 – 1993, 2009.

[248] J. H. Pollard and E. J. Valkovics, "The Gompertz distribution and its application," *Genus*, vol. 48, no. 3/4, pp. 15–28, 1992.

[249] J. Rieger, "The glass transition temperature T_g of polymers — comparison of the values from differential thermal analysis (DTA, DSC) and dynamic mechanical measurements (torsion pendulum)," *Polymer Testing*, vol. 20, pp. 199–204, 2001.

[250] V. M. Karbhari and Q. Wang, "Multi-frequency dynamic mechanical thermal analysis of moisture uptake in E-glass/vinylester composites," *Composites Part B: Engineering*, vol. 35, no. 4, pp. 299 – 304, 2004.

[251] F. H. Stillinger and T. A. Weber, "Hidden structure in liquids," *Phys. Rev. A*, vol. 25, pp. 978–989, Feb 1982.

[252] F. H. Stillinger and T. A. Weber, "Dynamics of structural transitions in liquids," *Phys. Rev. A*, vol. 28, pp. 2408–2416, Oct 1983.

[253] J. P. Foreman, D. Porter, S. Behzadi, and F. R. Jones, "A model for the prediction of structure-property relations in cross-linked polymers," *Polymer*, vol. 49, no. 25, pp. 5588 – 5595, 2008.

[254] V. Gumen, F. Jones, and D. Attwood, "Prediction of the glass transition temperatures for epoxy resins and blends using group interaction modelling," *Polymer*, vol. 42, no. 13, pp. 5717 – 5725, 2001.

[255] T. B. Lewis and L. E. Nielsen, "Dynamic mechanical properties of particulate-filled composites," *Journal of Applied Polymer Science*, vol. 14, no. 6, pp. 1449–1471, 1970.

[256] G. Edwards and L. Pacheco, "A Bayesian method for establishing fatigue design curves," *Structural Safety*, vol. 2, no. 1, pp. 27 – 38, 1984.